



MONTCLAIR STATE
UNIVERSITY

Montclair State University
**Montclair State University Digital
Commons**

Theses, Dissertations and Culminating Projects

1-2023

Destruction of PFOA on Ion-exchange Resin with Advanced Reduction Processes to Regenerate Resins for Addressing PFOA Pollution in Drinking Water

Junkui Cui
Montclair State University

Follow this and additional works at: <https://digitalcommons.montclair.edu/etd>



Part of the [Earth Sciences Commons](#), and the [Environmental Sciences Commons](#)

Recommended Citation

Cui, Junkui, "Destruction of PFOA on Ion-exchange Resin with Advanced Reduction Processes to Regenerate Resins for Addressing PFOA Pollution in Drinking Water" (2023). *Theses, Dissertations and Culminating Projects*. 1302.

<https://digitalcommons.montclair.edu/etd/1302>

This Dissertation is brought to you for free and open access by Montclair State University Digital Commons. It has been accepted for inclusion in Theses, Dissertations and Culminating Projects by an authorized administrator of Montclair State University Digital Commons. For more information, please contact digitalcommons@montclair.edu.

**Destruction of PFOA on Ion-exchange Resin with Advanced Reduction Processes to
Regenerate Resins for Addressing PFOA Pollution in Drinking Water**

A DISSERTATION

Submitted to the Faculty of
Montclair State University in partial fulfillment
of the requirements
for the degree of Doctor of Philosophy

by

Junkui Cui

Montclair State University

Upper Montclair, NJ

January 2023

Dissertation Chair: Dr. Yang Deng

MONTCLAIR STATE UNIVERSITY
THE GRADUATE SCHOOL
DISSERTATION APPROVAL

We hereby approve the Dissertation

**Destruction of PFOA on Ion-exchange Resin with Advanced Reduction Processes to
Regenerate Resins for Addressing PFOA Pollution in Drinking Water**

of

Junkui Cui

Candidate for the Degree:

Doctor of Philosophy

Graduate Program:

Environmental Science and Management

Certified by:


Dr. Kenneth Summer
Associate Provost for Academic Affairs
and Acting Dean of the Graduate School

Date:

12-15-22

Dissertation Committee:


Dr. Yang Deng
Dissertation Chair


Dr. Huan Feng


Dr. Jinshan Gao


Dr. Mengyan Li

Copyright © 2023 by Junkui Cui. All rights reserved.

Abstract**DESTRUCTION OF PFOA ON ION-EXCHANGE RESIN WITH ADVANCED REDUCTION PROCESSES TO REGENERATE RESINS FOR ADDRESSING PFOA POLLUTION IN DRINKING WATER**

by Junkui Cui

Per- and polyfluoroalkyl substances (PFAS) have been globally incorporated into various industrial and consumer products since the 1940s. However, concerns about PFAS have gradually grown because of their prevalence, mobility, persistence, bioaccumulation, and adverse impacts on human and environmental health. Unfortunately, traditional water treatment processes inefficiently remove PFAS. Therefore, there is an urgent research need to develop innovative, technically viable, and low cost-treatment processes for the removal of PFAS in water.

Among the established PFAS treatment technologies, ion-exchange (IX) has been extensively applied to drinking water treatment practices due to its adsorption capability and technology maturity. However, IX is highly cost-inefficient and environmentally unfriendly because of the expenses associated with off-site regeneration, no PFAS detoxification, and the production of harmful PFAS-containing regenerant waste required for careful disposal. In contrast, advanced reduction processes (ARPs) have demonstrated technical viability for PFAS degradation due to the powerful reducing potential of hydrated electron (e_{aq}^-) generated. Nevertheless, ARPs are restricted in realistic water treatment, particularly drinking water treatment, due to increased total dissolved solids in effluent, operational requirements in pH adjustment, and depletion of dissolved oxygen.

The primary objective of this dissertation is to advance the fundamental understanding of the interactions of e_{aq}^- and PFAS-laden IX resins, thereby providing a scientific basis for the development of an innovative on-site ARP-based IX resin regeneration method capable of recovering spent resins and degrading PFAS in drinking water treatment. Specifically, the design comprises repeated IX adsorption – ARP regeneration phases. In the first adsorption phase, trace PFAS in water is captured by IX resins until saturation. Subsequently, ARPs are launched to decompose PFAS laden on the resins for adsorption recovery before reuse. In the dissertation research, perfluorooctanoic acid (PFOA) was chosen as a model PFAS species owing to its prevalence in the aquatic environment, while ultraviolet (UV)/sulfite was selected as the representative ARP to generate e_{aq}^- . Five tasks were sequentially completed in this dissertation to achieve the primary objective.

In Task 1, a critical review of the destruction of aqueous PFAS with ARPs was conducted to retrospect the state-of-the-art knowledge on the emerging PFAS treatment technology and identify the critical knowledge gaps toward applications to drinking water treatment. In Task 2, bench-scale tests were performed to screen for a potentially durable resin to demonstrate the technical feasibility of e_{aq}^- -driven ARPs for mitigation and degradation of PFAS laden on resins. Specifically, IRA67 resins were selected among eight commercially available resins for the subsequent dissertation studies because of their excellent PFOA adsorption capability and durable physical/chemical properties for consistently high PFOA. In Task 3, bench-scale tests were carried out to elucidate the interactions of e_{aq}^- and PFOA sorbed on the PFOA/NOM-laden IRA67 resins and assess the role of NOM co-sorbed on the IX resins in the proposed PFAS treatment approach. Results showed that PFOA, regardless of sorbed or aqueous states, could be effectively degraded by e_{aq}^- . However, UV/SO₃²⁻ ARP treatment could not effectively decompose

co-sorbed NOM to substantially recover the resin adsorption effectively. The buildup of NOM on the resins finally led to the loss of the resin capacity for capturing PFOA in water with the increasing cycle number. Therefore, two pretreatment strategies (i.e., coagulation and UV/hydrogen peroxide (H_2O_2)-based advanced oxidation process (AOP)) were assessed in Task 4 to alleviate NOM loading on PFOA/NOM-laden IRA67 and to evaluate the effect of pH on desorption of co-sorbed NOM during the IRA67 regeneration processes, respectively. Moreover, the optimized cyclic adsorption-regeneration tests combined with the NOM mitigation strategies were evaluated for the repeated removal of PFOA in water. Results showed that alum coagulation at the optimized operational conditions (i.e., alum 60.0 mg/L; pH 6.0) significantly alleviated the NOM loading on IRA67, but the UV/ H_2O_2 -based AOP could not further reduce the PFOA loading on IRA67. The continuous adsorption of PFOA by IRA67 in the cyclic adsorption-regeneration process was ascribed to NOM desorption at pH 10.0 during the ARP regeneration process to release more occupied sites on IRA67. Therefore, the UV/ SO_3^{2-} process operated at an alkaline condition, if jointly used with alum coagulation as a pretreatment step, can enable a promising on-site regeneration process for the PFOA/NOM-laden IRA67 in drinking water. The information will be input to Task 5 in which the implications of the proposed ARP-based resin regeneration technologies were discussed in terms of economic, environmental, and social aspects, major conclusions were summarized, and future research directions were identified. The dissertation builds a basis for an innovative ARP-enabled on-site IX regeneration approach to PFAS pollution in drinking water treatment. The resin adsorption capacity can be substantially recovered, accompanied by the PFAS degradation and the production of a small volume of easily managed regenerant waste.

Keywords: Per- and polyfluoroalkyl substances (PFAS), Perfluorooctanoic acid (PFOA),

Advanced reduction processes (ARPs), Hydrated electron (e_{aq}^-), Ion-exchange resins, Resin regeneration

Acknowledgements

Many people have played a vital role in the development of this work. First and foremost, I am forever thankful to my advisor, Dr. Yang Deng, for his never-ending guidance and support throughout my PhD. He has always been a strong support for me and has given me the freedom to pursue anything I want. Only with such a free environment can I produce any good work. This dissertation would not have been possible without him – he was the best advisor that I could ever have asked for. I am certain that the experiences gained under his mentorship will serve me well in all my future endeavors.

I would also like to thank my fantastic committee members, Dr. Huan Feng, Dr. Jinshan Gao, and Dr. Mengyan Li, for their feedback and support during this dissertation study. I am grateful to have had them as mentors and role models.

Many thanks must go to Dr. Mark Chopping, Doctoral Program Director, Environmental Science and Management PhD program at Montclair State University (MSU), and Dr. Greg Pope, former Department Chair of Earth and Environmental Studies (EAES) at MSU, for your support and cooperation.

My sincerest gratitude goes to Dr. Xiaona Li, Dr. Laying Wu, and Dr. Kevin Olsen for their professional guidance on instrumental analysis. They are knowledgeable and happy to help me at any time. The experimental part of this dissertation would not have been accomplished without their support and dedication.

I would also like to thank all my present and past laboratory mates, Qiufeng Lin, Dr. Lei Zheng, Lisitai Yang, Dr. Zepei Tang, Ali Albalgane, Dr. Panpan Gao, and Dr. Hanieh Soleimanifar, who provided a supportive, collaborative, and exciting lab environment making these past five years of my PhD life a joyful ride. I am so lucky to meet you all in my life.

At MSU, I greatly appreciate my friends and classmates, Jing Nie, Linan Zhang, Woohee Kim, Sana Mirza, Archana Prasad, Oyindamola Fadipe, Dr. Xu Du, and Tina Wu. They made my stay at MSU easy, comfortable, and enjoyable, which was significant to overcome the difficulties of my PhD life. I will never forget our friendship.

I would like to convey my heartiest gratitude to my friends, Minghan Chi, Dr. Chengjun Quan, Quanrun Chen, Yulin Meng, Chongyang Ma, Joseph Li, Bin Li, Dr. Cong Luo, Kuinan Jin, Yan Tian, Weijie Piao, Mengtong Sun, and Yuejia Wang, who are not from MSU. They always encourage me when I am inclined to give up. I still remember those days and nights when we chatted and drank together. My PhD life would be much less awesome without them.

I would like to thank the funding and financial support from Doctoral Assistantship at MSU, Sokol Institute Fellowship, New Jersey Water Resources Research Institute (NJWRRI), American Water Works Association – New Jersey (AWWA-NJ), New Jersey Licensed Site Remediation Professionals Association (LSRPA), and New Jersey Water Environment Association (NJWEA).

Lastly, I owe my greatest gratitude to my wonderful family. My parents, Hongyan Jin and Dr. Songbiao Cui, have sacrificed a lot to help me achieve my dreams, and have always provided me with their unconditional love and support throughout my life. I am the luckiest son in the world. My lovely wife, Liling Piao, has always supported me as my best friend. She has been bearing my impatience and naiveness with her incredible patience and tolerance and is willing to bet on a man who wants to explore new things. I am certain that I am the luckiest husband in the world. Words are not enough to express my love and gratitude for them.

Dedication

*To my parents Hongyan and Songbiao, who gave me my life and strength,
to my friends who accompanied me through the last 29 years
and to Liling, who completed my soul.*

Table of Contents

Abstract	iv
Acknowledgements	viii
Dedication.....	x
List of Tables	xv
List of Figures.....	xvi
List of Abbreviations	xxiii
Chapter 1 Introduction and Objectives	1
1.1 Background and Problem Statement.....	1
1.1.1 An Overview of Per- and Polyfluoroalkyl Substances	1
1.1.2 Occurrence of PFAS in the Environment	4
1.1.3 Health Effects and Regulations.....	6
1.1.4 Challenges of PFAS Treatment in Drinking Water	7
1.1.5 Current Status of PFAS Treatment in Water	9
1.2 Rationales.....	29
1.3 Objectives and Hypothesis.....	30
References	33
Chapter 2 Critical Review of ARPs for PFAS Destruction	46
2.1 Introduction and Objectives	46
2.2 Hydrated Electrons and Their Generation for Destruction of PFAS	47
2.2.1 UV/sulfite	48
2.2.2 UV/iodide	50
2.2.3 UV/others.....	52

2.3 Mechanisms of PFAS Destruction	54
2.3.1 PFOA.....	55
2.3.2 PFOS.....	61
2.3.3 Other PFAS.....	64
2.4 Factors Affecting ARP Destruction of PFAS	70
2.4.1 Solution pH.....	70
2.4.2 Solute Dose	73
2.4.3 DO	74
2.4.4 Water Matrix Constituents.....	75
2.4.5 Temperature	78
2.5 Implication of the Knowledge for Water Industry	79
2.6 Future Research Needs on PFAS Destruction with ARPs.....	81
References	85
Chapter 3 Resin Screening and Technical Feasibility Studies	96
3.1 Introduction and Objectives	96
3.2 Materials and Methods.....	97
3.2.1 Chemical and Reagents	97
3.2.2 Experiments	98
3.2.3 Sample Analyses	101
3.3 Results.....	102
3.4 Discussion	105
3.5 Conclusions	110
References	126

Chapter 4 Hydrated Electron Degradation of PFOA Laden on IRA67 in the Presence of Natural Organic Matter	129
4.1 Introduction and Objectives	129
4.2 Materials and Methods.....	130
4.2.1 Chemical and Reagents	130
4.2.2 Experiments	131
4.2.3 Sample Analyses	137
4.3 Results.....	138
4.4 Discussion	143
4.5 Conclusions	149
References	163
Chapter 5 Mitigation of Co-sorbed NOM on PFOA/NOM-laden Ion Exchange Resins for Enhanced Hydrated Electron-induced Regeneration of Resins.....	167
5.1 Introduction and Objectives	167
5.2 Materials and Methods.....	168
5.2.1 Chemical and Reagents	168
5.2.2 Experiments	169
5.2.3 Sample Analyses	178
5.3 Results.....	179
5.4 Discussion	187
5.5 Conclusions	196
References	225
Chapter 6 Conclusions	228

6.1 Economic Analysis228

6.2 Implications in Environmental Management229

 6.2.1 Implication to the Water Treatment Industry229

 6.2.2 Environmental Benefits231

 6.2.3 Social Benefits234

6.3 Overall Conclusions.....236

6.4 Current Limitations of the Proposed IX Resin Regeneration Method238

6.5 Future Research239

References243

List of Tables

Table 3-1 Properties of eight selected resins used in this chapter.....	112
Table 3-2 Model parameters determined from non-linear regression analyses with the Langmuir isotherm model for PFOA adsorption on fresh resins (i.e., untreated) and fresh resins after e_{aq}^- -driven ARPs for eight selected resins	113
Table 3-3 Model parameters determined from non-linear regression analyses with the Freundlich isotherm model for PFOA adsorption on fresh resins (i.e., untreated) and fresh resins after e_{aq}^- -driven ARPs for eight selected resins	114
Table 3-4 Comparison of main chemical elements on PFOA sorbed fresh resins and PFOA sorbed e_{aq}^- -driven ARP treated resins.....	115

List of Figures

- Figure 1-1** Schematic overview of the classification of identified PFAS families.....32
- Figure 2-1** Proposed major pathways of reductive degradation of PFCAs with e_{aq}^- ($n = 7$ for PFOA) (initially, $n = m+2$; and numbers in parentheses represent the reaction numbers in this chapter).....83
- Figure 2-2** Proposed major pathways of reductive degradation of PFSAAs with e_{aq}^- (initially, $n=8$ for PFOS) ($n=m+2$; and numbers in parentheses represent the reaction numbers in this chapter)84
- Figure 3-1** The closed thermostatic cylindrical quartz photo-reactor for the UV/SO₃²⁻ treatment116
- Figure 3-2** Cyclic selected resin adsorption experiment - cumulative PFOA adsorption at different cycles (Experimental condition: initial pH = 3.0; resin dosage = 1.0 g/L; initial PFOA concentration = 200 mg/L; reaction volume = 500 mL; reaction time = 24 hours).117
- Figure 3-3** Measured and modeled adsorption isotherm data of PFOA on the fresh resins (i.e., untreated) and fresh resin after e_{aq}^- -driven ARPs (the scattered symbols, scattered lines, and solid lines represent measured, Langmuir modeled and Freundlich modeled data, respectively); a) IRA67; b) IRA96; c) IRA400; d) IRA900; e) IRA910; f) IRA958; g) XAD7HP; h) XAD4. (Experimental condition: initial pH = 7.0; resin dosage = 0.25 g/L; initial PFOA = 0.12 to 1.50 mmol/L; reaction volume = 40 mL; adsorption time = 24 hours)119
- Figure 3-4** SEM images (i.e., morphology) of 1) PFOA sorbed fresh resins and 2) PFOA sorbed e_{aq}^- -driven ARP treated resins: (a) IRA67; (b) IRA96; (c) IRA400; (d) IRA900; (e) IRA910; (f) IRA958; (g) XAD7HP; and (h) XAD4; (Experimental condition: initial pH = 10.0; resin

dosage = 0.2 g/L; sulfite dose = 10 mM; reaction volume = 500 mL; reaction time = 6 hours) 122

Figure 3-5 Residual concentrations of sulfate and dithionate in solution after ARP treatment of fresh resins (Experimental condition: initial pH = 10.0; Na₂SO₃ dose = 10 mM; resin dosage = 0.2 g/L (no resins in Control test); reaction volume = 1 L; reaction time = 6 hours) 123

Figure 3-6 IRA67 regeneration experiments under different operating conditions: 1) left Y axis - DOC released into regenerant; 2) right Y axis - F- released into the regenerant (Experimental condition: initial pH = 7.0 or 10.0; resin dosage = 0.2 g/L; reaction volume = 500 mL; reaction time = 6 or 12 hours)..... 124

Figure 3-7 IRA67 re-adsorption experiments under different operating conditions (Experimental condition: initial pH = 7.0; initial PFOA = 200 mg/L; resin dosage = 0.2 g/L; reaction volume = 500 mL; adsorption time = 24 hours) 125

Figure 4-1 Schematic overview of the cyclic adsorption-regeneration test using UV/SO₃²⁻ as an on-site PFOA/NOM-laden IRA67 regeneration method..... 152

Figure 4-2 Efficiencies of PFOA extracted from PFOA-preloaded resins in different extraction solutions (Experimental condition: PFOA preloaded resins = 13.25 μg/g, 1 g/L resins, pH 10.0, 1 L solution, and 24 hours) 153

Figure 4-3 Fate of PFOA and NOM in different phases over the UV/SO₃²⁻ ARP treatment of PFOA and NOM-preloaded IRA67 (Experimental condition: 1.0 L solution at pH 10.0, 1.0 g/L resins, and 5.0 mM SO₃²⁻) 154

Figure 4-4 Desorbed PFOA in the sulfite solution in the presence of SO₃²⁻ (Experimental condition: pH 10.0, 1 L SO₃²⁻ solution, resin dose = 1.0 g/L, and 13.25 μg/g PFOA on the resin before dosed to the solution) 155

- Figure 4-5** PFOA degradation in different phases over the UV/SO₃²⁻ treatment of PFOA and NOM-preloaded IRA67 (Experimental condition: 1.0 L solution at pH 10.0, 1.0 g/L resins, and 0.0-5.0 mM SO₃²⁻) 156
- Figure 4-6** PFOA and NOM adsorbed on IRA67 after each adsorption phase during six cyclic adsorption – regeneration tests: (a) PFOA adsorbed; and (b) NOM adsorbed (Experimental condition: no regeneration: no UV/SO₃²⁻ regeneration phase in each cycle; ARP treatment: UV/SO₃²⁻ used in the regeneration phase in each cycle, [SO₃²⁻] = 5.0 or 25.0 mM) 157
- Figure 4-7** Residual PFOA on WBA exchange resins and PFOA desorbed in solution under different experimental conditions (Experimental conditions: after addition of PFOA and NOM preloaded resins in pH 10.0 solution, the solutions were collected and then treated again by UV/SO₃²⁻ at 0.0-3.0 hrs. Then the collected resins were added to the UV/SO₃²⁻ treated solutions for the PFOA desorption tests. Reaction volume = 1.0 L; resin dose = 1.0 g/L; no oxygen during the UV/SO₃²⁻ treatment or desorption tests)..... 158
- Figure 4-8** Residual UV₂₅₄ absorbance, SUVA, and DOC in the NOM-simulated natural water at different experimental conditions (Experimental condition: Untreated: NOM-simulated natural water; UV only; pH 10.0: the control for ARP; pH 10.0; 1.0 mM sulfite; pH 10.0; UV irradiation time = 40 mins)..... 159
- Figure 4-9** The contents of carboxyl and phenolic functional groups in the NOM-simulated natural water at different experimental conditions (Experimental condition: Untreated: NOM-simulated natural water; UV only; pH 10.0: the control for ARP; 1.0 mM sulfite; pH 10.0, and UV irradiation duration = 40 mins)..... 160
- Figure 4-10** Comparison of SEM images of resins at three different conditions: a) fresh IRA67, b) IRA67 with UV irradiation only, and c) IRA67 with ARP treatment using 5 mM sulfite

(Experimental condition: reaction volume = 1.0 L; solution pH = 10.0; UV irradiation time = 3.0 hours).....	161
Figure 4-11 UV absorbance scan of IRA67 resins in water in a 1-cm quartz cell (wavelength = 200 – 400 nm).....	162
Figure 5-1 Visualization of alum coagulation process for simulated natural water: (a) mixing during coagulation; (b) collection of the supernatant; (c) membrane filtration; (d) simulated natural water before (left) and after (right) alum coagulation (alum 60.0 mg/L; pH 6.0)...	202
Figure 5-2 Visualization of (a) MW fractionation with a UF stirred cell; (b) SPE for the separation of FA and HPI isolates.....	203
Figure 5-3 Visualization of (a) NOM and PFOA loading tests on IRA67 in PFOA-containing pre-coagulated water using a jar tester; and (b) desorption of NOM and PFOA on IRA67 from multiple loading tests at different pH solutions using a shaker.....	204
Figure 5-4 Visualization of fresh IRA67 (left), IRA67 with no regeneration after six cyclic adsorption-regeneration tests (middle), and ARP regenerated IRA67 after six cyclic adsorption-regeneration tests (right)	205
Figure 5-5 Effect of coagulation pH and chemical dose: effect of pH (4.0 to 9.0) on (a) residual DOC and (b) residual UV ₂₅₄ absorbance of simulated natural water during alum coagulation (Experimental condition: alum dose = 40.0 mg/L; 500 mL); and effect of alum dose (20.0 to 120.0 mg/L) on (c) residual DOC and (d) residual UV ₂₅₄ absorbance in simulated natural water during alum coagulation (Experimental condition: pH = 6.0; 500 mL)	206
Figure 5-6 Residual DOC after the UV/H ₂ O ₂ -based AOP treatment of pre-coagulated water (Experimental condition: H ₂ O ₂ = 15.0 mg/L; initial pH = 7.5; UV irradiation time = 1 hour; reaction volume = 200 mL)	207

- Figure 5-7** Residual DOC in diluted simulated natural water and pre-coagulated water before and after IRA67 adsorption (Experimental condition: IRA67 dosage = 5.0 g/L; initial pH = 7.5; adsorption time = 24 hours; volume = 1.0 L)208
- Figure 5-8** Molecular size distribution of (a) residual DOC and (b) residual UV₂₅₄ absorbance as well as hydrophobic/hydrophilic fraction of (c) residual DOC and (d) residual UV₂₅₄ absorbance in simulated natural water, pre-coagulated water, and pre-coagulated water after resin (5.0 g/L) adsorption209
- Figure 5-9** Measured and modeled adsorption isotherms of PFOA in different PFOA-containing water systems (Experimental condition: initial pH = 7.5; reaction volume = 0.1 L; IRA67 dosage = 0.1 to 2.0 g/L; adsorption time = 24 hours; scattered symbols, scattered lines, and solid lines represent measured, Freundlich modeled, and Langmuir modeled data, respectively)210
- Figure 5-10** Effect of pH on the residual NOM and PFOA after the desorption from IRA67 (Experimental condition: (a) 20.0 µg PFOA/g IRA67; (b) 100.0 µg PFOA/g IRA67; (c, e, and g) 13.25 µg PFOA and 3.86 mg DOC/g IRA67; (d, f, and h) 21.12 µg PFOA and 11.55 mg DOC/g IRA67; volume = 0.1 L; IRA67 dosage = 1.0 g/L; desorption hour = 24 hours)212
- Figure 5-11** Fate of NOM and PFOA in PFOA-containing pre-coagulated water after each loading cycle during ten cyclic NOM and PFOA loading tests: (a) residual DOC in solution after each loading test and accumulative NOM adsorbed; and (b) residual PFOA in solution after each loading test and accumulative PFOA adsorbed (Experimental condition: pH = 7.5; volume = 0.2 L; IRA67 dosage = 0.5 g/L; reaction hour = 30 mins).....213

- Figure 5-12** Effect of pH on the fate of sorbed NOM and PFOA on IRA67 after ten cyclic loading tests: (a) NOM in solution (b) PFOA in solution (Experimental condition: volume = 0.1 L; IRA67 dosage = 1.0 g/L; desorption hour = 24 hours)214
- Figure 5-13** PFOA degradation at different sulfite dosages during the UV/SO₃²⁻ treatment of IRA67 from ten cyclic NOM and PFOA loading tests (Experimental condition: pH = 10.0; volume = 0.1 L; IRA67 dosage = 1.0 g/L; reaction hour = 3 hours)215
- Figure 5-14** Kinetic tests of the UV/SO₃²⁻ ARP treatment of IRA67 from ten cyclic NOM and PFOA loading tests: (a) PFOA decomposition and (b) sulfite decay (Experimental condition: pH = 10.0; volume = 0.1 L; IRA67 dosage = 1.0 g/L; reaction hour = 0 to 3 hours; sulfite dosage = 20.0 mM); symbols and lines represent measured data and the fit of the hypothetical reaction model, respectively.....216
- Figure 5-15** Ln C_n/C₀ vs. t for PFOA decomposition during the UV/SO₃²⁻ ARP treatment of IRA67 from ten cyclic NOM and PFOA loading tests (Experimental condition: pH = 10.0; volume = 0.1 L; IRA67 dosage = 1.0 g/L; reaction hour = 0 to 3 hours; sulfite dosage = 20.0 mM); symbols and lines represent measured data and non-linear regression modeled data, respectively)217
- Figure 5-16** NOM and PFOA during six cyclic adsorption-regeneration tests: (a) residual NOM in solution after each loading test; (b) accumulative NOM adsorbed; (c) residual PFOA in solution after each loading test; (d) accumulative NOM adsorbed; (e) DOC in solution before and after ARP regeneration (Experimental condition: adsorption phase: pH = 7.5; volume = 0.2 L; IRA67 dosage = 0.5 g/L; reaction hour = 30 mins; Control: no UV/SO₃²⁻ regeneration in each cycle; ARP treatment: pH = 10.0; volume = 0.1 L; IRA67 dosage = 1.0 g/L; reaction hour = 3 hours; sulfite dosage = 20.0 mM).....220

- Figure 5-17** Comparison of SEM images of three resins: a) fresh IRA67, b) IRA67 with no ARP regeneration after six cyclic adsorption-regeneration tests and c) ARP regenerated IRA67 after six cyclic adsorption-regeneration tests.....221
- Figure 5-18** Comparison of EDS spectra of three resins: a) fresh IRA67, b) IRA67 with no ARP regeneration after six cyclic adsorption-regeneration tests and c) ARP regenerated IRA67 after six cyclic adsorption-regeneration tests.....223
- Figure 5-19** Comparison of IEC of fresh IRA67, IRA67 with no regeneration after six cyclic adsorption-regeneration tests, and ARP regenerated IRA67 after six cyclic adsorption-regeneration tests.....224

List of Abbreviations

Activated Carbon (AC)

Aqueous Film-forming Form (AFFF)

Advanced Oxidation Processes (AOPs)

Aminopolycarboxylic Acids (APCAs)

Advanced Reduction Processes (ARPs)

Bromide (Br)

Boron-doped Diamond (BDD)

Bond Dissociation Energy (BDE)

Carbon (C)

Chlorine (Cl)

Comprehensive Environmental Response, Compensation, and Liability Act (CERCLA)

Critical Micelle Concentration (CMC)

Carbon Nanotubes (CNs)

Charge-transfer-to-solvent (CTTS)

Disinfection Byproducts (DBPs)

Difluoroacetic Acid (DFA)

Density Functional Theory (DFT)

Decarboxylation-hydroxylation-elimination-hydrolysis (DHEH)

Deionized (DI)

Dissolved Oxygen (DO)

Dissolved Organic Carbon (DOC)

Diocetyltrimethylammonium (DODMA)

Dissolved Organic Matter (DOM)

Dimensionally Stable Anode (DSA)

Electrochemical Fluorination (ECF)

Electron Donating Groups (EDGs)

Energy Dispersive X-Ray Spectroscopy (EDS)

Electrochemical Oxidation (EO)

Effluent Organic Matter (EfOM)

Environmental Protection Agency (EPA)

Electrospray Ionization (ESI)

Electron Withdrawing Groups (EWGs)

Fluorine (F)

Fluvic Acid (FA)

Fluoropolymer (FPs)

Fluorotelomer Carboxylic Acids (FTCAs)

Granular Activated Carbon (GAC)

Hydrogen (H)

Humic Acid (HA)

Hexadecylpyridinium (HDPY)

Hexadecyltrimethylammonium (HDTMA)

Hydrophilic (HPI)

Hydroperfluorocarboxylates (HPFCAs)

High-performance Liquid Chromatography-triple Quadrupole Mass Spectrometer (HPLC-MS/MS)

Hydrophobic (HPO)

Iodine (I)

Ion-exchange Capacity (IEC)

Ion Exchange (IX)

Life-cycle Analysis (LCA)

Lifetime Health Advisory (LHA)

Lowest Unoccupied Molecular Orbitals (LUMO)

Maximum Contaminant Levels (MCLs)

Monofluoroacetic Acid (MFA)

Montmorillonite (MM)

Mixed Metal Oxide (MMO)

Multiple Reaction Monitoring (MRM)

Molecular Weight (MW)

Nitrogen (N)

Nanofiltration (NF)

New Jersey (NJ)

Nitrilotriacetic Acid (NTA)

Natural Organic Matter (NOM)

Non-thermal Plasma (NTP)

Ozofractionative Catalyzed Reagent Addition (OCRA)

Organisation for Economic Co-operation and Development (OECD)

Operational and Maintenance (O&M)

Overhead and Profit (O&P)

Powdered Activated Carbon (PAC)

Perfluoroalkane Sulfonyl Fluorides (PASFs)

Perfluoroalkyl Acids (PFAAs)

Polyfluoroalkyl Acids (PolyFAAs)

Perfluoroalkyl Iodides (PFAIs)

Per- and Polyfluoroalkyl Substances (PFAS)

Perfluorobutanoic Acid (PFBA)

Perfluorobutane Sulfonates (PFBS)

Perfluoroalkyl Carboxylates (PFCAs)

Perfluoroalkylether Acids (PFEAAs)

Polyfluoroalkylether Acids (PolyFEAAs)

Polyfluoroalkylether Carboxylic Acid (PFECAs)

Polyfluoroalkylether Sulfonic Acid (PFESAs)

Perfluoropentanoic Acid (PFHeA)

Perfluoroheptanoic Acid (PFHpA)

Perluorohexanoic Acid (PFHxA)

Perfluoroalkyl Phosphinic Acids (PFPAAs)

Pentafluoropropionic Acid (PFPrA)

Perfluoropolyethers (PFPEs)

Perfluorononanoic Acid (PFNA)

Perfluorinated Sulfonates (PFSAs)

Reverse Osmosis (RO)

Relative Quasi-stationary Concentration (RQSC)

Strong Acid Cation (SAC)

Surface-active Foam Fractionation (SAFF)

Strong Base Anion (SBA)

Scanning Electron Microscopy (SEM)

Semifluorinated Alkanes (SFAs)

Soil Organic Matter (SOM)

Solid Phase Extraction (SPE)

Suwannee River Natural Organic Matter (SRNOM)

Specific Ultraviolet Absorbance (SUVA)

Total Dissolved Solids (TDS)

Techno-economic Assessment (TEA)

Trimethylphenylammonium (TMPA)

Total Organic Carbon (TOC)

Total Oxidizable Precursors (TOP)

Ultrafiltration (UF)

Ultraviolet (UV)

Vacuum Ultraviolet (VUV)

Weak Acid Cation (WAC)

Weak Base Anion (WBA)

Water Treatment Plants (WTPs)

Chapter 1 Introduction and Objectives

1.1 Background and Problem Statement

1.1.1 An Overview of Per- and Polyfluoroalkyl Substances

Per- and Polyfluoroalkyl Substances (PFAS) represent a family of fluorinated substances comprising at least one fully fluorinated methyl or methylene carbon atom without the attachment to any other atoms (e.g., hydrogen (H), chlorine (Cl), bromine (Br), and iodine (I)). Namely, except that a carbon atom is bonded to a H, Cl, Br, or I atom, any chemical compound with at least a perfluorinated methyl group (-CF₃) or a perfluorinated methylene group (-CF₂-) is considered as a PFAS (OECD, 2021; Z. Wang et al., 2021).

Over the past seven decades, PFAS have been synthesized through different manufacturing processes, among which electrochemical fluorination (ECF) and telomerization are the principal ones to produce compounds containing perfluoroalkyl chains, such as fluorosurfactants and side-chain fluorinated polymers (Buck et al., 2011). Specifically, the ECF technology generates a mixture of odd- and even-number perfluorinated carbon chain lengths of roughly 20% - 30% branched and 70% - 80% linear substances (Buck et al., 2011). On the other hand, the telomerization technology principally produces even-numbered, straight carbon chains (Buck et al., 2011; ITRC, 2020). Of note, because of the concerns about potential public health and environmental impacts, the major PFAS manufacturing companies (e.g., 3M) volunteered to phase out long-chain perfluoroalkyl acids (PFAAs) in 2000 (Buck et al., 2011; ITRC, 2020). The long-chain PFAAs encompass perfluorinated carboxylates (PFCAs) with eight or more fluorinated carbons (e.g., perfluorooctanoic acid (PFOA)) and perfluorinated sulfonates (PFSAs) with six or more fully fluorinated carbons (e.g., perfluorooctanesulfonic acid (PFOS)), as well as their salts and precursors (Buck et al., 2011; ITRC, 2020). To accomplish the global reduction in

the yield of products containing long-chain PFAAs, the technologies for substituting or reformulating longer-chain substances with nonfluorinated chemicals or shorter chain perfluoroalkyl or polyfluorinated substances have been developed to synthesize alternatives (e.g., short-chain PFAS) for the long-chain PFAAs (Glüge et al., 2020). Some representative alternative PFAS include HFPO-DA ammonium salt (GenX) in the manufacture of fluoropolymer, perfluorobutane sulfonate (PFBS) in place of PFOS, and 6:2 FTSA in the manufacture of aqueous film-forming foam (AFFF) (Gallen et al., 2018; Wang et al., 2019; Zhang et al., 2020). Generally, the alternatives are considered to be less bio-accumulative and much safer. However, information on the safety of PFAS alternatives remains inadequate (ITRC, 2020).

Over 4,700 PFAS were identified on the global market in 2018 (OECD, 2018). Based on the Report of the Organisation for Economic Co-operation and Development (OECD) in 2021, the PFAS family can be classified into four primary categories, i.e., PFAAs, polyfluoroalkyl acids (PolyFAAs), PFAA precursors, and other PFAS (OECD, 2021), as shown in **Figure 1-1**. PFAAs, including perfluoroalkylether acids (PFEAAs), are non-polymer PFAS with at least one perfluorocarbon moiety directly attached to an acid functional group (Kwarciak-Kozłowska, 2020). PFAAs are of importance because 1) they are highly persistent substances that have been commonly detected in the environment; and 2) they are or have been incorporated into various industrial and consumer goods (Buck et al., 2011). PolyFAAs, including polyfluoroalkylether acids (PolyFEAAs), are also non-polymer PFAS with at least one but not all C atoms attached to F atoms, such as polyfluoroalkylether carboxylic acid (PFECAs) and polyfluoroalkylether sulfonic acid (PFESAs) (OECD, 2021). Because many fluorochemicals can be biotically and abiotically transformed into PFAAs in the environment or biota, they are viewed as the PFAA

precursors. For example, PFAAs can be derived from perfluoroalkenes (C_nF_{2n} , $n>2$) and perfluoroalkane sulfonyl fluorides (PASFs, $C_nF_{2n+1}SO_2F$) (Buck et al., 2011; OECD, 2021).

Lastly, the PFAS that is not categorized into the above-mentioned three groups are referred to as other PFAS. Other PFAS not only contain non-polymeric PFAS (e.g., perfluoroalkanes (C_nF_{2n+2}) and perfluoroalkyl-*tert*-amines ($(C_nF_{2n+1})_3N$) with a limited reactivity, but also comprise polymer PFAS, such as fluoropolymers (FPs) and perfluoropolyethers (PFPEs) (OECD, 2021).

PFAS are globally utilized with different technological and economic advantages (Houde et al., 2011; Xiao, 2017). PFAS benefit from their highly strong bonds (i.e., C-F bond) in nature with a high bond dissociation energy ($115 \text{ kcal mol}^{-1}$) (Bentel, 2020). Moreover, the F atom contains the highest electronegativity of all elements, which enhances the electrostatic interaction and contributes to the total strength of the C-F bond (Epa, 2016). As a consequence of the greatest electronegativity of the F atom (i.e., lone pairs), PFAS are recalcitrant to common interactions (e.g., hydrogen bonding (Epa, 2016; M. Wang et al., 2021), resonance (Falzone et al., 2020), and conjugation (Y. Wang et al., 2021)). These lessened interactions dramatically decrease the surface free energy of PFAS (Houde et al., 2011). Because of their low surface free energy, PFAS are uniquely resistant to heat, water, oil, and stains, in addition to reducing friction (Cui et al., 2020). Therefore, PFAS have been historically and presently utilized in a broad range of products (e.g., paper, food packaging, clothing, cookware, carpet, textile, waxes, wipers, paints, medical products, mattresses, personal care products, and firefighting materials) and in many industries (e.g., semiconductor, metal plating and etching, photolithography, and building and construction) (Cui et al., 2020; ITRC, 2020). Accordingly, the PFAS industry claims that manufacturing PFAS to meet the demands of consumer goods and industrial applications brings value at \$2 billion a year in the U.S. fluoropolymer segment (Cordner et al., 2021; Wood, 2020).

1.1.2 Occurrence of PFAS in the Environment

A wide-ranging application of PFAS to different industrial and consumer goods has led to the substantial release of these emerging anthropogenic chemicals into the environment (Hekster et al., 2003; Li et al., 2020; Lu et al., 2021; Xu et al., 2021). Primary sources of PFAS in the environment include: 1) industrial facilities that manufacture, process, and/or apply PFAS chemicals; 2) locations where F-containing firefighting foams are released, stored, and used; 3) waste management facilities (e.g., landfills); and 4) the areas of biosolids application and production as well as wastewater management facilities (ITRC, 2021). Of interest, PFAS exhibit a high mobility in the aquatic environment (e.g., groundwater and surface water) (Hatton et al., 2018), strong partitioning behavior (e.g., liquid/solid and gas/liquid interface) (Munoz et al., 2019), and strong resistance to the biotic and abiotic transformation of perfluorinated moieties (i.e., the carbon center possessing only C-C or C-F bonds) in the environment (Bentel, 2020). Thus, various PFAS have been ubiquitously identified in most environmental media (e.g., air, soil, and water) (Evich et al., 2022). First, the atmospheric transport of PFAS plays a critical role in global PFAS distribution, as evidenced by the detection of PFAS in remote regions, such as the Arctic (Evich et al., 2022). Some PFAS have also been founded in the ambient air adjacent to the aforementioned four major emission areas due to the atmospheric release (Evich et al., 2022). Meanwhile, these anthropogenic chemicals have been detected in air and dust in indoor areas (e.g., homes and offices) (Barber et al., 2007). Studies showed that certain PFAS might have higher concentrations in indoor air than in an outdoor environment because of their emission from different indoor sources (e.g., carpet, clothing, food packaging, and personal care products) (Fraser et al., 2012; Fromme et al., 2015; ITRC, 2021).

Second, PFAS are identified in soil and sediment because these compounds from different sources can preserve soil and sediment via sorption, partitioning, and other complex reactions (Abunada et al., 2020). Specifically, atmospheric transportation and wet/dry deposition of PFAS occur globally, resulting in the PFAS pollution of soil and sediment (ITRC, 2021). Direct application of PFAS-containing products (e.g., AFFF), industrial discharge (e.g., pesticides and uncontrolled spills), or soil amendment with PFAS-affected media (e.g., biosolids, wastewater, and landfill leachate) are the potential PFAS pollution sources for soil (Lee et al., 2014). Furthermore, the presence of PFAS in sediments is likely ascribed to the PFAS discharge to surface water (ITRC, 2021).

Third, PFAS have been frequently observed in different water matrixes, such as surface freshwater, drinking water, groundwater, and landfill leachate (Albargane et al., 2022; Cui & Deng, 2022; Cui et al., 2020; Epa, 2016; ITRC, 2021). Of note, the water system is especially susceptible to PFAS contamination owing to its capability to act as a sink (González-Gaya et al., 2019; Yamashita et al., 2008). For example, PFAS may be directly discharged from primary pollution sources into water systems or enter into the aquatic environment through atmospheric transport and wet/dry deposition (Davis et al., 2007; Evich et al., 2022). Concentrations of PFAS in polluted water have been quantitatively correlated with neighboring fluorochemical manufacturing industries, AFFF-certified airports, wastewater treatment facilities, and military fire training areas (Hu et al., 2016). Different factors may influence their concentrations in water. For example, PFAS-containing soil and sediment can release PFAS into adjoining water bodies through leaching or percolation (ITRC, 2021). Sorption of PFAS to suspended microplastics, clays, or other particles can contribute to PFAS in surface water (Vickers, 2017). And PFAS-

containing stormwater runoff as a non-point source can widely contaminate receiving water bodies (Wilkinson et al., 2017).

1.1.3 Health Effects and Regulations

Humans are readily exposed to PFAS chemicals in their daily lives due to PFAS's prevalence, persistence, and mobility in the environment (Cui et al., 2020). Among different pathways for human exposure to PFAS, the path of dietary exposure via drinking water and polluted food sources (e.g., seafood and other animal products) is the greatest (Abunada et al., 2020; Chain et al., 2018; Evich et al., 2022; Lin et al., 2021; Sunderland et al., 2019). Human exposure to PFAS is validated by the detectable concentration of identified PFAS chemicals in the blood serum of almost all populations in developed countries (Fenton et al., 2021). Certain PFAS have been demonstrated to bioaccumulate, bind to blood proteins, and have long half-lives in humans (Cui et al., 2020). The unwanted exposure is connected to cancer, obesity, fertility reduction, enhanced cholesterol, immune suppression, and hormone interference (Bonato et al., 2020; Cui et al., 2020; Fenton et al., 2021; Sunderland et al., 2019). Although adverse health effects may be associated with exposure to specific PFAS at high concentrations, the knowledge concerning how different levels of exposure to various PFAS chemicals can result in different health outcomes remains limited (Abunada et al., 2020).

As the possible adverse effects of PFAS on human health arise, the guidelines and regulations regarding PFAS guidelines have emerged since the early 2000s (Brennan et al., 2021). To mitigate the human and ecological impacts of PFAS, different international treaties were signed in the early 2000s, such as the bans on the production of certain long-chain PFAS (Brennan et al., 2021). Meanwhile, the US guidelines and regulations on PFAS are implemented at national and state levels (Brennan et al., 2021). At the US national level, the US

Environmental Protection Agency (EPA) has issued lifetime health advisory (LHA) levels for perfluorooctanoic acid (PFOA) and perfluorooctanesulfonic acid (PFOS) at 0.004 and 0.02 ng/L, respectively, in 2022 (USEPA, 2022). Nevertheless, US EPA has not finished the regulatory processes to set maximum contaminant levels (MCLs) for PFOA and PFOS or designate PFOA and PFOS as hazardous substances under the Comprehensive Environmental Response, Compensation, and Liability Act (CERCLA) (Brennan et al., 2021). At the US state level, an increasing number of states executed their policies and regulations to alleviate PFAS contamination and diminish human exposure. Specifically, nine states in the US advanced drinking water standards or guidance values for PFOA and PFOS in 2020 due to the absence of mandatory federal drinking water standards for PFAS. The states' standards and guidance values are stricter than those released by the US EPA (Post, 2021). For example, the guidelines for PFAS (e.g., perfluorononanoic acid (PFNA)) other than PFOA and PFOS were developed in some states (Post, 2021). Additionally, if the concentration of PFAS in the drinking water system is greater than 20 ng/L (i.e., the health advisory level set by the State of Vermont), the public water systems are required to release a "do not drink" notification to the water consumers until the PFAS level is below the threshold (Brennan et al., 2021).

1.1.4 Challenges of PFAS Treatment in Drinking Water

The pursuit of public health and the potential regulatory pressure require the water industry to stay current and proactive in sufficiently eliminating PFAS in a water supply system. However, PFAS are challenging the water treatment industry, particularly the drinking water treatment, primarily for the following reasons. First, PFAS present at the trace levels (Anderson et al., 2016) are much less abundant than water matrix constituents (e.g., natural organic matter (NOM) at concentrations on the order of several mg/L) (Cui et al., 2018; Zheng et al., 2020),

making an effective abatement of PFAS extremely difficult. For example, a vast majority of active species in chemical oxidative or reductive processes (e.g., sulfate radical ($\text{SO}_4^{\cdot-}$ generated from persulfate based advanced oxidation processes (AOPs))) or active sorption sites in an adsorption or ion exchange process can be consumed by NOM, resulting in a highly low PFAS treatment efficiency. Second, the mandatory or non-enforceable PFAS regulations set incredibly high standards regarding the PFAS levels in drinking water. For example, New Jersey (NJ) was the first state in the US to develop an enforceable drinking water standard for PFAS in 2018. In 2020, the revised NJ MCL was set for PFOA (14 ng/L), PFOS (13 ng/L), and PFNA (13 ng/L) (NJDEP, 2021). Third, species of PFAS chemicals are a key factor affecting the PFAS treatment performance. Although the knowledge in removing long-chain PFAS has been dramatically advanced, the efficient removal or degradation of short-chain PFAS than long-chain PFAS remains challenging (Li et al., 2020). Fourth, as legacy PFAS with multiple strong C-F bonds are highly resistant to chemical, biological, and thermal degradation processes, conventional water treatment technologies, which are developed for effective removal of particulates and pathogens in raw water, poorly tackle the PFAS issues (Bentel, 2020; Shahsavari et al., 2021). Fifth, the prevalence of PFAS in water sources confronts many water treatment plants (WTPs) with PFAS pollution. One or more PFAAs are identified in 4% of the reporting public water systems (ITRC, 2021; USEPA, 2017a), considerably increasing the technical and financial difficulties in comprehensive PFAS monitoring and remediation efforts. Widespread PFAS particularly challenge small drinking water systems (more than 97% of 156,000 U.S. public water systems) that mostly suffer from lack of expertise to choose, operate, and maintain their systems, lack of sufficient financial resources, limited operation for residual disposal, and insufficient managerial support (USEPA, 2017b).

1.1.5 Current Status of PFAS Treatment in Water

Because of the aforementioned challenges, current efforts in the efficient removal of PFAS in drinking water are made in two aspects: 1) assessment and enhancement of established treatment technologies (e.g., activated carbon (AC), ion exchange (IX), and reverse osmosis (RO)); and 2) development of emerging treatment methods. Generally, the PFAS treatment options, regardless of established and burgeoning ones, can be divided into two categories, i.e., non-destruction and destruction technologies, which are discussed below. Information regarding different PFAS treatment technologies is available in many recent critical review articles (Ahmed et al., 2020; Crone et al., 2019; Kazwini et al., 2022; Kucharzyk et al., 2017; Verma et al., 2021; Wanninayake, 2021). Here some of these technologies are overviewed in terms of their technical specification, mechanism, treatment performance, and technical assessments.

1.1.5.1 Non-destruction Technologies. The non-destruction technologies covered in this chapter include adsorption enabled by various materials (e.g., AC, IX resins, biomaterial, minerals, and nanomaterials), membrane separation (e.g., nanofiltration (NF) and RO), and foam fractionation and ozofractionation.

1.1.5.1.1 Adsorption. AC adsorption. AC is a carbonaceous medium having a highly porous structure primarily composed of carbon atoms (Chada et al., 2012). Carbon-based materials (e.g., coconut shell, peat, wood, lignite coal, and olive pits) serving as AC feedstocks can be chemically or thermally activated to synthesize AC (Soo et al., 2013; TIGG, 2019). The manufactured AC has a high specific surface area. Their pore networks are channels formed within a rigid skeleton of disordered layers of carbon atoms (HAYCARB, 2019). The intrinsic pore network in the AC lattice structure provides the dominant sites where impurities are immobilized from gaseous and liquid media (HAYCARB, 2019).

The reactivity of AC for water treatment applications depends heavily on its physical and chemical properties. Pore size distribution quantifies the available pore volumes of AC over three pore size regions (i.e., micropore, mesopore, and macropore). Sorbate molecules tend to adsorb to the pores slightly greater than the sorbate sizes. Therefore, it is essential to examine whether the pore size of AC matches the molecule size of a target contaminant (TIGG, 2019). Moreover, other key properties encompass specific surface area, product density, mesh size, and ash content. For example, the specific surface area represents the availability of the AC surface on a given mass, typically ranging from 500 to 1500 m²/g. For a specific adsorbate, an enhanced internal surface area favors its removal efficiency (HAYCARB, 2019). Product density is the apparent density of AC, indicating the AC density at the maximum packing efficiency (TIGG, 2019). Mesh size measures the size range of a granular particle product. It is reported as a range of sieve openings (HAYCARB, 2019). Additionally, an ash content indicates the non-carbon fraction in an AC material. It differs from one base material to another (HAYCARB, 2019).

Adsorption processes can occur via two routes, i.e., physical adsorption and chemisorption. In a physical adsorption process, adsorbates in water can be adhered to the AC surface due to the differences in adsorbate concentrations between water and the carbon pores through weak force of attraction - Van Der Waals Forces or London Dispersion Forces (HAYCARB, 2019; TIGG, 2019). In contrast, the chemisorption process is enabled by a stronger force of attraction involved in forming chemical bonds between AC and target adsorbates (HAYCARB, 2019). For example, chlorine can be eliminated from water because of the chemisorption process between chlorine and AC to generate chloride ions.

AC is one of the most studied treatment processes for the removal of PFAS in drinking water (Du et al., 2014). US EPA has approved the commercial application of this established

technology (USEPA, 2018). AC was reported to achieve an adsorption efficiency of over 99% (Söregård et al., 2020). The commercial AC types utilized for PFAS removal include granular activated carbon (GAC) and powdered activated carbon (PAC) (USEPA, 2018). Compared to GAC, PAC gained much attention due to the better PFAS removal capability. For example, the PFAS adsorption capacity of PAC (~560 mg PFOS/g PAC and 290-500 mg PFOA/g PAC) was reported to be greater than that of GAC (71.6-290 mg PFOS/g GAC and 41.3-120 mg PFOA/g GAC) (Wanninayake, 2021; Zhang et al., 2019). Hydrophobic (HPO) and electrostatic interactions are viewed as two major mechanisms for AC adsorption of PFAS (Ateia et al., 2019). The legacy PFAS have relatively lower pK_a values (e.g., PFOA, $pK_a = 3.8$; PFOS, $pK_a = 3.27$) and a positive surface charge at $pH < 7.5$ ($pH_{pzc} = 7.5$) (Yu et al., 2009). Thus, the electrostatic interaction may occur between PFAS and ACs. Meanwhile, because of the presence of a HPO perfluorinated chain in PFOS and PFOA, HPO AC can also capture PFAS through HPO interactions (Yu et al., 2009).

Once AC becomes exhausted, PFAS-laden AC needs to be regenerated to alleviate a significant economic burden associated with AC consumption. Thermal regeneration is the most common method to regenerate the PFAS-spent AC, in which the contaminants (e.g., PFAS) sorbed on AC are thermally desorbed or degraded for recovering the AC adsorption capacity (Sonmez Baghirzade et al., 2021).

Benefits of AC for the PFAS treatment are clear. The water industry can easily accept the mature water treatment technology. The treatment can be readily incorporated into existing water treatment process trains with a small footprint, providing a viable PFAS removal (AWWA, 2020). However, the AC treatment for PFAS removal may suffer from different technical and economic restrictions. First, AC shows a relatively low adsorption capacity for short-chain PFAS

and their precursors (Ross et al., 2018). Second, improper disposal, transportation, and storage of PFAS-spent AC may introduce recalcitrant PFAS into the water system. Third, the regeneration or periodic replacement of AC is less economically feasible due to its elevated operational and maintenance costs (e.g., consumption of substantial energy). Fourth, the regeneration of PFAS-spent AC at a high temperature can accidentally alter the surface chemistry of AC and compromise its pore structure, resulting in a gradual decline in the adsorption capacity over the repeated thermal regeneration (Sonmez Baghirzade et al., 2021). Fifth, common water matrix constituents can co-adsorb to AC, thereby significantly reducing the number of active sites available for PFAS.

IX. IX is a reversible interchange of one kind of ion existing in an insoluble solid with another of like charge present in a solution neighboring the solid with the reaction being used (Helfferich, 1995). IX resin is a physical medium that enables IX reactions (Reichenberg, 1953). The resin encompasses organic polymers as a network of hydrocarbons across which “functional groups” of either cations or anions are affixed to provide IX sites to attract ions of an opposing charge (Pepper et al., 1952). Most IX resins are tiny, porous polystyrene or polyacrylic microbeads having a spherical shape with a diameter of 0.5 - 2.5 mm (SAMCO, 2017). The IX resin matrix is generated in a process called polymerization (i.e., cross-linking hydrocarbon chains), which produces a strong, resilient polymer structure with an excellent capacity due to its cross-linking (SAMCO, 2017). In other words, the degree of cross-linking strengthens the internal pore structure of the resin to benefit the internal movement of exchanging ions. The IX resin structure comprises a three-dimensional, cross-link polymer matrix that has covalently bonded functional groups with fixed ionic charges (Crittenden et al., 2012).

The properties of IX resin primarily vary with the polymer matrix, porosity, and functional groups, thus affecting the sorption capacity and rate (Deng et al., 2010). Specifically, the polymer matrix is an essential factor influencing the sorption rate, which can be attributed to the different intraparticle diffusion rates induced by different polymer matrixes (Deng et al., 2010). As aforementioned, polystyrene and polyacrylic polymer matrix prevail in the current IX application market. A polystyrene matrix tends to be more HPO, while a polyacrylic matrix tends to be more hydrophilic (HPI) (Crittenden et al., 2012). The resin polymer plays a critical role in binding functional groups serving as the IX sites throughout the matrix. Resins are divided into gel-type and microporous (or macroreticular)-type (Crittenden et al., 2012). The separation capability of the IX resin is ascribed to the species and surface density of these functional groups. These functional groups on one IX resin might be significantly different between various IX resins (Topp & Pepper, 1949).

It has been demonstrated that commercial resins, especially IX (with functional groups) and non-ionic (without functional groups) resins, are capable of removing PFAS in drinking water (Contea et al., 2015; Deng et al., 2010; Garg et al., 2021; Senevirathna, 2010; Wanninayake, 2021; Yu et al., 2009). Because IX resins (210-2575 mg PFOS/g resin and 1206 mg PFOA/g resin) can effectively adsorb PFAS in solution through ion-exchange processes, they have higher adsorption capacities than non-ionic resins (37-41 mg PFOS/g resin and 38-46 mg PFOA/g resin) (Chularueangaksorn et al., 2014; Contea et al., 2015; Garg et al., 2021). IX resins are classified into cationic and anionic (USEPA, 2018). The most frequently used IX resins include strong acid cation (SAC) exchange resins, weak acid cation (WAC) exchange resins, strong base anion (SBA) exchange resins, weak base anion (WBA) exchange resins, and chelating resins (SAMCO, 2017). Because PFAS (i.e., lower pK_a) possess negative charges in

water, anion-exchange resins rather than cation-exchange resins are preferentially utilized for better PFAS removal (Garg et al., 2021; Maimaiti et al., 2018; McCleaf et al., 2017; Wanninayake, 2021; Zaggia et al., 2016). The adsorption capacity of anion exchange resins for PFAS ranges from 1 - 6000 μmol PFAS/g resin, with an average kinetic uptake capacity of \sim 1350 μmol PFAS/g resin and isotherm uptake capacity of 1550 μmol PFAS/g resin (Dixit et al., 2021). While WBA exchange resins have widely been proven for the effective removal of PFAS in drinking water, SBA resins, particularly PFAS-selective resins, can be applied (AWWA, 2020).

The adsorption mechanisms of IX removal of PFAS are ascribed to HPO interaction, IX, PFAS self-aggregation, and hydrogen bonding (Boyer et al., 2021; Dixit et al., 2021; Du et al., 2014). First, HPO interaction can be involved in the sorption process because the HPO IX polymer backbones or cross-links tend to capture a PFOA or PFOS due to its HPO perfluorinated chain (Dixit et al., 2021). The role of IX in the PFAS removal was demonstrated in previous studies. Second, when the resins with chloride as exchange anions to adsorb PFOS were used, the ratios of PFOS adsorbed to chloride released from anion-exchange resins were reported to vary from 1.0 to 1.28, indirectly indicating that the anion exchange reactions were involved in the sorption of PFOS on the resins (Deng et al., 2010). Thus, the negatively charged head of the PFAS molecule is attracted to the positively charged IX site on the resin (Boyer et al., 2021). Third, studies showed that admicelle, hemi-micelles, and micelle could be produced via the PFAS self-aggregation of C-F chains in the inner pores of IX resins when substantial PFAS adsorb on the IX resins, particularly the concentration of PFAS on the resin surface is much greater than that in solution (Dixit et al., 2021; Yu et al., 2009). Fourth, another possible PFAS adsorption mechanism is hydrogen bonding (Dixit et al., 2021). For example, PFAS containing

oxygen atoms in their functional head can serve as accepters and attract the IX resins' hydrogen atoms (Lu et al., 2016).

Proper disposal or regeneration of PFAS-laden IX resins is of importance. Waste industry will dispose of non-regenerable or single-use IX resins at waste disposal sites or incinerate these resins for PFAS destruction (AWWA, 2020; Boyer et al., 2021). In contrast, the more popular IX resins for the PFAS treatment need to be regenerated. The regeneration is enabled with brine solutions (e.g., sodium chloride (NaCl)), alkaline aqueous solution (e.g., sodium hydroxide (NaOH)), and/or a combination of organic solvents (e.g., methanol or ethanol) with brine or alkaline solution for effective desorption of PFAS (Boyer et al., 2021; Dixit et al., 2021).

The advantage of IX resin applications to the PFAS treatment is primarily ascribed to a reliable treatment performance. Meanwhile, IX resins exhibit the potential to remove other contaminants during the PFAS removal process (AWWA, 2020). Generally, IX resins are also superior to GAC for PFAS removal because of their smaller footprints, shorter empty bed contact time, and longer replacement frequency (AWWA, 2020). Nevertheless, this treatment option has its limitations. First, though the recovery efficiency of spent IX resin is high after regeneration, the organic solvents for regeneration of IX resins are toxic and volatile, making *in-situ* regeneration dangerous (Du et al., 2014). Second, it is essential to decompose the PFAS-containing wastes generated from the regeneration before water disposal or recycling. However, very few efforts were made to treat waste eluate compared to the regeneration of resins via solvent elution (Ateia et al., 2019). Third, IX resin regeneration is commonly off-site implemented, and transportation between the treatment and regeneration facilities increases costs and the risk of secondary pollution. Fourth, IX resins can bind molecules (e.g., NOM) in water other than PFAS to significantly decrease their capacity for PFAS. Fifth, IX resins are ineffective

for the adsorption of some short-chain PFAS (Wanninayake, 2021). Sixth, applying non-regenerable IX resins for PFAS is not economically feasible as IX resins on a pound-for-pound basis are more expensive than GAC media (AWWA, 2020; USEPA, 2018).

Other Adsorbents. Besides the commercially available adsorbents (i.e., AC and IX resins) for PFAS adsorption in drinking water, others are applied as emerging PFAS adsorbents (Chi et al., 2022; Du et al., 2014; Garg et al., 2021; Wanninayake, 2021; Zhang et al., 2019), including natural adsorbents (e.g., minerals and biomaterial) and nanomaterials.

Minerals are attractive alternatives for PFAS adsorption because they are relatively abundant, have a low price, and have environmental sustainability (Ochoa-Herrera & Sierra-Alvarez, 2008; Zhou et al., 2010). Minerals have changeable stratified structures and tunable mesopores. Many adsorbents (e.g., montmorillonite (MM), boehmite, zeolite, kaolinite, alumina, silica, and goethite) have been extensively investigated for the PFAS adsorption in water (Du et al., 2014; Tang et al., 2010; Wang et al., 2012; Zhao et al., 2014; Zhou et al., 2010). The mineral-enabled PFAS adsorption mechanisms are highly dependent on the mineral properties. Although many mechanisms may be involved in the PFAS adsorption, electrostatic attraction and HPO interactions prevail (Du et al., 2014; Zhang et al., 2019).

Of note, the adsorption capacities for PFAS (< 10 mg PFAS/g for most minerals) are typically limited, which are much less than the other adsorbents (Zhang et al., 2019). The buck structure of the mineral possesses a high mass transfer resistance, which can significantly limit the substrate diffusion in the adsorption process (Li et al., 2015).

Similar to minerals, biomaterials have gained much attention because of their enhanced adsorption performance and lower costs (Zhang et al., 2019). Thus, the environmentally friendly and cost-effective adsorbents are considered as the promising alternatives for the PFAS removal

in water. The commonly studied biomaterials for PFAS adsorption are rice husk, chitosan, and quaternized cotton (Deng et al., 2013; Deng et al., 2012; Inyang & Dickenson, 2017; Zhang et al., 2011). Their dominant sorption mechanisms for PFAS are also electrostatic attraction and HPO interactions (Zhang et al., 2021; Zhang et al., 2019). Of interest, high adsorption capacities have been accomplished by biomaterials (91.6 - 2170 mg PFOS/g and 21.7 - 1350 mg PFOA/g) compared to other adsorbents (Zhang et al., 2019). There are other advantages for the applications of biomaterial, in addition to the strong PFAS adsorption capacities. First, the conversion of spent biomass wastes into value-added biomaterials represents an economical and sustainable approach to the waste management (Ahmad et al., 2014). Second, the biomaterials can concurrently remove other water contaminants, such as heavy metals, during the PFAS adsorption process (Wanninayake, 2021). However, there are some disadvantages to applying biomaterials for PFAS removal. For example, off-site disposal and incineration of waste biomaterials can assume substantial energy. Although some biomaterials can be disposed of via low energy-burning, the incomplete decomposition or defluorination of PFAS adsorbed on the biomaterials can introduce the persistent contaminants back to the environment.

Unlike traditional adsorption materials, nanomaterials can solve many problems associated with their counterpart bulk materials due to their unique properties (Oyetade et al., 2018). Among many nanomaterials used for PFAS removal in water, carbon nanotubes (CNTs) are widely used because they possess unique hollow nanostructures and unusual chemophysical properties (Zhang et al., 2019). The high specific surface area and strong hydrophobicity of CNTs have resulted in an excellent PFAS adsorption capability (382 – 1651 mg PFOS/g and 140 – 1110 mg PFOA/g), which are higher than other adsorbents (Zhang et al., 2019). Moreover, the CNTs are capable of rapidly reaching equilibrium (2 hr) advantageous over

chars (384 hr) and ash (48 hr) (Zhang et al., 2019). In addition to the CNTs, other nanomaterials (e.g., modified nanosized iron oxides and mesoporous silica materials) also exhibit excellent PFAS removal capabilities in water (Wanninayake, 2021; Zhang et al., 2019). The PFAS removal by these nanomaterials is largely attributed to electrostatic forces and HPO interactions. Although it has been demonstrated that hydrogen bonding interaction is not a dominant mechanism for PFAS removal by CNTs (Du et al., 2014), the interaction may occur between the carboxylate group of PFAS and the oxygen-containing functional group on the CNT surface via charge-assisted hydrogen bonding. Of note, this method for PFAS removal also has its restrictions. For instance, these nanomaterials are more expensive than other adsorbents or their counterpart bulk materials. Moreover, because of the smaller size of nanomaterials, the spent nanomaterials can be possibly introduced back into the finished water to result in secondary pollution (Zhang et al., 2019).

1.1.5.1.2 NF&RO. Membrane technology has been widely applied in clean water production and seawater desalination (Ali et al., 2018; Tang et al., 2018). Among commonly used membrane technologies for water purification, NF and RO membrane separation has gained much attention (Mondal & Wickramasinghe, 2008). RO membrane is a semi-permeable membrane that effectively rejects dissolved and suspended constituents in the feed water, such as ions and large particles, under a high pressure (100 – 800 psi) (Malaeb & Ayoub, 2011). Therefore, the unwanted solute (e.g., NaCl) cannot pass through the RO membrane. Instead, the solvent molecular can pass through the membrane to become a good tasting permeate water (Warsinger et al., 2016). Meanwhile, the NF membrane technology, a pressure-driven process, was introduced in the 1980s (Eriksson, 1988). The typical difference between RO and NF is that an NF membrane can reject hardness to a high degree but pass sodium chloride, whereas a RO

membrane can reject all salts to a high degree (USEPA, 2018). Due to the greater pore size, NF (i.e., 1-10 nm) provides a few advantages, such as high flux and relatively low operation pressure, as compared to RO (i.e., < 1 nm) (Hilal et al., 2004). Additionally, the costs of the NF separation can be largely reduced because this separation process can be operated at room temperature, different from a distillation process (Earle et al., 2006).

It has been reported that RO or NF membrane effectively removes a variety of PFAS, regardless of their chain length and chemical structure (Lee et al., 2021; Mastropietro et al., 2021; Tow et al., 2021). The removal mechanism is dependent on the PFAS species, water quality parameters, and membrane properties (AWWA, 2020). The size exclusion is considered as the major PFAS rejection mechanism, especially for RO membranes (AWWA, 2020; Mastropietro et al., 2021). Besides, other PFAS rejection mechanisms contain adsorption, which can also be involved in membrane applications, particularly with NF membranes (AWWA, 2020).

Regarding the PFAS rejection performance with NF or RO treatment, the maximum removal of different PFAS, including short- and long-chain ones, ranges from 84.0% to 99.9% (AWWA, 2020). The first studies concerning the RO removal of PFAS showed that 99% of PFOS was successfully rejected at an initial concentration of PFOS ranging from 0.5 to 1500 mg/L (Tang et al., 2006). Additionally, an appreciable PFAS removal rate was achieved with the NF and RO membrane combination in the testing on a feed of 10 parts per million PFOS over four days (Tang et al., 2007). The removal efficiencies of PFOS by the RO and NF treatments are typically >99% and 90-99%, respectively. (Kucharzyk et al., 2017). After NF or RO filtration, a small portion of feedwater containing PFAS can be retained as a high-strength concentrated waste (USEPA, 2018).

After PFAS rejection, the RO or NF's membrane concentrate needs to be disposed appropriately. The concentrate disposal methods are site-specific, including thermal incineration, evaporation ponds, land application, discharge to an outfall, deep well injection, discharged to regional concentrate treatment facilities, or discharge to the sanitary sewer (AWWA, 2020). The advantages of RO or NF membrane separation for PFAS rejection are summarized below. First, they can effectively and reliably remove different PFAS. Second, small footprints are required for the operation of the modular and compact systems. Third, other contaminants or unwanted water matrix constituents (e.g., NOM) in water can be simultaneously removed. However, the disadvantages of their application cannot be ignored. The membrane separation technologies are typically prohibitive and energy-intensive due to the membrane fouling (Deng, 2007). Moreover, the membrane separation technologies require the costly disposal of PFAS-containing brines. In other words, the retentates (i.e., PFAS concentrates) from high-pressure membranes need to be disposed of, otherwise, PFAS contaminants may return to the environment (Mastropietro et al., 2021). Additionally, pre- and post-membrane treatments are typically demanded to mitigate membrane fouling and extend the lifetime of membranes water (AWWA, 2020).

1.1.5.1.3 Foam Fractionation and Ozofractionation. Foam fractionation is a chemical process for the separation or concentration of components from a mixture based on selective adsorption (Nakabayashi et al., 2011). A gas-liquid interface is involved in this chemical process where air bubbles are introduced into a liquid solution, allowing surface-active substances (e.g., HPO molecules) dissolved in the solution to be selectively adsorbed onto the bubbles (Burghoff, 2012). Instead, the surface-inactive components remain in the bulk solution (Wanninayake, 2021). The foam formation can be attributed to dispersed or dissolved substances. As the surface tension of the gas-liquid interface declines, the foam increasingly stabilizes (Burghoff, 2012).

Therefore, the generated bubbles create a rising foam column above the liquid level. The foam fractionation is an emerging treatment technology to remove PFAS in water (Wanninayake, 2021). For example, the OPEC systems in Australia applied its surface-active foam fractionation (SAFF) technology for the effective removal of PFAS below Australian Drinking Water guidelines in 20 million liters of groundwater while concentrating PFAS into low volumes (500 liters) of final PFAS concentrate. Because PFAS typically contain a C-F “tail” with HPO properties, PFAS can act as surfactants preferentially affinity to gas bubble surface via adsorption mechanism. The extent of PFAS adsorption by SAFF is closely associated with the adsorption coefficient of the molecules at the gas-liquid interface (Burns et al., 2021). Concerning the benefits of foam fractionation technology, the separation process can be accomplished within a minute utilizing a low-cost simple apparatus. Moreover, any chemicals or sorbents are not utilized throughout the PFAS removal process. However, this technology has its disadvantage. First, because of the low surfactant abilities of short-chain PFAS, the removal efficiency of short-chain PFAS by foam fractionation is poor compared to the removal of long-chain PFAS (Dai et al., 2019). Second, foam-induced PFAS wastes are generated, which need further treatment and waste management (Wanninayake, 2021).

Ozofractionation is a type of foam fractionation that combines ozone (O_3) with foam fractionation (Wanninayake, 2021). The significant difference between ozofractionation and air-based foam fractionation is that ozofractionation applies O_3 to form bubbles in the foam. The generation of smaller-sized bubbles (i.e., surface area) with a higher electrostatic charge on the surface can result in better removal efficiency of PFAS because foam fractionation is heavily dependent on PFAS (i.e., the surfactant nature) attached to the bubbles. The emerging ozofractionation technology has been demonstrated to effectively remove aqueous PFAS and

their precursors, including total oxidizable precursors (TOP) (Horst et al., 2018). It was reported that 99.99% of different PFAS (< 2 ng/L to 28.8 µg/L) was successfully removed by an ozofractionative catalyzed reagent addition (OCRA) process (Horst et al., 2018). The PFAS separation mechanism of ozofractionation is that the generated hydroxyl radicals (i.e., •OH; strong electron binders) after O₃ injection in water play a critical role in separating more PFAS in water, in addition to the separated PFAS from air-based foam fractionation (Dai et al., 2019). Specifically, a •OH-rich layer around the interface of the gas bubbles is formed because of the O₃ diffusion from the gas phase into the water phase (Dai et al., 2019; Von Gunten & Hoigne, 1994). According to the affinity theory, the negatively charged HPI “head” of PFAS can bind the hydroxyl radical electron binders, thereby concentrating more PFAS in proximity to the interface of the gas bubbles (Dai et al., 2019). Thus, the ozofractionation can improve PFAS separation efficiency in water than air-based foam fractionation. A benefit of the ozofractionation technology is that this technology can effectively remove a wide array of PFAS, including long-chain and short-chain ones (Ross et al., 2018). It can also concurrently mitigate other contaminants without compromising PFAS removal efficiency (Wanninayake, 2021). Furthermore, a small footprint is required for the application of ozofractionation. Nevertheless, similar to air-based foam fractionation, this technology struggles to further treat PFAS-enriched waste stream (Horst et al., 2018).

1.1.5.2 Destruction Technologies. The destruction technologies covered in this chapter encompass advanced oxidation with chemical, photochemical, and electrochemical methods, advanced reduction, ultrasonication, biological degradation, non-thermal plasma, and hydrothermal treatment.

1.1.5.2.1 AOPs. AOPs are defined as the oxidation processes involving the formation of sufficient free radicals for the degradation of organic or inorganic contaminants in water or wastewater (Deng & Zhao, 2015). The generated free radicals during AOPs are $\bullet\text{OH}$ or $\text{SO}_4^{\bullet-}$. The AOPs have been extensively studied for the degradation of PFAS in water (Ahmed et al., 2020; Gao et al., 2021; Garg et al., 2021; Vo et al., 2020; X. Wang et al., 2021; Wanninayake, 2021).

The currently studied AOPs using $\bullet\text{OH}$ for destruction of PFAS include the ozone process (i.e., O_3 and hydrogen peroxide (H_2O_2)) (Dombrowski et al., 2018), catalyst-enabled oxidation (e.g., $\text{Fe}^{2+}/\text{H}_2\text{O}_2$) (Lu et al., 2020), ultraviolet (UV)-based oxidation (185 and 254 nm) (Leonello et al., 2021; Vo et al., 2020), electrochemical oxidation (Sharma et al., 2022), and others (e.g., ultrasonication (Cao et al., 2020), air fractionation (Wanninayake, 2021), and non-thermal plasma (Palma et al., 2022)). The explored AOPs utilizing $\text{SO}_4^{\bullet-}$ for PFAS degradation is the activated persulfate ($\text{S}_2\text{O}_8^{2-}$) oxidation (e.g., heat activation (Gao et al., 2021), UV activation (Lutze et al., 2018), microwave activation (Lee et al., 2012), iron activation (Yang et al., 2013), and ultrasound activation (Gray, 2018)).

The mechanism of PFAS degradation with $\bullet\text{OH}$ involves two plausible pathways. First, $\bullet\text{OH}$ can replace the H atom on the C-F bonding (Vo et al., 2020). Second, $\bullet\text{OH}$ can break up the backbone of the PFAS chain into small fractions. The mechanism of PFAS degradation by $\text{SO}_4^{\bullet-}$ was widely studied using PFOS and PFOA as model PFAS (Yang et al., 2020). Decarboxylation is the predominant mechanisms for PFAS defluorination (Yang et al., 2020). The degradation efficiencies of PFAS during the AOP treatment can range from 0 to 100% when the initial PFAS concentration falls within several ng/L to a few mg/L (Vo et al., 2020). It is heavily dependent on

initial PFAS concentrations, PFAS types (e.g., short chain vs. long-chain), radical generation methods (e.g., types of catalysts), and radical species ($\bullet\text{OH}$ vs. $\text{SO}_4^{\bullet-}$).

AOPs have been proven a promising method for degradation of aqueous PFAS because of their unique advantages (e.g., high redox potential, convenient storage, transportation, and longevity of precursor chemical reagents) (Yang et al., 2020). However, this technology still has some restrictions for full-scale applications. First, the degradation pathway of PFAS by AOPs is still under debate. Second, some AOPs are not cost-effective and produce harmful by-products (e.g., bromate and perchlorate). Third, some AOPs may produce byproducts (e.g., iron sludge from the Fenton-related AOP systems), which need extra steps to be removed in the water systems.

1.1.5.2.2 Ultrasonication/sonolysis. Sonochemical degradation of PFAS has gained much interest due to its excellent PFAS removal potential in several lab-scale studies (Cao et al., 2020; Javed, 2020). Ultrasonication or sonolysis uses high-frequency ultrasound (20 to 1100 kHz) to facilitate cavitation and induce cavitation bubbles in water (Wanninayake, 2021). The bubbles subsequently collapse (implode) due to quasi-adiabatic compression to produce bubble-interface temperatures near 1000 k and average vapor temperatures near 5000 k (Cao et al., 2020; Javed, 2020; Wanninayake, 2021). The water vapor undergoes pyrolysis to generate hydrogen radical ($\bullet\text{H}$) and $\bullet\text{OH}$ (Garg et al., 2021). Regarding the PFAS degradation mechanism, PFAS initially diffuse to the bubble-water interface and undergo cavitation pyrolysis to cleavage ionic functional groups, thereby forming fluorochemical intermediates (Cao et al., 2020; Garg et al., 2021). The fluorochemical intermediates are subsequently defluorinated via pyrolytic reaction within the bubble gas phase to generate low molecular PFAS, carbon dioxide (CO_2), and fluorine ions (F^-) (Cao et al., 2020; Javed, 2020; Wanninayake, 2021). Legacy PFAS have been

reported to be effectively degraded by sonolysis at different initial concentrations (up to mg/L level) with short degradation half-lives of < 30 mins (Cao et al., 2020). There are several advantages for the sonochemical degradation of PFAS, such as safety, cleanliness, energy-efficiency, and no secondary pollution (Cao et al., 2020). However, this technology has some drawbacks. First, applying the sonochemical method for large-scale PFAS removal is still challenging because it is energy intensive (Javed, 2020). Meanwhile, this process is inefficient in terms of total input energy, which may influence the PFAS degradation efficiency. Second, large-scale ultrasonic reactors have the potential to corrode the transducer material after long-term repeated use, which leads to severe problems, such as poor heat dissipation and reduced energy transfer (Cao et al., 2020).

1.1.5.2.3 Electrochemical Oxidation (EO). EO has been extensively studied for PFAS removal in water in recent years because of its capabilities for complete mineralizing legacy and emerging PFAS (Garg et al., 2021; Radjenovic et al., 2020; Sharma et al., 2022; Wanninayake, 2021). The typical layout of the EO system is composed of two electrodes (i.e., anode and cathode) connected to a power source. When an appropriate electrolyte and an energy input are applied to the system, strong oxidizing species are generated from a steady-state anodic current to degrade the target contaminants (Anglada et al., 2009). There are two mechanisms for PFAS destruction using EO: direct electron transfer and electrogenerated oxidants (Wanninayake, 2021). First, strong oxidants ($\bullet\text{OH}$ and $\text{SO}_4^{\bullet-}$) are electrogenerated on the anode, and the PFAS are decomposed in the bulk solution (Nzeribe et al., 2019; Ross et al., 2018). Second, the direct electron transfer step occurs at the anode via active oxygen (e.g., $\bullet\text{OH}$) when PFAS adsorbed onto the anodic surface (Wanninayake, 2021). Thus, selecting an appropriate anode for PFAS degradation is of importance in the EO system because it influences the PFAS degradation

efficiency (Radjenovic et al., 2020). Among various available electrode materials, boron-doped diamond (BDD) anodes, mixed metal oxide (MMO), and dimensionally stable anode (DSA) have been primarily investigated for EO of PFAS (Sharma et al., 2022). With an appropriate application of the EO system (e.g., suitable electrode materials), a promising PFAS removal efficiency can be achieved. For instance, many studies showed that over 90% of identified legacy PFAS were effectively removed with an initial concentration of PFAS from 4 to 200 mg/L (Ross et al., 2018; Sharma et al., 2022). Generally, EO exhibits high energy efficiency, convenient set-up, and scalability, in addition to the discontinuous operability at mild conditions (Sharma et al., 2022). Additionally, this technology can be achieved at atmospheric pressure and ambient temperature without external reagents required (Sharma et al., 2022). Furthermore, this method is cost-effective because a small quantity of electrolyte is required for the reaction to enhance the process. However, this method has its limitations. First, it is less effective for the degradation of short-chain PFAS in real contaminated water (Radjenovic et al., 2020; Wanninayake, 2021). Second, potential electrode corrosion may occur during PFAS treatment. Third, undesirable toxic by-products can possibly be generated with the presence of co-contaminants (e.g., chlorine gas, perchlorate, and bromate) (Wanninayake, 2021). Fourth, PFAS treatment using the EO system can be negatively affected by electrode fouling due to the adsorption NOM in drinking water (Radjenovic et al., 2020). Fifth, because of the trace level of PFAS in drinking water, mass transfer of PFAS may be significantly limited.

1.1.5.2.4 Non-thermal Plasma (NTP). NTP is an AOP that has recently been applied for PFAS destruction in water (Palma et al., 2022). NTP is electrically energized matter in a gaseous state. It can be formed by passing gases through the electric field. During the NTP production, most electrical energy is used for the formation of energetic matters instead of gas heating.

Therefore, the energy in NTP results in the high-energy electrical discharges and ionization of background gas, thereby producing NTP species. The NTP species are generally highly reactive radicals (e.g., $\bullet\text{OH}$, $\bullet\text{H}$, peroxide ($\text{O}_2^{\bullet-}$), perhydroxyl radical ($\text{HO}_2\bullet$) and hydrated electron (e_{aq}^-)), which can significantly decompose recalcitrant PFAS (Wanninayake, 2021). According to the literature, the PFAS removal efficiency using the NTP process can reach up to 99.9% when the initial concentration of PFAS is from several ng/L to a few mg/L in different water systems (Palma et al., 2022). Specifically, the removal efficiency of long-chain PFAS is higher than that of short-chain PFAS (Palma et al., 2022). There is limited information regarding the PFAS removal mechanism by NTP processes in the academic community. The possible PFAS removal mechanisms by NTP are 1) that NTP can generate different reactive species having both oxidative ($\bullet\text{OH}$) and reductive properties (e_{aq}^- and $\text{H}\bullet$); 2) that NTP may activate not only the direct photolysis of photochemical labile compounds but also the direct pyrolysis of the compounds in the plasma-generated hot spots (Palma et al., 2022). The advantage of this technique is that because plasma discharge itself activates all the processes, chemicals are not added to perform the treatment. Moreover, the removal efficiency of PFAS is greater than the conventional AOPs. However, this technology needs high cost and energy for full-scale treatment compared to AOPs using strong oxidants (Palma et al., 2022).

1.1.5.2.5 Biological Treatment. Biological treatment of PFAS also received much interest due to its lower investment and less disruption to the soil and water environment than physical and chemical methods (Zhang et al., 2022). The biological treatment method uses biological cultures (aerobic and/or anaerobic) for effective degradation of recalcitrant organic compounds present in the water (Lawrence & McCarty, 1970). In terms of the PFAS degradation mechanisms with microbial species, the proposed mechanisms for PFAS degradation processes

vary significantly in the literature, indicating that none of biological PFAS degradation pathways has been confirmed (Zhang et al., 2022). A few studies showed that some enzymes (e.g., extracted from *Cannabis sativa* L.) could either cleave the C-F bond via either oxidation by inserting oxygen atoms or reduction by adding extra electrons to the bonds to biodegrade certain PFAS (Shahsavari et al., 2021). Nevertheless, most reported PFAS biodegradation processes are still limited to remove fluorinated moieties instead of defluorination by the cleave of C-F bonds (Zhang et al., 2022). The PFAS degradation efficiency with biological treatment can reach up to 100% under an aerobic or anaerobic condition depending on the target PFAS species when the initial concentration of PFAS ranges from 0.1 to 1000 mg/L (Zhang et al., 2022). Although PFAS removal using biological treatment has many advantages, such as high degradation efficiency of certain PFAS, environment friendliness, safety, and cost-effectiveness, there are still some limitations on this method. First, the information regarding more detailed and accurate PFAS degradation pathways is limited (Zhang et al., 2022). Some of the intermediate forms are still unknown. Second, this method cannot completely degrade certain PFAS because of the restriction of microbial enzymatic reactions in cleaving C-F bonds. Third, biological treatment typically requires a long time for completion of the PFAS degradation. Even under ideal laboratory conditions, this method can still take more time to degrade PFAS than other methods that applied for PFAS degradation (Wanninayake, 2021). For instance, aerobic or anaerobic microorganisms can take more than 100 days to degrade certain PFAS (Vo et al., 2020).

1.1.5.2.6 Hydrothermal Treatment. Hydrothermal treatment is also an emerging technology for the PFAS destruction in condensed water, such as the brine from membrane separation or regeneration of exhausted IX resins (Hori et al., 2006; Wu et al., 2019). The hydrothermal treatment process uses elevated temperatures and pressures to treat water in a

subcritical state, in which the water can be maintained in a liquid state at $>100^{\circ}\text{C}$ and a high pressure between 16.5 and 23.3 Mpa (Javed, 2020; Li et al., 2022). The subcritical water creates a unique reactive environment to degrade persistent organic compounds (e.g., PFAS) (Möller et al., 2011). A hydrothermal treatment process is reported to significantly degrade over 90% of PFOS with a defluorination rate of 80% in a subcritical and alkaline condition (350°C ; 16.5 Mpa; $\text{pH} > 9$ (NaOH)) (Hao et al., 2021; Wu et al., 2019). A plausible degradation mechanism of alkaline hydrothermal treatment has been proposed (Wu et al., 2019). PFAS was initially involved in a nucleophilic attack at the polar head group (i.e., functional group) via OH^- substitution (Hao et al., 2021; Wu et al., 2019). Thereafter, PFAS were further degraded by sequential decarboxylation and hydrolysis reactions (Wu et al., 2019). The main advantage of this technology is that the hydrothermal processing of PFAS-impacted water requires dramatically lower energy inputs than incineration of the same material (Hao et al., 2021). However, most alkaline hydrothermal treatment processes for PFAS degradation were studied in bench scales. Further pilot and full-scale investigations need to be conducted in real water samples.

1.1.5.2.7 Advanced Reduction Processes (ARPs). ARPs are an emerging and promising PFAS destruction technology with high degradation efficiencies (Cui et al., 2020). A critical review on this subject is provided in **Chapter 2**.

1.2 Rationales

Although IX has been extensively practiced for technically effective adsorption of PFAS in drinking water treatment, the technology is restricted by multiple limits, including mostly cost and/or energy inefficiency due to prohibitive off-site regeneration, no PFAS detoxification, the generation of toxic PFAS-containing regenerant required for careful waste disposal, and

interference with co-existing water matrix constituents. In contrast, ARPs have demonstrated technical effectiveness in degrading PFAS in water (Cui et al., 2020). However, ARPs are barely applied to aqueous PFAS mitigation, particularly for drinking water treatment, because of the increased total dissolved solids (TDS) in effluent, pH adjustment (ARPs require an alkaline condition), and dissolved oxygen (DO) elimination. Therefore, either of the two PFAS treatment processes alone cannot provide an efficient PFAS treatment in a drinking water treatment scenario.

Here a treatment scheme combining IX and ARP is proposed. Specifically, ARP serves as an on-site regeneration method for degradation and detoxification of PFAS sorbed on IX resins to overcome the shortcomings mentioned above. **The expected benefits of this dissertation research** are summarized as follows. 1) The on-site resin regeneration can degrade and detoxify PFAS by producing a small volume of non-toxic and easily managed regenerant waste. 2) The regenerated IX resins can be repeatedly used to alleviate PFOA in water to significantly reduce the overall PFOA treatment costs. 3) Although this research focused on PFAS, the innovative regeneration method can be transferred to the mitigation of other trace amounts of persistent organic pollutants in water. And, 4) given that IX resins are widely used in chemical and environmental engineering industries, the study profoundly impacts the broader fields.

1.3 Objectives and Hypothesis

The **long-term goal** of this study is to develop innovative, technically viable, and low-cost treatment processes for the removal of PFAS in drinking water. The **primary objective** of this dissertation is to advance the fundamental understanding of the interactions of hydrated electrons and PFOA-spent IX resins, while providing a scientific basis for the development of an

innovative ARP-based IX resin regeneration technology capable of recovering spent resins and degrading PFOA in drinking water treatment. The **central hypothesis** is that hydrated electrons generated from ARPs can effectively degrade PFOA sorbed on the IX resins without significantly compromising the structures of IX resins, thereby regenerating exhausted resins in combination with the strategies for mitigation of NOM loadings on the IX resins. To achieve the overall objective, the following five **specific objectives** were pursued:

Objective I: To perform a critical literature review on the destruction of aqueous PFAS with ARPs to retrospect the state-of-the-art knowledge on the emerging PFAS treatment technology and identify the critical knowledge gaps toward applications to drinking water treatment.

Objective II: To screen for a potentially durable resin capable of effective adsorbing PFOA and resisting PFAS-caused damage to ARPs, and demonstrate the technical feasibility of the e_{aq}^- -driven ARPs for mitigation and degradation of PFAS sorbed on resins to alleviate PFOA in a laboratory-controlled water environment.

Objective III: To elucidate the interactions of e_{aq}^- and PFOA sorbed on the PFOA/NOM-laden IRA67 resins and assess the role of NOM co-sorbed on the IX resins in the proposed PFAS treatment approach.

Objective IV: To evaluate applicable strategies for mitigation of NOM loadings on PFOA-laden resins for cyclic use of regenerated IRA67 resins in a laboratory-controlled water environment.

Objective V: To comprehensively assess the novel ARP-based resin regeneration technologies.

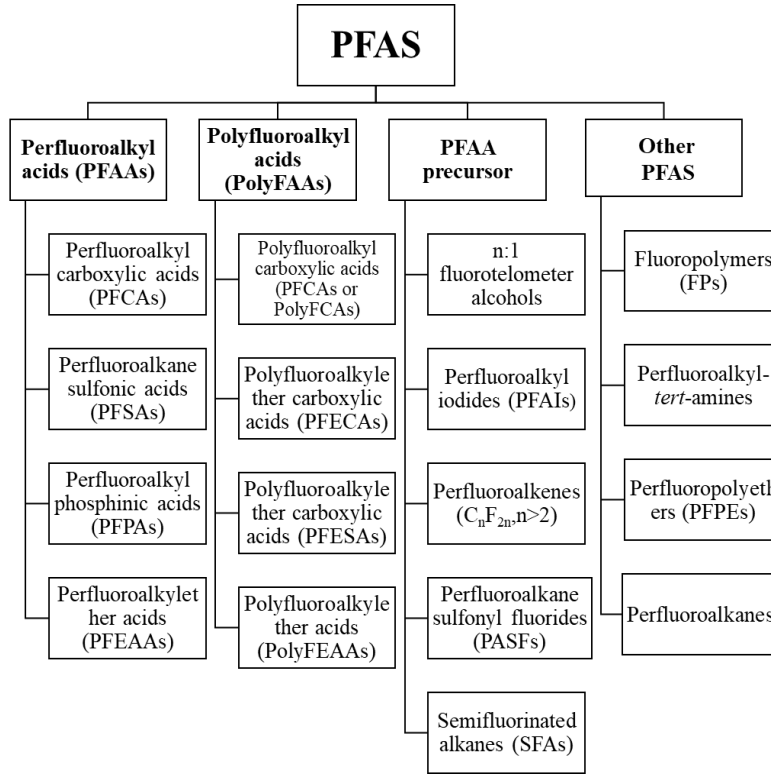


Figure 1-1 Schematic overview of the classification of identified PFAS families

References

- Abunada, Z., Alazaiza, M. Y., & Bashir, M. J. (2020). An overview of per-and polyfluoroalkyl substances (Pfas) in the environment: source, fate, risk and regulations. *Water*, *12*(12), 3590.
- Ahmad, M., Rajapaksha, A. U., Lim, J. E., Zhang, M., Bolan, N., Mohan, D., Vithanage, M., Lee, S. S., & Ok, Y. S. (2014). Biochar as a sorbent for contaminant management in soil and water: a review. *Chemosphere*, *99*, 19-33.
- Ahmed, M. B., Alam, M. M., Zhou, J. L., Xu, B., Johir, M. A. H., Karmakar, A. K., Rahman, M. S., Hossen, J., Hasan, A. K., & Moni, M. A. (2020). Advanced treatment technologies efficacies and mechanism of per-and poly-fluoroalkyl substances removal from water. *Process Safety and Environmental Protection*, *136*, 1-14.
- Albalgane, A., Cui, J., Song, W., & Deng, Y. (2022). Advanced Reduction Processes for Degradation of Refractory Organics in Landfill Leachate. *Journal of Environmental Engineering*, *148*(9), 04022046.
- Ali, A., Tufa, R. A., Macedonio, F., Curcio, E., & Drioli, E. (2018). Membrane technology in renewable-energy-driven desalination. *Renewable and Sustainable Energy Reviews*, *81*, 1-21.
- Anderson, R. H., Long, G. C., Porter, R. C., & Anderson, J. K. (2016). Occurrence of select perfluoroalkyl substances at US Air Force aqueous film-forming foam release sites other than fire-training areas: Field-validation of critical fate and transport properties. *Chemosphere*, *150*, 678-685.
- Anglada, A., Urtiaga, A., & Ortiz, I. (2009). Contributions of electrochemical oxidation to wastewater treatment: fundamentals and review of applications. *Journal of Chemical Technology & Biotechnology*, *84*(12), 1747-1755.
- Ateia, M., Maroli, A., Tharayil, N., & Karanfil, T. (2019). The overlooked short-and ultrashort-chain poly-and perfluorinated substances: A review. *Chemosphere*, *220*, 866-882.
- AWWA. (2020). *Drinking Water Treatment for PFAS Selection Guide*.
- Barber, J. L., Berger, U., Chaemfa, C., Huber, S., Jahnke, A., Temme, C., & Jones, K. C. (2007). Analysis of per-and polyfluorinated alkyl substances in air samples from Northwest Europe. *Journal of environmental monitoring*, *9*(6), 530-541.
- Bentel, M. J. (2020). *Understanding Structure–Reactivity Relationships for Aqueous Per-and Polyfluoroalkyl Substances (PFAS) Within the UV/Sulfite System UC Riverside*].
- Bonato, M., Corrà, F., Bellio, M., Guidolin, L., Tallandini, L., Irato, P., & Santovito, G. (2020). PFAS environmental pollution and antioxidant responses: an overview of the impact on

- human field. *International journal of environmental research and public health*, 17(21), 8020.
- Boyer, T. H., Fang, Y., Ellis, A., Dietz, R., Choi, Y. J., Schaefer, C. E., Higgins, C. P., & Strathmann, T. J. (2021). Anion exchange resin removal of per-and polyfluoroalkyl substances (PFAS) from impacted water: A critical review. *Water research*, 200, 117244.
- Brennan, N. M., Evans, A. T., Fritz, M. K., Peak, S. A., & von Holst, H. E. (2021). Trends in the Regulation of Per-and Polyfluoroalkyl Substances (PFAS): A Scoping Review. *International journal of environmental research and public health*, 18(20), 10900.
- Buck, R. C., Franklin, J., Berger, U., Conder, J. M., Cousins, I. T., De Voogt, P., Jensen, A. A., Kannan, K., Mabury, S. A., & van Leeuwen, S. P. (2011). Perfluoroalkyl and polyfluoroalkyl substances in the environment: terminology, classification, and origins. *Integrated environmental assessment and management*, 7(4), 513-541.
- Burghoff, B. (2012). Foam fractionation applications. *Journal of Biotechnology*, 161(2), 126-137.
- Burns, D. J., Stevenson, P., & Murphy, P. J. (2021). PFAS removal from groundwaters using Surface-Active Foam Fractionation. *Remediation Journal*, 31(4), 19-33.
- Cao, H., Zhang, W., Wang, C., & Liang, Y. (2020). Sonochemical degradation of poly-and perfluoroalkyl substances—a review. *Ultrasonics Sonochemistry*, 69, 105245.
- Chada, N., Romanos, J., Hilton, R., Suppes, G., Burrell, J., & Pfeifer, P. (2012). Activated carbon monoliths for methane storage. APS March Meeting Abstracts,
- Chain, E. P. o. C. i. t. F., Knutsen, H. K., Alexander, J., Barregård, L., Bignami, M., Brüschweiler, B., Ceccatelli, S., Cottrill, B., Dinovi, M., & Edler, L. (2018). Risk to human health related to the presence of perfluorooctane sulfonic acid and perfluorooctanoic acid in food. *EFSA journal*, 16(12), e05194.
- Chi, M., Li, N., Cui, J., Karlin, S., Rohr, N., Sharma, N., & Thieringer, F. M. (2022). Biomimetic, mussel-inspired surface modification of 3D-printed biodegradable polylactic acid scaffolds with nano-hydroxyapatite for bone tissue engineering. *Frontiers in Bioengineering and Biotechnology*, 1646.
- Chularueangaksorn, P., Tanaka, S., Fujii, S., & Kunacheva, C. (2014). Batch and column adsorption of perfluorooctane sulfonate on anion exchange resins and granular activated carbon. *Journal of Applied Polymer Science*, 131(3).
- Contea, L., Fallettia, L., Zaggiaa, A., & Milanb, M. (2015). Polyfluorinated organic micropollutants removal from water by ion exchange and adsorption. *Chemical Engineering*, 43.

- Cordner, A., Goldenman, G., Birnbaum, L. S., Brown, P., Miller, M. F., Mueller, R., Patton, S., Salvatore, D. H., & Trasande, L. (2021). The true cost of PFAS and the benefits of acting now. *Environmental Science & Technology*, 55(14), 9630-9633.
- Crittenden, J. C., Trussell, R. R., Hand, D. W., Howe, K. J., & Tchobanoglous, G. (2012). *MWH's water treatment: principles and design*. John Wiley & Sons.
- Crone, B. C., Speth, T. F., Wahman, D. G., Smith, S. J., Abulikemu, G., Kleiner, E. J., & Pressman, J. G. (2019). Occurrence of per-and polyfluoroalkyl substances (PFAS) in source water and their treatment in drinking water. *Critical Reviews in Environmental Science and Technology*, 49(24), 2359-2396.
- Cui, J., & Deng, Y. (2022). Hydrated Electron Degradation of PFOA Laden on Ion-Exchange Resins in the Presence of Natural Organic Matter. *ACS ES&T Engineering*.
- Cui, J., Gao, P., & Deng, Y. (2020). Destruction of per-and polyfluoroalkyl substances (PFAS) with advanced reduction processes (ARPs): A critical review. *Environmental Science & Technology*, 54(7), 3752-3766.
- Cui, J., Zheng, L., & Deng, Y. (2018). Emergency water treatment with ferrate (VI) in response to natural disasters. *Environmental Science: Water Research & Technology*, 4(3), 359-368.
- Dai, X., Xie, Z., Dorian, B., Gray, S., & Zhang, J. (2019). Comparative study of PFAS treatment by UV, UV/ozone, and fractionations with air and ozonated air. *Environmental Science: Water Research & Technology*, 5(11), 1897-1907.
- Davis, K. L., Aucoin, M. D., Larsen, B. S., Kaiser, M. A., & Hartten, A. S. (2007). Transport of ammonium perfluorooctanoate in environmental media near a fluoropolymer manufacturing facility. *Chemosphere*, 67(10), 2011-2019.
- Deng, S., Niu, L., Bei, Y., Wang, B., Huang, J., & Yu, G. (2013). Adsorption of perfluorinated compounds on aminated rice husk prepared by atom transfer radical polymerization. *Chemosphere*, 91(2), 124-130.
- Deng, S., Yu, Q., Huang, J., & Yu, G. (2010). Removal of perfluorooctane sulfonate from wastewater by anion exchange resins: Effects of resin properties and solution chemistry. *Water research*, 44(18), 5188-5195.
- Deng, S., Zhang, Q., Nie, Y., Wei, H., Wang, B., Huang, J., Yu, G., & Xing, B. (2012). Sorption mechanisms of perfluorinated compounds on carbon nanotubes. *Environmental Pollution*, 168, 138-144.
- Deng, Y. (2007). Physicochemical removal of organic contaminants in municipal landfill leachate. *Landfill Research Focus*, 5-26.

- Deng, Y., & Zhao, R. (2015). Advanced oxidation processes (AOPs) in wastewater treatment. *Current Pollution Reports*, 1(3), 167-176.
- Dixit, F., Dutta, R., Barbeau, B., Berube, P., & Mohseni, M. (2021). PFAS removal by ion exchange resins: A review. *Chemosphere*, 272, 129777.
- Dombrowski, P. M., Kakarla, P., Caldicott, W., Chin, Y., Sadeghi, V., Bogdan, D., Barajas-Rodriguez, F., & Chiang, S. Y. (2018). Technology review and evaluation of different chemical oxidation conditions on treatability of PFAS. *Remediation Journal*, 28(2), 135-150.
- Du, Z., Deng, S., Bei, Y., Huang, Q., Wang, B., Huang, J., & Yu, G. (2014). Adsorption behavior and mechanism of perfluorinated compounds on various adsorbents—A review. *Journal of hazardous materials*, 274, 443-454.
- Earle, M. J., Esperança, J. M., Gilea, M. A., Canongia Lopes, J. N., Rebelo, L. P., Magee, J. W., Seddon, K. R., & Widegren, J. A. (2006). The distillation and volatility of ionic liquids. *Nature*, 439(7078), 831-834.
- Epa, U. (2016). Lifetime health advisories and health effects support documents for perfluorooctanoic acid and perfluorooctane sulfonate. *Fed. Reg.* 81(101), 33250-33251.
- Eriksson, P. (1988). Nanofiltration extends the range of membrane filtration. *Environmental Progress*, 7(1), 58-62.
- Evich, M. G., Davis, M. J., McCord, J. P., Acrey, B., Awkerman, J. A., Knappe, D. R., Lindstrom, A. B., Speth, T. F., Tebes-Stevens, C., & Strynar, M. J. (2022). Per- and polyfluoroalkyl substances in the environment. *Science*, 375(6580), eabg9065.
- Falzone, S., Slater, L., Keating, K., Caro, C., Rodriguez, K., & Schaefer, C. (2020). Characterizing PFAS contamination from bench-top assessment of complex resistivity (CR) and nuclear magnetic resonance (NMR) measurements. In *SEG Technical Program Expanded Abstracts 2020* (pp. 1994-1998). Society of Exploration Geophysicists.
- Fenton, S. E., Ducatman, A., Boobis, A., DeWitt, J. C., Lau, C., Ng, C., Smith, J. S., & Roberts, S. M. (2021). Per- and polyfluoroalkyl substance toxicity and human health review: Current state of knowledge and strategies for informing future research. *Environmental toxicology and chemistry*, 40(3), 606-630.
- Fraser, A. J., Webster, T. F., Watkins, D. J., Nelson, J. W., Stapleton, H. M., Calafat, A. M., Kato, K., Shoeib, M., Vieira, V. M., & McClean, M. D. (2012). Polyfluorinated compounds in serum linked to indoor air in office environments. *Environmental Science & Technology*, 46(2), 1209-1215.

- Fromme, H., Dreyer, A., Dietrich, S., Fembacher, L., Lahrz, T., & Völkel, W. (2015). Neutral polyfluorinated compounds in indoor air in Germany—The LUPE 4 study. *Chemosphere*, *139*, 572-578.
- Gallen, C., Eaglesham, G., Drage, D., Nguyen, T. H., & Mueller, J. (2018). A mass estimate of perfluoroalkyl substance (PFAS) release from Australian wastewater treatment plants. *Chemosphere*, *208*, 975-983.
- Gao, P., Cui, J., & Deng, Y. (2021). Direct regeneration of ion exchange resins with sulfate radical-based advanced oxidation for enabling a cyclic adsorption–regeneration treatment approach to aqueous perfluorooctanoic acid (PFOA). *Chemical Engineering Journal*, *405*, 126698.
- Garg, S., Wang, J., Kumar, P., Mishra, V., Arafat, H., Sharma, R. S., & Dumée, L. F. (2021). Remediation of water from per-/poly-fluoroalkyl substances (PFAS)—Challenges and perspectives. *Journal of Environmental Chemical Engineering*, *9*(4), 105784.
- Glüge, J., Scheringer, M., Cousins, I. T., DeWitt, J. C., Goldenman, G., Herzke, D., Lohmann, R., Ng, C. A., Trier, X., & Wang, Z. (2020). An overview of the uses of per-and polyfluoroalkyl substances (PFAS). *Environmental Science: Processes & Impacts*, *22*(12), 2345-2373.
- González-Gaya, B., Casal, P., Jurado, E., Dachs, J., & Jiménez, B. (2019). Vertical transport and sinks of perfluoroalkyl substances in the global open ocean. *Environmental Science: Processes & Impacts*, *21*(11), 1957-1969.
- Gray, K. M. (2018). Sonochemical Defluorination of Perfluorinated Compounds by Activated Persulfate Ions. *Environmental Engineering*.
- Hao, S., Choi, Y.-J., Wu, B., Higgins, C. P., Deeb, R., & Strathmann, T. J. (2021). Hydrothermal alkaline treatment for destruction of per-and polyfluoroalkyl substances in aqueous film-forming foam. *Environmental Science & Technology*, *55*(5), 3283-3295.
- Hatton, J., Holton, C., & DiGuseppi, B. (2018). Occurrence and behavior of per-and polyfluoroalkyl substances from aqueous film-forming foam in groundwater systems. *Remediation Journal*, *28*(2), 89-99.
- HAYCARB. (2019). *Activated Carbon Basics*.
- Hekster, F. M., Laane, R. W., & Voogt, P. d. (2003). Environmental and toxicity effects of perfluoroalkylated substances. *Reviews of environmental contamination and toxicology*, 99-121.
- Helfferrich, F. G. (1995). *Ion exchange*. Courier Corporation.

- Hilal, N., Al-Zoubi, H., Darwish, N., Mohamma, A., & Arabi, M. A. (2004). A comprehensive review of nanofiltration membranes: Treatment, pretreatment, modelling, and atomic force microscopy. *Desalination*, 170(3), 281-308.
- Hori, H., Nagaoka, Y., Yamamoto, A., Sano, T., Yamashita, N., Taniyasu, S., Kutsuna, S., Osaka, I., & Arakawa, R. (2006). Efficient decomposition of environmentally persistent perfluorooctanesulfonate and related fluorochemicals using zerovalent iron in subcritical water. *Environmental Science & Technology*, 40(3), 1049-1054.
- Horst, J., McDonough, J., Ross, I., Dickson, M., Miles, J., Hurst, J., & Storch, P. (2018). Water treatment technologies for PFAS: the next generation. *Groundwater Monitoring & Remediation*, 38(2), 13-23.
- Houde, M., De Silva, A. O., Muir, D. C., & Letcher, R. J. (2011). Monitoring of perfluorinated compounds in aquatic biota: an updated review: PFCs in aquatic biota. *Environmental Science & Technology*, 45(19), 7962-7973.
- Hu, X. C., Andrews, D. Q., Lindstrom, A. B., Bruton, T. A., Schaidler, L. A., Grandjean, P., Lohmann, R., Carignan, C. C., Blum, A., & Balan, S. A. (2016). Detection of poly-and perfluoroalkyl substances (PFASs) in US drinking water linked to industrial sites, military fire training areas, and wastewater treatment plants. *Environmental science & technology letters*, 3(10), 344-350.
- Inyang, M., & Dickenson, E. R. (2017). The use of carbon adsorbents for the removal of perfluoroalkyl acids from potable reuse systems. *Chemosphere*, 184, 168-175.
- ITRC. (2020). *History and Use of Per- and Polyfluoroalkyl Substances (PFAS)*.
- ITRC. (2021). *PFAS — Per- and Polyfluoroalkyl Substances*.
- Javed, H. (2020). *Mechanistic insights on the merits and limitations of advanced treatment processes for removal of contaminants of emerging concern* [Rice University].
- Kazwini, T., Yadav, S., Ibrar, I., Al-Juboori, R. A., Singh, L., Ganbat, N., Karbassiyazdi, E., Samal, A. K., Subbiah, S., & Altaee, A. (2022). Updated review on emerging technologies for PFAS contaminated water treatment. *Chemical Engineering Research and Design*.
- Kucharzyk, K. H., Darlington, R., Benotti, M., Deeb, R., & Hawley, E. (2017). Novel treatment technologies for PFAS compounds: A critical review. *Journal of Environmental Management*, 204, 757-764.
- Kwarciak-Kozłowska, A. (2020). Methods used for the removal of disinfection by-products from water. In *Disinfection By-products in Drinking Water* (pp. 1-21). Elsevier.

- Lawrence, A. W., & McCarty, P. L. (1970). Unified basis for biological treatment design and operation. *Journal of the Sanitary Engineering Division*, 96(3), 757-778.
- Lee, H., Tevlin, A. G., Mabury, S. A., & Mabury, S. A. (2014). Fate of polyfluoroalkyl phosphate diesters and their metabolites in biosolids-applied soil: biodegradation and plant uptake in greenhouse and field experiments. *Environmental Science & Technology*, 48(1), 340-349.
- Lee, T., Speth, T. F., & Nadagouda, M. N. (2021). High-pressure Membrane Filtration Processes for separation of Per-and polyfluoroalkyl substances (PFAS). *Chemical Engineering Journal*, 134023.
- Lee, Y., Lo, S., Kuo, J., & Hsieh, C. (2012). Decomposition of perfluorooctanoic acid by microwaveactivated persulfate: Effects of temperature, pH, and chloride ions. *Frontiers of Environmental Science & Engineering*, 6(1), 17-25.
- Leonello, D., Fendrich, M. A., Parrino, F., Patel, N., Orlandi, M., & Miotello, A. (2021). Light-Induced Advanced Oxidation Processes as PFAS Remediation Methods: A Review. *Applied Sciences*, 11(18), 8458.
- Li, F., Duan, J., Tian, S., Ji, H., Zhu, Y., Wei, Z., & Zhao, D. (2020). Short-chain per-and polyfluoroalkyl substances in aquatic systems: Occurrence, impacts and treatment. *Chemical Engineering Journal*, 380, 122506.
- Li, J., Pinkard, B. R., Wang, S., & Novosselov, I. V. (2022). Hydrothermal treatment of per-and polyfluoroalkyl substances (PFAS). *Chemosphere*, 135888.
- Li, K., Zeng, Z., Xiong, J., Yan, L., Guo, H., Liu, S., Dai, Y., & Chen, T. (2015). Fabrication of mesoporous Fe₃O₄@ SiO₂@ CTAB-SiO₂ magnetic microspheres with a core/shell structure and their efficient adsorption performance for the removal of trace PFOS from water. *Colloids and Surfaces A: Physicochemical and Engineering Aspects*, 465, 113-123.
- Lin, Q., Dong, F., Li, C., & Cui, J. (2021). Disinfection byproduct formation from algal organic matters after ozonation or ozone combined with activated carbon treatment with subsequent chlorination. *Journal of Environmental Sciences*, 104, 233-241.
- Lu, D., Sha, S., Luo, J., Huang, Z., & Jackie, X. Z. (2020). Treatment train approaches for the remediation of per-and polyfluoroalkyl substances (PFAS): A critical review. *Journal of hazardous materials*, 386, 121963.
- Lu, X., Deng, S., Wang, B., Huang, J., Wang, Y., & Yu, G. (2016). Adsorption behavior and mechanism of perfluorooctane sulfonate on nanosized inorganic oxides. *Journal of colloid and interface science*, 474, 199-205.

- Lu, Y., Meng, L., Ma, D., Cao, H., Liang, Y., Liu, H., Wang, Y., & Jiang, G. (2021). The occurrence of PFAS in human placenta and their binding abilities to human serum albumin and organic anion transporter 4. *Environmental Pollution*, 273, 116460.
- Lutze, H. V., Brekenfeld, J., Naumov, S., von Sonntag, C., & Schmidt, T. C. (2018). Degradation of perfluorinated compounds by sulfate radicals—New mechanistic aspects and economical considerations. *Water research*, 129, 509-519.
- Maimaiti, A., Deng, S., Meng, P., Wang, W., Wang, B., Huang, J., Wang, Y., & Yu, G. (2018). Competitive adsorption of perfluoroalkyl substances on anion exchange resins in simulated AFFF-impacted groundwater. *Chemical Engineering Journal*, 348, 494-502.
- Malaeb, L., & Ayoub, G. M. (2011). Reverse osmosis technology for water treatment: State of the art review. *Desalination*, 267(1), 1-8.
- Mastropietro, T. F., Bruno, R., Pardo, E., & Armentano, D. (2021). Reverse osmosis and nanofiltration membranes for highly efficient PFASs removal: overview, challenges and future perspectives. *Dalton Transactions*, 50(16), 5398-5410.
- McCleaf, P., Englund, S., Östlund, A., Lindegren, K., Wiberg, K., & Ahrens, L. (2017). Removal efficiency of multiple poly-and perfluoroalkyl substances (PFASs) in drinking water using granular activated carbon (GAC) and anion exchange (AE) column tests. *Water research*, 120, 77-87.
- Möller, M., Nilges, P., Harnisch, F., & Schröder, U. (2011). Subcritical water as reaction environment: fundamentals of hydrothermal biomass transformation. *ChemSusChem*, 4(5), 566-579.
- Mondal, S., & Wickramasinghe, S. R. (2008). Produced water treatment by nanofiltration and reverse osmosis membranes. *Journal of membrane science*, 322(1), 162-170.
- Munoz, G., Budzinski, H., Babut, M., Lobry, J., Selleslagh, J., Tapie, N., & Labadie, P. (2019). Temporal variations of perfluoroalkyl substances partitioning between surface water, suspended sediment, and biota in a macrotidal estuary. *Chemosphere*, 233, 319-326.
- Nakabayashi, T., Takakusagi, Y., Iwabata, K., & Sakaguchi, K. (2011). Foam fractionation of protein: correlation of protein adsorption onto bubbles with a pH-induced conformational transition. *Analytical biochemistry*, 419(2), 173-179.
- NJDEP. (2021). *Per- and Polyfluoroalkyl Substances (PFAS) in Drinking Water*.
- Nzeribe, B. N., Crimi, M., Mededovic Thagard, S., & Holsen, T. M. (2019). Physico-chemical processes for the treatment of per-and polyfluoroalkyl substances (PFAS): a review. *Critical Reviews in Environmental Science and Technology*, 49(10), 866-915.

- Ochoa-Herrera, V., & Sierra-Alvarez, R. (2008). Removal of perfluorinated surfactants by sorption onto granular activated carbon, zeolite and sludge. *Chemosphere*, 72(10), 1588-1593.
- OECD. (2018). *Toward a new comprehensive global database of perand polyfluoroalkyl substances (PFASs)*.
- OECD. (2021). *Reconciling Terminology of the Universe of Per- and Polyfluoroalkyl Substances: Recommendations and Practical Guidance. Series on Risk Management No. 61*.
- Oyetade, O. A., Varadwaj, G., Nyamori, V. O., Jonnalagadda, S. B., & Martincigh, B. S. (2018). A critical review of the occurrence of perfluoroalkyl acids in aqueous environments and their removal by adsorption onto carbon nanotubes. *Reviews in Environmental Science and Bio/Technology*, 17(4), 603-635.
- Palma, D., Richard, C., & Minella, M. (2022). State of the art and perspectives about non-thermal plasma applications for the removal of PFAS in water. *Chemical Engineering Journal Advances*, 100253.
- Pepper, K., Reichenberg, D., & Hale, D. (1952). 599. Properties of ion-exchange resins in relation to their structure. Part IV. Swelling and shrinkage of sulphonated polystyrenes of different cross-linking. *Journal of the Chemical Society (Resumed)*, 3129-3136.
- Post, G. B. (2021). Recent US state and federal drinking water guidelines for per-and polyfluoroalkyl substances. *Environmental toxicology and chemistry*, 40(3), 550-563.
- Radjenovic, J., Duinslaeger, N., Avval, S. S., & Chaplin, B. P. (2020). Facing the challenge of poly-and perfluoroalkyl substances in water: is electrochemical oxidation the answer? *Environmental Science & Technology*, 54(23), 14815-14829.
- Reichenberg, D. (1953). Properties of ion-exchange resins in relation to their structure. III. Kinetics of exchange. *Journal of the American Chemical Society*, 75(3), 589-597.
- Ross, I., McDonough, J., Miles, J., Storch, P., Thelakkat Kochunarayanan, P., Kalve, E., Hurst, J., S. Dasgupta, S., & Burdick, J. (2018). A review of emerging technologies for remediation of PFASs. *Remediation Journal*, 28(2), 101-126.
- SAMCO. (2017). *What Is Ion Exchange Resin and How Does It Work?*
- Senevirathna, S. T. M. L. D. (2010). Development of effective removal methods of PFCs (perfluorinated compounds) in water by adsorption and coagulation.
- Shahsavari, E., Rouch, D., Khudur, L. S., Thomas, D., Aburto-Medina, A., & Ball, A. S. (2021). Challenges and current status of the biological treatment of PFAS-contaminated soils. *Frontiers in Bioengineering and Biotechnology*, 1493.

- Sharma, S., Shetti, N. P., Basu, S., Nadagouda, M. N., & Aminabhavi, T. M. (2022). Remediation of per-and polyfluoroalkyls (PFAS) via electrochemical methods. *Chemical Engineering Journal*, 430, 132895.
- Sonmez Baghirzade, B., Zhang, Y., Reuther, J. F., Saleh, N. B., Venkatesan, A. K., & Apul, O. G. (2021). Thermal regeneration of spent granular activated carbon presents an opportunity to break the forever PFAS cycle. *Environmental Science & Technology*, 55(9), 5608-5619.
- Soo, Y., Chada, N., Beckner, M., Romanos, J., Burrell, J., & Pfeifer, P. (2013). Adsorbed methane film properties in nanoporous carbon monoliths. APS March Meeting Abstracts,
- Söregård, M., Östblom, E., Köhler, S., & Ahrens, L. (2020). Adsorption behavior of per-and polyfluoroalkyl substances (PFASs) to 44 inorganic and organic sorbents and use of dyes as proxies for PFAS sorption. *Journal of Environmental Chemical Engineering*, 8(3), 103744.
- Sunderland, E. M., Hu, X. C., Dassuncao, C., Tokranov, A. K., Wagner, C. C., & Allen, J. G. (2019). A review of the pathways of human exposure to poly-and perfluoroalkyl substances (PFASs) and present understanding of health effects. *Journal of exposure science & environmental epidemiology*, 29(2), 131-147.
- Tang, C. Y., Fu, Q. S., Criddle, C. S., & Leckie, J. O. (2007). Effect of flux (transmembrane pressure) and membrane properties on fouling and rejection of reverse osmosis and nanofiltration membranes treating perfluorooctane sulfonate containing wastewater. *Environmental Science & Technology*, 41(6), 2008-2014.
- Tang, C. Y., Fu, Q. S., Gao, D., Criddle, C. S., & Leckie, J. O. (2010). Effect of solution chemistry on the adsorption of perfluorooctane sulfonate onto mineral surfaces. *Water research*, 44(8), 2654-2662.
- Tang, C. Y., Fu, Q. S., Robertson, A., Criddle, C. S., & Leckie, J. O. (2006). Use of reverse osmosis membranes to remove perfluorooctane sulfonate (PFOS) from semiconductor wastewater. *Environmental Science & Technology*, 40(23), 7343-7349.
- Tang, C. Y., Yang, Z., Guo, H., Wen, J. J., Nghiem, L. D., & Cornelissen, E. (2018). Potable water reuse through advanced membrane technology.
- TIGG. (2019). *What Is Activated Carbon?*
- Topp, N., & Pepper, K. (1949). 690. Properties of ion-exchange resins in relation to their structure. Part I. Titration curves. *Journal of the Chemical Society (Resumed)*, 3299-3303.
- Tow, E. W., Ersan, M. S., Kum, S., Lee, T., Speth, T. F., Owen, C., Bellona, C., Nadagouda, M. N., Mikelonis, A. M., & Westerhoff, P. (2021). Managing and treating per-and

- polyfluoroalkyl substances (PFAS) in membrane concentrates. *AWWA water science*, 3(5), e1233.
- USEPA. (2017a). *Basic Information about Per- and Polyfluoroalkyl Substances (PFASs)*.
- USEPA. (2017b). *Small Drinking Water Systems Research*.
- USEPA. (2018). *Reducing PFAS in Drinking Water with Treatment Technologies*.
- USEPA. (2022). Lifetime Drinking Water Health Advisories for Four Perfluoroalkyl Substances.
- Verma, S., Varma, R. S., & Nadagouda, M. N. (2021). Remediation and mineralization processes for per-and polyfluoroalkyl substances (PFAS) in water: A review. *Science of the Total Environment*, 794, 148987.
- Vickers, N. J. (2017). Animal communication: when i'm calling you, will you answer too? *Current biology*, 27(14), R713-R715.
- Vo, H. N. P., Ngo, H. H., Guo, W., Nguyen, T. M. H., Li, J., Liang, H., Deng, L., Chen, Z., & Nguyen, T. A. H. (2020). Poly-and perfluoroalkyl substances in water and wastewater: a comprehensive review from sources to remediation. *Journal of Water Process Engineering*, 36, 101393.
- Von Gunten, U., & Hoigne, J. (1994). Bromate formation during ozonization of bromide-containing waters: interaction of ozone and hydroxyl radical reactions. *Environmental Science & Technology*, 28(7), 1234-1242.
- Wang, F., Liu, C., & Shih, K. (2012). Adsorption behavior of perfluorooctanesulfonate (PFOS) and perfluorooctanoate (PFOA) on boehmite. *Chemosphere*, 89(8), 1009-1014.
- Wang, M., Orr, A. A., Jakubowski, J. M., Bird, K. E., Casey, C. M., Hearon, S. E., Tamamis, P., & Phillips, T. D. (2021). Enhanced adsorption of per-and polyfluoroalkyl substances (PFAS) by edible, nutrient-amended montmorillonite clays. *Water research*, 188, 116534.
- Wang, X., Chen, Z., Wang, Y., & Sun, W. (2021). A review on degradation of perfluorinated compounds based on ultraviolet advanced oxidation. *Environmental Pollution*, 291, 118014.
- Wang, Y., Chang, W., Wang, L., Zhang, Y., Zhang, Y., Wang, M., Wang, Y., & Li, P. (2019). A review of sources, multimedia distribution and health risks of novel fluorinated alternatives. *Ecotoxicology and environmental safety*, 182, 109402.
- Wang, Y., Darling, S. B., & Chen, J. (2021). Selectivity of Per-and Polyfluoroalkyl Substance Sensors and Sorbents in Water. *ACS Applied Materials & Interfaces*.

- Wang, Z., Buser, A. M., Cousins, I. T., Demattio, S., Drost, W., Johansson, O., Ohno, K., Patlewicz, G., Richard, A. M., & Walker, G. W. (2021). A New OECD Definition for Per- and Polyfluoroalkyl Substances. *Environmental Science & Technology*, 55(23), 15575-15578.
- Wanninayake, D. M. (2021). Comparison of currently available PFAS remediation technologies in water: A review. *Journal of Environmental Management*, 283, 111977.
- Warsinger, D. M., Tow, E. W., Nayar, K. G., & Maswadeh, L. A. (2016). Energy efficiency of batch and semi-batch (CCRO) reverse osmosis desalination. *Water research*, 106, 272-282.
- Wilkinson, J. L., Hooda, P. S., Swinden, J., Barker, J., & Barton, S. (2017). Spatial distribution of organic contaminants in three rivers of Southern England bound to suspended particulate material and dissolved in water. *Science of the Total Environment*, 593, 487-497.
- Wood. (2020). *Socio-Economic Assessment of the US Fluoropolymer Industry -Executive Summary*.
- Wu, B., Hao, S., Choi, Y., Higgins, C. P., Deeb, R., & Strathmann, T. J. (2019). Rapid destruction and defluorination of perfluorooctanesulfonate by alkaline hydrothermal reaction. *Environmental science & technology letters*, 6(10), 630-636.
- Xiao, F. (2017). Emerging poly- and perfluoroalkyl substances in the aquatic environment: a review of current literature. *Water research*, 124, 482-495.
- Xu, B., Liu, S., Zhou, J. L., Zheng, C., Weifeng, J., Chen, B., Zhang, T., & Qiu, W. (2021). PFAS and their substitutes in groundwater: Occurrence, transformation and remediation. *Journal of hazardous materials*, 412, 125159.
- Yamashita, N., Taniyasu, S., Petrick, G., Wei, S., Gamo, T., Lam, P. K., & Kannan, K. (2008). Perfluorinated acids as novel chemical tracers of global circulation of ocean waters. *Chemosphere*, 70(7), 1247-1255.
- Yang, L., He, L., Xue, J., Ma, Y., Xie, Z., Wu, L., Huang, M., & Zhang, Z. (2020). Persulfate-based degradation of perfluorooctanoic acid (PFOA) and perfluorooctane sulfonate (PFOS) in aqueous solution: Review on influences, mechanisms and prospective. *Journal of hazardous materials*, 393, 122405.
- Yang, S., Cheng, J., Sun, J., Hu, Y., & Liang, X. (2013). Defluorination of aqueous perfluorooctanesulfonate by activated persulfate oxidation. *PloS one*, 8(10), e74877.
- Yu, Q., Zhang, R., Deng, S., Huang, J., & Yu, G. (2009). Sorption of perfluorooctane sulfonate and perfluorooctanoate on activated carbons and resin: kinetic and isotherm study. *Water research*, 43(4), 1150-1158.

- Zaggia, A., Conte, L., Falletti, L., Fant, M., & Chiorboli, A. (2016). Use of strong anion exchange resins for the removal of perfluoroalkylated substances from contaminated drinking water in batch and continuous pilot plants. *Water research*, *91*, 137-146.
- Zhang, B., He, Y., Huang, Y., Hong, D., Yao, Y., Wang, L., Sun, W., Yang, B., Huang, X., & Song, S. (2020). Novel and legacy poly-and perfluoroalkyl substances (PFASs) in indoor dust from urban, industrial, and e-waste dismantling areas: the emergence of PFAS alternatives in China. *Environmental Pollution*, *263*, 114461.
- Zhang, D., He, Q., Wang, M., Zhang, W., & Liang, Y. (2021). Sorption of perfluoroalkylated substances (PFASs) onto granular activated carbon and biochar. *Environmental technology*, *42*(12), 1798-1809.
- Zhang, D., Zhang, W., & Liang, Y. (2019). Adsorption of perfluoroalkyl and polyfluoroalkyl substances (PFASs) from aqueous solution-A review. *Science of the Total Environment*, *694*, 133606.
- Zhang, Q., Deng, S., Yu, G., & Huang, J. (2011). Removal of perfluorooctane sulfonate from aqueous solution by crosslinked chitosan beads: sorption kinetics and uptake mechanism. *Bioresource technology*, *102*(3), 2265-2271.
- Zhang, Z., Sarkar, D., Biswas, J. K., & Datta, R. (2022). Biodegradation of per-and polyfluoroalkyl substances (PFAS): A review. *Bioresource technology*, *344*, 126223.
- Zhao, L., Bian, J., Zhang, Y., Zhu, L., & Liu, Z. (2014). Comparison of the sorption behaviors and mechanisms of perfluorosulfonates and perfluorocarboxylic acids on three kinds of clay minerals. *Chemosphere*, *114*, 51-58.
- Zheng, L., Cui, J., & Deng, Y. (2020). Emergency water treatment with combined ferrate (vi) and ferric salts for disasters and disease outbreaks. *Environmental Science: Water Research & Technology*, *6*(10), 2816-2831.
- Zhou, Q., Deng, S., Yu, Q., Zhang, Q., Yu, G., Huang, J., & He, H. (2010). Sorption of perfluorooctane sulfonate on organo-montmorillonites. *Chemosphere*, *78*(6), 688-694.

Chapter 2 Critical Review of ARPs for PFAS Destruction

2.1 Introduction and Objectives

Among very few technically effective PFAS treatment methods, ARPs have recently emerged as a promising option (Cui et al., 2020). The term of ARPs was used in the late 1990s to explain the unintended degradation of highly oxidized organic compounds (e.g., carbon tetrachloride) by reducing radical species (e.g., e_{aq}^- and $H\cdot$) produced during electron beam irradiation of polluted groundwater (Gehring & Eschweiler, 1999). As a purposeful water treatment option, ARPs were proposed to address water contaminants more than one decade later (Vellanki et al., 2013; Yoon et al., 2011). ARPs represent a chemical degradation process producing sufficient and highly reducing radicals for destruction of contaminants in water (Cui et al., 2020). ARPs employ strong reducing agents with $E^\circ \leq -2.3$ V vs. normal hydrogen electrode at 25°C [which is the potential equal to or lower than that of e_{aq}^- and its conjugate acid (i.e., $H\cdot$)] (Waclawek et al., 2022). Although the term has been very recently adopted in water and wastewater treatment, the investigations on the reactions of these reducing agents with different chemicals in the water began several decades ago (S Gordon et al., 1963; Sheffield Gordon et al., 1963; Hart et al., 1964; Keene, 1964; OZAWA et al., 1974). For environmental applications, ARPs have proven very effective for the removal of various oxidized contaminants, such as vinyl chloride (Liu et al., 2013a, 2013b), perchlorate (Vellanki & Batchelor, 2013), bromate (Botlaguduru et al., 2015; Jung et al., 2014), nitrate (Bensalah et al., 2014), chromium (VI) (Moussavi et al., 2015; Xie et al., 2017), and 2, 4, 6-trichlorophenol (Yazdanbakhsh et al., 2018). Special attention has been recently directed to ARPs due to their capability of effectively destructing different PFAS chemicals in water (Bao et al., 2018; Bentel et al., 2019; Cao et al., 2022; J. Gu et al., 2017; Gu et al., 2016; Y. Gu et al., 2017; Jiao et al., 2022; Kugler et al., 2021;

C. J. Liu et al., 2021; Z. Liu et al., 2022; Lyu et al., 2015; Park et al., 2009; Qu et al., 2014; Qu et al., 2010; Ren et al., 2021; Song et al., 2013; M. Sun et al., 2018; Sun et al., 2017; Z. Sun et al., 2018; Vellanki et al., 2013; Zhang et al., 2015). These encouraging findings demonstrate that ARPs are a promising approach to the mitigation of the PFAS impacts in an aqueous environment.

The objective of this chapter was to provide a state-of-the-art review on e_{aq}^- and its generation for PFAS destruction, mechanisms of reductive destruction of PFAS by e_{aq}^- , and the evaluation of effects of critical factors affecting the PFAS degradation and defluorination efficiencies in an ARP. Furthermore, environmental implications of the knowledge for water industries were discussed, and future research needs were identified.

2.2 Hydrated Electrons and Their Generation for Destruction of PFAS

Although different activation methods (e.g., photolysis, radiolysis, and sonolysis) with or without the assistance of chemical solutes can produce different free reducing radicals in water, photo-irradiation of sulfite (SO_3^{2-}), iodide (I^-), dithionite ($S_2O_6^{2-}$), ferrocyanide ($Fe(CN)_6^{4-}$), or certain organic compounds (e.g., phenol, aminopolycarboxylic acids (APCAs), and indole derivatives) was reported for effective decomposition of PFAS chemicals in water in the literature (Buxton et al., 1988; Huang et al., 2007; Z. Sun et al., 2018; Tian et al., 2016; Tian & Gu, 2018; Trojanowicz et al., 2018; Vellanki et al., 2013; Waclawek et al., 2022). SO_3^{2-} and I^- are the most frequently used among these solutes. The effective destruction of PFAS molecules during the ARP treatment is principally ascribed to the generation of e_{aq}^- , rather than other reducing agents produced, as evidenced by the results of scavenging experiments (Z. Sun et al., 2018).

Excess electrons can be generated in electrically neutral water directly by pulse radiolysis or using ionization or detachment of a specific solute that enables the existence of electrons in water rather than association with their parent cations (Devonshire & Weiss, 1968; Larsen et al., 2010). Negative charges of the secondary electrons polarize neighboring neutral water molecules so that the electrons are bound to these water molecules to create a metastable localized species called hydrated electrons (Hart, 1964; Larsen et al., 2010). Experimental evidence for the detection of e_{aq}^- was first found in the late 1950s (Hart, 1964). Afterwards, substantial debates have remained over the different models proposed to describe the molecular structure of e_{aq}^- (Herbert & Coons, 2017). In a traditionally accepted cavity model, a hydrated electron excludes water to create and occupy a small quasi-spherical region, which is surrounded by water molecules with O-H bonds pointing toward the cavity (Kevan, 1981). However, the existence of a cavity structure has been occasionally questioned (Casey et al., 2013; Larsen et al., 2010).

Hydrated electrons are a potent reducing agent with an extremely negative standard reduction potential of -2.9 V (Schwarz, 1981; Swallow, 1973). The short-lived radicals can have a half-life of more than 300 microseconds (Hart, 1964). It is conventionally believed that they tend to react with chemical species via a one-electron transfer mechanism (Hart & Anbar, 1970). Whereas rate constants of these reactions broadly vary from $\sim 10 \text{ M}^{-1}\cdot\text{s}^{-1}$ to a diffusion-controlled mode, the activation energies range narrowly within 6-30 $\text{kJ}\cdot\text{mol}^{-1}$, suggesting that the kinetics is limited by the availability of a vacant orbital on the target reactant species (Buxton et al., 1988).

2.2.1 UV/sulfite

The occurrence of a chain reaction during photoionization of sulfite in water was early reported in the 1920s (Bäckström, 1927). Efforts were later made to elucidate the underlying reaction mechanisms (Chawla et al., 1973; Deister & Warneck, 1990; Dogliotti & Hayon, 1968;

Fischer & Warneck, 1996; Hayon et al., 1972). Because the UV/sulfite system for reductive destruction of PFAS is mostly operated at an alkaline condition (the effect of pH would be discussed later) and bisulfite (HSO_3^-) has a pK_a of 7.21 (Haynes, 2014), the major sulfite species in the PFAS treatment system is SO_3^{2-} rather than HSO_3^- . The photoionization of SO_3^{2-} produces e_{aq}^- together with equimolar $\text{SO}_3^{\cdot-}$ as shown in Eq. (2-1).



When vacuum UV (VUV) irradiation (185 nm) is adopted in a UV/sulfite system, additional e_{aq}^- can be directly created from the photoionization of water, but the phenomena cannot be observed using other spectral regions (e.g., 254 nm) (Y. Gu et al., 2017; Zoschke et al., 2014).

Under anoxic conditions, $\text{SO}_3^{\cdot-}$ is subsequently recombined through two parallel pathways to generate $\text{S}_2\text{O}_6^{2-}$ (Eq. (2-2)) (Eriksen, 1974; Hayon et al., 1972) and sulfate (SO_4^{2-}) (Eq. (2-3)) (Fischer & Warneck, 1996), respectively.



Meanwhile, e_{aq}^- may be consumed through three mechanisms in the absence of target chemical species. Firstly, e_{aq}^- can react with H^+ to produce the conjugate acid, $\text{H}\cdot$ (Eq. (2-4)) (Buxton et al., 1988). Subsequently, the produced $\text{H}\cdot$ can further promptly react with e_{aq}^- to form hydrogen gas (H_2) (Eq. (2-5)) (Buxton et al., 1988).



Secondly, e_{aq}^- can be recombined to produce H_2 and OH^- (Eq. (2-6)) (Buxton et al., 1988).



Thirdly, e_{aq}^- may react with $S_2O_6^{2-}$ generated from Eq. (2-2) (Eq. (2-7)) (Fischer & Warneck, 1996).



Of note, SO_3^{2-} can be partially recycled from Eq. (2-2) and (2-7) for generation of additional e_{aq}^- . The final photo-decomposition products of SO_3^{2-} are sulfate and dithionite with a reported approximate molar ratio of SO_4^{2-} to $S_2O_6^{2-}$ of 2:1 (Deister & Warneck, 1990; Fischer & Warneck, 1996).

When DO is present, e_{aq}^- generated can be substantially consumed by O_2 to produce superoxide ($O_2^{\cdot-}$) (Eq. (2-8)), which may further react with e_{aq}^- as in Eq. (2-9) (Buxton et al., 1988).



2.2.2 UV/iodide

The photochemistry of iodide in water was also early investigated (Franck & Scheibe, 1928; Jortner et al., 1961; Jortner et al., 1964). Photoexcitation of I^- in water first occurs to produce an excited iodide (I^*H_2O) (Eq. (2-10)).



I^*H_2O can decay to its ground state (I^-) through Eq. (2-11). It can also be thermally degraded to an intermediate state, i.e., a caged complex ($I\cdot, e^-$), in which electrons are less confined and undergo a quasi-random walk diffusion process in the proximity of I atom ($I\cdot$) over water molecules (Eq. (2-12)) (Jortner et al., 1961). Finally, e_{aq}^- can be generated through

dissociation of the caged complex, accompanied by the production of $I\cdot$ (Eq. (2-13)) (Jortner et al., 1964).

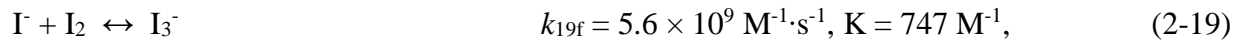
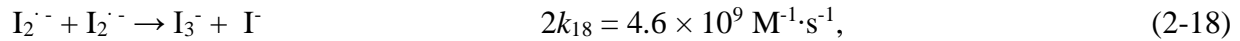
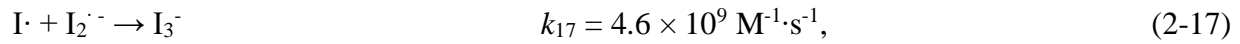
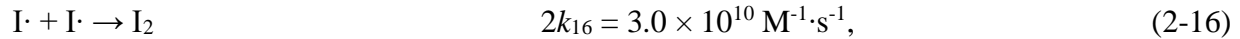
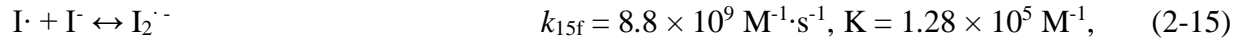


Here () represents the solvent cage in which $I\cdot$ and e_{aq}^- are formed in pairs.

More detailed mechanistic information regarding the e_{aq}^- generation from photo-irradiation of I^- in water was further explored. Initial photoexcitation involves a state above the charge-transfer-to-solvent (CTTS) absorption, an absorption band for detachment of the electron from I^- . The photo-detached electron is an electron (e_{trapped}^-) trapped in a polarization well created by water molecules oriented around I^- (Long, Lu, Shi, et al., 1990; Long et al., 1994). The trapped electron would subsequently experience electron solvation, which is viewed as an excited state relaxation process between different electronic energy levels of the solvated electrons (Long, Lu, & Eisenthal, 1990; Sheu & Rossky, 1996; Shi et al., 1996). Consequently, two other electron species are sequentially produced primarily through a nonadiabatic electron transfer process (Long, Lu, Shi, et al., 1990), including wet electrons (e_{wet}^-) and e_{aq}^- . e_{wet}^- is a pre-solvated electron with the lowest excited state, while e_{aq}^- is the equilibrium solvated electron with the ground state (Eq. (2-14)) (Shi et al., 1996). Transitions among the three electron species are extremely rapid with a time scale in the order of femtoseconds (Long, Lu, & Eisenthal, 1990; Long, Lu, Shi, et al., 1990; Tang et al., 2010).



$I\cdot$ generated from Eq. (2-13) can react with the added I^- to generate various I species, which react with another one in the water as shown in Eq. (2-15) to (2-19) (Elliot, 1992).



Here, the subscript of f in the above rate constants means that the rate constant is for the forward reaction. In the absence of target pollutants, $e_{aq}\dot{-}$ can be consumed by several I species (Eq. (2-20) and (2-21)) (Qu et al., 2010), besides reactions with H^+ (Eq. (2-4) and (2-5)) and self-recombination (Eq. (2-6)).



2.2.3 UV/others

Other solutes were also used under the UV irradiation to generate $e_{aq}\dot{-}$ for the destruction of PFAS in water, such as $Fe(CN)_6^{4-}$, which can be photolyzed to generate $e_{aq}\dot{-}$ (Eq. (2-22)) for degradation of PFAS (Huang et al., 2007).



It should be noted that a fraction of $e_{aq}\dot{-}$ generated from the UV/sulfite or UV/iodide system can be scavenged by oxidizing species, leading to a low utilization efficiency and a short lifetime of $e_{aq}\dot{-}$. To address this issue, organic compounds were proposed to generate $e_{aq}\dot{-}$. One such example is nitrilotriacetic acid (NTA), which plays a dual role in water (Z. Sun et al., 2018). It is firstly fully hydrated with hydration spheres and then serves as a photosensitizer to facilitate water photo-dissociation and photo-ionization for the generation of $e_{aq}\dot{-}$ and $\cdot OH$ (Eq. (2-23)) (Lian et al., 2004).



Afterwards, NTA with a high reactivity toward $\cdot\text{OH}$ (rate constant = $4.2 \times 10^9 \text{ M}^{-1}\cdot\text{s}^{-1}$ at pH 10.0) minimizes the germinate recombination between e_{aq}^- and $\cdot\text{OH}$ (Sahul & Sharma, 1987), promoting the e_{aq}^- utilization for PFAS. Therefore, under the identical conditions (0.01 mM PFOS; 2 mM NTA or SO_3^{2-} ; pH 10.0), UV/NTA was reported to achieve better degradation and defluorination of PFOS than UV/sulfite (Z. Sun et al., 2018). Furthermore, UV/ Fe^{II} NTA system was proposed to minimize the scavenging effect of H^+ on e_{aq}^- by combining Fe(II/III)-ligand complexes with UV/NTA system to degrade PFAS under relatively mild conditions (pH 8.0) (Sun et al., 2022). Specifically, PFOS, $\text{Fe}(\text{H}_2\text{O})_6^{2+}$, and NTA can form a penta-coordinated metal-ligand complex that undergoes a UV-induced directional electron transfer from Fe^{II} NTA to PFOS so that PFOS was decomposed through a concerted photoinduced intramolecular charge transfer instead of direct attack by e_{aq}^- (Sun et al., 2022).

The other organic solutes used are indole (Eq. (2-24)) and its derivatives (e.g., 3-indole-acetic-acid (IAA)) to generate organic radical cations and e_{aq}^- for the destruction of PFAS in water (Kugler et al., 2021; Mialocq et al., 1982; Tian et al., 2015).



The reductive degradation can be dramatically enhanced in the presence of organomodified montmorillonite (a naturally occurring clay) (Kugler et al., 2021; Tian et al., 2016; Tian & Gu, 2018). The organic modification materials are cationic surfactants, including hexadecyltrimethylammonium (HDTMA) bromide, dioctodecyldimethylammonium (DODMA) bromide, hexadecylpyridinium (HDPY) bromide, and trimethylphenylammonium (TMPA) bromide. Moreover, 12-aminolauric acid (ALA), a saturated omega fatty acid with a 12-carbon atom chain, was proposed to pre-intercalate into the interlayer space of montmorillonite to

greatly expand the interlayer space (Kugler et al., 2021). The modified clay possesses an excellent adsorption capability for both PFAS and indole solutes, creating a constrained interlayer space for ensuing reactions. When e_{aq}^- and organic radical cations are simultaneously generated there upon photolysis, the cationic radicals can be rapidly stabilized by the negatively charged planar clay structure to minimize their recombination reactions with e_{aq}^- . Consequently, e_{aq}^- can more efficiently attack the co-sorbed PFAS on the clay. The degradation performance of this approach is only slightly inhibited in the presence of DO or with a pH decrease (Tian et al., 2016).

2.3 Mechanisms of PFAS Destruction

Fundamental information regarding the ARP degradation of PFAS in water has been explored using different approaches, including identifying intermediate and final degradation products, closing mass balance of F and C over the reaction time, measurements of PFAS degradation and defluorination rates, and calculation with density functional theory (DFT). Of note, the extent of defluorination has been quantified using three parameters with different meanings, including the F index (Eq. (2-25)) (Park et al., 2009), overall defluorination ratio (overall deF%) (Eq. (2-26)) (Bentel et al., 2019), and molecular defluorination ratio (molecular deF%) (Eq. (2-27)) (Bentel et al., 2019).

$$\text{F index} = \frac{[\text{F}^-]_{\text{released}}}{[\text{PFAS}]_{\text{degraded}}} \quad (2-25)$$

$$\text{Overall deF\%} = \frac{[\text{F}^-]_{\text{released}}}{[\text{PFAS}]_0 \times N_{\text{C-F}}} \times 100\% \quad (2-26)$$

$$\text{Molecular deF\%} = \frac{[\text{F}^-]_{\text{released}}}{[\text{PFAS}]_{\text{degraded}} \times N_{\text{C-F}}} \times 100\% = \frac{\text{Overall deF\%}}{\text{DP}} \quad (2-27)$$

Here, $[F^-]_{\text{released}}$ is the molar concentration of F^- released due to degradation; $[PFAS]_0$ is the initial molar concentration of a specific parent PFAS chemical; $[PFAS]_{\text{degraded}}$ is the molar concentration of the PFAS that has been degraded; N_{C-F} is the number of C-F bonds in the parent PFAS molecule; and DP is the degradation portion of the parent PFAS (i.e., $\frac{[PFAS]_{\text{degraded}}}{[PFAS]_0}$). The F index indicates the average number of F^- produced from each decomposed parent PFAS molecule at a specific reaction time. Overall and molecular deF% are the ratios of F^- released at a specific reaction time to F present in the total (i.e., degraded + residual) and degraded parent PFAS, respectively. Overall deF% indicates an overall conversion efficiency from organic F in the original PFAS to inorganic F anions, while molecular deF% shows the average conversion efficiency of organic F to inorganic F on each decomposed parent PFAS molecule. Overall deF% has been the most commonly used among the three defluorination parameters. In the following discussion, the defluorination efficiency used is an overall defluorination ratio.

2.3.1 PFOA

Reductive degradation of PFOA with e_{aq}^- follows a second-order kinetic reaction pattern with a rate constant of $(1.7 \pm 0.5) \times 10^7 \text{ M}^{-1} \cdot \text{s}^{-1}$ (0.01 M NaClO_4 ; pH 10.0) (Huang et al., 2007). The rate of PFOA defluorination is lower than its degradation rate (Bentel et al., 2019; G. Liu et al., 2021; Ren et al., 2021; Song et al., 2013), typically at the initial reaction phase, implying that part of PFOA degradation reactions, such as the cleavage of C-C bonds on PFOA for production of F-containing intermediate products, cannot synchronously translate into the release of F^- . PFOA degradation efficiencies can reach up to 100% in an ARP system (Bentel, Liu, et al., 2020; Guo et al., 2019; G. Liu et al., 2021; Qu et al., 2010; Ren et al., 2021; Song et al., 2013; Z. Sun et al., 2018; Tian et al., 2016; Tian & Gu, 2018; Zhang et al., 2015), while the maximum defluorination efficiencies are observed to broadly vary between ~55% and 98% in the most

literature (Bentel, Liu, et al., 2020; Bentel et al., 2019; Guo et al., 2019; Qu et al., 2010; Ren et al., 2021; Song et al., 2013; Z. Sun et al., 2018; Tian et al., 2016; Tian & Gu, 2018; Zhang et al., 2015), except for two studies that reported nearly complete defluorination (Qu et al., 2010; Tian et al., 2016). The disparity of the maximum defluorination efficiencies is likely ascribed to the different experimental conditions used in these studies. However, a complete defluorination is argued to be hardly achieved from the perspective of the reductive degradation mechanisms of PFOA, as discussed later (Bentel, Liu, et al., 2020; Bentel et al., 2019).

Two major intermediate product types are identified from the PFOA reactions with e_{aq}^- , including less fluorinated carboxylic acids and shorter-chain PFCAs (Bentel et al., 2019; Qu et al., 2014; Qu et al., 2010; Ren et al., 2021; Song et al., 2013). The presence of the former products indicates the cleavage of C-F bonds as well as the ensuing H/F exchange, while the formation of the latter ones implies the scission of C-C bonds (Qu et al., 2010). Concentrations of the aforementioned degradation intermediate products are typically increased with time as a result of accumulation due to the degradation of parent compounds at the initial reaction phase, followed by a gradual decrease because the intermediates are increasingly degraded due to their reactivity toward e_{aq}^- and with the decrease of the parent compound concentrations (Bentel, Liu, et al., 2020; Bentel et al., 2019; Qu et al., 2010; Ren et al., 2021; Song et al., 2013).

Two major parallel reaction pathways have been proposed for the PFOA degradation with e_{aq}^- (**Figure 2-1**), including H/F exchange and chain shortening (Cui et al., 2020). Among all the $-CF_2-$ in a PFOA molecule, the α -position one adjacent to the carboxyl group has exhibited a high activity, likely due to the inductive effect of the head group, thereby providing the preferential reaction center (Bentel, Liu, et al., 2020; Bentel et al., 2019; Qu et al., 2010; Ren et al., 2021). Furthermore, DFT calculations reveal that for the PFCA radical anion produced

after the attachment of an extra electron, α -position C-F bonds are spontaneously stretched, facilitating the bond cleavage (Bentel et al., 2019). The ensuing cleavage of C-F bonds leads to the formation of less fluorinated organic radical anions and the elimination of F^- (Eq. (2-28)) followed by H addition (Eq. (2-29)) to accomplish H/F exchange (for PFOA, $n = 7$) (Qu et al., 2010).



The most probable structure after the two sequential H/F exchanges on α -position C-F bonds is $C_{n-1}F_{2n-1}-CH_2-COOH$ (Bentel et al., 2019). Specifically, for PFOA ($n = 7$), the intermediate is $C_6F_{13}-CH_2-COOH$ (Bentel et al., 2019). The presence of $-CH_2-$ is believed to increase the chemical recalcitrance of the degradation product (Bentel et al., 2019). Meanwhile, other hydrofluorinated degradation products generated from more H/F exchanges are identified (e.g., $C_7F_{12}H_3-COO^-$, $C_7F_{11}H_4-COO^-$, and $C_7F_9H_6-COO^-$), suggesting that the C-F bonds on the middle positions of carbon chain can also be cleaved (Bentel et al., 2019). Furthermore, the H/F exchange can occur similarly on shorter-chain PFCAAs that are produced via chain shortening.

Chain shortening is acknowledged as the other primary PFOA degradation pathway with the formation of shorter-chain PFCAAs due to the scission of C-C bonds. However, controversial pathways have been proposed to explain the mechanism. In an early study (Qu et al., 2010), photo-reductive destruction of PFOA in a UV/iodide system was investigated in ^{18}O -water with the approach used previously to explore the mechanisms governing direct UV irradiation of PFOA (Hori et al., 2004). Experimental evidence showed the formation of $[C_6F_{13}C(^{16}O)(^{16}O)]^-$, $[C_6F_{13}C(^{16}O)(^{18}O)]^-$, and $[C_6F_{13}C(^{18}O)(^{18}O)]^-$. Therefore, two C-C scission routes were presumed to simultaneously occur during reductive degradation of PFOA with e_{aq}^- (Qu et al., 2014; Qu et

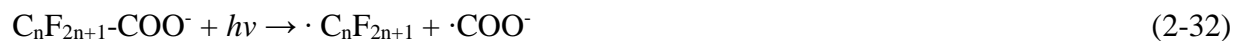
al., 2010; Song et al., 2013), which led to the production of $[\text{C}_6\text{F}_{13}\text{C}(^{16}\text{O})(^{16}\text{O})]^-$ and $[\text{C}_6\text{F}_{13}\text{C}(^{16}\text{O})(^{18}\text{O})]^- / [\text{C}_6\text{F}_{13}\text{C}(^{18}\text{O})(^{18}\text{O})]^-$, respectively.

In the first one, UV photolysis is believed to excite the PFCA degradation products after two H/F exchanges (i.e., $\text{C}_n\text{F}_{2n-1}\text{H}_2\text{-COO}^-$) to form $\cdot\text{C}_{n-1}\text{F}_{2n-1}$, $\cdot\text{COO}^-$, and CH carbenes (i.e., $:\text{CH}_2$) (Eq. (2-30)). The produced $\cdot\text{C}_{n-1}\text{F}_{2n-1}$ and $\cdot\text{COO}^-$ can be recombined to form $\text{C}_{n-1}\text{F}_{2n-1}\text{-COO}^-$ with one fewer CF_2 unit than its parent compound (Eq. (2-31)) (Qu et al., 2014; Qu et al., 2010; Song et al., 2013; Z. Sun et al., 2018).



The stepwise $-\text{CH}_2-$ removal through direct UV irradiation and aforementioned hydrolysis explains further the C-C scission of PFOA. However, the pathway has recently been questioned for two reasons (Bentel et al., 2019). Firstly, the degradation of $\text{C}_{n-1}\text{F}_{2n-1}\text{-CH}_2\text{-COO}^-$ is challenging due to the presence of $-\text{CH}_2-$, which is supported by the sluggish degradation of $\text{CF}_3\text{-CH}_2\text{-COO}^-$ with e_{aq}^- . If the above pathway were the case, all the PFOA molecules would finally be shortened to trifluoroacetic acid (TFA). Bentel et al. (Bentel et al., 2019) found that TFA could be completely defluorinated in an advanced reduction system, but a complete defluorination of PFOA was barely achieved (Bentel, Liu, et al., 2020; Bentel et al., 2019). Secondly, even though Eq. (2-30) truly occurs, the possibility of recombination of $\cdot\text{C}_{n-1}\text{F}_{2n-1}$ and $\cdot\text{COO}^-$ (Eq. (2-31)) is low due to their low concentrations (Bentel et al., 2019).

The second route is involved four sequential steps, including decarboxylation initiated by direct UV irradiation (Eq. (2-32)), hydroxylation (Eq. (2-33)), F elimination (Eq. (2-34)), and hydrolysis (Eq. (2-35)) (Bentel et al., 2019; Qu et al., 2010). The pathway is called the decarboxylation-hydroxylation-elimination-hydrolysis (DHEH) mechanism.



Among the reactions, speculative Eq. (2-32) and (2-33) were proposed in a prior study on the direct UV irradiation of PFOA (Hori et al., 2004). HF elimination from $\text{C}_n\text{F}_{2n+1}\text{OH}$ in Eq. (2-34) was previously proposed for chlorine atom - initiated photo-oxidation of methyl perfluoroalkyl ethers (Nohara et al., 2001). Along the DHEH pathway, the produced $\text{C}_{n-1}\text{F}_{2n-1}\text{COOH}$ can be further degraded repeatedly in a similar manner so that multiple CF_2 units can be stepwise lost. However, the direct photolysis hypothesis for scission of C-C bonds on PFOA is not supported by the reported evidence that a very limited defluorination efficiency is achieved during direct UV photolysis of PFOA in water (Qu et al., 2010; Song et al., 2013). In another study supporting the DHEH for chain shortening (Bentel et al., 2019; Ren et al., 2021), how the decarboxylation is initiated is not clearly stated (Cui et al., 2020). Particularly, whether or how hydrated electrons are involved in the C-C cleavage of PFOA via the DHEH mechanism was not clarified in the available literature.

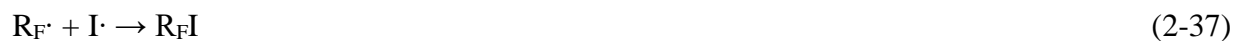
Of note, low-energy electrons can induce decarboxylation of formic acid (HCOOH) and TFA in a condensed phase (Bertin et al., 2009; Lafosse et al., 2009). Therefore, it is plausible that photo-induced hydrated electrons can initiate decarboxylation of PFOA in water in a similar manner, which may serve as the first step of the DHEH mechanism. The hypothesis was proposed to explain the scission of C-C bonds on PFOA during TiO_2 photocatalytic decomposition of PFOA in the presence of oxalic acid (Wang & Zhang, 2011). The hydrated electron-driven decarboxylation of PFCAs in water is as follows.



Following the decarboxylation involved with e_{aq}^- , the PFOA degradation product would be further degraded via Eq. (2-33) to (2-35) to accomplish the cleavage of C-C bonds via a new probable DHEH pathway. Between the two aforementioned chain shortening mechanisms (i.e., Eq. (2-30) to (2-31) and Eq. (2-32) to (2-36)), the DHEH route seems more plausible. In-depth mechanistic studies are required to elucidate the detailed C-C scission mechanisms.

Quantitative information regarding the relative contributions of the H/F exchange and chain shortening pathways to PFOA degradation is not reported. However, the measurement of the overall defluorination ratio may be informative in determining the relative importance of the two competitive mechanisms. Theoretically, a complete defluorination is barely accomplished via the H/F exchange due to the chemical persistence of the degradation products, while 100% defluorination can be achieved by chain shortening via the DHEH pathway with the final products of CO_2 , H_2O , and F^- , as shown in **Figure 2-1** (Bentel et al., 2019).

Besides the two aforementioned reaction pathways, other side reactions may simultaneously occur, as evidenced by the identification of other intermediate products, depending on the activation modes of e_{aq}^- . Various gaseous intermediates produced in the UV/iodide system are identified, such as CFHI_2 , $\text{C}_2\text{F}_4\text{HI}$, $\text{C}_5\text{F}_6\text{HI}$, $\text{C}_6\text{F}_{13}\text{I}$, and $\text{C}_6\text{F}_{10}\text{HI}$. Their formation may be a result of the incorporation of $\text{I}\cdot$ (Eq. (2-13)) into fluoridated intermediates ($\text{R}_{\text{F}}\cdot$) as follows (Park et al., 2009).



Similarly, in the UV/sulfite system, shorter chain-length fluorinated alkyl sulfonates are also observed, such as $\text{C}_7\text{F}_{15}\text{SO}_3^-$, $\text{C}_6\text{F}_{13}\text{SO}_3^-$, $\text{C}_5\text{F}_{11}\text{SO}_3^-$, $\text{C}_4\text{F}_9\text{SO}_3^-$, and $\text{C}_3\text{F}_7\text{SO}_3^-$ (Ren et al., 2021; Song et al., 2013), likely due to the incorporation of SO_3^- generated from Eq. (2-1).

2.3.2 PFOS

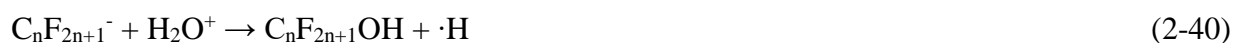
PFOS degradation with e_{aq}^- occurs through mechanisms different from the decomposition of PFOA owing to the presence of a different head group (i.e., sulfonic group) (Bentel et al., 2019; Gong & He, 2021; Gu et al., 2016; Y. Gu et al., 2017; Kugler et al., 2021; Park et al., 2009; M. Sun et al., 2018; Sun et al., 2022; Z. Sun et al., 2018). Two types of intermediate PFOS degradation products are identified, including 1) short-chain fully and partially fluorinated PFSA; and 2) PFOA and short-chain fully and partially fluorinated PFCAs (e.g., perfluoroheptanoic acid (PFHpA), perfluorohexanoic acid (PFHxA), perfluoropentanoic acid (PFPeA), and perfluorobutanoic acid (PFBA)) (Gong & He, 2021; Gu et al., 2016; M. Sun et al., 2018; Z. Sun et al., 2018). Other degradation products are also observed due to the incorporation of I⁻ or SO₃^{·-}. Particularly in a UV/iodide system, more diverse iodinated gaseous products are produced from the degradation of PFOS than the decomposition of PFOA (Park et al., 2009). Similar to the intermediate products of PFOA degradation, these daughter chemicals gradually build up and subsequently diminish in an ARP system as the reactions proceed (Bentel et al., 2019; Gu et al., 2016; Y. Gu et al., 2017). The formation of the different intermediate degradation products implies that the PFOS decomposition with e_{aq}^- occurs through multiple competitive reaction mechanisms.

Three reaction pathways have been proposed to explain the reductive destruction of PFOS with e_{aq}^- , including desulfonation, H/F exchange, and chain shortening via direct C-C cleavage (**Figure 2-2**) (Bentel et al., 2019; Gu et al., 2016; Y. Gu et al., 2017; M. Sun et al., 2018). During desulfonation, the attachment of e_{aq}^- breaks down the C-S bond between the head group and perfluoroalkyl chain. The C-S scission relatively readily occurs (Eq. (2-38) to (2-40)) because C-S (272 kJ/mol) in PFOS has lower bond energy than C-C (346 kJ/mol). Moreover, the

distance between C and S atoms (4.463 Å) is longer than that of C-C (1.529-1.627 Å) or S-O (1.651 Å) on PFOS (Erkoç & Erkoç, 2001). DFT calculations also indicate the C-S bond stretching after the formation of $\cdot C_nF_{2n+1}SO_3^{2-}$ (n=8) in Eq. (2-38), suggesting dissociation of the sulfonate group and the perfluoroalkyl chain (Bentel et al., 2019).



However, two slightly different dissociation routes have been proposed to describe the following C-S scission. In the first one, the desulfonation leads to the formation of $C_nF_{2n+1}^-$ (Eq. (2-39)) followed by the production of $C_8F_{17}OH$ (Eq. (2-40)), which would be subsequently transformed to PFOA (n=8) via Eq. (2-34) and (2-35) (Gu et al., 2016).



In the other pathway, the dissociation produces $\cdot C_nF_{2n+1}$ (Eq. (2-41)), which can be transformed to PFOA (n=8) through Eq. (2-33) to (2-35) (Bentel et al., 2019).



The second desulfonation pathway may be more plausible because the alkaline condition for the ARP treatment disfavors the occurrence of Eq. (2-40). Although desulfonation does not directly eliminate F or shorten the C-C chain, H/F exchange and chain shortening can occur during the subsequent reductive destruction of PFOA, as discussed above.

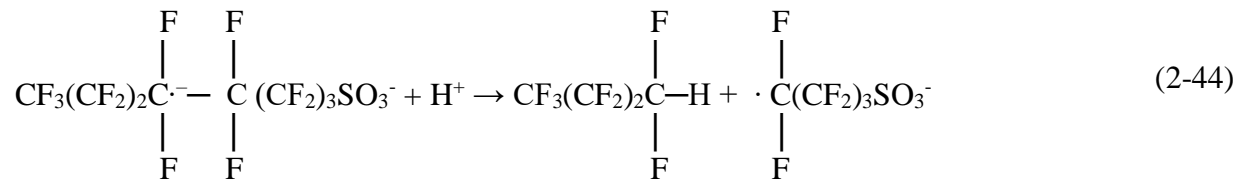
H-F exchange represents another PFOS degradation pathway that can eliminate F but cannot break down C-C bonds. Besides the occurrence of the aforementioned H/F exchange on the PFCAs (the PFOS degradation products), H/F exchange may happen on relatively weak C-F bonds of PFOS after the attachment of e_{aq}^- (Bentel et al., 2019; Y. Gu et al., 2017; Park et al., 2009). The e_{aq}^- attachment preferentially attacks one of the centermost C-F bonds, producing

PFOS radicals (Gu et al., 2016; Park et al., 2009; Paul et al., 2004). Recent DFT calculations show that the two center ones on PFOS have the lowest bond dissociation energy (BDE) ($446.31 \text{ kJ}\cdot\text{mol}^{-1}$) among all the C-F bonds, implying that the C-F cleavages preferentially take place in the middle $-\text{CF}_2-$ chain (Bentel et al., 2019). One H/F exchange plausibly proceeds successively through Eq. (2-42) and (2-43), (Y. Gu et al., 2017) in a manner similar to the H/F exchange for PFOA (Eq. ((2-28) and (2-29)) except for the different C-F locations.

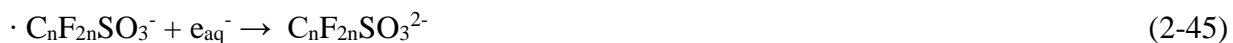


Cyclic H/F exchanges can form multiple H/F exchange products, depending on the C-F BDE (Bentel et al., 2019).

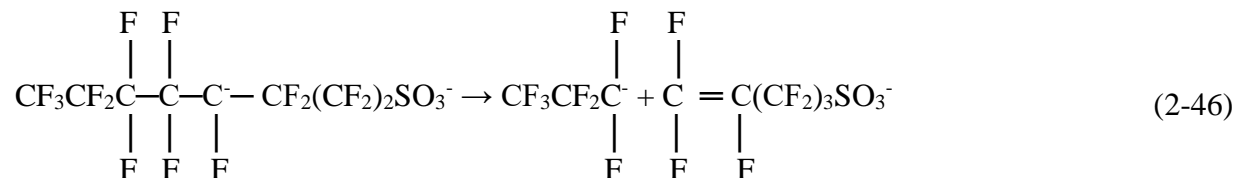
The third degradation mechanism is the direct cleavage of C-C bonds on PFOS. The lowest unoccupied molecular orbitals (LUMO) of PFOS are situated on the moiety of C4 - C8 atoms in the perfluoroalkyl chain, which exhibits a sigma antibonding nature (Gu et al., 2016). Following the attachment of e_{aq}^- on the middle $-\text{CF}_2-$, the binding between the C and C atoms would be attenuated, facilitating the breakdown of these C-C bonds. Particularly, from a thermodynamic point of view, the formation of C_3F_7^- , C_4F_9^- , and $\text{C}_5\text{F}_{11}^-$ is favorable because these dissociation fragments of PFOS have the lowest relative energies (ΔE) with respect to $\text{PFOS}\cdot$ (Gu et al., 2016). For example, two pathways are proposed to explain the plausible occurrence of reductive C-C scission on C5. The first C-C scission mechanism begins with the attachment of e_{aq}^- on the middle $-\text{CF}_2-$ to produce $\text{CF}_3(\text{CF}_2)_2\text{CF}_2\cdot^-(\text{CF}_2)_4\text{SO}_3^-$, which then complexes with a proton followed by C-C scission due to an intramolecular e transfer (Eq. (2-44)) (Park et al., 2009).



However, the contribution of Eq. (2-44) to the overall chain shortening is insignificant because of the limited availability of protons in an alkaline condition typically used for ARP treatment of PFAS. The other reaction pathway firstly proceeds through F elimination (Eq. (2-42)) to produce $\cdot\text{C}_n\text{F}_{2n}\text{SO}_3^-$, which subsequently transforms to a carbanion ($\text{C}_8\text{F}_{16}\text{SO}_3^{2-}$) after e_{aq}^- attachment (Eq. (2-45)) (Gu et al., 2016).



Thereafter, the carbanion is dissociated due to reductive cleavage of C-C to generate a shorter chain carbanion $\text{CF}_3\text{CF}_2\text{CF}_2^-$ (i.e., C_3F_7^- fragment) and an olefin (Eq. (2-46)) (Gu et al., 2016; Park et al., 2009).



Carbanion C_3F_7^- would recombine $\cdot\text{COOH}$ from the PFOA degradation to generate PFBA. The reaction pathway is indirectly evidenced by the abundance of PFBA observed among the PFOS degradation products (Gu et al., 2016). Alternatively, the carbanion reacts with H_2O^+ (Eq. (2-40)), followed by F elimination (Eq. (2-34)) and hydrolysis (Eq. (2-35)) to produce pentafluoropropionic acid (PFPrA).

2.3.3 Other PFAS

ARP destruction of other PFAS chemicals in water has also been investigated, including shorter chain PFCAs and PFSAs, per- and polyfluoro dicarboxylic acids (PFdiCAs, $\text{HOOC}-$

$C_nF_{2n}-COOH$), fluorotelomer carboxylic acids (FTCAs, $C_nF_{2n+1}-CH_2CH_2-COOH$), Perfluoroalkyl Ether Carboxylic Acids (PFECAs), and omega-hydroperfluorocarboxylates (ω -HPFCAs; $HCF_2-(CF_2)_{n-1}-COO^-$), in addition to PFOA and PFOS alternatives (e.g., F-53B and OBS (sodium ρ -perfluorous nonenoxybenzenesulfonate)) (Abusallout et al., 2021; Bao et al., 2020; Bao et al., 2018; Bao et al., 2019; Bentel, Yu, et al., 2020; Bentel et al., 2019; Cao et al., 2022; Gao et al., 2021; Jiao et al., 2022; L. Liu et al., 2022; Z. Liu et al., 2021; Park et al., 2009). Generally, degradation behaviors of the PFAS chemicals rely heavily upon their head groups. For specific PFAS types, the degradation patterns may also be influenced by chain length of the fluoroalkyl moieties, oxygen-segregated fluoroalkyl moieties, and branching extents (Bentel, Yu, et al., 2020; Bentel et al., 2019; Park et al., 2009). Below is an in-depth discussion on hydrated electron reductive degradation of other PFCAs and PFSAs, PFdiCAs, FTCAs, PFECAs, and ω -HPFCAs in water.

Degradation of other PFCAs ($n \geq 2$) in an ARP system proceeds through the two aforementioned competitive PFOA decomposition mechanisms (i.e., H/F exchange and chain shortening via DHEH). Their decomposition rates are typically greater than the rates of F^- release (Bentel et al., 2019). Moreover, both the degradation and defluorination rates of these PFCAs ($n \geq 2$) appear independent of their chain lengths. Park et al. (Park et al., 2009) found that three PFCAs ($n = 4, 6, \text{ and } 8$) had similar pseudo-first-order rate constants ($\sim 1.3 \times 10^{-3} \text{ min}^{-1}$) in a UV/iodide system, and their F indexes slightly varied between 1 and 2, suggesting a chain length-independent degradation mechanism. And, Bentel et al. (Bentel et al., 2019) reported that the overall defluorination ratios of PFCAs ($n = 2-10$) ranged narrowly within 49.1-58.2% in a UV/sulfite system.

In contrast, different mechanisms for reductive degradation of TFA ($n = 1$ PFCA) with e_{aq}^- have been proposed (Bentel et al., 2019; Jiao et al., 2022; Qu et al., 2010). One viewpoint ascribes the decomposition of TFA to two parallel pathways:(Qu et al., 2010) 1) sequential H/F exchange (Eq. (2-28) and (2-29)) that successively produces difluoroacetic acid (DFA, CF_2HCOOH) and monofluoroacetic acid (MFA, CFH_2COOH), finally generating acetic acid (CH_3COOH); and 2) the direct cleavage of C-C leads to the formation of fluoroform (CHF_3) and CO_2 , and/or generates two fragments (i.e., $\cdot CF_3$ and $\cdot COOH$), which react with water to form fluoroform and formic acid, respectively, or $\cdot CF_3$ of which recombines with itself to generate hexafluoroethane (C_2F_6). Acetic acid, formic acid, fluoroform, and hexafluoroethane are identified among the intermediate products of e_{aq}^- -initiated degradation of PFOA, which can be stepwise degraded to TFA (Qu et al., 2014; Qu et al., 2010).

However, the aforementioned TFA degradation pathways are not supported by experimental evidence from direct UV/sulfite degradation of TFA, DFA, and MFA (Bentel et al., 2019). ARP is observed to achieve complete defluorination for TFA, but not for DFA or MFA, thereby ruling out the principal role of the sequential H/F exchange pathway. Meanwhile, the rates of TFA degradation and defluorination are nearly synchronized, indicating that F^- is rapidly released, accompanied by TFA degradation. The observation does not support the aforementioned direct C-C cleavage route because the alteration of the TFA structure cannot cause an immediate release of F^- . Instead, the two unique properties of the TFA degradation, i.e., 100% defluorination and the synchronized degradation and defluorination patterns, suggest that the DHEH route is a plausibly dominant mechanism, which finally leads to the production of inorganic F^- , H_2O , and CO_2 (**Figure 2-1**) (Bentel et al., 2019).

Of interest, a different TFA degradation pathway was proposed in the UV/KI system (Jiao et al., 2022). Two major reactions occurred in this proposed pathway. First, e_{aq}^- and UV irradiation break the C-C bonds of the TFA. Second, the C-F bonds are further attacked by nucleophile e_{aq}^- and finally broken in the hydrolysis or photoreduction reaction. The experimental evidence does not support the H/F exchange process because no DFA was detected in the UV/KI system (Jiao et al., 2022). Meanwhile, the DHEH route is not the dominant mechanism in the UV/KI system, as evidenced by the formation of $HCOO^-$, CH_3COO^- , and CF_3H as the intermediate products before generating the final products CO_2 and F^- in the UV/KI system (Jiao et al., 2022). Specifically, the intermediate products in the UV/KI system (e.g., $HCOO^-$) would not be generated during the DHEH pathway because the intermediate product of DHEH was CF_3OH , which could not be detected in the UV/KI system (Jiao et al., 2022).

In contrast with PFCAs, degradation and defluorination rates of different PFSA are noticeably reduced with the decreasing chain length (Bentel et al., 2019; Park et al., 2009). For example, in a UV/iodide system, the decay rate of perfluorobutane sulfonate (PFBS) was reported to be only 13% of the PFOS decomposition rate under identical experimental conditions (Park et al., 2009). At $n = 1$, the decay and F^- release of $CF_3SO_3^-$ are almost marginal (Bentel et al., 2019). The chain-length reliance is ascribed to the increasing strengths of primary and secondary C-F bonds with the decreasing chain length. F^- release preferentially occurs from the middle – CF_2 – where extra electrons tend to attach during the initial defluorination phase.

Reductive destruction of four other PFAS, including PFdiCAs, FTCAs, PFECAs, and ω -HPFCAs in water has also been studied (Bao et al., 2018; Bentel, Yu, et al., 2020; Bentel et al., 2019; Gao et al., 2021). PFdiCAs have two – COO^- on the two chain ends, different from corresponding PFCAs (with the same perfluoroalkyl chain length), having a – COO^- on one end

and a recalcitrant – CF₃ on the other. One more relatively weak link between the perfluoroalkyl chain and – COO⁻ on PFdiCA favors its degradation via H/F exchange and/or DHEH mechanisms. Bentel et al. (Bentel et al., 2019) found that PFdiCAs were more rapidly decomposed than corresponding PFCAs (n=3-10) in a UV/sulfite system. Moreover, they observed very similar overall deF% (~67%) of these compounds, indicating that defluorination of PFdiCAs is independent of their chain lengths.

Reductive degradation of FTCAs was investigated in detail (Bentel et al., 2019; Z. Liu et al., 2021). The presence of – CH₂CH₂ – considerably increases chemical persistence to e_{aq}⁻ attack, so FTCAs are more recalcitrant to reductive degradation or defluorination than the PFCAs with the same perfluoroalkyl chain length (Bentel et al., 2019). As their perfluoroalkyl chain lengths decrease, the reactivity of FTCAs is lowered. Consequently, significant degradation can only be observed for n ≥ 6 FTCAs. Similar to the degradation of PFSAs, the decay of FTCAs is believed to firstly occur on the middle C-F bonds with relatively low BDEs via H/F exchange. The assumption is supported by the identification of H/F exchange degradation products of FTCAs. In the degradation product analysis, shorter-chain PFCAs are also found in low abundance, implying that dissociation of the head group simultaneously plays a role in the FTCA degradation (Bentel et al., 2019).

Unlike PFCAs, PFECAs (e.g., GenX) contain ether C-O bonds in molecules. The degradation of PFECAs was investigated in detail (Bentel, Yu, et al., 2020). The three degradation pathways of PFECAs were proposed in the UV/SO₃²⁻ system: 1) ether C-O bond cleavage, 2) C-C bond cleavage, including the decarboxylation step of DHEH and the cleavage of -CF₃ from branched PFECAs, and 3) direct C-F bond cleavage followed by H-F exchange (Bentel, Yu, et al., 2020). Compared with traditional full-carbon-chain PFCAs, the distinct

degradation behavior of PFECAs is ascribed to their ether structure. The ether oxygen atoms enhance the bond dissociation energy of the C-F bonds on the adjacent $-CF_2-$ moieties (Bentel, 2020), which decreases the generation of H/F-exchanged polyfluorinated products that are recalcitrant to reductive defluorination. In contrast, the cleavage of ether C-O bonds produces unstable perfluoroalcohols, thereby promoting defluorination of short fluoroalkyl moieties. Of interest, the rate and extent of PFECA degradation are heavily relying on both branching extent and the chain length of oxygen-segregated fluoroalkyl moieties (Bentel, Yu, et al., 2020). It has been demonstrated that PFECAs containing longer fluorocarbon moieties (rather than a longer length of the molecule) had a lower defluorination rate, as evidenced by the higher defluorination rate of linear PFECA with short oxygen-segregated fluorocarbon moieties. Additionally, the branched PFECA showed lower defluorination percentages compared to linear PFECAs because they have a higher tendency of H/F exchange on the tertiary carbon (Bentel, Yu, et al., 2020).

The degradation of ω -HPFCAs was assessed in the UV/sulfite system (Gao et al., 2021). ω -HPFCAs have an F atom of the ω -position (i.e., terminal) CF_3 in the PFCAs replaced by an H atom (Gao et al., 2021). Two major degradation pathways of ω -HPFCAs in the UV/sulfite systems were proposed: decarboxylation and H/F exchange (Gao et al., 2021). Like PFCAs, the direct linkage between $HC_nF_{2n}-$ and $-COO^-$ enables facile degradation under UV/sulfite treatment. Surprisingly, the presence of the H atom on the remote carbon makes ω -HPFCAs more susceptible than PFCAs to decarboxylation (i.e., C-C bond cleavage from α - CF_2 to form shorter-chain ω -HPFCAs) and less susceptible to hydrodefluorination (i.e., H/F exchange) because terminal H in the ω -HPFCAs plays a critical role in lowering the BDEs of the terminal C-F bonds, based on the DFT calculations (Gao et al., 2021). However, the terminal H in ω -HPFCAs does not enable the cleavage of more C-F bonds. For instance, although the

defluorination of ω -HPFCAs ($n = 3-8$) reached 88-94%, corresponding to an increase of 3-20% compared to individual PFCAs with the same n , the total number of C–F bonds cleaved from ω -HPFCA and PFCA in the same chain length were not significantly different (Gao et al., 2021). This phenomenon can be attributed to one less C–F bond in ω -HPFCA than in the corresponding PFCA. The other potential reason is that only a limited number of fluorinated carbons (e.g., HCF_2^- , CF_3^- , and $-\text{CF}_2^-$) can be segregated by hydrocarbon moieties, thereby becoming resistant to UV/sulfite treatment.

2.4 Factors Affecting ARP Destruction of PFAS

Hydrated electron-driven reductive degradation has proven highly effective for the chemical destruction of PFAS in water. Nearly complete degradation of various PFAS can be accomplished at appropriate operating conditions (Bentel, Liu, et al., 2020; Cao et al., 2021; Gu et al., 2016; Jiao et al., 2022; Z. Liu et al., 2021; Qu et al., 2014; Qu et al., 2010; Ren et al., 2021; Song et al., 2013; M. Sun et al., 2018; Sun et al., 2017; Z. Sun et al., 2018; Tian et al., 2016; Tian & Gu, 2018). Key factors affecting the PFAS decomposition behaviors are discussed as follows.

2.4.1 Solution pH

Initial pH can significantly influence PFAS reductive degradation and defluorination with e_{aq}^- . Meanwhile, pH may evolve as the reaction proceeds, depending on the degradation extent and solution buffer capacity. The pH range studied in literature broadly varies from 2.4 - 13 (Bentel, Liu, et al., 2020; Y. Gu et al., 2017; Jiao et al., 2022; Lyu et al., 2015; Ren et al., 2021; Song et al., 2013; Sun et al., 2017; Z. Sun et al., 2018). Experimental evidence unanimously indicates that an increasing pH favors the reductive destruction, and thus the optimal pH for reductive degradation of PFAS falls within an alkaline range.

The enhancement effect of an alkaline pH is principally because less H^+ scavenges e_{aq}^- (Eq. (2-4) to (2-5)) with the increasing pH so that e_{aq}^- can be more efficiently utilized for the degradation of PFAS (Buxton et al., 1988). Based on Eq. (2-4), a pH increases by 1.0 means that the reaction rate of H^+ scavenging by e_{aq}^- is decreased by one order of magnitude. Therefore, a slight pH change may noticeably alter the PFAS degradation rate.

In a UV/NTA system, the presence of NTA can greatly eliminate $\cdot OH$ due to its high reactivity toward $\cdot OH$, thereby promoting the utilization efficiency of e_{aq}^- for the destruction of PFAS (Z. Sun et al., 2018). Distributions of successively deprotonated NTA species with the pK_a values of 0.8, 1.9, 2.48, and 9.65 depending on solution pH. Because a fully deprotonated NTA is more reactive toward $\cdot OH$ than its fully or partially protonated forms, an alkaline solution would benefit the reactions of NTA and $\cdot OH$ to reduce the consumption of $\cdot OH$ for e_{aq}^- (Z. Sun et al., 2018).

However, in an ARP system using photo-irradiation of indole derivatives with organomodified clay, the inhibiting effect of pH decrease (3.0-11.0) on the PFAS degradation was reported to be insignificant (Tian & Gu, 2018). The pH-independence is ascribed to a unique micro-environment on the modified clay, where protons in the clay interlayers are appreciably replaced by large modification organic cations and e_{aq}^- is generated in the vicinity of sorbed PFAS.

On the other hand, solution pH may change as the PFAS degradation proceeds in an ARP system with limited pH buffering capacity (Y. Gu et al., 2017; Park et al., 2009; M. Sun et al., 2018). Various pH evolution patterns have been reported in literature, likely because the pH variation is simultaneously controlled by multiple factors. A major reason for the pH increase is the H^+ consumption by e_{aq}^- (Eq. (2-4)). Moreover, when direct photolysis (e.g., VUV irradiation)

generates $\cdot\text{OH}$ in the presence of sulfite, $\cdot\text{OH}$ can react with sulfite to generate OH^- and increase pH (Eq. (2-47)) (Fischer & Warneck, 1996).



For example, in a UV/sulfite system (2.4 g/L sulfite; UV irradiation: 500 W and 365 nm; and 400 mL solution), pH at an initial level of 7.00 was reported to consistently increase by 0.16 and 0.22 during the degradation of PFOA (20 mg/L) and PFOS (20 mg/L), respectively (M. Sun et al., 2018).

In contrast, other reasons can contribute to a pH decrease. For example, a rapid F^- release from PFAS defluorination can form a weak acid HF ($\text{pK}_a = 3.45$) in water, thus reducing solution pH (Y. Gu et al., 2017; Park et al., 2009). In a UV/iodide solution (10 mM iodide; UV irradiation: 8 W and 254 nm; and 30 mL solution) for the destruction of PFOS (24 μM), pH was noticed to initially increase and then decrease, exhibiting a unique bell-shaped pH curve (Park et al., 2009).

Besides the aforementioned reasons, others, such as concentrations and species of intermediate degradation products generated over the reactions, likely influence the activity of H^+ in water. Consequently, the final pH change patterns may be complex, depending on specific operational conditions. Gu et al. (Y. Gu et al., 2017) treated PFOS with VUV/sulfite (37.2 μM PFOS; pH 10; UV irradiation: 10 W and 185 nm; and 800 mL solution) using a broad range of sulfite doses (1-20 mM). A consistent pH decrease was observed at 1 mM sulfite, whereas the pH exhibited an initial decrease followed by an increase for other doses, at which the pH increase extent was increased with the increasing sulfite dose.

2.4.2 Solute Dose

The dose of the chemical solute for photo-production of e_{aq}^- is essential to the reductive degradation patterns of PFAS because it is directly related to the yield of e_{aq}^- . When SO_3^{2-} or I^- is used, the PFAS degradation and defluorination efficiencies are typically increased with an increasing solute dose until a critical level, beyond which the PFAS destruction efficiencies would decrease as the dose further increases (Qu et al., 2010; Song et al., 2013; M. Sun et al., 2018). For example, Sun et al. (M. Sun et al., 2018) reported that the degradation efficiencies of five PFAS all increased with the SO_3^{2-} dose, peaked almost at 100% at 2.4 g/L SO_3^{2-} , and decreased, to different degrees, as the SO_3^{2-} concentration increased to 4.0 g/L (20 mg/L PFDA, PFNA, PFOA, PFBA, or PFOS; pH 7.0; UV irradiation: 500 W and 365 nm; and 400 mL solution). And Qu et al. (Qu et al., 2010) found that the initial PFOA decomposition rate increased with an increase in the I^- concentration within $[I^-]:[PFOA] = 0-12$, but declined as the I^- concentration increased at $[I^-]:[PFOA] = 12-28$ (25 μ M PFOA; 0.0-0.7 mM I^- ; pH 9.0; UV irradiation: 15 W and 254 nm; and 740 mL solution).

The positive dependence of solute dose observed within a low solute dose range is ascribed to the fact that more solutes for photo-excitation can translate into more e_{aq}^- through Eq. (2-1) or Eq. (2-10) to (2-13), provided that sufficient photons are available. For example, the relative quasi-stationary concentration (RQSC) of e_{aq}^- in a UV/ SO_3^{2-} / N_2 system was concluded to reveal that RQSC is approximately linearly increased with the increasing sulfite dose at pH > 9 (Song et al., 2013). However, the potential scavenging effects for e_{aq}^- can also be gradually enhanced with the increase in the solute dose. In a UV/sulfite system, e_{aq}^- can be increasingly consumed with the increasing sulfite dose through the enhanced self-recombination of e_{aq}^- (Eq. (2-6)) and/or reaction with intermediate $S_2O_6^{2-}$ (Eq. (2-7)). Moreover, for a UV/iodide system, an

increasing I^- dose can enhance the reactions of e_{aq}^- with different I species (Eq. (2-20) and (2-21)), besides its self-recombination. Once the solute dose reaches a specific level beyond which the scavenging begins to outweigh the e_{aq}^- generation, the negative dependence of the solute dose would become dominant.

2.4.3 DO

The presence of DO can substantially decrease rates and efficiencies of PFAS degradation and defluorination in most ARP systems (Y. Gu et al., 2017; Lyu et al., 2015; Park et al., 2009; Qu et al., 2010; Song et al., 2013). The negative impact is principally attributed to the scavenging effects of O_2 (Eq. (2-8) and (2-9)) (Buxton et al., 1988). Moreover, DO can adsorb part of UV photons to reduce the yield of e_{aq}^- and thus compromise the PFAS decomposition (Hasson & Nicholls, 1971; Lyu et al., 2015). Of note, the inhibiting extent of PFAS decomposition due to DO is typically substantial. For example, in a UV/sulfite system for PFOA degradation (20 μ M PFOA; 10 mM sulfite; UV irradiation: 10 W and 254 nm; 200 mL solution; and pH 10.3), an overall defluorination ratio was reported to considerably decline from 88.5% in an N_2 purged solution to 6.4% in an air-aerated solution within 24 hours (Song et al., 2013). These findings suggest that effective destruction of PFAS mostly occurs in a strictly oxygen-deficient condition.

Efforts have been made to mitigate the negative DO impact. A strategy is the use of a high photon flux UV irradiation. Gu et al. (Gu et al., 2016) found that PFOS maintained a rapid decomposition at an initial 5 mg/L DO in an open UV/sulfite system (9.93×10^{-8} einstein/cm²·s) using a high-pressure mercury UV lamp. The UV lamp provided a higher emission density and a broader emission spectrum than low or medium-pressure UV lamps, thus promoting the e_{aq}^- quantum yield. Another approach is the adoption of appropriate chemical solutes for photo-

ionization to minimize the scavenging effect of DO for e_{aq}^- . Sun et al. (Z. Sun et al., 2018) noticed a slight difference of PFOS degradation and defluorination at oxic and anoxic conditions in a UV/NTA treatment, because NTA and UV-excited NTA (NTA^{*}) could rapidly react with O₂ and different reactive oxygen species (ROS) (e.g., O₂^{·-}) produced in the presence of O₂. Consequently, the quenching of e_{aq}^- by O₂ or ROS was lessened (Larson & Stabler, 1978; Sahul & Sharma, 1987; Sørensen & Frimmel, 1995).

2.4.4 Water Matrix Constituents

Water matrix constituents co-existing with PFAS may significantly affect the reductive destruction of PFAS in water through different mechanisms. Two constituents extensively studied are humic acid (HA) and nitrate (NO₃⁻).

2.4.4.1 HA. Dissolved organic matter (DOM) is ubiquitously present in different PFAS-polluted water matrixes, such as NOM in surface freshwater (Croue et al., 2000; Frimmel, 1998; Ma et al., 2001), effluent organic matter (EfOM) in biologically treated municipal wastewater (Jin et al., 2016; Shon et al., 2006), soil organic matter (SOM) in groundwater, and leachate organic matter (LOM) in landfill leachate (Andreottola & Cannas, 1992; Shouliang et al., 2008; Zhao et al., 2018). Because DOM is typically much more abundant than PFAS in polluted water, its impact on ARP destruction of PFAS is of interest. Although various organic types are comprised in aquatic DOM, only the effect of HA, a primary HPO DOM fraction, was investigated in the literature (Y. Gu et al., 2017; Guo et al., 2019; Ren et al., 2021; Sun et al., 2017), among which in-depth studies for evaluation of the role of HA were implemented in a UV/iodide system, rather than for a UV/sulfite ARP.

For a UV/iodide ARP treatment, enhanced and inhibiting effects of HA on the PFAS decomposition are observed at different HA concentrations (Guo et al., 2019; Sun et al., 2017),

suggesting that multiple competitive mechanisms govern the influence of HA. Experimental evidence reveals that HA can accelerate the PFAS degradation with the increasing HA concentration, but the decomposition is slowed down once HA is beyond a specific concentration. At a too high HA concentration, the PFAS degradation kinetic rate is even below that in the absence of HA. Therefore, an optimal HA exists to maximize the rate of PFAS decomposition in a UV/iodide system (Sun et al., 2017). Although HA may considerably alter the kinetic patterns of PFAS degradation, it may not accordingly change the final PFAS degradation efficiency. On the other hand, HA may exhibit different impacts on the defluorination behaviors. In a UV/iodide system (30 μ M PFOA; 0.3 mM iodide; UV irradiation: 14 W and 254 nm; and pH 10.0), rapid PFOA degradation and defluorination were noticed in the presence of HA (1.0 mg/L) only within the initial 3 hours. Thereafter, the PFOA decomposition and defluorination efficiencies with time were independent of the initial HA concentration (Guo et al., 2019). In another set of PFOS degradation experiments with nearly identical operational conditions (Sun et al., 2017), HA (0.0-30.0 mg/L) played a more complicated role. HA at 1.0 and 30.0 mg/L significantly promoted and inhibited the initial PFOS decomposition rate, respectively. However, the greatest defluorination efficiency (almost 100%) was finally achieved at 30.0 mg/L HA (Sun et al., 2017).

Four mechanisms governing HA-enhanced PFAS degradation are proposed for the UV/iodide system. The principal enhancement pathway is that HA reacts with oxidizing I-containing intermediates (e.g., I_2 , HOI, IO_3^- and I_3^-) to produce I^- , which is subsequently photo-activated to generate additional e_{aq}^- (Qu et al., 2014; Sun et al., 2017). In the second mechanism, specific functional groups on HA (e.g., quinone moieties) may serve as an electron shuttle (Kang & Choi, 2008; Scott et al., 1998), thereby mediating electron transfer between I^- and PFAS. The

third one is associated with the confinement effect of HA, in which HA bridges I^- and PFAS to form I^- -HA-PFAS adducts (Sun et al., 2017). The adducts can enable the occurrence of ensuing e_{aq}^- formation and PFAS decomposition in a local region so that the quenching of e_{aq}^- by others becomes minimal and the diffusion distance for e_{aq}^- to PFAS is shortened. Moreover, the fourth mechanism is the direct formation of extra e_{aq}^- from photo-ionization of HA in water (Wang et al., 2007). However, the contribution of this pathway is minor due to its low quantum yield of e_{aq}^- (Sun et al., 2017).

Meanwhile, three plausible mechanisms can inhibit the reductive degradation of PFAS in the presence of HA. Firstly, inhibition can be potentially caused by the UV quenching property of HA. UV blocking effects of HA fractions in NOM, EfOM, and LOM have been reported elsewhere (Lester et al., 2013; Zhang et al., 2014; Zhao et al., 2018). Competitive adsorption of HA with SO_3^{2-} or I^- for photons can directly alleviate the yield of e_{aq}^- . Secondly, the HA absorption of UV can generate various reactive species (e.g., $\cdot OH$, 1O_2 , H_2O_2 , and excited triplet state DOM (DOM^{*})), which ineffectually decompose PFAS but can oxidize the generated e_{aq}^- (Lyu et al., 2015). Thirdly, the presence or absence of specific moieties may inhibit the reductive decomposition of PFAS. Electron withdrawing groups (EWGs) (e.g., carboxylic acids on aromatic rings) on HA preferentially react with the generated e_{aq}^- (Li et al., 2019). Furthermore, the scarcity of quinone moieties would lessen electron transfer mediation. Both of them disfavor the reductive destruction of PFAS.

A net effect of HA on the PFAS degradation in the UV/iodide system relies upon competition among the aforementioned enhancement and inhibiting mechanisms. For the e_{aq}^- reductive decomposition of PFAS, the high molecular weight (MW) HA faction with more electron donating groups (EDGs) and electron transfer mediators exhibit an overall enhancement

effect, whereas the low MW molecules characterized with abundant EWGs and saturated aliphatic moieties marginally promote or even inhibit the PFAS degradation (Sun et al., 2017).

2.4.4.2 Nitrate. NO_3^- is a common surface water and groundwater solute. NO_3^- -N concentrations in the U.S. groundwater are mostly below 3 mg/L (Spalding & Exner, 1993), while its level in surface freshwater without nutrient pollution is typically less than 1 mg/L (USEPA, 2014). Gu et al. (Y. Gu et al., 2017) observed that PFAS degradation was slowed down with the increasing NO_3^- level (0.0-0.5 mM) in a VUV/sulfite system (37.2 μM PFOS; pH 10; UV irradiation: 10 W and 185 nm; and 800 mL solution). However, a significant difference among the final PFOS degradation efficiencies was not observed at 0.0-0.5 mM NO_3^- , unless the NO_3^- was increased to 1.0 mM. The NO_3^- suppression of PFAS decomposition is due to its rapid reactions with e_{aq}^- (Eq. (2-48) to (2-50))(Gonzalez et al., 2004). Ren et al. (Ren et al., 2021) displayed similar results that PFOA degradation was significant restricted when the initial NO_3^- level reached 2 mM in the UV/sulfite system (10 mg/L PFOA; sulfite 10 mM; pH 10; UV irradiation: 11 W and 254 nm; and 500 mL solution).



2.4.5 Temperature

Hydrated electron destruction of PFAS is also influenced by temperature. The reductive degradation of PFAS is improved with an increasing temperature (Lyu et al., 2015; Zhang et al., 2015), likely due to the growing collision frequency of molecules in water as the temperature increases. Pseudo-first-order rate constants of PFAS degradation or defluorination are reported to fit the Arrhenius equation at different temperature ranges (20-40°C for PFOA;(Zhang et al.,

2015) and 35-100°C for PFOS (Lyu et al., 2015)). Moreover, the same intermediate degradation products are identified in the UV/iodide degradation of PFOA at different temperatures, suggesting that the temperature change cannot alter the pathways of PFAS degradation (Zhang et al., 2015). However, the time required for a specific intermediate product to reach its maximum concentration declines with the increasing temperature because intermediate products become more reactive at a higher temperature and thus tend to react more promptly with e_{aq}^- rather than accumulate in the system (Zhang et al., 2015).

2.5 Implication of the Knowledge for Water Industry

Destruction of aqueous PFAS through e_{aq}^- -driven chemical reduction provides a technically viable treatment approach to mitigating PFAS pollution for water and wastewater industries. This approach can effectively degrade a broad range of PFAS molecules as compared to many other chemical oxidative or reductive methods, offering a promising ultimate solution to the PFAS impacts. The unique nature of the chemical reductive process has profound implications for its application in realistic treatment.

First, effluent TDS can influence how ARPs are applied to treat different PFAS-polluted water matrixes. TDS would be inevitably increased after the ARP treatment due to the formation of inert salt residuals, such as sulfate and iodide. In the literature, a typical dose of sulfite or iodide for the generation of e_{aq}^- for PFAS treatment ranges from several to a few tens of mM, leading to a TDS increase by several hundreds to thousands mg/L. Further TDS increase is expected when acid and/or alkaline is used for pH adjustment. Consequently, the direct application mode is infeasible for drinking water treatment or municipal wastewater reuse, which typically has a strict limit on the effluent salinity. For example, TDS and sulfate in the U.S. potable water should be ≤ 500 and 250 mg/L, respectively, according to the U.S. secondary

drinking water standards. Instead, under the circumstances, the indirect application of ARPs to the water or wastewater treatment may be considered. One example is that RO concentrates PFAS into membrane brine, which is later treated with ARPs to remove the accumulated PFAS in the brine. For remediating subsurface PFAS-polluted groundwater, TDS is not a limiting factor in most cases. However, *in-situ* remediation with the ARPs is impossible because direct UV irradiation is barely applied to the subsurface. Rather, PFAS-polluted groundwater, after being pumped out, can be readily *ex-situ* treated with ARPs.

Second, the complexity of the system design, operation, and maintenance can be significantly increased due to the pH adjustment and the requirement for an anoxic environment. Solution pH in most water, particularly drinking water sources and municipal wastewater, is nearly neutral. However, a moderately to highly alkaline pH is preferred to ensure an effective reductive destruction of PFAS, thus requiring a pH adjustment. However, the addition of acid and/or base increases the system complexity, effluent TDS, and treatment costs. Another factor inhibiting the PFAS decomposition efficiency is DO, which is ubiquitous in various PFAS-polluted water. To remove DO from water and subsequently maintain a low or no oxygen condition in realistic water and wastewater treatment is challenging, particularly for high-capacity treatment facilities. Controlling DO in water and wastewater typically requires additional treatment devices and costs. However, DO may not be an issue for the treatment of low-DO water or wastewater, such as landfill leachate and groundwater.

Third, the formation of undesirable degradation byproducts is a concern. Various fluoride-containing degradation products may be produced, of which some remain toxic or are greenhouse gases. Furthermore, when I^- is adopted for the e_{aq}^- generation, different iodinated byproducts have been identified due to iodide incorporation. The formation and toxicity of iodide-

containing byproducts produced from drinking water disinfection have been well documented (Bichsel & Von Gunten, 2000; Hua et al., 2006; Pan et al., 2016; Plewa et al., 2004; Richardson et al., 2008). These compounds generally exhibit more significant mammalian cell cytotoxicity and genotoxicity than their brominated and chlorinated analogues (Richardson et al., 2008).

2.6 Future Research Needs on PFAS Destruction with ARPs

Although current studies well demonstrate encouraging results on e_{aq}^- destruction of PFAS in water, further investigations are needed, including:

- 1) The dilemma of ARPs for realistic treatment is that e_{aq}^- generated is highly reactive toward both target PFAS compounds and certain water matrix constituents, which are typically much more abundant than PFAS at trace concentrations. Consequently, the fraction of e_{aq}^- allocated for the PFAS degradation is limited, leading to a low treatment efficiency. Therefore, novel approaches to minimizing the scavenging effects of different co-existing species (e.g., H^+ , DO, and NOM) for e_{aq}^- are highly demanded. Particularly, alleviation of the H^+ inhibition can reduce the reliance of ARPs on an alkaline pH and thus avoid costly pH adjustment. Another strategy is to improve the yield of e_{aq}^- using new and more efficient e_{aq}^- generation methods.
- 2) Can ARPs be combined with other physical/chemical processes and even biological methods to build more efficient multiple barriers for PFAS in water? For example, the PFAS reduction products generated from the ARP treatment may be efficiently degraded by specific chemical oxidation processes if abundant reducing functional groups remain on them or further removed by biological degradation when ARPs improve the biodegradability of these compounds.

- 3) Developing cost and energy-efficient ARP technologies using less-energy demanding activation methods (e.g., visible light) with minimal environmental impacts is essential to address the PFAS pollution. However, it is inappropriate now to carry out the techno-economic assessment (TEA) and life-cycle analysis (LCA) for ARPs and compare the technologies with existing PFAS treatment options, considering that the emerging treatment process is still at the early stage. With the advances in ARP chemistry and the technology development and optimization, the TEA and LCA will be needed in a future and more-developed phase. Residual disposal and management will also need to be considered during this assessment.

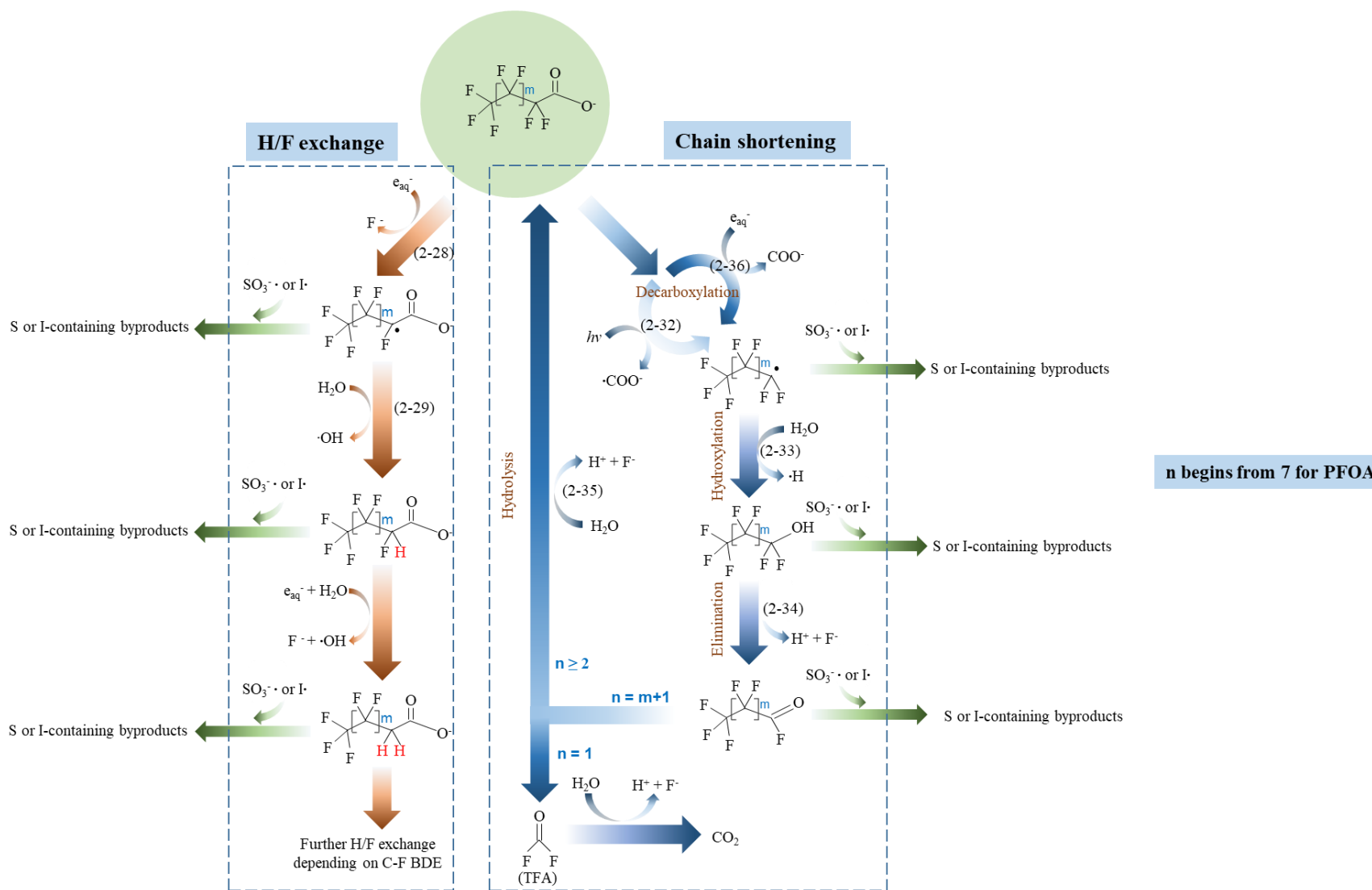


Figure 2-1 Proposed major pathways of reductive degradation of PFCAs with e_{aq}^- ($n = 7$ for PFOA) (initially, $n = m+2$; and numbers in parentheses represent the reaction numbers in this chapter).

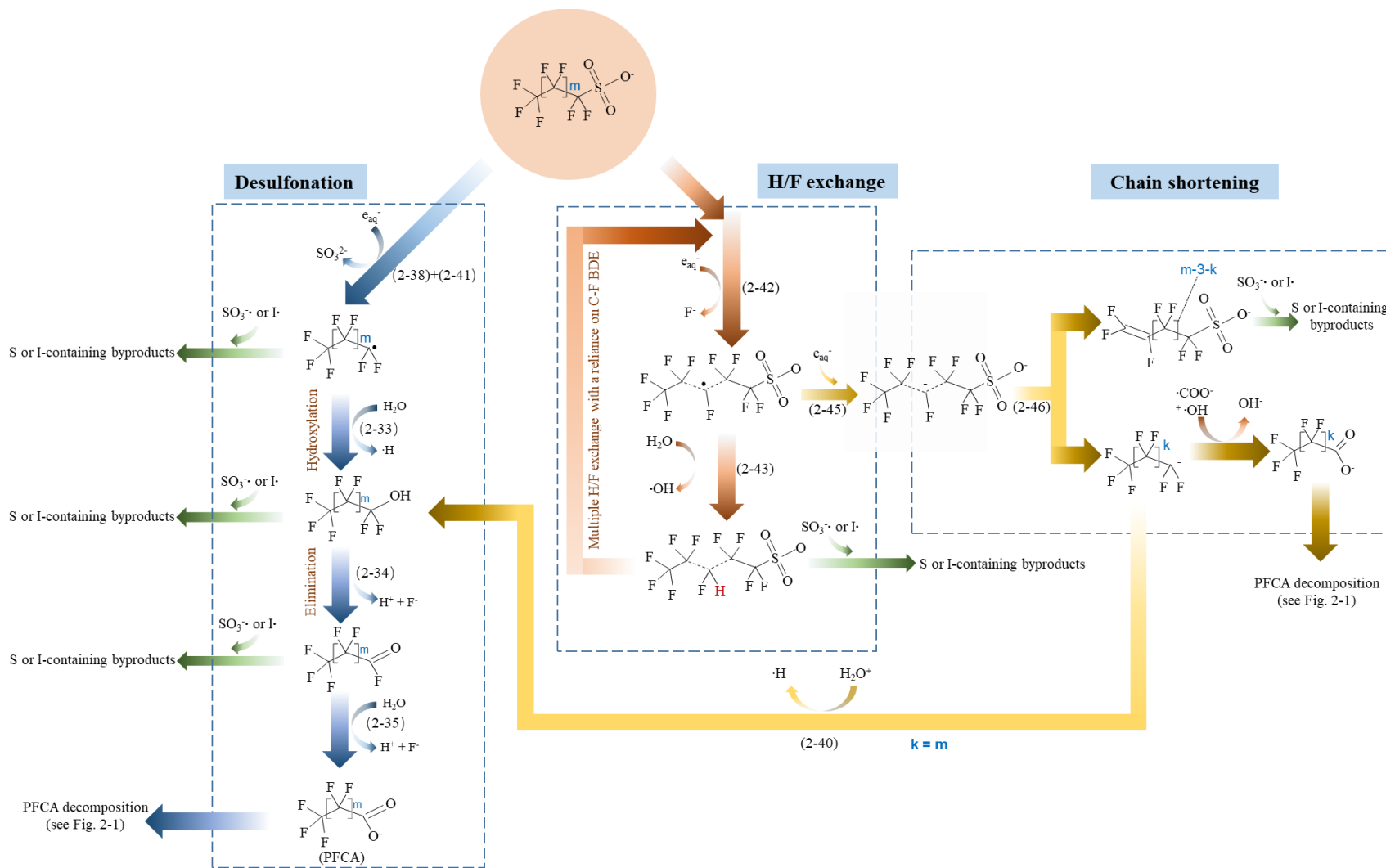


Figure 2-2 Proposed major pathways of reductive degradation of PFSAs with e_{aq}^- (initially, $n = 8$ for PFOS) ($n = m+2$; and numbers in parentheses represent the reaction numbers in this chapter)

References

- Abusallout, I., Wang, J., & Hanigan, D. (2021). Emerging investigator series: rapid defluorination of 22 per-and polyfluoroalkyl substances in water using sulfite irradiated by medium-pressure UV. *Environmental Science: Water Research & Technology*, 7(9), 1552-1562.
- Andreottola, G., & Cannas, P. (1992). 2.4 Chemical and Biological Characteristics of Landfill Leachate. *Landfilling of waste: leachate*, 1, 65.
- Bäckström, H. L. (1927). The chain-reaction theory of negative catalysis1. *Journal of the American Chemical Society*, 49(6), 1460-1472.
- Bao, Y., Cagnetta, G., Huang, J., & Yu, G. (2020). Degradation of hexafluoropropylene oxide oligomer acids as PFOA alternatives in simulated nanofiltration concentrate: Effect of molecular structure. *Chemical Engineering Journal*, 382, 122866.
- Bao, Y., Deng, S., Jiang, X., Qu, Y., He, Y., Liu, L., Chai, Q., Mumtaz, M., Huang, J., & Cagnetta, G. (2018). Degradation of PFOA Substitute: GenX (HFPO–DA Ammonium Salt): Oxidation with UV/Persulfate or Reduction with UV/Sulfite? *Environmental science & technology*, 52(20), 11728-11734.
- Bao, Y., Huang, J., Cagnetta, G., & Yu, G. (2019). Removal of F–53B as PFOS alternative in chrome plating wastewater by UV/Sulfite reduction. *Water research*, 163, 114907.
- Bensalah, N., Nicola, R., & Abdel-Wahab, A. (2014). Nitrate removal from water using UV-M/S $2 O_4^{2-}$ advanced reduction process. *International Journal of Environmental Science and Technology*, 11(6), 1733-1742.
- Bentel, M. J. (2020). *Understanding Structure–Reactivity Relationships for Aqueous Per-and Polyfluoroalkyl Substances (PFAS) Within the UV/Sulfite System UC Riverside*].
- Bentel, M. J., Liu, Z., Yu, Y., Gao, J., Men, Y., & Liu, J. (2020). Enhanced degradation of perfluorocarboxylic acids (PFCAs) by UV/sulfite treatment: Reaction mechanisms and system efficiencies at pH 12. *Environmental science & technology letters*, 7(5), 351-357.
- Bentel, M. J., Yu, Y., Xu, L., Kwon, H., Li, Z., Wong, B. M., Men, Y., & Liu, J. (2020). Degradation of Perfluoroalkyl Ether Carboxylic Acids with Hydrated Electrons: Structure–Reactivity Relationships and Environmental Implications. *Environmental Science & Technology*.
- Bentel, M. J., Yu, Y., Xu, L., Li, Z., Wong, B. M., Men, Y., & Liu, J. (2019). Defluorination of Per-and Polyfluoroalkyl Substances (PFASs) with Hydrated Electrons: Structural Dependence and Implications to PFAS Remediation and Management. *Environmental science & technology*.

- Bertin, M., Martin, I., Duvernay, F., Theulé, P., Bossa, J.-B., Borget, F., Illenberger, E., Lafosse, A., Chiavassa, T., & Azria, R. (2009). Chemistry induced by low-energy electrons in condensed multilayers of ammonia and carbon dioxide. *Physical Chemistry Chemical Physics*, *11*(11), 1838-1845.
- Bichsel, Y., & Von Gunten, U. (2000). Formation of iodo-trihalomethanes during disinfection and oxidation of iodide-containing waters. *Environmental science & technology*, *34*(13), 2784-2791.
- Botlaguduru, V. S. V., Batchelor, B., & Abdel-Wahab, A. (2015, Apr). Application of UV-sulfite advanced reduction process to bromate removal. *Journal of Water Process Engineering*, *5*, 76-82. <https://doi.org/10.1016/j.jwpe.2015.01.001>
- Buxton, G. V., Greenstock, C. L., Helman, W. P., & Ross, A. B. (1988). Critical review of rate constants for reactions of hydrated electrons, hydrogen atoms and hydroxyl radicals ($\cdot\text{OH}/\cdot\text{O}^-$) in aqueous solution. *Journal of Physical and Chemical Reference Data*, *17*(2), 513-886.
- Cao, H., Zhang, W., Wang, C., Liang, Y., & Sun, H. (2022). Photodegradation of F-53B in aqueous solutions through an UV/Iodide system. *Chemosphere*, *292*, 133436.
- Cao, Y., Qiu, W., Li, J., Jiang, J., & Pang, S. (2021). Review on UV/sulfite process for water and wastewater treatments in the presence or absence of O_2 . *Science of the Total Environment*, *765*, 142762.
- Casey, J. R., Kahros, A., & Schwartz, B. J. (2013). To be or not to be in a cavity: the hydrated electron dilemma. *The Journal of Physical Chemistry B*, *117*(46), 14173-14182.
- Chawla, O. P., Arthur, N., & Fessenden, R. W. (1973). Electron spin resonance study of the photolysis of aqueous sulfite solutions. *The Journal of Physical Chemistry*, *77*(6), 772-776.
- Croue, J.-P., Korshin, G. V., & Benjamin, M. M. (2000). *Characterization of natural organic matter in drinking water*. American Water Works Association.
- Cui, J., Gao, P., & Deng, Y. (2020). Destruction of per-and polyfluoroalkyl substances (PFAS) with advanced reduction processes (ARPs): A critical review. *Environmental Science & Technology*, *54*(7), 3752-3766.
- Deister, U., & Warneck, P. (1990). Photooxidation of sulfite (SO_3^{2-}) in aqueous solution. *Journal of Physical Chemistry*, *94*(5), 2191-2198.
- Devonshire, R., & Weiss, J. J. (1968). Nature of the transient species in the photochemistry of negative ions in aqueous solution. *The Journal of Physical Chemistry*, *72*(11), 3815-3820.

- Dogliotti, L., & Hayon, E. (1968). Flash photolysis study of sulfite, thiocyanate, and thiosulfate ions in solution. *The Journal of Physical Chemistry*, 72(5), 1800-1807.
- Elliot, A. J. (1992). A pulse radiolysis study of the reaction of OH with I₂ and the decay of I₂⁻. *Canadian Journal of Chemistry*, 70(6), 1658-1661.
- Eriksen, T. E. (1974). pH Effects on the pulse radiolysis of deoxygenated aqueous solutions of sulphur dioxide. *Journal of the Chemical Society, Faraday Transactions 1: Physical Chemistry in Condensed Phases*, 70, 208-215.
- Erkoç, Ş., & Erkoç, F. (2001). Structural and electronic properties of PFOS and LiPFOS. *Journal of Molecular Structure: THEOCHEM*, 549(3), 289-293.
- Fischer, M., & Warneck, P. (1996). Photodecomposition and photooxidation of hydrogen sulfite in aqueous solution. *The Journal of Physical Chemistry*, 100(37), 15111-15117.
- Franck, J., & Scheibe, G. (1928). Über absorptionsspektren negativer halogenionen in lösung. *Zeitschrift für Physikalische Chemie*, 139(1), 22-31.
- Frimmel, F. (1998). Characterization of natural organic matter as major constituents in aquatic systems. *Journal of Contaminant Hydrology*, 35(1-3), 201-216.
- Gao, J., Liu, Z., Bentel, M. J., Yu, Y., Men, Y., & Liu, J. (2021). Defluorination of Omega-Hydroperfluorocarboxylates (ω -HPFCAs): Distinct Reactivities from Perfluoro and Fluorotelomeric Carboxylates. *Environmental Science & Technology*, 55(20), 14146-14155.
- Gehring, P., & Eschweiler, H. (1999). Ozone/electron beam process for water treatment: design, limitations and economic considerations. *Ozone: science & engineering*, 21(5), 523-538.
- Gong, X.-B., & He, Z.-W. (2021). Perfluorooctane sulfonate decomposition by a high photon flux UV/SO₃²⁻/N₂ system: kinetics and influence factors. *Water, Air, & Soil Pollution*, 232(5), 1-11.
- Gonzalez, M. G., Oliveros, E., Wörner, M., & Braun, A. M. (2004). Vacuum-ultraviolet photolysis of aqueous reaction systems. *Journal of Photochemistry and Photobiology C: Photochemistry Reviews*, 5(3), 225-246.
- Gordon, S., Hart, E., Matheson, M., Rabani, J., & Thomas, J. (1963). Reactions of the hydrated electron. *Discussions of the Faraday Society*, 36, 193-205.
- Gordon, S., Hart, E. J., Matheson, M. S., Rabani, J., & Thomas, J. (1963). Reaction constants of the hydrated electron. *Journal of the American Chemical Society*, 85(10), 1375-1377.

- Gu, J., Ma, J., Jiang, J., Yang, L., Yang, J. X., Zhang, J. Q., Chi, H. Z., Song, Y., Sun, S. F., & Tian, W. Q. (2017, Jan). Hydrated electron ($e(aq)(-)$) generation from phenol/UV: Efficiency, influencing factors, and mechanism. *Applied Catalysis B-Environmental*, 200, 585-593. <https://doi.org/10.1016/j.apcatb.2016.07.034>
- Gu, Y., Dong, W., Luo, C., & Liu, T. (2016). Efficient reductive decomposition of perfluorooctanesulfonate in a high photon flux UV/sulfite system. *Environmental science & technology*, 50(19), 10554-10561.
- Gu, Y., Liu, T., Wang, H., Han, H., & Dong, W. (2017). Hydrated electron based decomposition of perfluorooctane sulfonate (PFOS) in the VUV/sulfite system. *Science of the Total Environment*, 607, 541-548.
- Guo, C., Zhang, C., Sun, Z., Zhao, X., Zhou, Q., & Hoffmann, M. R. (2019). Synergistic impact of humic acid on the photo-reductive decomposition of perfluorooctanoic acid. *Chemical Engineering Journal*, 360, 1101-1110.
- Hart, E. J. (1964). The hydrated electron. *Science*, 146(3652), 1664-1664.
- Hart, E. J., & Anbar, M. (1970). Hydrated electron.
- Hart, E. J., Gordon, S., & Thomas, J. (1964). Rate Constants of Hydrated Electron Reactions with Organic Compounds¹. *The Journal of Physical Chemistry*, 68(6), 1271-1274.
- Hasson, V., & Nicholls, R. (1971). Absolute spectral absorption measurements on molecular oxygen from 2640-1920 AA. II. Continuum measurements 2430-1920 AA. *Journal of Physics B: Atomic and Molecular Physics*, 4(12), 1789.
- Haynes, W. M. (2014). *CRC handbook of chemistry and physics*. CRC press.
- Hayon, E., Treinin, A., & Wilf, J. (1972). Electronic spectra, photochemistry, and autoxidation mechanism of the sulfite-bisulfite-pyrosulfite systems. SO_2^- , SO_3^- , SO_4^- , and SO_5^- radicals. *Journal of the American Chemical Society*, 94(1), 47-57.
- Herbert, J. M., & Coons, M. P. (2017). The hydrated electron. *Annual review of physical chemistry*, 68, 447-472.
- Hori, H., Hayakawa, E., Einaga, H., Kutsuna, S., Koike, K., Ibusuki, T., Kiatagawa, H., & Arakawa, R. (2004). Decomposition of environmentally persistent perfluorooctanoic acid in water by photochemical approaches. *Environmental science & technology*, 38(22), 6118-6124.
- Hua, G., Reckhow, D. A., & Kim, J. (2006). Effect of bromide and iodide ions on the formation and speciation of disinfection byproducts during chlorination. *Environmental science & technology*, 40(9), 3050-3056.

- Huang, L., Dong, W., & Hou, H. (2007). Investigation of the reactivity of hydrated electron toward perfluorinated carboxylates by laser flash photolysis. *Chemical physics letters*, 436(1-3), 124-128.
- Jiao, H., Zhang, C., Yang, M., Wu, Y., Zhou, Q., & Hoffmann, M. R. (2022). Photoreductive defluorination of trifluoroacetic acid (TFA) in the aqueous phase by hydrated electrons. *Chemical Engineering Journal*, 430, 132724.
- Jin, P., Jin, X., Bjerkelund, V. A., Østerhus, S. W., Wang, X. C., & Yang, L. (2016). A study on the reactivity characteristics of dissolved effluent organic matter (EfOM) from municipal wastewater treatment plant during ozonation. *Water research*, 88, 643-652.
- Jortner, J., Levine, R., Ottolenghi, M., & Stein, G. (1961). The photochemistry of the iodide ion in aqueous solution. *The Journal of Physical Chemistry*, 65(7), 1232-1238.
- Jortner, J., Ottolenghi, M., & Stein, G. (1964). On the photochemistry of aqueous solutions of chloride, bromide, and iodide ions. *The Journal of Physical Chemistry*, 68(2), 247-255.
- Jung, B., Nicola, R., Batchelor, B., & Abdel-Wahab, A. (2014, Dec). Effect of low- and medium-pressure Hg UV irradiation on bromate removal in advanced reduction process. *Chemosphere*, 117, 663-672. <https://doi.org/10.1016/j.chemosphere.2014.09.086>
- Kang, S.-H., & Choi, W. (2008). Oxidative degradation of organic compounds using zero-valent iron in the presence of natural organic matter serving as an electron shuttle. *Environmental science & technology*, 43(3), 878-883.
- Keene, J. (1964). The absorption spectrum and some reaction constants of the hydrated electron. *Radiation Research*, 22(1), 1-13.
- Kevan, L. (1981). Solvated electron structure in glassy matrixes. *Accounts of Chemical Research*, 14(5), 138-145.
- Kugler, A., Dong, H., Li, C., Gu, C., Schaefer, C. E., Choi, Y. J., Tran, D., Spraul, M., & Higgins, C. P. (2021). Reductive defluorination of Perfluorooctanesulfonic acid (PFOS) by hydrated electrons generated upon UV irradiation of 3-Indole-acetic-acid in 12-Aminolauric-Modified montmorillonite. *Water research*, 200, 117221.
- Lafosse, A., Bertin, M., & Azria, R. (2009). Electron driven processes in ices: Surface functionalization and synthesis reactions. *Progress in Surface Science*, 84(5-6), 177-198.
- Larsen, R. E., Glover, W. J., & Schwartz, B. J. (2010). Does the hydrated electron occupy a cavity? *Science*, 329(5987), 65-69.
- Larson, R. A., & Stabler, P. P. (1978). Sensitized photooxidation of nitrilotriacetic and iminodiacetic acids. *Journal of Environmental Science & Health Part A*, 13(8), 545-552.

- Lester, Y., Sharpless, C. M., Mamane, H., & Linden, K. G. (2013). Production of photo-oxidants by dissolved organic matter during UV water treatment. *Environmental science & technology*, 47(20), 11726-11733.
- Li, C., Zheng, S. S., Li, T. T., Chen, J. W., Zhou, J. H., Su, L. M., Zhang, Y. N., Crittenden, J. C., Zhu, S. Y., & Zhao, Y. H. (2019, Mar). Quantitative structure-activity relationship models for predicting reaction rate constants of organic contaminants with hydrated electrons and their mechanistic pathways. *Water research*, 151, 468-477.
<https://doi.org/10.1016/j.watres.2018.12.010>
- Lian, R., Oulianov, D. A., Shkrob, I. A., & Crowell, R. A. (2004). Geminate recombination of electrons generated by above-the-gap (12.4 eV) photoionization of liquid water. *Chemical physics letters*, 398(1-3), 102-106.
- Liu, C. J., McKay, G., Jiang, D., Tenorio, R., Cath, J. T., Amador, C., Murray, C. C., Brown, J. B., Wright, H. B., & Schaefer, C. (2021). Pilot-scale field demonstration of a hybrid nanofiltration and UV-sulfite treatment train for groundwater contaminated by per-and polyfluoroalkyl substances (PFASs). *Water research*, 205, 117677.
- Liu, G., Feng, C., & Shao, P. (2021). Degradation of Perfluorooctanoic Acid with Hydrated Electron by a Heterogeneous Catalytic System. *Environmental Science & Technology*.
- Liu, L., Deng, S., Bao, Y., Huang, J., & Yu, G. (2022). Degradation of OBS (Sodium p-Perfluorooxide Nonenoxybenzenesulfonate) as a Novel Per-and Polyfluoroalkyl Substance by UV/Persulfate and UV/Sulfite: Fluorinated Intermediates and Treatability in Fluoroprotein Foam. *Environmental Science & Technology*.
- Liu, X., Yoon, S., Batchelor, B., & Abdel-Wahab, A. (2013a, Jun). Degradation of vinyl chloride (VC) by the sulfite/UV advanced reduction process (ARP): Effects of process variables and a kinetic model. *Science of the Total Environment*, 454, 578-583.
<https://doi.org/10.1016/j.scitotenv.2013.03.060>
- Liu, X., Yoon, S., Batchelor, B., & Abdel-Wahab, A. (2013b, Jan). Photochemical degradation of vinyl chloride with an Advanced Reduction Process (ARP) - Effects of reagents and pH. *Chemical Engineering Journal*, 215, 868-875.
<https://doi.org/10.1016/j.cej.2012.11.086>
- Liu, Z., Bentel, M. J., Yu, Y., Ren, C., Gao, J., Pulikkal, V. F., Sun, M., Men, Y., & Liu, J. (2021). Near-quantitative defluorination of perfluorinated and fluorotelomer carboxylates and sulfonates with integrated oxidation and reduction. *Environmental Science & Technology*, 55(10), 7052-7062.
- Liu, Z., Chen, Z., Gao, J., Yu, Y., Men, Y., Gu, C., & Liu, J. (2022). Accelerated Degradation of Perfluorosulfonates and Perfluorocarboxylates by UV/Sulfite+ Iodide: Reaction Mechanisms and System Efficiencies. *Environmental Science & Technology*, 56(6), 3699-3709.

- Long, F. H., Lu, H., & Eisenthal, K. B. (1990). Femtosecond studies of the presolvated electron: An excited state of the solvated electron? *Physical review letters*, *64*(12), 1469.
- Long, F. H., Lu, H., Shi, X., & Eisenthal, K. B. (1990). Femtosecond studies of electron photodetachment from an iodide ion in solution: The trapped electron. *Chemical physics letters*, *169*(3), 165-171.
- Long, F. H., Shi, X., Lu, H., & Eisenthal, K. B. (1994). Electron photodetachment from halide ions in solution: Excited-state dynamics in the polarization well. *The Journal of Physical Chemistry*, *98*(30), 7252-7255.
- Lyu, X.-J., Li, W.-W., Lam, P. K., & Yu, H.-Q. (2015). Insights into perfluorooctane sulfonate photodegradation in a catalyst-free aqueous solution. *Scientific reports*, *5*, 9353.
- Ma, H., Allen, H. E., & Yin, Y. (2001). Characterization of isolated fractions of dissolved organic matter from natural waters and a wastewater effluent. *Water research*, *35*(4), 985-996.
- Mialocq, J., Amouyal, E., Bernas, A., & Grand, D. (1982). Picosecond laser photolysis of aqueous indole and tryptophan. *The Journal of Physical Chemistry*, *86*(16), 3173-3177.
- Moussavi, G., Jiani, F., & Shekoohian, S. (2015, Sep). Advanced reduction of Cr(VI) in real chrome-plating wastewater using a VUV photoreactor: Batch and continuous-flow experiments. *Separation and Purification Technology*, *151*, 218-224.
<https://doi.org/10.1016/j.seppur.2015.07.047>
- Nohara, K., Toma, M., Kutsuna, S., Takeuchi, K., & Ibusuki, T. (2001). Cl atom-initiated oxidation of three homologous methyl perfluoroalkyl ethers. *Environmental science & technology*, *35*(1), 114-120.
- OZAWA, T., SETAKA, M., YAMAMOTO, H., & KWAN, T. (1974). On the reaction of the sulfite radical anions with thioureas. *Chemical and Pharmaceutical Bulletin*, *22*(4), 962-964.
- Pan, Y., Li, W., An, H., Cui, H., & Wang, Y. (2016). Formation and occurrence of new polar iodinated disinfection byproducts in drinking water. *Chemosphere*, *144*, 2312-2320.
- Park, H., Vecitis, C. D., Cheng, J., Choi, W., Mader, B. T., & Hoffmann, M. R. (2009). Reductive defluorination of aqueous perfluorinated alkyl surfactants: effects of ionic headgroup and chain length. *The Journal of Physical Chemistry A*, *113*(4), 690-696.
- Paul, A., Wannere, C. S., & Schaefer, H. F. (2004). Do linear-chain perfluoroalkanes bind an electron? *The Journal of Physical Chemistry A*, *108*(43), 9428-9434.

- Plewa, M. J., Wagner, E. D., Richardson, S. D., Thruston, A. D., Woo, Y.-T., & McKague, A. B. (2004). Chemical and biological characterization of newly discovered iodoacid drinking water disinfection byproducts. *Environmental science & technology*, 38(18), 4713-4722.
- Qu, Y., Zhang, C.-J., Chen, P., Zhou, Q., & Zhang, W.-X. (2014). Effect of initial solution pH on photo-induced reductive decomposition of perfluorooctanoic acid. *Chemosphere*, 107, 218-223.
- Qu, Y., Zhang, C., Li, F., Chen, J., & Zhou, Q. (2010). Photo-reductive defluorination of perfluorooctanoic acid in water. *Water research*, 44(9), 2939-2947.
- Ren, Z., Bergmann, U., & Leiviskä, T. (2021). Reductive degradation of perfluorooctanoic acid in complex water matrices by using the UV/sulfite process. *Water research*, 205, 117676.
- Richardson, S. D., Fasano, F., Ellington, J. J., Crumley, F. G., Buettner, K. M., Evans, J. J., Blount, B. C., Silva, L. K., Waite, T. J., & Luther, G. W. (2008). Occurrence and mammalian cell toxicity of iodinated disinfection byproducts in drinking water. *Environmental science & technology*, 42(22), 8330-8338.
- Sahul, K., & Sharma, B. (1987). Gamma radiolysis of nitrilotriacetic acid (NTA) in aqueous solutions. *Journal of radioanalytical and nuclear chemistry*, 109(2), 321-327.
- Schwarz, H. A. (1981). Free radicals generated by radiolysis of aqueous solutions. *Journal of Chemical Education*, 58(2), 101-105.
- Scott, D. T., McKnight, D. M., Blunt-Harris, E. L., Kolesar, S. E., & Lovley, D. R. (1998). Quinone moieties act as electron acceptors in the reduction of humic substances by humics-reducing microorganisms. *Environmental science & technology*, 32(19), 2984-2989.
- Sheu, W.-S., & Rossky, P. J. (1996). Electronic and solvent relaxation dynamics of a photoexcited aqueous halide. *The Journal of Physical Chemistry*, 100(4), 1295-1302.
- Shi, X., Long, F. H., Lu, H., & Eisenthal, K. B. (1996). Femtosecond electron solvation kinetics in water. *The Journal of Physical Chemistry*, 100(29), 11903-11906.
- Shon, H., Vigneswaran, S., & Snyder, S. A. (2006). Effluent organic matter (EfOM) in wastewater: constituents, effects, and treatment. *Critical reviews in environmental science and technology*, 36(4), 327-374.
- Shouliang, H., Beidou, X., Haichan, Y., Liansheng, H., Shilei, F., & Hongliang, L. (2008). Characteristics of dissolved organic matter (DOM) in leachate with different landfill ages. *Journal of Environmental Sciences*, 20(4), 492-498.

- Song, Z., Tang, H., Wang, N., & Zhu, L. (2013). Reductive defluorination of perfluorooctanoic acid by hydrated electrons in a sulfite-mediated UV photochemical system. *Journal of hazardous materials*, 262, 332-338.
- Sörensen, M., & Frimmel, F. H. (1995). Photodegradation of EDTA and NTA in the UV/H₂O₂ process. *Zeitschrift für Naturforschung B*, 50(12), 1845-1853.
- Spalding, R. F., & Exner, M. E. (1993). Occurrence of nitrate in groundwater—a review. *Journal of environmental quality*, 22(3), 392-402.
- Sun, M., Zhou, H., Xu, B., & Bao, J. (2018). Distribution of perfluorinated compounds in drinking water treatment plant and reductive degradation by UV/SO₃²⁻ process. *Environmental Science and Pollution Research*, 25(8), 7443-7453.
- Sun, Z., Zhang, C., Chen, P., Zhou, Q., & Hoffmann, M. R. (2017). Impact of humic acid on the photoreductive degradation of perfluorooctane sulfonate (PFOS) by UV/Iodide process. *Water research*, 127, 50-58.
- Sun, Z., Zhang, C., Jiang, J., Wen, J., Zhou, Q., & Hoffmann, M. R. (2022). UV/FelINTA as a novel photoreductive system for the degradation of perfluorooctane sulfonate (PFOS) via a photoinduced intramolecular electron transfer mechanism. *Chemical Engineering Journal*, 427, 130923.
- Sun, Z., Zhang, C., Xing, L., Zhou, Q., Dong, W., & Hoffmann, M. R. (2018). UV/nitritotriacetic acid process as a novel strategy for efficient photoreductive degradation of perfluorooctanesulfonate. *Environmental Science & Technology*, 52(5), 2953-2962.
- Swallow, A. J. (1973). Radiation chemistry. An introduction.
- Tang, Y., Shen, H., Sekiguchi, K., Kurahashi, N., Mizuno, T., Suzuki, Y.-I., & Suzuki, T. (2010). Direct measurement of vertical binding energy of a hydrated electron. *Physical Chemistry Chemical Physics*, 12(15), 3653-3655.
- Tian, H., Gao, J., Li, H., Boyd, S. A., & Gu, C. (2016). Complete defluorination of perfluorinated compounds by hydrated electrons generated from 3-indole-acetic-acid in organomodified montmorillonite. *Scientific reports*, 6, 32949.
- Tian, H., & Gu, C. (2018). Effects of different factors on photodefluorination of perfluorinated compounds by hydrated electrons in organo-montmorillonite system. *Chemosphere*, 191, 280-287.
- Tian, H., Guo, Y., Pan, B., Gu, C., Li, H., & Boyd, S. A. (2015). Enhanced photoreduction of nitro-aromatic compounds by hydrated electrons derived from indole on natural montmorillonite. *Environmental science & technology*, 49(13), 7784-7792.

- Trojanowicz, M., Bojanowska-Czajka, A., Bartosiewicz, I., & Kulisa, K. (2018). Advanced oxidation/reduction processes treatment for aqueous perfluorooctanoate (PFOA) and perfluorooctanesulfonate (PFOS)—a review of recent advances. *Chemical Engineering Journal*, 336, 170-199.
- USEPA. (2014). *Monitoring and Assessing Water Quality - Volunteer Monitoring*. <http://water.epa.gov/type/rsl/monitoring/vms510.cfm>
- Vellanki, B. P., & Batchelor, B. (2013, Nov). Perchlorate reduction by the sulfite/ultraviolet light advanced reduction process. *Journal of hazardous materials*, 262, 348-356. <https://doi.org/10.1016/j.jhazmat.2013.08.061>
- Vellanki, B. P., Batchelor, B., & Abdel-Wahab, A. (2013). Advanced reduction processes: a new class of treatment processes. *Environmental engineering science*, 30(5), 264-271.
- Waclawek, S., Ma, X., Sharma, V. K., Xiao, R., O'Shea, K. E., & Dionysiou, D. D. (2022). Making Waves: Defining Advanced Reduction Technologies from the Perspective of Water Treatment. *Water research*, 118101.
- Wang, W., Zafiriou, O. C., Chan, I.-Y., Zepp, R. G., & Blough, N. V. (2007). Production of hydrated electrons from photoionization of dissolved organic matter in natural waters. *Environmental science & technology*, 41(5), 1601-1607.
- Wang, Y., & Zhang, P. (2011). Photocatalytic decomposition of perfluorooctanoic acid (PFOA) by TiO₂ in the presence of oxalic acid. *Journal of hazardous materials*, 192(3), 1869-1875.
- Xie, B., Shan, C., Xu, Z., Li, X., Zhang, X., Chen, J., & Pan, B. (2017). One-step removal of Cr (VI) at alkaline pH by UV/sulfite process: reduction to Cr (III) and in situ Cr (III) precipitation. *Chemical Engineering Journal*, 308, 791-797.
- Yazdanbakhsh, A., Eslami, A., Moussavi, G., Rafiee, M., & Sheikhmohammadi, A. (2018). Photo-assisted degradation of 2, 4, 6-trichlorophenol by an advanced reduction process based on sulfite anion radical: Degradation, dechlorination and mineralization. *Chemosphere*, 191, 156-165.
- Yoon, S. H., Abdel-Wahab, A., & Batchelor, B. (2011). Advanced Reduction Processes for Hazardous Waste Treatment. Qatar Foundation Annual Research Forum Proceedings,
- Zhang, C., Qu, Y., Zhao, X., & Zhou, Q. (2015). Photoinduced reductive decomposition of Perfluorooctanoic acid in water: effect of temperature and ionic strength. *CLEAN—Soil, Air, Water*, 43(2), 223-228.
- Zhang, D., Yan, S., & Song, W. (2014). Photochemically induced formation of reactive oxygen species (ROS) from effluent organic matter. *Environmental science & technology*, 48(21), 12645-12653.

Zhao, R., Jung, C., Trzopek, A., Torrens, K., & Deng, Y. (2018). Characterization of ultraviolet-quenching dissolved organic matter (DOM) in mature and young leachates before and after biological pre-treatment. *Environmental Science: Water Research & Technology*, 4(5), 731-738.

Zoschke, K., Börnick, H., & Worch, E. (2014). Vacuum-UV radiation at 185 nm in water treatment—a review. *Water research*, 52, 131-145.

Chapter 3 Resin Screening and Technical Feasibility Studies

3.1 Introduction and Objectives

Among the established PFAS treatment processes, the commercially available resin (e.g., IX and non-ionic resins)-based IX is a non-destruction technology to mitigate PFAS in drinking water. IX for the PFAS removal is reviewed in **Chapter 1** (Contea et al., 2015; Deng et al., 2010; Garg et al., 2021; Senevirathna, 2010; Wanninayake, 2021; Yu et al., 2009). Although the IX applications have advantages in the alleviation of PFAS from water, they are restricted by limitations (e.g., prohibitive off-site regeneration and the production of toxic PFAS-containing regenerant waste), as discussed in **Chapter 1**.

On the other hand, the e_{aq}^- -driven ARPs have been appreciated due to their capabilities for effective degradation of a broad range of PFAS molecules in water compared to many other chemical oxidative or reductive methods. The burgeoning technology offers a promising ultimate solution to the PFAS impacts (Bao et al., 2018; Bentel et al., 2019; J. Gu et al., 2017; Gu et al., 2016; Y. Gu et al., 2017; Lyu et al., 2015; Park et al., 2009; Qu et al., 2014; Qu et al., 2010; Song et al., 2013; M. Sun et al., 2018; Sun et al., 2017; Z. Sun et al., 2018; Vellanki et al., 2013; Zhang et al., 2015), as illustrated in **Chapter 2**. However, the application of e_{aq}^- -driven ARPs to the PFAS treatment is also limited in realistic water treatment because of the increased TDS in the effluent, pH adjustment, and practical difficulty in eliminating DO from substantial water, as discussed in **Chapter 2** (Cui et al., 2020). Thus, further investigations are needed to explore a novel approach to the application of e_{aq}^- -driven ARPs to the PFAS removal in realistic water.

In this chapter, an innovative on-site cyclic PFAS treatment system based on IX and ARP is proposed to degrade PFAS sorbed on resins and regenerate resin. This approach attempted to overcome the respective shortcomings of the IX and ARP for cost and energy efficient removal

of PFAS. In the proposed scheme, each cycle is separated into two phases, i.e., IX adsorption and ARP degradation for resin regeneration and reductive PFAS defluorination. In the PFAS adsorption phase, trace PFAS in considerable water is concentrated onto a small number of resins. In the ensuing resin regeneration phase, PFAS sorbed on resins is directly destructed through e_{aq}^- -driven ARPs, accompanied by the generation of a small volume of easily managed regenerant.

The objectives of the research described in this chapter include 1) to screen for a potentially durable resin among several commercially available resins for effective PFAS adsorption; and 2) to evaluate the technical feasibility of e_{aq}^- -driven ARPs to achieve PFAS-spent resin regeneration for repeated alleviation of PFAS in water. There are two criteria for the selection of a technically durable resin with an excellent PFAS adsorption capability. First, the selected resins possess a high PFAS adsorption capability. Second, the selected resins are relatively resistant to physical and chemical destruction of the resin materials during an e_{aq}^- -driven ARP to enable cyclic PFAS adsorption. The technical feasibility is evaluated in two aspects. First, e_{aq}^- -driven ARPs could destruct the PFAS sorbed on the PFAS-laden resins for resin regeneration. Second, the ARP-treated resins could adsorb more aqueous PFAS than untreated resins. The study described in **Chapter 3** represents the first step toward developing an innovative ARP-based resin regeneration approach capable of cyclic removal of PFAS in drinking water.

3.2 Materials and Methods

3.2.1 Chemical and Reagents

All the reagents used were at least analytical grade, except as noted. WBA exchange resins (Amberlite™ IRA67 and IRA96) were purchased from Fisher Scientific. Non-ionic resins

(Amberlite™ XAD7HP and XAD4), SBA exchange resins (Amberlite™ IRA400, 900, 910, and 958), and sodium dithionate ($\text{Na}_2\text{S}_2\text{O}_6$; > 90%) were obtained from Sigma-Aldrich. PFOA (96%, ACROS Organics™), hydrochloric acid (HCl; 37% solution in water), and NaOH (> 97%) were purchased from Fisher Scientific. Sodium sulfite (Na_2SO_3 ; > 98%) and sodium sulfate (Na_2SO_4 ; > 99%) were purchased from Millipore Sigma (Burlington, MA, USA.). All the solutions were prepared using ultrapure water (> 18.2 M Ω ·cm) generated from a Milli-Q® water purification system (Milli-Q Direct 8).

3.2.2 Experiments

Eight resins were selected in this study. Selected resins are well-performed in terms of their demonstrated capability for adsorption of aqueous PFAS based on the literature data (Du et al., 2014). The resins were first rinsed to remove possible impurities on the surface by adding 0.50 g resins into 500 mL ultrapure water in a 1 L conical flask. After 20-min mixing at 60 rpm on an orbital reciprocating shaker (Thermo Scientific MaxQ™ 2508) at room temperature (25 °C), the sample was filtered with 0.45 μm nylon membrane (Corning™ nylon syringe filters). Rinsed fresh resins were collected for further analysis.

PFOA was chosen as a model PFAS species owing to its prevalence in the aquatic environment (Domingo & Nadal, 2019; Hoffman et al., 2011; Post et al., 2012). PFOA was first pre-loaded to the resins to compare the adsorption capacity among eight resins and prepare for the ensuing experiment. The preloading procedure is as follows. Selected resins (1.0 g/L) were introduced to a 500-mL 200 mg/L PFOA solution in a 1-L flask on a thermostat shaker at 150 rpm at room temperature (25°C). The initial pH was 3.0. The adsorption proceeded 24 hours before the solution was filtered using a 0.45 μm nylon membrane. Filtrate PFOA was measured to quantify pre-loaded PFOA on the resins, while the resins were collected for another run of

preloading. Overall, seven pre-loading tests were carried out for each type of resin. The PFOA pre-loaded resins were collected for further analysis.

Resin screening tests were first carried out for each type of resin to compare the adsorption isotherms of the fresh resins (i.e., untreated) and ARP-treated resins. The experiments aimed to examine whether e_{aq}^- -driven ARPs might affect the adsorption performance of the resins after the ARP treatment. Here, UV/SO₃²⁻ was selected as the representative ARP to generate e_{aq}^- . A 1 L solution containing 0.2 g rinsed fresh resins and 10 mM Na₂SO₃ was loaded in a 1 L closed thermostatic cylindrical quartz photo-reactor (model 7840-185, ACE Glass Inc.) for the UV/SO₃²⁻ treatment (**Figure 3-1**). The cylinder-shaped reactor had a height of 440 mm and a diameter of 85.5 mm. The inner and outer diameters of a 450-mm high quartz immersion well in the cylinder center were 31 and 48 mm, respectively. A 450 W medium-pressure (200 to 400 nm) mercury lamp with a UV intensity of 187 μW/cm² was placed in the quartz immersion well. Of total energy radiated, approximately 40% to 48% is in the ultraviolet portion of the spectrum. Before reactions, the solution was purged with N₂ for 40 min to eliminate DO. The initial pH was adjusted to 10.0 with 1.0 mM NaOH solution. During the UV irradiation, pH was not controlled or buffered. Cooling water was continuously circulated to control the solution temperature at 25 ± 1 °C. A magnetic stirrer was used to ensure a completely mixed state. All the UV irradiation tests were conducted in a photochemical safety cabinet. The UV/SO₃²⁻ treatment proceeded for six hours. Of note, no fresh resins were introduced in the control tests, in which the ARP degradation of PFOA occurred in a homogeneous system. After the ARP treatment, the solutions were filtered with a 0.45 μm nylon membrane and collected for further analysis. Meanwhile, the resins were collected and rinsed with ultrapure water for subsequent sorption isotherm tests. A typical batch adsorption run was performed in a 50-mL polypropylene

centrifuge tube with 40-mL of PFOA-containing solution and 0.25 g/L (i.e., 10 mg resin) of fresh or ARP-treated resins. The initial PFOA concentrations ranged from 0.12 to 1.50 mmol/L. The initial solution pH was adjusted to 7.0 with 0.1 mM NaOH. The tubes were shaken on the shaker at 150 rpm for 24 hours at room temperature. After 24 hours, the solution was filtered with a 0.45 μm nylon membrane. The filtrate was stored to measure residual PFOA to quantify the loaded PFOA on the resins, while the resins were collected for further analysis.

Feasibility tests for the PFOA-sorbed resin regeneration were performed to measure the fluoride and dissolved organic carbon (DOC) in the regenerant under different operating conditions. PFOA was initially loaded on the resins (1000 mg PFOA/g resin) before regeneration tests using the above-mentioned PFOA pre-loading method. IRA67 was selected in the regeneration tests. Seven different operating conditions include 1) control (untreated; pH = 7.0); 2) pH = 10.0 only (six hours); 3) UV only (six hours); 4) simultaneous UV (six hours) + sulfite (10 mM); 5) sulfite only (10 mM; six hours); 6) sulfate only (10 mM; six hours); and 7) sulfite only (10 mM, six hours) and ensuing UV (six hours). Specifically, a 500 mL solution containing 0.1 g PFOA pre-loaded resin was introduced in a 1 L closed thermostatic cylindrical quartz photo-reactor. The solution pH was adjusted to pH 10.0 with 1 M NaOH except for the control test (i.e., pH = 7.0). All the regeneration procedures were identical to the abovementioned UV/SO₃²⁻ treatment procedure, except that different chemicals were dosed to the regeneration solution at each operating condition. Experiments were continuously run for six or twelve hours as needed. After the regeneration test, the solution was filtered with a 0.45 μm nylon membrane. The filtrate was collected to measure DOC and fluoride in the regenerant.

The re-adsorption tests were carried out using the PFOA pre-loaded (1000 mg PFOA/g IRA67) and regenerated IRA67, which were collected from PFOA pre-loading and resin

regeneration tests, respectively. Results will be used to evaluate the feasibility of the on-site ARP-based cyclic treatment system. A typical batch adsorption run was performed in 500 mL 200 mg/L PFOA solution in a 1-L flask with 0.2 g/L IRA67 (i.e., 0.1 g) on a thermostat shaker. The initial solution pH was adjusted to 7.0 with 0.1 mM NaOH. The flasks were shaken on the shaker at 150 rpm for 24 hours at room temperature. After 24 hours, the solution was filtered with a 0.45 μm nylon membrane. The filtrate was collected for the measurement of residual PFOA.

3.2.3 Sample Analyses

Solution pH was measured with a Thermo Scientific Orion 5-Star Plus pH meter. DOC was analyzed by measuring total organic carbon (TOC) in the water filtered by a 0.45 μm nylon membrane with a TOC analyzer (TOC-L_{CPH}, Shimadzu Corp., Kyoto, Japan). The concentrations of fluoride (F_{aq}^-), SO_4^{2-} , and $\text{S}_2\text{O}_6^{2-}$ were measured using ion chromatography (881 Compact IC Pro, Metrohm) with the Standard Method 4110. Morphology and elemental analysis of the resins were determined using scanning electron microscopy (SEM) (Hitachi S-3400N) with Energy Dispersive X-Ray Spectroscopy (EDS). Concentrations of PFOA in the adsorption phase were determined by measuring TOC using a TOC analyzer. Two adsorption isotherm models were used to fit the experimental data at chemical equilibrium, including the Langmuir and Freundlich models, as shown in Eq. (3-1) and (3-2), respectively (Rahimi et al., 2014).

$$q_e = \frac{bC_e q_{\text{max}}}{1 + bC_e} \quad \text{Langmuir} \quad (3-1)$$

$$q_e = K_f C_e^{1/n} \quad \text{Freundlich} \quad (3-2)$$

Where C_e (mmol/L) is the adsorbate concentration in water at chemical equilibrium; q_{max} (mmol/g) is the maximum adsorption capacity; q_e (mmol/g) is the equilibrium sorption amount; and b , K_f , and n are constants. The non-linear least-square optimization technique was used to

evaluate how the experimentally measured data fit either adsorption isotherm model using the Solver Add-In in Microsoft Excel (Version 2020). Chi-square tests were used as a statistical “goodness-of-fit” criterion. The chi-square goodness-of-fit test is based on Eq. (3-3) and (3-4).

$$\chi^2 = \sum_{i=1}^n \frac{(\text{observed value}_i - \text{expected value}_i)^2}{\text{expected value}_i} \quad (3-3)$$

Where χ^2 is the chi-square value; the observed and expected values are experimentally measured and modeled data, respectively; and i is the number of experimental measurements.

The criterion for acceptable fit is:

$$P(\chi^2 \leq \chi_0^2) = 1 - \alpha \quad (3-4)$$

Where α is the confidence level and $\leq \chi_0^2$ is the chi-square distribution value for $n - 1$ degree of freedom. The equilibrium sorption amounts of PFOA on the fresh resins (i.e., untreated) and ARP-treated resins were compared with the Students’ t-tests (95% confidence limits) using the Solver Add-In of Microsoft Excel. All analytical results reported represent the mean of three replicate samples, with error bars corresponding to one standard deviation.

3.3 Results

For each resin, the accumulative PFOA sorbed over seven preloading cycles is shown in **Figure 3-2**. The cumulative PFOA on the resins increased with the cycle number. After each preloading cycle, the cumulative PFOA adsorbed on the resins followed the order of IRA67>IRA958>IRA910>IRA900>IRA96>IRA400>XAD4>XAD7HP. Among the eight selected resins, IRA67 was the best resin in terms of the PFOA sorption capacity. Although IRA958 and IRA910 were ranked as the second and third best-performed resins for the PFOA capture, respectively, their adsorption capacity for PFOA gradually reached a plateau after the sixth adsorption cycle.

Adsorption isotherms of PFOA on the fresh and ARP-treated resins are in **Figure 3-3**. Model parameters obtained by non-linear regression analyses with Langmuir and Freundlich model are summarized in **Tables 3-2** and **3-3**, respectively. Two different adsorption isotherm models were fit with experimental equilibrium data at ten different aqueous PFOA concentrations (i.e., 0.12, 0.18, 0.24, 0.30, 0.48, 0.60, 0.72, 0.96, 1.20, and 1.50 mmol/L). At a 95% confidence level, both the Langmuir and Freundlich models passed the goodness-of-fit tests in all the studied experimental conditions. Results showed that adsorption isotherms of PFOA on all the selected SBA exchange resins (i.e., IRA400, IRA900, IRA910, and IRA958) after e_{aq}^- -driven ARP treatment were significantly different ($p < 0.05$) from the fresh SBA exchange resins in this study. In contrast, the adsorption isotherms of PFOA on the selected WBA exchange resins (i.e., IRA67 and IRA96) and non-ionic resins (i.e., XAD4 and XAD7HP) were not significantly different ($p > 0.05$) from the fresh SBA exchange resins in the studied experimental conditions.

Residual concentrations of sulfate and dithionate in the regenerant after ARP treatment of fresh resins are illustrated in **Figure 3-5**. Although the sulfate and dithionate are the possible final products of SO_3^{2-} during the UV/ SO_3^{2-} -ARP treatment (Cui et al., 2020), the major final product in the study was sulfate, as evidenced by **Figure 3-5**. Here, no resins were used in the control test. The results showed that the concentrations of sulfate and dithionate in the SBA exchange resins were significantly different ($p < 0.05$) compared to those in the control test, indicating that the final product of SO_3^{2-} was adsorbed on the SBA exchange resins. However, the concentrations of sulfate and dithionate were not significantly different ($p > 0.05$) from the control test in the WBA exchange resins and non-ionic resins.

The DOC and fluoride released into the regenerant after regeneration of PFOA pre-loaded IRA67 (1000 mg PFOA/g resin) in different operating conditions are shown in **Figure 3-6**. When the PFOA pre-loaded resins were introduced to the control solution at pH 7.0, PFOA was desorbed from the resin to the solution based on the observation of DOC in the regenerant (2.62 mg/L) in **Figure 3-6**. More PFOA were desorbed from IRA67 to the solution at pH 10.0, as evidenced by the higher DOC in the regenerant at pH 10.0 only solution (8.73 mg/L) than DOC at pH 7.0. Meanwhile, PFOA was not further desorbed from the IRA67 with the addition of sulfite or sulfate (10 mM) because the similar regenerant DOC were observed at the pH 10.0 only, sulfite only (8.80 mg/L), and sulfate only (8.73 mg/L) solutions. The regenerant DOC after UV regeneration remained constant. However, after the ARP regeneration of resins, DOC in the simultaneous UV + sulfite and sulfite (initial) + UV (following) was dramatically decreased to 1.66 and 3.03 mg/L, respectively. The fluoride concentrations in the regenerant were 4.00 and 3.75 mg/L in simultaneous UV + sulfite and sulfite (initial) + UV (following), respectively, indicating that ARPs can degrade PFOA in the solution. This finding is in agreement with the observations reported in previous studies (Liu et al., 2022; Ren et al., 2021). In contrast, only 0.35 mg/L of fluorine was detected in regenerant in the UV only solution. No fluoride was detected in the control, pH 10.0 only, sulfite only, and sulfate only groups.

Residual DOC in the adsorption solution after re-adsorption tests of IRA67 is shown in **Figure 3-7**. The initial DOC was 46.17 mg/L. The DOC in the control test was reduced to 29.78 mg/L, indicating that the IRA67 was not fully saturated. Compared with the findings of the control tests, more PFOA was removed from the solution in the pH 10.0 only and UV only groups, as evidenced by the lower residual DOC (23.91 mg/L and 22.58 mg/L), respectively. Meanwhile, similar PFOA removals from the adsorption solution were noticed in the sulfite only

(23.34 mg/L DOC) and sulfate only (23.56 mg/L DOC) tests. Of interest, a dramatic reduction in the residual DOC was obtained in simultaneous UV + sulfite (13.89 mg/L) and sulfite (initial) + UV (following) (16.80 mg/L) tests.

3.4 Discussion

As shown in **Figure 3-2**, the cumulative PFOA adsorbed was resin-type specific. The non-ionic resins had the lowest PFOA adsorption capacity. This phenomenon can be explained from the perspective of the adsorption mechanism for IX removal of PFOA. The mechanisms governing resin removal of PFOA are complex due to the multiple interacting phenomena (Boyer et al., 2021; Dixit et al., 2021), relying heavily on the properties of resins in this study. Among the different underlying mechanisms, IX, HPO interaction, PFAS self-aggregation, and hydrogen bonding may play a potentially essential role (Boyer et al., 2021; Dixit et al., 2021; Du et al., 2014), as described in **Chapter 1**. IX has been considered as the primary reason for the PFOA removal by many IX resins (Boyer et al., 2021; Dixit et al., 2021). Because non-ionic resins (i.e., XAD4 and XAD7HP) used in this study are the ones without active charged functional groups, they had the lower PFOA adsorption capacity. Of interest, the high adsorption percentages of PFOA in non-ionic resins are likely due to its strongly HPO interaction with non-ionic resins' non-polar structure. This conclusion is supported by the fact that the resins with a more non-polar character (i.e., XAD4; HPO polystyrene matrix) have a better PFOA adsorption than those with the moderately polar character (i.e., XAD7HP; HPI polyacrylic matrix). Furthermore, as shown in **Figure 3-2**, both SBA and WBA exchange resins could effectively capture aqueous PFOA because the functional groups on WBA exchange resins remained positively charged, which allowed the interactions with negatively charged PFOA at pH 3.0. The difference in PFOA adsorption capacity in these IX resins is primarily ascribed to the difference

in the resin properties, especially matrix and porosity. The properties of eight selected resins used in **Chapter 3** is shown in **Table 3-1**. Specifically, though IRA67 and IRA958 had different porosities, they both outperformed other IX resins in terms of PFOA adsorption capacity after seven adsorption cycles. Namely, regardless of a macroporous or gel-type, all the polystyrene IX resins displayed a relatively lower PFOA adsorption capacity than polyacrylic resins, highlighting that the polymer matrix of IX resins plays a dominant role in affecting PFOA adsorption due to their various interparticle diffusion rates through different polymer matrixes. Because the polyacrylic matrix is more HPI than the polystyrene matrix, PFOA can readily transport into the resin pores (Deng et al., 2010). Moreover, among four polystyrene IX resins, IRA400 had the lowest PFOA adsorption capacity. This result can be explained based on the consideration of the porosity of IX resins. It has been shown that the microporous IX resin differs from the gel-type IX resin in physical morphology (Boyer et al., 2021). A single microporous IX particle can be considered as an ensemble of tiny microgels with an interconnected network of pores (i.e., 10-100 nm). In contrast, gel resin may be considered as a homogeneous solid phase without any significant pores in between. Only micropores (less than 2 nm) can be generated after IX resin is saturated (Li & Sengupta, 2000). Thus, it could be anticipated that the microporous resins had the potential to adsorb more PFOA because of the larger pores. However, the resin porosity barely affected the adsorption capacity of PFOA on the polyacrylic resins in this study. For example, although IRA67 possesses a gel structure, IRA67 is more HPI due to its polyacrylic matrix. As the polyacrylic matrix resins can adsorb more water in an aqueous solution than polystyrene resins (Parrish, 1977), the open structure of IRA67 in the gel phase allows faster and easier entry of PFOA.

In addition to the PFOA adsorption capacity, the durable resin structure and persistent adsorption behaviors after the ARP treatment are of essence during the technology evaluation. As shown in **Figure 3-3**, the equilibrium sorption amounts of PFOA on all the selected ARP-treated SBA exchange resins were dramatically reduced compared to the fresh resins in the studied experimental conditions, while the sorption amounts of PFOA on selected WBA exchange resins and non-ionic resins almost remained constant. This phenomenon can be explained by the following reasons. First, the active functional sites available for aqueous PFOA adsorption on the SBA resins decreased after e_{aq}^- -driven ARP treatment. Because ARP regeneration requires a basic pH for minimal H^+ scavenging of e_{aq}^- and SBA resins have a broad service pH range (0-14), SO_3^{2-} and its oxidation products (i.e., SO_4^{2-}) can considerably adsorb to the SBA exchange resins during regeneration in an alkaline environment. Consequently, the ARP-regenerated SBA exchange resins, when reused for PFOA adsorption, are expected to poorly capture aqueous PFOA because anionic SO_3^{2-} and SO_4^{2-} have occupied substantial functional sites. In contrast, the adsorption of SO_3^{2-} to WBA exchange resins at such a pH is minimal over the UV/ SO_3^{2-} treatment. Meanwhile, the adsorption of SO_3^{2-} to non-ionic resins is strictly restricted because these resins do not possess actively charged functional groups for SO_3^{2-} adsorption. These explanations are supported by the results from **Figure 3-5** and **Table 3-4**. The major chemical elements on PFOA sorbed fresh resins as well as PFOA sorbed e_{aq}^- -driven ARP treated resins using EDS spectra are compared in **Table 3-4**. Results showed that the composition fraction of sulfur on e_{aq}^- -driven ARP treated SBA exchange resins was greater than that of PFOA sorbed fresh SBA exchange resins, indirectly validating that the final product of SO_3^{2-} was adsorbed on the SBA exchange resins to occupy certain functional sites before subsequent PFOA adsorption. Second, the reduction of PFOA adsorption by SBA exchange

resins after e_{aq}^- -driven ARP treatment can be attributed to the damage to resin morphology. The SEM method was applied to visualize the evolution of resin morphology to examine the effects of UV-excited e_{aq}^- on the selected resins. The SEM images of PFOA sorbed fresh resins and PFOA sorbed e_{aq}^- -driven ARP treated resins are shown in **Figure 3-4**. After the PFOA preloading on fresh resins, most resin beads still possessed intact, smooth, and spherical structures. However, the surface of some PFOA sorbed e_{aq}^- -driven ARP treated SBA exchange resins became much coarse, accompanied by the formation of many larger cracks (e.g., IRA400 and IRA910), indicating severe material damage. As discussed above, the matrix of resins plays a critical role in the PFOA adsorption. The damage to the resin matrix can adversely influence the following PFOA adsorption, as evidenced by **Figure 3-3** regarding the sorption isotherms of PFOA on fresh resins and e_{aq}^- -driven ARP treated resins.

Here, IRA67 was selected because IRA67 showed a promising adsorption capability for aqueous PFOA (ranked No.1 among eight selected resins) and proved a stable performance for PFOA adsorption after e_{aq}^- -driven ARPs (i.e., sorption isotherm tests) in the resin screening tests. Thus, subsequent technical feasibility tests were conducted with IRA67. The DOC and fluoride released into the regenerant after regeneration of PFOA pre-loaded IRA67 (1000 mg PFOA/g resin) in different operating conditions are shown in **Figure 3-6**. The PFOA was partially desorbed in the control solution based on the DOC (2.62 mg/L) in the regenerant. The solution pH can significantly affect the PFOA adsorption capacity of WBA exchange resins. For example, the functional groups on the WBA exchange resins (e.g., tertiary amino groups on IRA67) can be gradually deprotonated as solution pH reaches the pK_a (e.g., pK_a of IRA67 = 9.3 (Miyazaki & Nakai, 2011)) of WBA resins. Therefore, more PFOA retained by electrostatic interactions are desorbed from the WBA exchange resins as solution pH increases. This

conclusion is supported by the observation of higher DOC at pH 10.0 only (8.73 mg/L). Of interest, as DOC remained constant in sulfite only (8.80 mg/L) and sulfate only (8.73 mg/L), the plausible reason for PFOA desorption in this study is the alkaline environment. This result further confirms that the adsorption of sulfite and sulfate to IRA67 resin at pH 10.0 is restricted during the UV/SO₃²⁻ regeneration. The DOC was not decreased after direct UV irradiation. Meanwhile, the observation of low concentrations of fluoride in the regenerant of UV only solution suggests that UV irradiation barely destructed PFOA in the solution. In contrast, e_{aq}⁻ generated from UV/SO₃²⁻ plays a primary role in degrading PFOA in the solution, as evidenced by the reduced DOC and high concentration of aqueous fluoride after regeneration in simultaneous UV + sulfite and sulfite (initial) + UV (following) condition. The mechanism for e_{aq}⁻-induced reductive degradation of PFOA involves H/F exchange and/or carbon chain shortening (Cui et al., 2020), as discussed in **Chapter 2**.

The IRA67, after different regeneration tests, was applied in the re-adsorption tests. The residual DOC in the adsorption solution after re-adsorption tests of IRA67 is shown in **Figure 3-7**. Compared with the results in the control test, more PFOA adsorption was observed at pH 10.0 only because more functional sites were released through PFOA desorption at pH 10.0 during the regeneration test. Further adsorption of PFOA was not observed in the UV only test compared to that of the pH 10.0 only test, which indirectly validates that direct UV irradiation did not degrade PFOA sorbed on IRA67 to release additional functional sites. Compared with the pH 10.0 only test, similar PFOA removal was noticed in the sulfite only and sulfate only tests, suggesting that the sulfite and sulfate do not occupy the additional functional sites in the previous regeneration tests at pH 10.0 to adversely affect the subsequent PFOA adsorption. A significant decrease in residual DOC was noticed in the simultaneous UV + sulfite and sulfite (initial) + UV (following)

test, indicating that e_{aq}^- can degrade PFOA sorbed on resins to release more occupied sites for capturing more PFOA in the following phase.

3.5 Conclusions

Although IX is viewed as one of the established technologies for PFAS removal, the current application of IX for alleviation of PFAS in drinking water is challenged by prohibitive off-site regeneration and the production of PFAS-containing toxic regenerant, which requires proper disposal. More importantly, because IX only transfers PFAS from water to another phase without degradation, the PFAS toxicity for public and environmental health remains. Therefore, developing an innovative and environmentally friendly IX regeneration method is urgently needed. On the other hand, ARPs have been extensively studied on a laboratory scale over the past decade. Efforts were made to advance the understanding of the PFAS degradation mechanisms and assess critical factors affecting the PFAS degradation and defluorination efficiencies. However, ARPs are barely applied to the mitigation of aqueous PFAS in realistic water treatment because of the increased TDS in effluent, DO elimination, pH adjustment, and scavenging effects of water matrix constituents. Thus, there is a significant knowledge gap in the application of ARPs to the PFAS treatment in practical water treatment.

Of note, the findings presented in this chapter serve as the first step toward developing an on-site ARP-based IX resin regeneration process for concurrently restoring resin capacity and degrading sorbed PFAS on resins to address PFAS pollution in realistic water. The major contributions from this work are summarized as follows.

- 1) IRA67 resin is selected as the promising one among eight commercially available resins for the subsequent dissertation studies because of its excellent PFOA adsorption capability

and durable physical/chemical properties for consistently high PFOA adsorption performance after e_{aq}^- -driven ARPs.

2) Results from the regeneration tests show that aqueous PFOA can be defluorinated during the UV/SO₃²⁻ ARP treatment processes to generate fluoride, implying that the regenerant waste may be less and even non-toxic.

3) The re-adsorption tests show that the UV/SO₃²⁻ ARP treatment can degrade sorbed PFOA on IRA67 and release more functional sites for capturing more aqueous PFOA in drinking water.

The encouraging results from this chapter demonstrate that an on-site ARP-based IX resin regeneration process can overcome the respective shortcomings of IX and ARP to alleviate PFOA pollution in drinking water. Therefore, the proposed IX resin regeneration process deserves further investigation for its engineering applications. As discussed in **Chapter 2**, water matrix constituents may significantly affect the PFAS degradation or defluorination efficiencies with ARPs. NOM is a ubiquitous water matrix constituent in raw water, and its concentration is several magnitudes greater than that of PFAS in water sources. In the IX adsorption phase, PFAS and NOM can be unavoidably co-loaded on IX resins, indicating that NOM may play a vital role in the proposed ARP-based IX resin regeneration process. Thus, a few key questions are raised for the in-depth development of PFOA degradation and detoxification technologies with the innovative on-site ARP-based IX resin regeneration process, including 1) Can PFOA sorbed on IRA67 be effectively degraded in a UV/SO₃²⁻ system in the presence of NOM? 2) What role does the co-sorbed NOM on the resin play during the adsorption and regeneration process? Answers will be sought in the next chapter.

Table 3-1 Properties of eight selected resins used in this chapter

Resin	Ionic vs. Non-ionic	Strong base vs. Weak base	Matrix	Porosity	Functional Group
IRA67	Ionic	Weak base	Polyacrylic	Gel	Tertiary amine
IRA96	Ionic	Weak base	Polystyrene	Macroporous	Tertiary amine
IRA400	Ionic	Strong base (Type I)	Polystyrene	Gel	Quaternary ammonium
IRA900	Ionic	Strong base (Type I)	Polystyrene	Macroporous	Trimethylammonium
IRA910	Ionic	Strong base (Type II)	Polystyrene	Macroporous	Dimethylethanol ammonium
IRA958	Ionic	Strong base (Type I)	Polyacrylic	Macroporous	Quaternary ammonium
XAD7HP	Non-ionic	N/A	Polyacrylic	Macroporous	N/A
XAD4	Non-ionic	N/A	Polystyrene	Macroporous	N/A

Note: N/A = Not applicable

Table 3-2 Model parameters determined from non-linear regression analyses with the Langmuir isotherm model for PFOA adsorption on fresh resins (i.e., untreated) and fresh resins after e_{aq}^- -driven ARPs for eight selected resins

Adsorbent	Adsorbate	Langmuir constants				
		q_{max}	b	χ^2	DF	χ_0^2
IRA67 (untreated)	PFOA	0.642	15.02	0.03	9	3.32
IRA67 (ARP treated)	PFOA	0.638	14.67	0.02	9	3.32
IRA96 (untreated)	PFOA	0.426	11.67	0.41	9	3.32
IRA96 (ARP treated)	PFOA	0.424	11.59	1.41	9	3.32
IRA400 (untreated)	PFOA	0.413	15.12	0.58	9	3.32
IRA400 (ARP treated)	PFOA	0.328	12.57	0.87	9	3.32
IRA900 (untreated)	PFOA	0.445	10.96	0.94	9	3.32
IRA900 (ARP treated)	PFOA	0.334	10.56	0.88	9	3.32
IRA910 (untreated)	PFOA	0.481	12.82	1.21	9	3.32
IRA910 (ARP treated)	PFOA	0.413	8.90	0.22	9	3.32
IRA958 (untreated)	PFOA	0.557	14.21	0.25	9	3.32
IRA958 (ARP treated)	PFOA	0.449	12.40	0.12	9	3.32
XAD7HP (untreated)	PFOA	0.284	15.90	0.33	9	3.32
XAD HP (ARP treated)	PFOA	0.276	16.61	0.23	9	3.32
XAD4 (untreated)	PFOA	0.299	9.65	0.55	9	3.32
XAD4 (ARP treated)	PFOA	0.276	9.98	0.22	9	3.32

Note: q_{max} : the maximum adsorption capacity of PFOA (mmol/g); the unit for b: L/mmol; DF: degree of freedom; χ^2 : chi-square; χ_0^2 : the chi-square at the degree of freedom of 9 at a 95% confidence level.

Table 3-3 Model parameters determined from non-linear regression analyses with the Freundlich isotherm model for PFOA adsorption on fresh resins (i.e., untreated) and fresh resins after e_{aq}^- -driven ARPs for eight selected resins

Adsorbent	Adsorbate	Freundlich constants				
		K_f	n	χ^2	DF	χ_0^2
IRA67 (untreated)	PFOA	0.639	4.61	0.23	9	3.32
IRA67 (ARP treated)	PFOA	0.633	4.60	0.11	9	3.32
IRA96 (untreated)	PFOA	0.422	3.98	1.21	9	3.32
IRA96 (ARP treated)	PFOA	0.419	3.97	1.23	9	3.32
IRA400 (untreated)	PFOA	0.404	5.18	0.31	9	3.32
IRA400 (ARP treated)	PFOA	0.326	4.34	0.43	9	3.32
IRA900 (untreated)	PFOA	0.446	3.68	0.44	9	3.32
IRA900 (ARP treated)	PFOA	0.332	3.72	0.34	9	3.32
IRA910 (untreated)	PFOA	0.486	4.06	0.12	9	3.32
IRA910 (ARP treated)	PFOA	0.412	3.22	0.44	9	3.32
IRA958 (untreated)	PFOA	0.543	4.71	0.21	9	3.32
IRA958 (ARP treated)	PFOA	0.434	4.42	0.84	9	3.32
XAD7HP (untreated)	PFOA	0.287	5.10	0.22	9	3.32
XADHP (ARP treated)	PFOA	0.280	5.25	0.22	9	3.32
XAD4 (untreated)	PFOA	0.294	3.55	0.29	9	3.32
XAD4 (ARP treated)	PFOA	0.272	3.62	0.39	9	3.32

Note: the unit for K_f : $\text{mmol}^{(1-1/n)} \text{L}^{1/n}/\text{g}$; DF: degree of freedom; χ^2 : chi-square; χ_0^2 : the chi-square at the degree of freedom of 9 at a 95% confidence level.

Table 3-4 Comparison of main chemical elements on PFOA sorbed fresh resins and PFOA sorbed e_{aq}^- -driven ARP treated resins

Resin	Carbon (C)	Nitrogen (N)	Fluorine (F)	Sulfur (S)	Chlorine (Cl)
IRA67	≈	≈	≈	≈	≈
IRA96	≈	≈	↓	≈	≈
IRA400	≈	↓	↓	↑	↓
IRA900	≈	≈	↓	↑	↓
IRA910	≈	↓	↓	↑	↓
IRA958	≈	≈	↓	↑	≈
XAD7HP	≈	≈	≈	≈	≈
XAD4	≈	≈	≈	↑	≈

Note: ≈: Composition fraction of chemical element on PFOA sorbed UV-excited e_{aq}^- -treated resins is similar to that of the PFOA sorbed fresh resins.

↑: Composition fraction of chemical element on PFOA sorbed UV-excited e_{aq}^- -treated resins is greater than that of the PFOA sorbed fresh resins.

↓: Composition fraction of chemical element on PFOA sorbed UV-excited e_{aq}^- -treated resins is lower than that of the PFOA sorbed fresh resins.

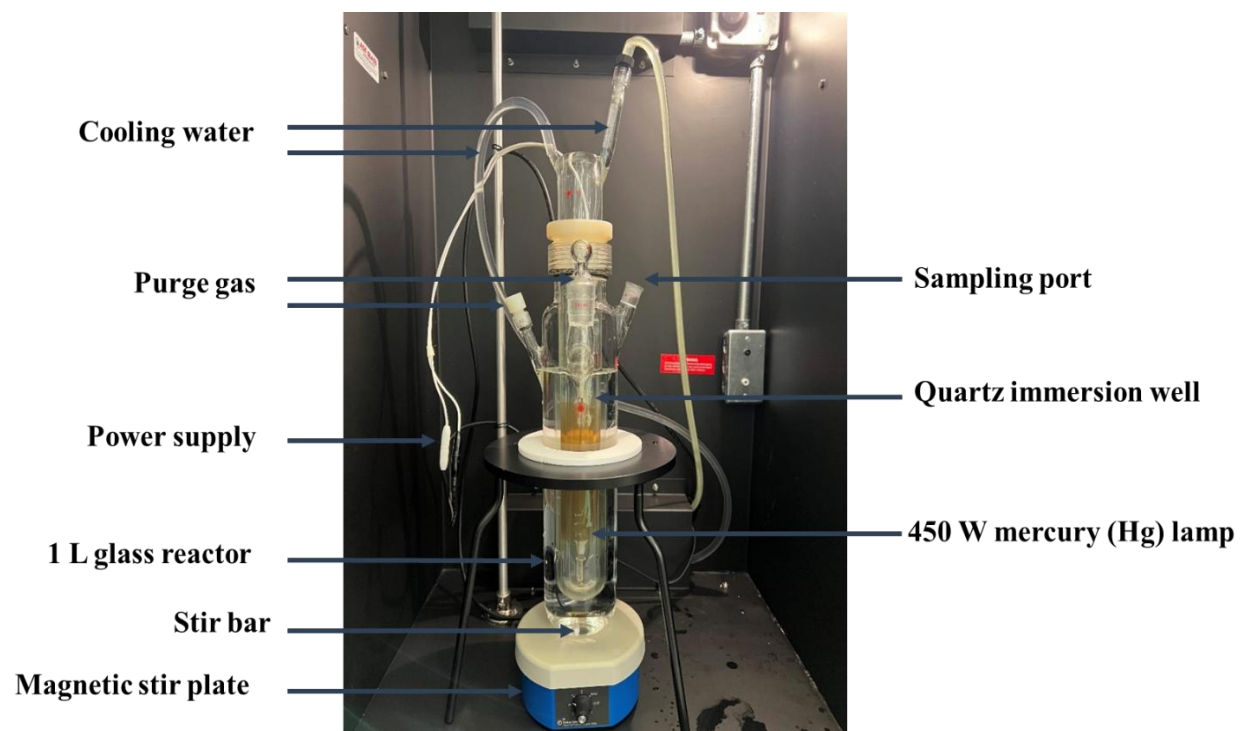


Figure 3-1 The closed thermostatic cylindrical quartz photo-reactor for the UV/SO₃²⁻ treatment

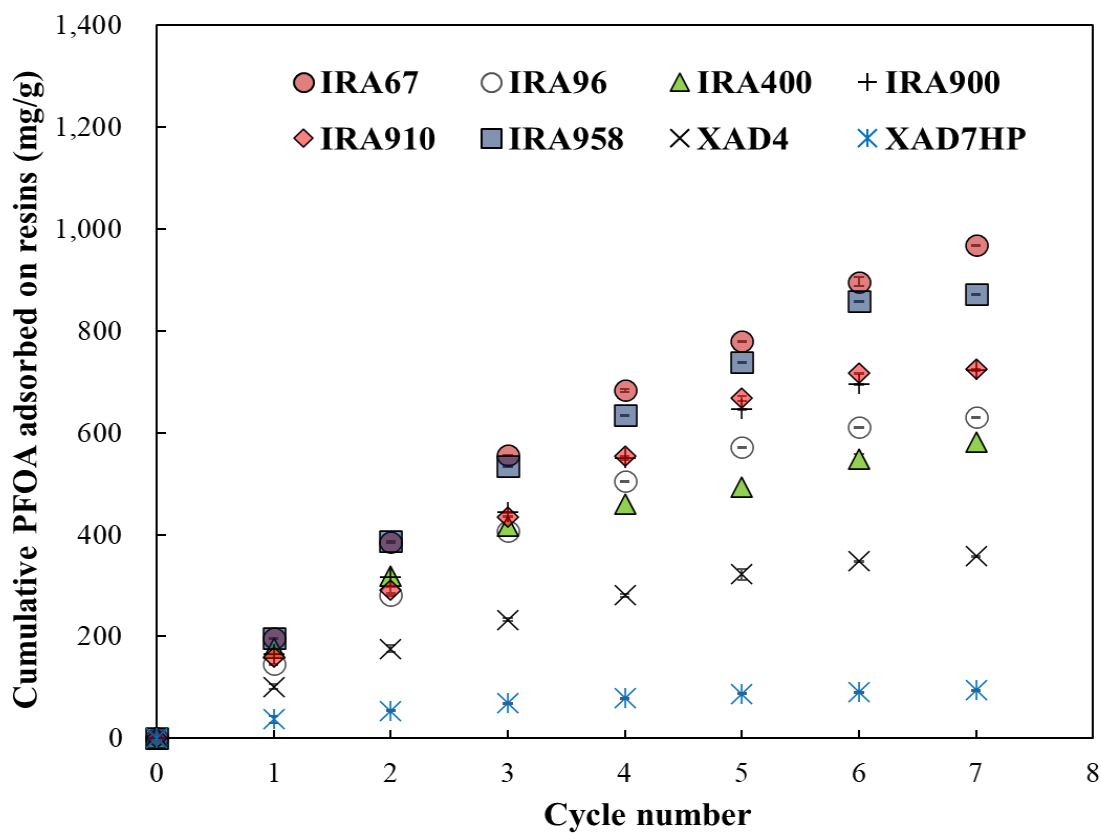
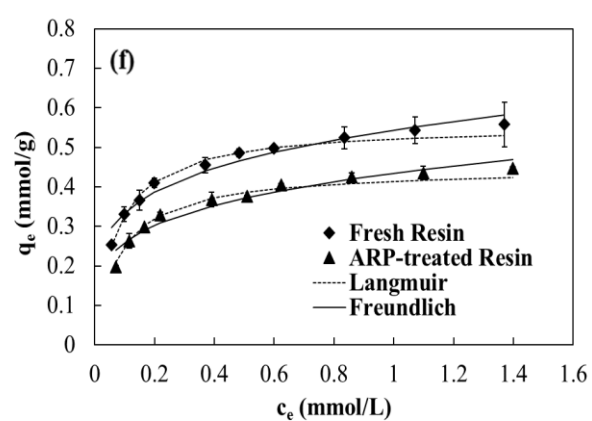
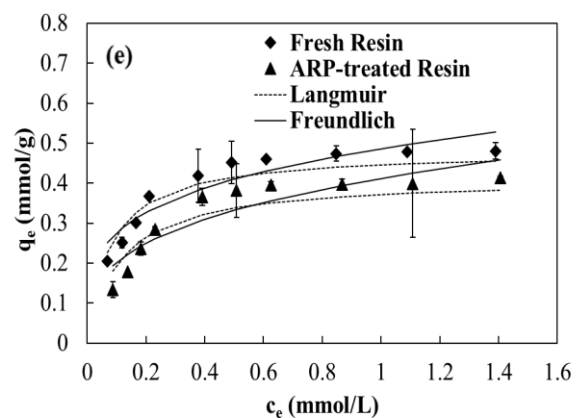
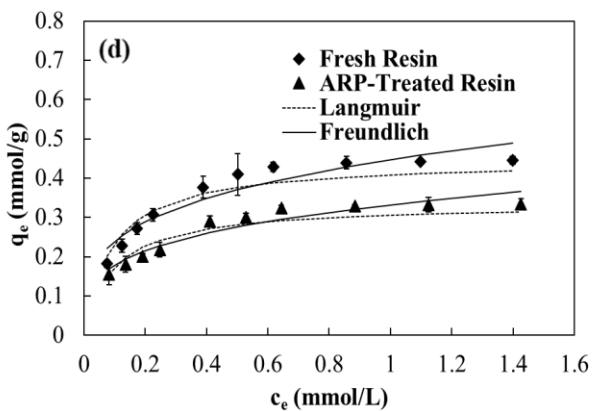
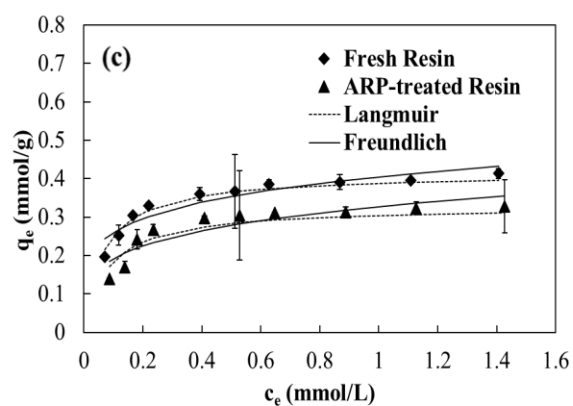
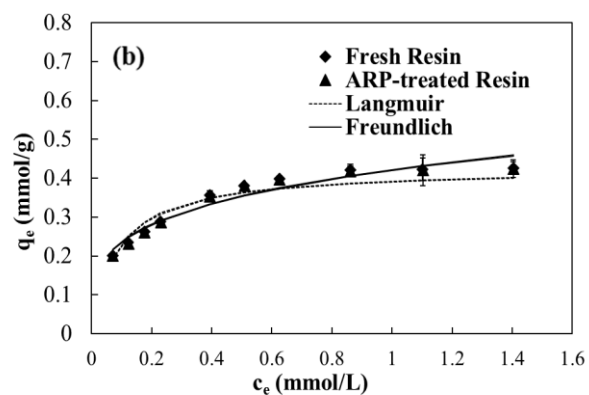
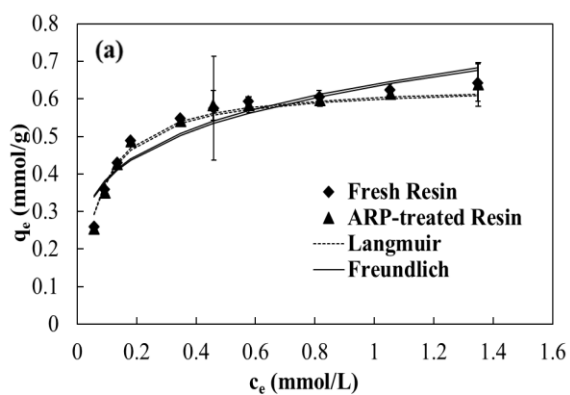


Figure 3-2 Cyclic selected resin adsorption experiment - cumulative PFOA adsorption at different cycles (Experimental condition: initial pH = 3.0; resin dosage = 1.0 g/L; initial PFOA concentration = 200 mg/L; reaction volume = 500 mL; reaction time = 24 hours)



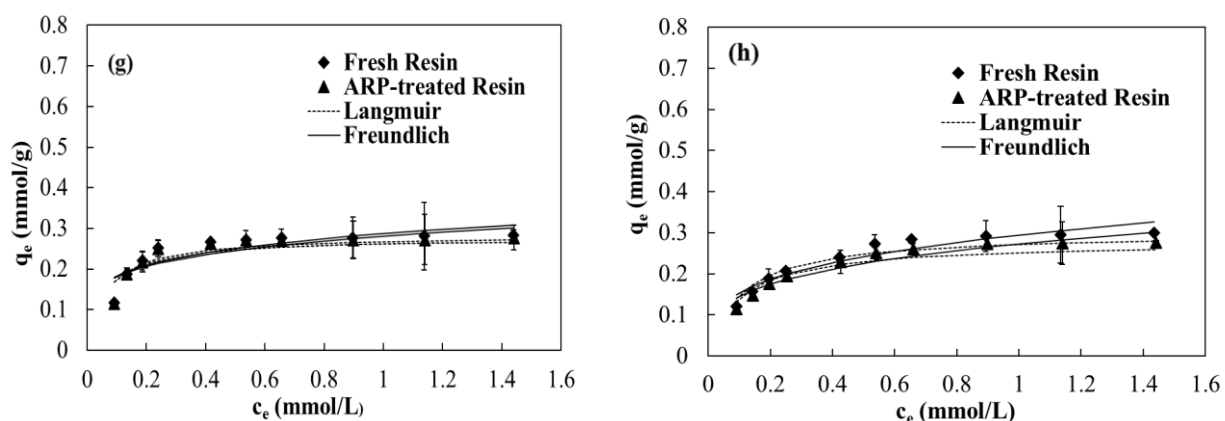
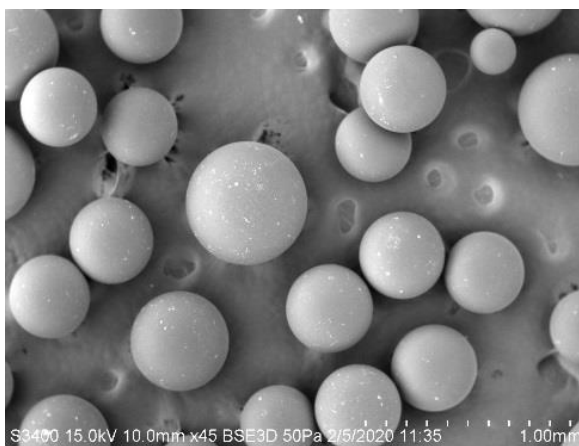
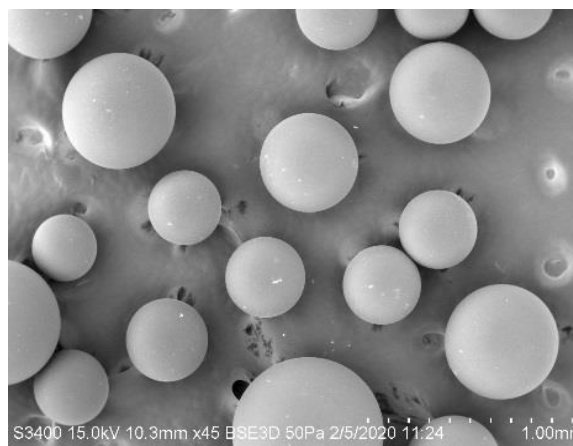


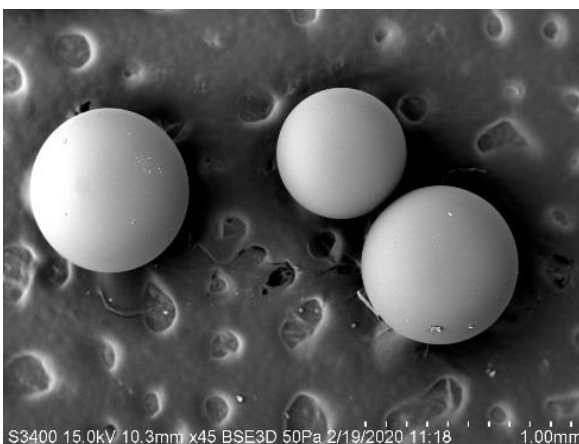
Figure 3-3 Measured and modeled adsorption isotherm data of PFOA on the fresh resins (i.e., untreated) and fresh resin after e_{aq}^- -driven ARPs (the scattered symbols, scattered lines, and solid lines represent measured, Langmuir modeled and Freundlich modeled data, respectively); a) IRA67; b) IRA96; c) IRA400; d) IRA900; e) IRA910; f) IRA958; g) XAD7HP; h) XAD4. (Experimental condition: initial pH = 7.0; resin dosage = 0.25 g/L; initial PFOA = 0.12 to 1.50 mmol/L; reaction volume = 40 mL; adsorption time = 24 hours)



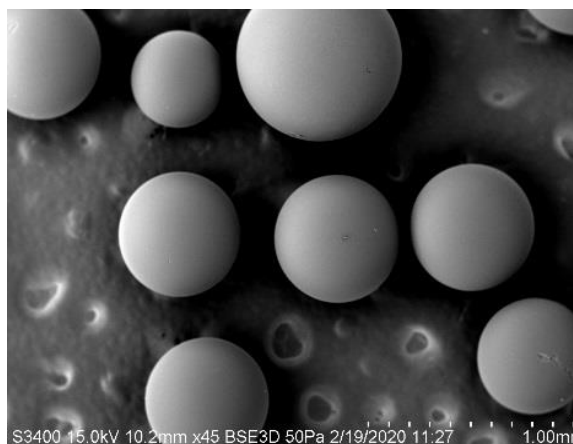
(a-1)



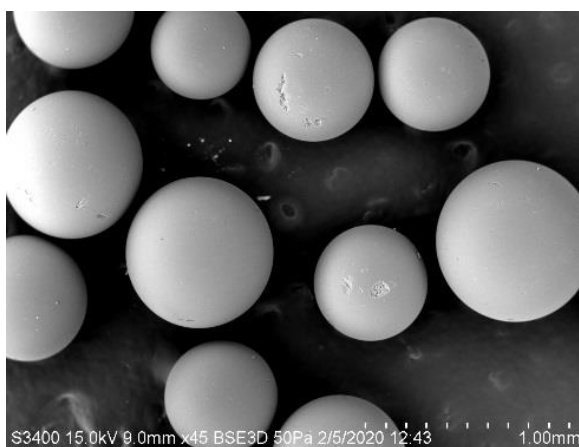
(a-2)



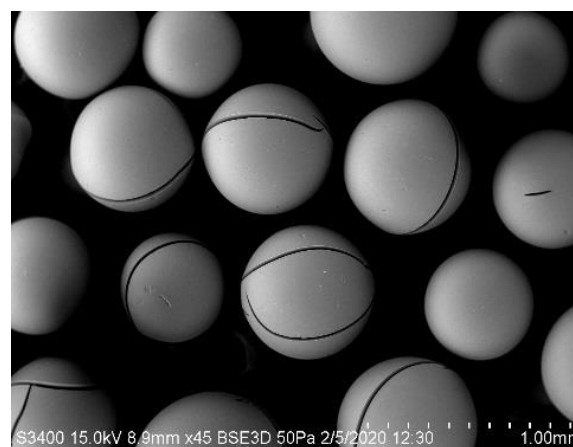
(b-1)



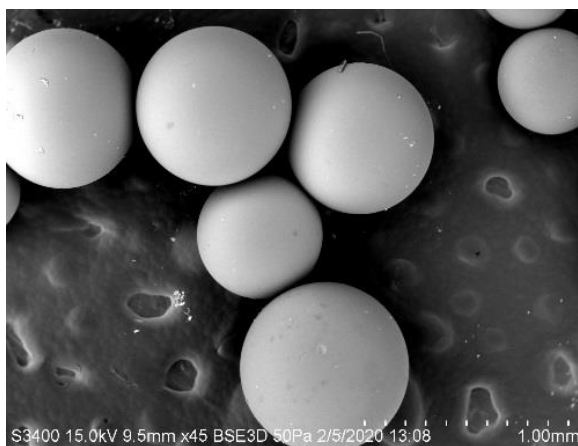
(b-2)



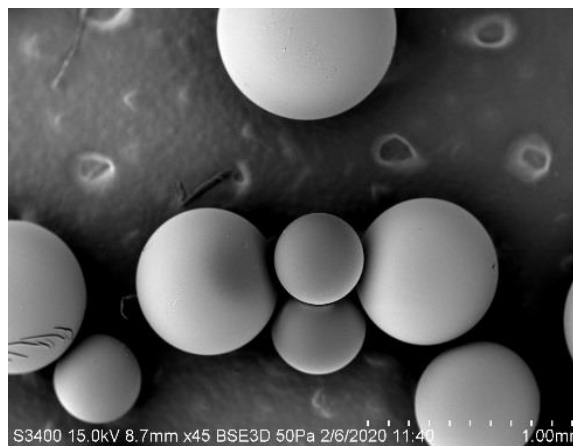
(c-1)



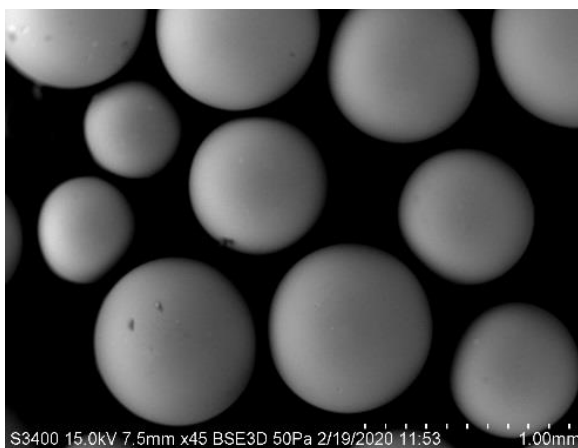
(c-2)



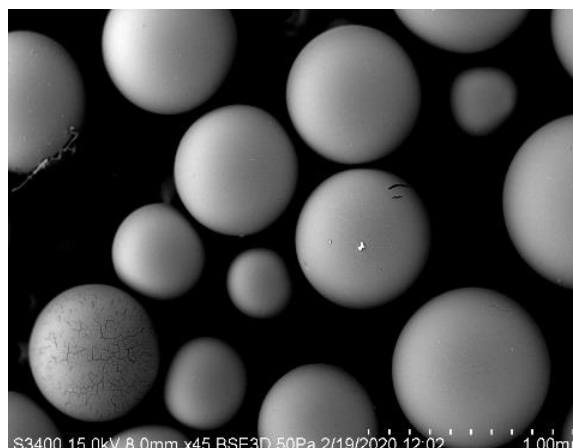
(d-1)



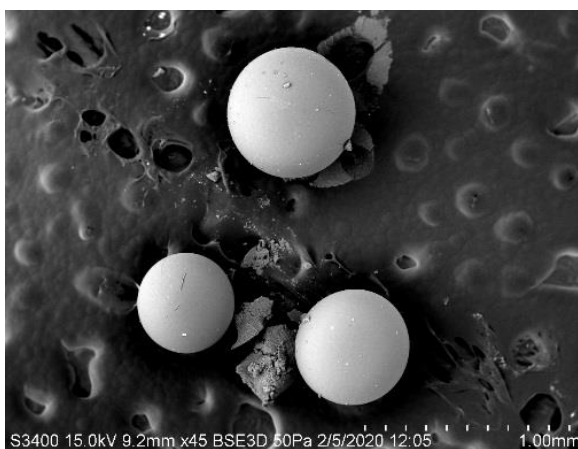
(d-2)



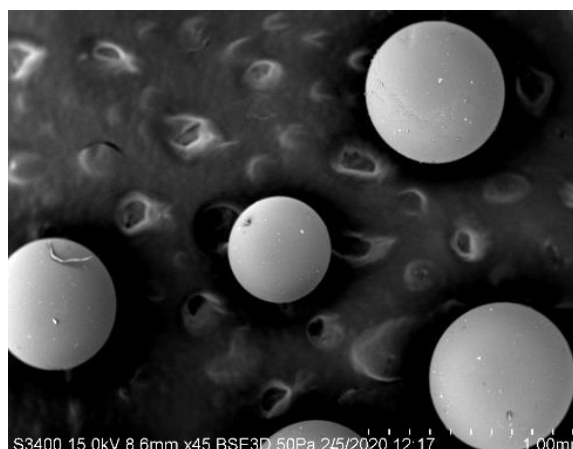
(e-1)



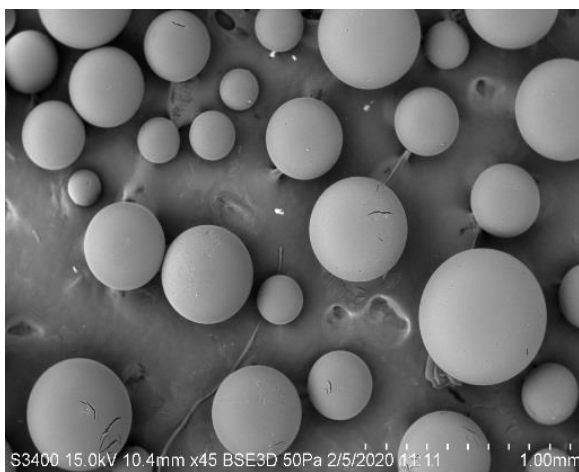
(e-2)



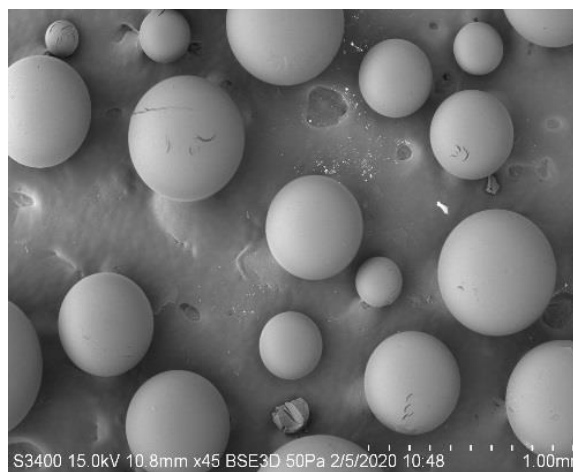
(f-1)



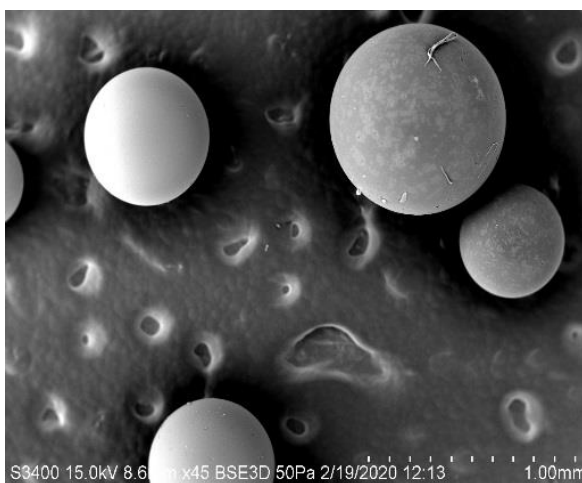
(f-2)



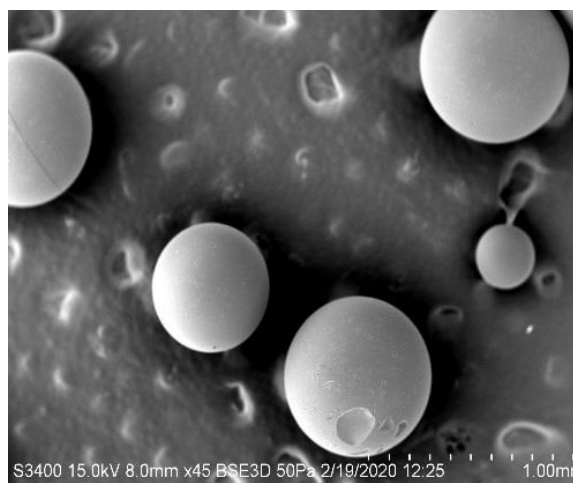
(g-1)



(g-2)



(h-1)



(h-2)

Figure 3-4 SEM images (i.e., morphology) of 1) PFOA sorbed fresh resins and 2) PFOA sorbed e_{aq}^- -driven ARP treated resins: (a) IRA67; (b) IRA96; (c) IRA400; (d) IRA900; (e) IRA910; (f) IRA958; (g) XAD7HP; and (h) XAD4; (Experimental condition: initial pH = 10.0; resin dosage = 0.2 g/L; sulfite dose = 10 mM; reaction volume = 500 mL; reaction time = 6 hours)

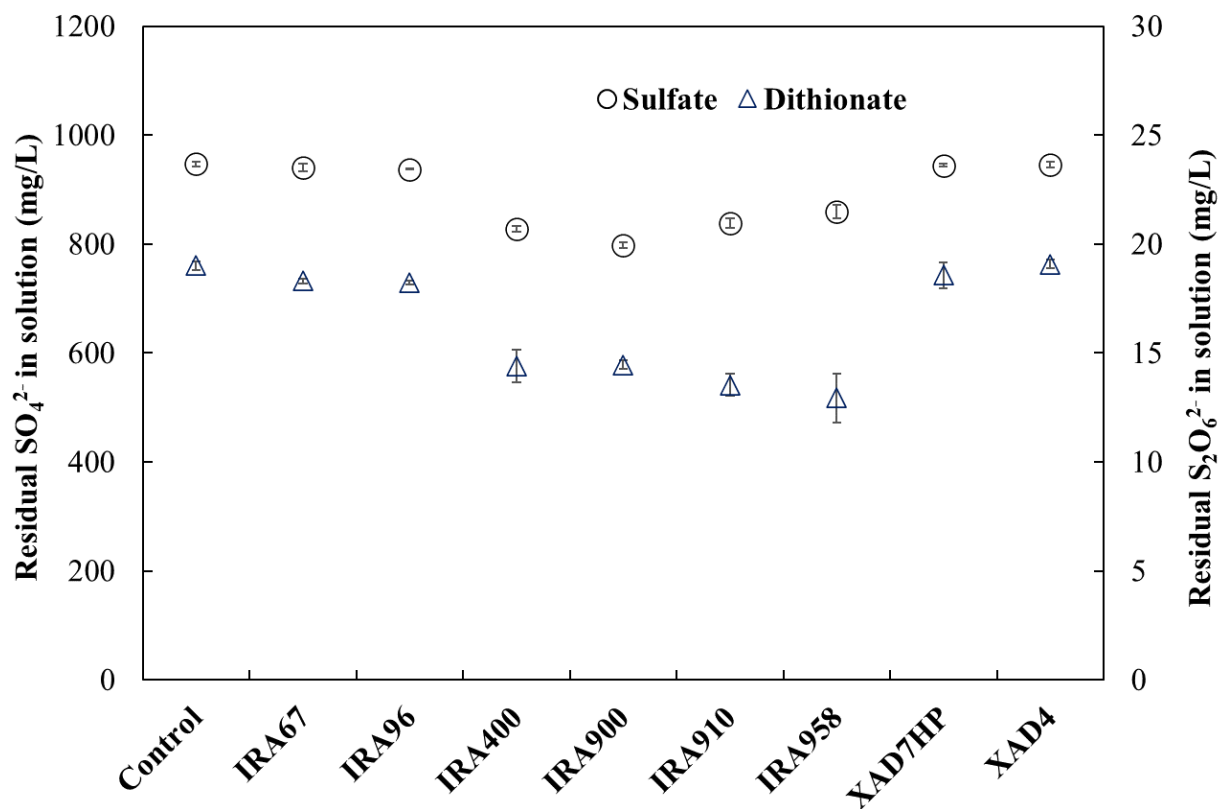


Figure 3-5 Residual concentrations of sulfate and dithionate in solution after ARP treatment of fresh resins (Experimental condition: initial pH = 10.0; Na_2SO_3 dose = 10 mM; resin dosage = 0.2 g/L (no resins in Control test); reaction volume = 1 L; reaction time = 6 hours)

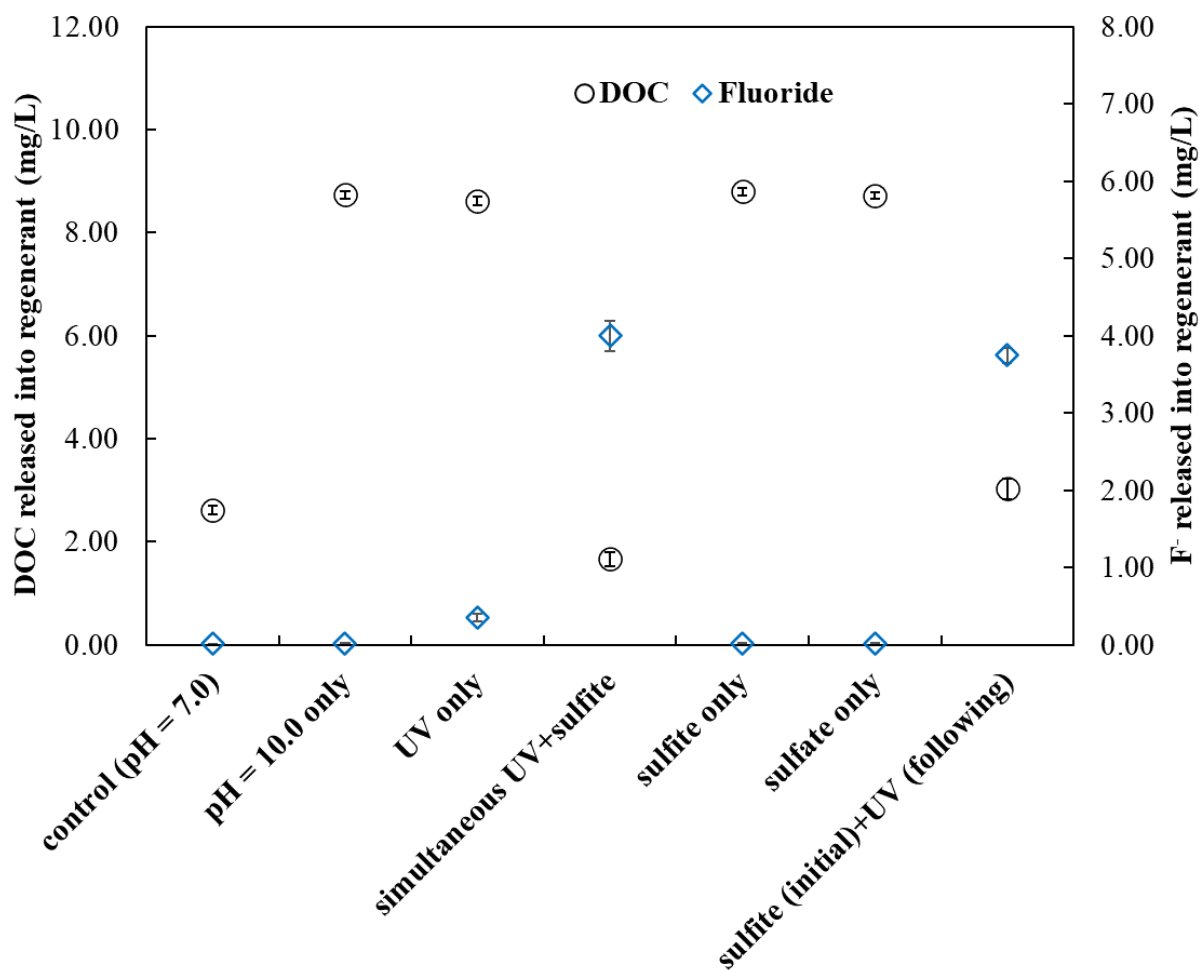


Figure 3-6 IRA67 regeneration experiments under different operating conditions: 1) left Y axis - DOC released into regenerant; 2) right Y axis - F⁻ released into the regenerant (Experimental condition: initial pH = 7.0 or 10.0; resin dosage = 0.2 g/L; reaction volume = 500 mL; reaction time = 6 or 12 hours)

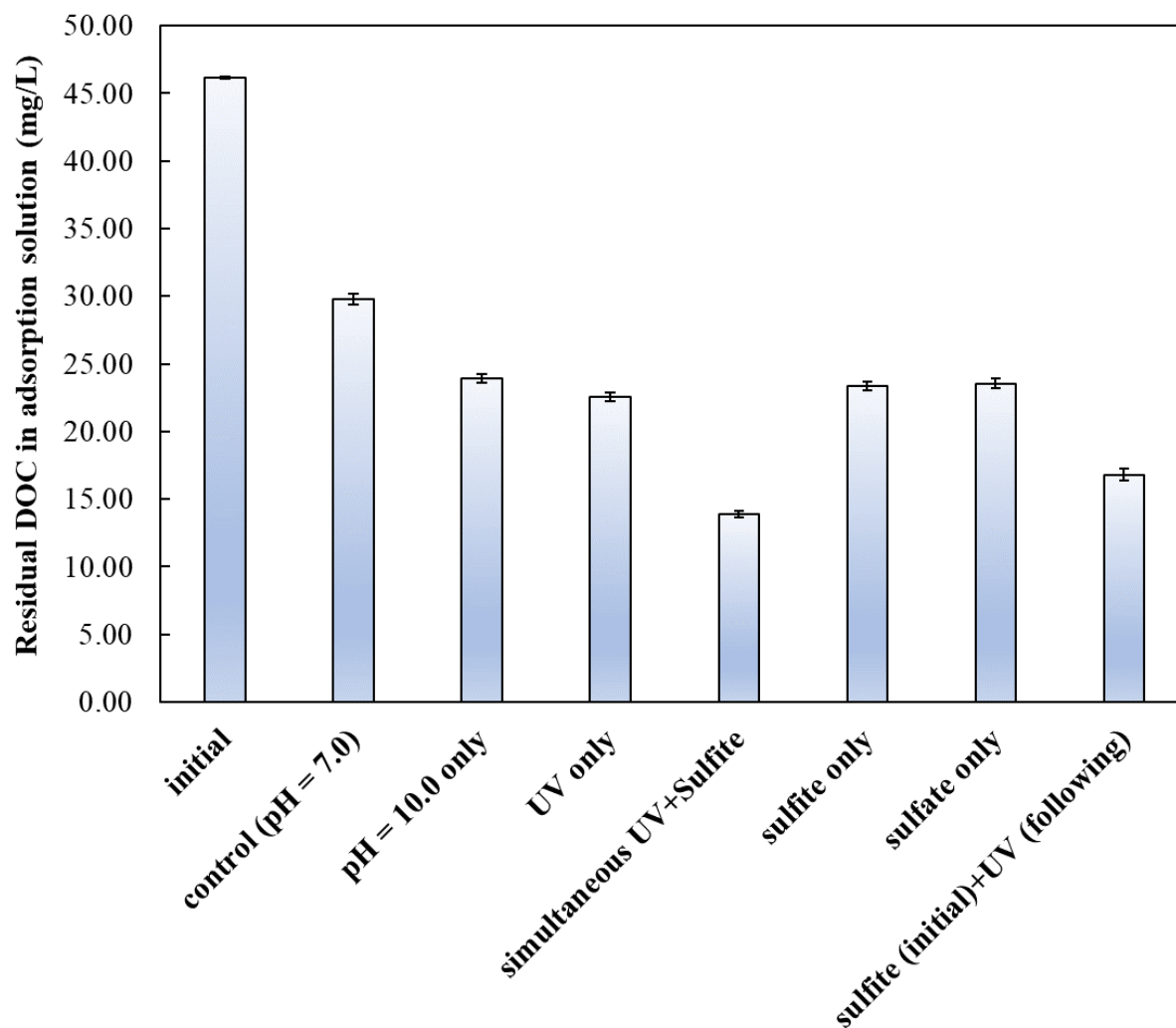


Figure 3-7 IRA67 re-adsorption experiments under different operating conditions (Experimental condition: initial pH = 7.0; initial PFOA = 200 mg/L; resin dosage = 0.2 g/L; reaction volume = 500 mL; adsorption time = 24 hours)

References

- Bao, Y., Deng, S., Jiang, X., Qu, Y., He, Y., Liu, L., Chai, Q., Mumtaz, M., Huang, J., & Cagnetta, G. (2018). Degradation of PFOA Substitute: GenX (HFPO–DA Ammonium Salt): Oxidation with UV/Persulfate or Reduction with UV/Sulfite? *Environmental science & technology*, 52(20), 11728-11734.
- Bentel, M. J., Yu, Y., Xu, L., Li, Z., Wong, B. M., Men, Y., & Liu, J. (2019). Defluorination of Per-and Polyfluoroalkyl Substances (PFASs) with Hydrated Electrons: Structural Dependence and Implications to PFAS Remediation and Management. *Environmental science & technology*.
- Boyer, T. H., Fang, Y., Ellis, A., Dietz, R., Choi, Y. J., Schaefer, C. E., Higgins, C. P., & Strathmann, T. J. (2021). Anion exchange resin removal of per-and polyfluoroalkyl substances (PFAS) from impacted water: A critical review. *Water research*, 200, 117244.
- Contea, L., Fallettia, L., Zaggiaa, A., & Milanb, M. (2015). Polyfluorinated organic micropollutants removal from water by ion exchange and adsorption. *Chemical Engineering*, 43.
- Cui, J., Gao, P., & Deng, Y. (2020). Destruction of per-and polyfluoroalkyl substances (PFAS) with advanced reduction processes (ARPs): A critical review. *Environmental Science & Technology*, 54(7), 3752-3766.
- Deng, S., Yu, Q., Huang, J., & Yu, G. (2010). Removal of perfluorooctane sulfonate from wastewater by anion exchange resins: Effects of resin properties and solution chemistry. *Water research*, 44(18), 5188-5195.
- Dixit, F., Dutta, R., Barbeau, B., Berube, P., & Mohseni, M. (2021). PFAS removal by ion exchange resins: A review. *Chemosphere*, 272, 129777.
- Domingo, J. L., & Nadal, M. (2019). Human exposure to per-and polyfluoroalkyl substances (PFAS) through drinking water: a review of the recent scientific literature. *Environmental research*, 177, 108648.
- Du, Z., Deng, S., Bei, Y., Huang, Q., Wang, B., Huang, J., & Yu, G. (2014). Adsorption behavior and mechanism of perfluorinated compounds on various adsorbents—A review. *Journal of hazardous materials*, 274, 443-454.
- Garg, S., Wang, J., Kumar, P., Mishra, V., Arafat, H., Sharma, R. S., & Dumée, L. F. (2021). Remediation of water from per-/poly-fluoroalkyl substances (PFAS)—Challenges and perspectives. *Journal of Environmental Chemical Engineering*, 9(4), 105784.
- Gu, J., Ma, J., Jiang, J., Yang, L., Yang, J. X., Zhang, J. Q., Chi, H. Z., Song, Y., Sun, S. F., & Tian, W. Q. (2017, Jan). Hydrated electron (e(aq)(-)) generation from phenol/UV:

- Efficiency, influencing factors, and mechanism. *Applied Catalysis B-Environmental*, 200, 585-593. <https://doi.org/10.1016/j.apcatb.2016.07.034>
- Gu, Y., Dong, W., Luo, C., & Liu, T. (2016). Efficient reductive decomposition of perfluorooctanesulfonate in a high photon flux UV/sulfite system. *Environmental science & technology*, 50(19), 10554-10561.
- Gu, Y., Liu, T., Wang, H., Han, H., & Dong, W. (2017). Hydrated electron based decomposition of perfluorooctane sulfonate (PFOS) in the VUV/sulfite system. *Science of the Total Environment*, 607, 541-548.
- Hoffman, K., Webster, T. F., Bartell, S. M., Weisskopf, M. G., Fletcher, T., & Vieira, V. M. (2011). Private drinking water wells as a source of exposure to perfluorooctanoic acid (PFOA) in communities surrounding a fluoropolymer production facility. *Environmental health perspectives*, 119(1), 92-97.
- Li, P., & Sengupta, A. K. (2000). Intraparticle diffusion during selective sorption of trace contaminants: the effect of gel versus macroporous morphology. *Environmental Science & Technology*, 34(24), 5193-5200.
- Liu, F., Guan, X., & Xiao, F. (2022). Photodegradation of Per- and Polyfluoroalkyl Substances in Water: A Review of Fundamentals and Applications. *Journal of hazardous materials*, 129580.
- Lyu, X.-J., Li, W.-W., Lam, P. K., & Yu, H.-Q. (2015). Insights into perfluorooctane sulfonate photodegradation in a catalyst-free aqueous solution. *Scientific reports*, 5, 9353.
- Miyazaki, Y., & Nakai, M. (2011). Protonation and ion exchange equilibria of weak base anion-exchange resins. *Talanta*, 85(4), 1798-1804.
- Park, H., Vecitis, C. D., Cheng, J., Choi, W., Mader, B. T., & Hoffmann, M. R. (2009). Reductive defluorination of aqueous perfluorinated alkyl surfactants: effects of ionic headgroup and chain length. *The Journal of Physical Chemistry A*, 113(4), 690-696.
- Parrish, J. (1977). Macroporous resins as supports for a chelating liquid ion-exchanger in extraction chromatography. *Analytical Chemistry*, 49(8), 1189-1192.
- Post, G. B., Cohn, P. D., & Cooper, K. R. (2012). Perfluorooctanoic acid (PFOA), an emerging drinking water contaminant: a critical review of recent literature. *Environmental research*, 116, 93-117.
- Qu, Y., Zhang, C.-J., Chen, P., Zhou, Q., & Zhang, W.-X. (2014). Effect of initial solution pH on photo-induced reductive decomposition of perfluorooctanoic acid. *Chemosphere*, 107, 218-223.

- Qu, Y., Zhang, C., Li, F., Chen, J., & Zhou, Q. (2010). Photo-reductive defluorination of perfluorooctanoic acid in water. *Water research*, 44(9), 2939-2947.
- Rahimi, M., Wadi, D., & Vadi, M. (2014). Langmuir, freundlich and temkin adsorption isotherm of captopril an ace inhibitor (or angiotensin-converting-enzyme inhibitor) is a pharmaceutical drug used for the treatment of hypertension by multi-wall carbon nanotube. *Ind. J. Fund. Appl. Life Sci*, 4, 933-937.
- Ren, Z., Bergmann, U., & Leiviskä, T. (2021). Reductive degradation of perfluorooctanoic acid in complex water matrices by using the UV/sulfite process. *Water research*, 205, 117676.
- Senevirathna, S. T. M. L. D. (2010). Development of effective removal methods of PFCs (perfluorinated compounds) in water by adsorption and coagulation.
- Song, Z., Tang, H., Wang, N., & Zhu, L. (2013). Reductive defluorination of perfluorooctanoic acid by hydrated electrons in a sulfite-mediated UV photochemical system. *Journal of hazardous materials*, 262, 332-338.
- Sun, M., Zhou, H., Xu, B., & Bao, J. (2018). Distribution of perfluorinated compounds in drinking water treatment plant and reductive degradation by UV/SO₃²⁻ process. *Environmental Science and Pollution Research*, 25(8), 7443-7453.
- Sun, Z., Zhang, C., Chen, P., Zhou, Q., & Hoffmann, M. R. (2017). Impact of humic acid on the photoreductive degradation of perfluorooctane sulfonate (PFOS) by UV/Iodide process. *Water research*, 127, 50-58.
- Sun, Z., Zhang, C., Xing, L., Zhou, Q., Dong, W., & Hoffmann, M. R. (2018). UV/nitritotriacetic acid process as a novel strategy for efficient photoreductive degradation of perfluorooctanesulfonate. *Environmental Science & Technology*, 52(5), 2953-2962.
- Vellanki, B. P., Batchelor, B., & Abdel-Wahab, A. (2013). Advanced reduction processes: a new class of treatment processes. *Environmental engineering science*, 30(5), 264-271.
- Wanninayake, D. M. (2021). Comparison of currently available PFAS remediation technologies in water: A review. *Journal of Environmental Management*, 283, 111977.
- Yu, Q., Zhang, R., Deng, S., Huang, J., & Yu, G. (2009). Sorption of perfluorooctane sulfonate and perfluorooctanoate on activated carbons and resin: kinetic and isotherm study. *Water research*, 43(4), 1150-1158.
- Zhang, C., Qu, Y., Zhao, X., & Zhou, Q. (2015). Photoinduced reductive decomposition of Perfluorooctanoic acid in water: effect of temperature and ionic strength. *CLEAN–Soil, Air, Water*, 43(2), 223-228.

Chapter 4 Hydrated Electron Degradation of PFOA Laden on IRA67 in the Presence of Natural Organic Matter

4.1 Introduction and Objectives

To overcome the respective shortcomings of IX and e_{aq}^- -driven ARPs for PFAS treatment (demonstrated in **Chapters 1 and 2**) in the drinking water treatment scenario, an on-site ARP-based IX resin regeneration approach was proposed in **Chapter 3**. Moreover, the proof-of-concept for degradation of PFOA sorbed on IX resins was validated in **Chapter 3**. These findings show that the innovative on-site ARP-based IX resin regeneration approach was capable of concurrently restoring resin capacity and degrading sorbed PFAS on resins to address PFAS pollution in water treatment. Among the eight commercially available resins, IRA67 has proven as the best-performed one for the application to the intended purpose due to its excellent PFOA adsorption capabilities and durable physical and chemical properties over the e_{aq}^- -driven ARP treatment, as discussed in **Chapter 3**. This study also highlights that a UV/SO₃²⁻ ARP treatment process can effectively degrade PFOA sorbed on IRA67 and release previously occupied functional sites on the resins for capturing more PFOA in the ensuing adsorption process. Although the technical feasibility of this proposed method was validated in **Chapter 3**, two critical questions need to be answered before applying the innovative on-site ARP-based IX resin regeneration method to the mitigation of aqueous dissolved PFAS in realistic water treatment. First, NOM, defined as a complex matrix of organic material in water sources (Matilainen et al. 2010), has a concentration with several magnitudes greater than that of PFAS in raw water (Benjamin, 2014; Chellam & Sari, 2016; Exner & Färber, 2006; Xu et al., 2021; Zareitalabad et al., 2013). When IX is applied to the removal of PFAS in natural water, PFAS and NOM are unavoidably co-sorbed on IX resins. Can PFAS sorbed on IX resins be effectively degraded in a

UV/SO₃²⁻ ARP system in the presence of co-sorbed NOM to release more previously occupied functional sites on the IX resins? Second, what is the role of co-sorbed NOM during the PFAS adsorption and ARP-based resin regeneration phases? The study described in **Chapter 4** can advance our understanding of the treatment behaviors and underlying mechanisms of the new on-site ARP-based resin regeneration method for PFAS mitigation in water.

The objective of the research described in this chapter aimed to answer the two questions by probing the interactions of e_{aq}⁻ and PFOA-laden IRA67 in the presence of NOM. Here, PFOA was chosen as a model PFAS species owing to its prevalence in the aquatic environment, while UV/SO₃²⁻ was selected as the representative ARP to generate e_{aq}⁻ (Eq. (2-1)).

4.2 Materials and Methods

4.2.1 Chemical and Reagents

All the reagents used were at least analytical grade, except as noted. WBA exchange resins (Amberlite™ IRA67) and ammonium acetate (CH₃CO₂NH₄; > 97%) were obtained from Sigma-Aldrich. PFOA (96%, ACROS Organics™), NaCl (99%), sodium bicarbonate (NaHCO₃; 99%), HCl (37% solution in water), nitric acid (HNO₃; 70% solution in water), and NaOH (> 97%) were purchased from Fisher Scientific. PFOA analytical standard solution (100 µg/mL in methanol), Na₂SO₃ (> 98%), and methanol (LC-MS grade) were purchased from Millipore Sigma (Burlington, MA, USA.). Suwannee River Natural Organic Matter (SRNOM) was purchased from the International Humic Substance Society (IHSS, St. Paul, MN, USA). All the solutions were prepared using ultrapure water (> 18.2 MΩ·cm) generated from a Milli-Q® water purification system (Milli-Q Direct 8).

4.2.2 Experiments

4.2.2.1 UV/SO₃²⁻ Treatment of PFOA/NOM Preloaded IRA67. IRA67 resins were rinsed using the method detailed elsewhere (Gao et al., 2021). To prepare PFOA and SRNOM preloaded resins, 1.0 g resins were introduced to 1.0 L PFOA-containing simulated natural water (20.0 µg/L PFOA, 5.0 mg/L DOC, 84.0 mg/L NaHCO₃, 1.0 mg/L NaCl, and pH 7.5) in a 1 L beaker on a four-paddle programmable jar tester (Phipps & Bird - 7790-950) (Cui & Deng, 2022). The occurrence of PFOA in surface water and groundwater typically ranges within a broad range over several orders of magnitude (Zareitalabad et al., 2013). Although PFOA is mostly below 100 ng/L, high concentrations (up to several – a few tens of µg/L) were reported (Exner & Färber, 2006; Xu et al., 2021; Zareitalabad et al., 2013). In this chapter, a high initial PFOA level of 20.0 µg/L was selected to represent PFAS pollution in the worst scenario (Cui & Deng, 2022). A 120-rpm stirring proceeded for 24 hours at 25 °C before filtration with 0.1 µm Durapore® PVDF membrane. The preloaded resins (13.25 µg/g PFOA and 3.86 mg/L DOC) were collected for the UV/SO₃²⁻ treatment in a 1 L closed thermostatic cylindrical quartz photo-reactor (model 7840-185, ACE Glass Inc.) (**Figure 3-1**). The cylinder-shaped reactor had a height of 440 mm and a diameter of 85.5 mm. The inner and outer diameters of a 450-mm high quartz immersion well in the cylinder center were 31 and 48 mm, respectively. A 450 W medium-pressure (200 to 400 nm) mercury lamp with a UV intensity of 187 µW/cm² was placed in the quartz immersion well. Of total energy radiated, approximately 40% to 48% is in the ultraviolet portion of the spectrum. Before reactions, the solution was purged with N₂ for 40 min to eliminate DO. Initial pH was adjusted to 10.0 with 1.0 mM NaOH solution. During the UV irradiation, pH was not controlled or buffered. Cooling water was continuously circulated to maintain the solution temperature at 25 ± 1 °C. A magnetic stirrer was used to ensure a

completely mixed state during the ARP treatment. All the UV irradiation tests were conducted in a photochemical safety cabinet. To initiate the e_{aq}^- generation, appropriate amounts of Na_2SO_3 were dosed to the solution before the UV lamp was turned on. The UV/ SO_3^{2-} treatment proceeded for three hours. Control tests were carried out at identical conditions in the absence of Na_2SO_3 .

4.2.2.2 Cyclic Adsorption-regeneration Tests. Cyclic adsorption-regeneration experiments were carried out over six cycles. The schematic overview of the cyclic adsorption-regeneration experiment using UV/ SO_3^{2-} as an on-site PFOA/NOM-laden IRA67 regeneration method is shown in **Figure 4-1**. Each cycle comprised an adsorption phase and a UV/ SO_3^{2-} treatment phase. The adsorption tests were performed at the conditions similar to the aforementioned adsorption experiments in **Section 4.2.2.1**, except that the volume of PFOA-containing simulated natural water was increased to 5.0 L to make the resins nearly exhausted with PFOA and NOM. The following UV/ SO_3^{2-} treatment (i.e., regeneration) experiments were identical to the UV/ SO_3^{2-} tests described in **Section 4.2.2.1**. Two SO_3^{2-} doses of 5.0 and 25.0 mM were used. Control experiments were conducted without the UV/ SO_3^{2-} treatment phase in each cycle.

4.2.2.3 PFOA Extraction Tests. PFOA sorbed on the IRA67 was extracted to a solution as follows. IRA67 resins (1.0 g) were dosed to a 1 L of 10% NaCl (w/v) in a 2 L beaker. The beaker was covered with parafilm tape to minimize the water loss due to evaporation. The beaker was shaken on an orbital reciprocating shaker at 150 rpm for 24 hours at room temperature (25 °C). Thereafter, the mixture was filtered by 0.1 μm Durapore[®] PVDF membrane. PFOA in the filtrate was measured to quantify sorbed-PFOA on the resins. To validate whether the extraction could adequately desorb sorbed PFOA from IRA67, a set of validation tests were

conducted as follows. The preloaded resins (13.25 $\mu\text{g/g}$ PFOA and 3.86 mg/L DOC) were prepared as described in the **Section 4.2.2.1**. Afterwards, the PFOA sorbed on IRA67 was extracted with three different extraction solutions with the aforementioned PFOA extraction procedures. The three solutions include: 1) 10% NaCl (w/v); 2) 1% NaOH (w/v) and 70% MeOH (v/v); and 3) 1% NaCl (w/v) and 70% MeOH (v/v). The last two solutions were selected because they were used for effective PFOA desorption from anion exchange resins in the literature (Boyer et al., 2021).

4.2.2.4 PFOA Desorption from IRA67 in An Alkaline Sulfite Solution. A group of tests were performed to assess the effect of SO_3^{2-} dose on the desorption of PFOA from the WBA exchange resins in an alkaline sulfite solution. One liter of water was adjusted to pH 10.0 with 1.0 mM NaOH solution, followed by 40-min nitrogen gas purging to eliminate DO. Then 1.0 g of PFOA preloaded resins ($13.25 \pm 0.04 \mu\text{g/g}$ PFOA) was added to the solution. A magnetic stirrer mixer was used to ensure a completely mixed state. Throughout the mixing, pH was manually controlled at pH 10.0 with 0.1 mM NaOH solution, and nitrogen gas was continuously purged. At each 30-min time interval, an aliquot of solution sample was collected for PFOA analysis, immediately before an appropriate weight of Na_2SO_3 was added. The SO_3^{2-} doses were gradually increased from 0.0, 0.5, 1.0, 2.0, 3.0, 4.0, to 5.0 mM.

4.2.2.5 PFOA Desorption from IRA67 during the UV/ SO_3^{2-} Treatment. A set of tests were carried out to evaluate the effect of PFOA degradation products during UV/ SO_3^{2-} treatment on PFOA desorption from IRA67. Solution pH of 1 L water was adjusted to 10.0 with 1.0 mM NaOH solution, followed by 40-min nitrogen gas purging to eliminate DO. One gram of PFOA and NOM preloaded resins (13.25 $\mu\text{g/g}$ PFOA; 3.86 mg DOC/g) was added to the solution. A magnetic stirrer mixer was used to ensure a completely mixed state. The pH was manually

controlled at pH 10.0 with 0.1 mM NaOH solution throughout the mixing, and nitrogen gas was continuously purged. After 30 mins of mixing, the IRA67 was collected from the solution for further analysis and the following experiment. Thereafter, the resin-free solution was transferred to the 1 L closed thermostatic cylindrical quartz photo-reactor. Subsequently, an appropriate weight of Na₂SO₃ was added to the resin-free solution to make the initial SO₃²⁻ concentration at 5.0 mM. Before using a 450 W medium-pressure (200-400 nm) mercury lamp in the UV/SO₃²⁻ treatment, the solution was purged with nitrogen gas for 40 mins to eliminate DO. Different UV irradiation times, including 0.0, 0.5, 1.0, 2.0, and 3.0 hours, were used in each resin-free solution. After the UV/SO₃²⁻ treatment, the collected IRA67 was introduced back to each UV/SO₃²⁻ treated solution before three-hour mixing. A magnetic stirrer mixer was used to ensure a completely mixed state, and nitrogen gas was continuously purged. After mixing, the IRA67 resin was collected from each UV/SO₃²⁻ treated solution to quantify sorbed PFOA. As described in the **Section 4.2.2.3**, the remaining PFOA sorbed on IRA67 was extracted using the 10% NaCl only method.

4.2.2.6 UV/SO₃²⁻ Treatment of NOM in Water. NOM might play an important role in the UV/SO₃²⁻ treatment of PFOA and NOM laden on resins. However, the degradation of NOM by UV/SO₃²⁻ remains unknown. Here, the UV/SO₃²⁻ decomposition of NOM in water was evaluated. A NOM-simulated natural water (4.95 mg/L DOC) was synthesized using the SRNOM. All bench-scale experiments were conducted in a 1 L closed thermostatic cylindrical quartz photo-reactor with a reaction volume of 1 L. The quartz reactor was equipped with a 450 W medium-pressure mercury lamp. The lamp was placed in a quartz tube located centrally in the reactor. The NOM-simulated natural water was loaded in the reactor and continuously purged with nitrogen gas for at least 40 mins to deplete DO before the photolysis experiments.

Thereafter, the initial solution pH was adjusted to 10.0 with 1.0 mM NaOH, before an appropriate weight of Na₂SO₃ was added to the NOM-simulated natural water to ensure the initial SO₃²⁻ concentration at 1.0 mM. Cooling water was continuously circulated in the reactor to control the solution temperature at room temperature (25 ± 1 °C). The solution was continuously stirred using a magnetic bar stirrer during the reaction. The reaction was initiated once the UV lamp was switched on. The photoreactor was placed in a steel cabinet to safely operate the photochemical reaction. Each photochemical reaction lasted for 40 mins. Control tests were carried out at the identical conditions in the absence of Na₂SO₃. After the photochemical reaction, the treated NOM-simulated natural water was collected for further analysis.

The potentiometric titration method was used to measure the concentrations of carboxyl and phenolic functional groups in NOM-simulated natural water, which served as the representatives of EWGs and EDGs, respectively (Ma et al., 2001; Ritchie & Perdue, 2003). For the analyses, 100 mL deionized (DI) water (i.e., blank), fresh, and treated NOM-simulated natural water were collected and acidified to pH 3.0 with 0.1 mM HNO₃. After an overnight settling, the solutions were filtered by 0.45 µm microfiltration membranes. Ionic strength of the filtrate was then adjusted to 0.1 M with 5.0 M NaCl. Subsequently, the solution was purged by nitrogen gas for at least 10 mins to remove any dissolved CO₂. Finally, the samples were titrated with 0.1 M NaOH from pH 3.0 to 10.0. During the titration, the solutions were continuously stirred using a magnetic bar stirrer and purged by nitrogen gas. The volumetric difference of the NaOH solutions to increase pH to 10.0 in the NOM-simulated natural water and DI water could be used to quantify titratable functional groups (i.e., carboxyl and phenolic) in the NOM-simulated natural water. A pH of 8.0 was commonly chosen as the carboxyl equivalence point,

while the phenol content was estimated as twice as the NaOH consumption between 8.0 to 10.0 (Ma et al., 2001).

4.2.2.7 Morphology of IRA67 during the UV/SO₃²⁻ Treatment. A set of tests were carried out to evaluate the evolution of resin morphology to examine the effect of UV/SO₃²⁻ on the morphology IRA67. One gram of fresh resins was prepared for the UV/SO₃²⁻ treatment in a 1 L closed thermostatic cylindrical quartz photo-reactor. A 450 W medium-pressure (200-400 nm) mercury lamp placed in a quartz tube was inserted in the center of the reactor. Before reactions, the solution was purged with nitrogen gas for 40 min to eliminate DO. Initial pH was adjusted to 10.0 with 1.0 mM NaOH solution. During the UV irradiation, pH was not controlled or buffered. Cooling water was continuously circulated to maintain the solution temperature at 25 ± 1 °C. A magnetic stirrer was used to ensure a completely mixed state during the ARP treatment. All the UV irradiation tests were conducted in a photochemical safety cabinet. To initiate the e_{aq}⁻ generation, an appropriate weight of Na₂SO₃ was dosed to ensure the initial SO₃²⁻ concentration at 5 mM. The UV/SO₃²⁻ treatment proceeded for three hours. Control tests were carried out at the identical conditions in the absence of Na₂SO₃. After treatment, the resins were collected for the SEM analysis.

4.2.2.8 UV Absorbance Scan of IRA67 Resins in Water. UV absorbance of the IRA67 resin beads in water (wavelength = 200 to 400 nm) was scanned to evaluate whether UV light could travel from the resin surface to its center. The fresh IRA67 resins were filled in a 1-cm quartz cell before DI water was introduced to the 1-cm quartz cell. Subsequently, the UV absorbance of IRA67 resin beads in water was scanned using a UV/Vis spectrophotometer (HACH, DR5000).

4.2.3 Sample Analyses

Solution pH was measured with a Thermo Scientific Orion 5-Star Plus pH meter. SO_3^{2-} concentration in water was quantified using sulfite test kits (Model SU-5, HACH). DOC was analyzed through the measurement of TOC in the water filtered by a 0.45 μm nylon membrane with a TOC analyzer (TOC-L_{CPH}, Shimadzu Corp., Kyoto, Japan). UV_{254} absorbance was analyzed using a UV/Vis spectrophotometer (HACH, DR5000). PFOA in water was analyzed with a high-performance liquid chromatography-triple quadrupole mass spectrometer (HPLC-MS/MS; Agilent 6460C). To quantify PFOA sorbed on the resins, the sorbed PFOA was extracted from the resins to water before analysis of aqueous PFOA. In terms of the aqueous PFOA analysis, the Agilent MassHunter Workstation Software was used for data acquisition and analysis. The HPLC system was equipped with a BEH C18 column (2.1 x 50 mm, 1.7 μm). Methanol (solvent A) and 20 mM ammonium acetate (solvent B) were used in the mobile phase. The injection volume was 2.0 μL , and the column temperature was set at 50 °C. The elution flow rate was maintained at 0.25 mL/min. Electrospray ionization (ESI) mass spectrometry in the negative mode was used to identify PFOA. The ion spray voltage was set to -4500 V. The source temperature was set to 450 °C. Multiple reaction monitoring (MRM) mode was used for identification and quantification. Analytes were measured with a standard target approach that included a calibration curve and the use of PFOA analytical standard solutions. Specifically, the PFOA calibration samples (0.1-20.0 $\mu\text{g/L}$) were prepared by diluting the PFOA analytical standard solution with methanol. The detection limit of PFOA was 0.1 $\mu\text{g/L}$. The PFOA extraction was described in **Section 4.2.2.3**. After the cyclic tests, PFOA remaining on the resins was extracted to the aqueous phase before analyses of dissolved PFOA, representing overall residual PFOA on the resins. After the UV/SO_3^{2-} treatment of the resin, the amount of degraded

PFOA was the difference between PFOA sorbed on the resins before the treatment and dissolved PFOA after treatment and extraction. The morphology of the resins was determined using SEM (Hitachi S-3400N). The emitted intensity of the UV lamp was measured with an UV intensity radiometer (UVP, UVX-25 Sensor). All analytical results reported represented the mean of three replicate samples, with error bars corresponding to one standard deviation of these measurements.

4.3 Results

The initial effort was to determine a method that can adequately extract PFOA sorbed on resins to quantify PFOA on the solid phase. PFOA extraction tests were conducted to validate the sufficient desorption of all the sorbed PFOA from IRA67. The efficiencies of PFOA extracted from PFOA-preloaded resins in different extraction solutions are shown in **Figure 4-2**. Results showed that the recovery efficiencies of adsorbed PFOA from IRA67 using 10% NaCl (w/v), 1% NaOH (w/v) and 70% MeOH (v/v), as well as 1% NaCl (w/v) and 70% MeOH (v/v) were 98%, 99%, and 97%, respectively, indicating that the extraction with 10% NaCl only is a reliable method for sufficient extraction of sorbed PFOA from IRA67 in this study. Extraction with NaCl only was also used for extraction of PFAS from spent resins in many other studies (Dixit et al., 2020; Dixit, Barbeau, et al., 2021; Park et al., 2020).

Following the resin preloading, 13.25 $\mu\text{g/g}$ PFOA was immobilized to the IRA67, accompanied by significant NOM adsorption (3.86 mg DOC/g). The ensuing UV/SO₃²⁻ treatment of the PFOA/NOM-laden resins comprised two sequential steps, i.e., dosing the resins into an alkaline SO₃²⁻ solution and turning on the UV lamp for e_{aq}⁻ generation, at an anoxic condition. Once the preloaded resins were added to the 5.0 mM SO₃²⁻ solution at pH 10.0, 51% of the sorbed PFOA desorbed to the solution with 6.49 $\mu\text{g/g}$ PFOA remaining on the resins (**Figure 4-**

3a). Similarly, NOM partially desorbed with 68% (i.e., 2.62 mg DOC/g) on the resins and 32% in the solution (i.e., 1.24 mg DOC/L) (**Figure 4-3b**).

SO_3^{2-} dosed to solution might play a potential role in IX with PFOA sorbed on the resin. Before further evaluation, the effect of SO_3^{2-} in the PFOA desorption should be assessed. Therefore, a set of tests were performed to assess the effect of SO_3^{2-} dose on the desorption of PFOA from IRA67 in an alkaline sulfite solution. Effect of SO_3^{2-} doses on the desorbed PFOA and the percentage of remaining SO_3^{2-} in solution at various ultimate SO_3^{2-} dosages are shown in **Figure 4-4**. Regardless of the SO_3^{2-} dose, the desorbed PFOA remained nearly constant, while all SO_3^{2-} remained in solution. This finding indicated that IX between sorbed PFOA and SO_3^{2-} in water played a minor role in the PFOA desorption.

After the subsequent UV/ SO_3^{2-} treatment, PFOA on the resins and in the solution nearly vanished (**Figure 4-3a**). No degradation of the sorbed PFOA was observed after the UV irradiation alone (**Figure 4-5**) or in an alkaline SO_3^{2-} solution only (**Figure 4-4**). Therefore, these findings highlight the principal role of e_{aq}^- in the PFOA degradation. In contrast, DOC in the solution remained constant, while NOM on the resins could not be quantified due to technical difficulties (**Figure 4-3b**).

The effect of SO_3^{2-} dose on the UV/ SO_3^{2-} degradation of PFOA in the heterogeneous system was subsequently assessed. As shown in **Figure 4-5**, approximately equal amounts of PFOA (6.53 μg vs. 6.70 μg) on the resins (1.0 g) and in the solution (1.0 L) were present at 0.0 mM SO_3^{2-} . As $[\text{SO}_3^{2-}]$ increased from 1.0 to 5.0 mM, PFOA in the two phases were both degraded, but exhibited different patterns. At 1.0 mM SO_3^{2-} , little PFOA on the resins began to decay, while PFOA in solution dramatically declined to 0.12 $\mu\text{g}/\text{L}$ (i.e., 98% removal). When $[\text{SO}_3^{2-}]$ was further increased to 3.0 and 5.0 mM, PFOA on the resins decreased to 1.49 and 0.12

$\mu\text{g/g}$, respectively. The finding demonstrates that e_{aq}^- generated preferentially attacks PFOA in the solution rather than PFOA on the resins.

Cyclic adsorption - regeneration tests were conducted to examine the adsorption recovery and PFOA degradation robustness. Each cycle comprised adsorption and UV/ SO_3^{2-} -based regeneration phases. As shown in **Figure 4-6(a)**, the resins could capture 31.38 $\mu\text{g/g}$ PFOA and 17.57 mg/g DOC in the 1st cycle. For the resins treated with 25.0 mM SO_3^{2-} , the PFOA sorbed moderately declined to 20.07 $\mu\text{g/g}$ in the 2nd cycle and then almost remained in the following two cycles. Finally, PFOA sorbed appreciably decreased to 8.22 and 7.34 $\mu\text{g/g}$ at the 5th and 6th cycles, respectively. The adsorption of NOM and PFOA was compared between the different resins using the Students' t-tests (95% confidence limits). Of interest, the PFOA adsorption in each cycle was not significantly different ($p > 0.05$) for the resins regenerated at 25.0 and 5.0 mM SO_3^{2-} . In contrast, NOM adsorption with the resins regenerated at 25.0 mM SO_3^{2-} slightly declined to 15.31 mg/g DOC with the increasing cycle number to 4 (**Figure 4-7(b)**), then dramatically dropped to 5.16 and 3.48 mg/g DOC at the 5th and 6th cycles, respectively. When $[\text{SO}_3^{2-}]$ was reduced to 5.0 mM for regeneration, the NOM adsorption was slightly lower in most cycles except the 6th cycle. When $[\text{SO}_3^{2-}]$ was reduced to 5.0 mM for regeneration, the NOM adsorption was slightly lower in most cycles except the 6th one.

The effect of PFOA degradation products generated during UV/ SO_3^{2-} treatment on the desorption of PFOA from IRA67 was evaluated. The residual PFOA sorbed on the IRA67 and PFOA desorbed in solution after different experimental conditions are shown in **Figure 4-7**. It should be noted that some PFOA and its degradation intermediates existed in the solution after UV/ SO_3^{2-} treatment. Concentrations of PFOA and its degradation products mostly likely varied, depending on the irradiation durations. After the resins initially collected were added to the

solutions, the remaining PFOA on the WBA exchange resins was not changed, regardless of the irradiation durations, suggesting that the PFOA degradation products formed at different UV/SO₃²⁻ treatment conditions could not enhance the desorption of PFOA from the WBA exchange resins.

To evaluate the influence of UV/SO₃²⁻ on NOM, the UV/SO₃²⁻ treatment of NOM was conducted in a homogeneous system. Residual UV₂₅₄ absorbance, specific UV absorbance (SUVA), and DOC in the NOM-simulated natural water under different experimental conditions are shown in **Figure 4-8**. The fresh NOM-simulated natural water was represented as an “untreated” group with a DOC of 4.95 mg/L and UV₂₅₄ absorbance of 0.129 cm⁻¹. After the UV irradiation only, the UV₂₅₄ absorbance declined to 0.069 cm⁻¹ owing to the direct photolysis and/or indirect photodegradation. In the indirect photodegradation, certain NOM molecules could be excited by the absorption of photons to form a triplet excited state of NOM (i.e., ³NOM*), which could initiate the reaction with substrates via triplet energy transfer or oxidation routes (Canonica et al., 2006; Zhang et al., 2014; Zhang et al., 2012). Interestingly, the UV₂₅₄ absorbance further decreased to 0.010 cm⁻¹ in the ARP treatment group (sulfite 1.0 mM), as presented in **Figure 4-8**. The enhanced NOM degradation was principally ascribed to chemical degradation of NOM by different reactive species, particularly e_{aq}⁻, in the ARP system. Drastically different from UV₂₅₄ absorbance, DOC did not markedly decline under any experimental conditions, suggesting that C-C bonds of the NOM could not be noticeably cleaved by the UV irradiation or e_{aq}⁻-induced reductive degradation. To better understand the influences of ARP on the NOM characteristics, SUVA was calculated after different treatment processes based on Eq. (4-1).

$$\text{SUVA}\left(\frac{\text{L}}{\text{mg}\cdot\text{m}}\right) = \frac{\text{UV}_{254} \text{ absorbance } \left(\frac{1}{\text{cm}}\right)}{\text{DOC}\left(\frac{\text{mg}}{\text{L}}\right)} \times 100 \frac{\text{cm}}{\text{m}} \quad (4-1)$$

SUVA represents the UV absorbance at 254 nm (cm^{-1}) divided by DOC concentration (mg/L) (Weishaar et al., 2003). It is widely used as a surrogate measurement for DOC aromaticity (Traina et al., 1990). The SUVA in the untreated simulated natural water was 2.60 $\text{L}/(\text{mg}\cdot\text{m})$. After the UV irradiation only, SUVA decreased to 1.38 $\text{L}/\text{mg}\cdot\text{m}$. Similar to the evolution of UV_{254} absorbance, SUVA in the ARP treatment dramatically decreased to 0.19 $\text{L}/\text{mg}\cdot\text{m}$, indicating that the remaining NOM possessed a high fraction of non-humic and HPI NOM molecules after the ARP treatment.

To further understand the changes of specific functional groups on NOM after $\text{UV}/\text{SO}_3^{2-}$ ARP treatment, the contents of carboxyl and phenolic functional groups in the NOM-simulated natural water after different treatments are demonstrated in **Figure 4-9**. The contents were 6.06 and 2.02 meq/g , respectively, in the untreated simulated natural water. Following the UV irradiation only treatment at pH 10.0, carboxyl functional groups' content declined to 3.99 meq/g . After ARP treatment in a sulfite dose of 1.0 mM , it further decreased to 0.98 meq/g . In contrast, the phenolic $-\text{OH}$ content narrowly remained constant after the UV irradiation alone or ARP treatment, suggesting that e_{aq}^- is almost ineffective for phenolic $-\text{OH}$ groups in the NOM molecules. The aforementioned findings suggest that, in a $\text{UV}/\text{SO}_3^{2-}$ system, UV-absorbing moieties in NOM can be mitigated by both UV irradiation and reactive species (e.g., e_{aq}^-) produced from $\text{UV}/\text{SO}_3^{2-}$. Meanwhile, EWGs are readily degraded, while EDGs are recalcitrant in the $\text{UV}/\text{SO}_3^{2-}$ system.

Because maintaining the stable physical structure and chemical properties of resin materials during resin regeneration processes are a key for continuous PFOA adsorption, a set of tests was carried out to evaluate the evolution of resin morphology to examine the effects of

UV/SO₃²⁻ on IRA67 during UV/SO₃²⁻ treatment. The SEM images of IRA67 after UV/SO₃²⁻ ARP treatments are shown in **Figure 4-10**. SEM analysis was applied to visualize the evolution of resin morphology (e.g., the formation of cracks on the resin surface) to examine the effects of UV/SO₃²⁻ on IRA67. The results showed that the resin beads still possessed an intact, smooth, and spherical structure after UV irradiation and ARP treatment compared to fresh IRA67. There were no evident changes in the morphology, suggesting that the polymeric structure on IRA67 adequately withstood the attack of UV irradiation and/or e_{aq}⁻.

4.4 Discussion

IRA67 are WBA exchange resins with a gel structure bearing polyacrylic-divinylbenzene (matrix) and tertiary amine (functional group) (Cui & Deng, 2022). The WBA exchange resins, when applied to the removal of PFOA in the simulated natural water (**Figure 4-6**), could capture PFOA accompanied by immobilization of much more abundant NOM (Cui & Deng, 2022). Therefore, the resin saturation during IX application to drinking water treatment is principally governed by the sorption of substantial NOM instead of trace PFOA.

IRA67 resins without exchangeable ionic sites have a pK_a of 9.3 (Miyazaki & Nakai, 2011).



Here, overbars represent a resin phase. Because PFOA is a weak acid with a pK_a of 3.8 (Burns et al., 2008), IRA67 resins can capture PFOA⁻ (i.e., deprotonated PFOA), which is the dominant PFOA species at a typical water treatment pH condition, as shown in Eq. (4-2) and (4-3).



Electrostatic attraction is viewed as the primary reaction pathway of IRA67 removal of aqueous PFOA (Du et al., 2015). In contrast, the PFOA uptake through HPO interaction was limited due to the presence of a HPI polyacrylic backbone. On the other hand, though the PFOA concentration was much below its critical micelle concentration (CMC) (15,696 mg/L) (Kissa, 2001), the formation of micelle or hemimicelle was likely because the concentration of PFOA in proximity to the resin functional sites or in the pore water within the resin framework might be much higher than in bulk solution (Boyer et al., 2021). Even at concentrations below their CMCs, low-order pre-micellar aggregates of surfactant molecules can form (Ben-Amotz & Mendes de Oliveira, 2021; LeBard et al., 2012).

Besides PFOA, the WBA exchange resins simultaneously captured substantial NOM (Cui & Deng, 2022). The competition between the IX removal of PFAS and NOM has been reviewed elsewhere (Boyer et al., 2021). However, the mechanisms governing IX removal of NOM are complex due to the involvement of multiple interacting phenomena (Rahmani & Mohseni, 2017), relying heavily on the properties of both resins and NOM (Bolto et al., 2004; Bolto et al., 2002). For the NOM removal by WBA exchange resins, a non-electrostatic mechanism involving H bonding of undissociated acidic species (e.g., carboxylic acid and phenol) in NOM molecules with amino groups on the resins was also proposed (Bolto et al., 2004; Bolto et al., 2002).

Investigation of the two sequential steps during the UV/SO₃²⁻ treatment of PFOA/NOM-laden resins (**Figure 4-3**) provides deeper insights. In the first step, partial desorption of PFOA and NOM occurred when PFOA/NOM-laden resins were added to a DO-free alkaline SO₃²⁻ solution. As presented in **Figure 4-4**, regardless of the SO₃²⁻ dose (0.0-5.0 mM), PFOA desorbed into the water was nearly constant (6.66 - 6.85 µg/L), while all the SO₃²⁻ remained in solution. These findings suggest that the partial PFOA desorption is not caused by ion exchange between

sorbed PFOA/NOM and SO_3^{2-} ($\text{pK}_{a2} = 7.17$) (Siddiqi et al., 1996) in water. Instead, the plausible reason for PFOA desorption is the alkaline environment (Boyer et al., 2021). As shown in Eq. (4-2), The enhancement of pH disfavors the formation of the protonated tertiary amine groups on the WBA exchange resins, resulting in the release of sorbed PFOA (Cui & Deng, 2022). Here, pH 10.0 was chosen because an alkaline pH can minimize the H^+ scavenging effect for e_{aq}^- (Cui & Deng, 2022). Because pH 10.0 is slightly above the pK_a of IRA67 (i.e., 9.3), a partial release of PFOA from the WBA exchange resins was observed before initiating the UV/ SO_3^{2-} treatment.

In the second step, given that most SO_3^{2-} remained in the water, e_{aq}^- is generated in the solution immediately before the PFOA decomposition in bulk solution and on the resins (**Figure 4-3a**) in the following UV/ SO_3^{2-} step. While UV/ SO_3^{2-} degradation of PFOA in water has been well documented (Cui et al., 2020), the finding on the degradation of PFOA on the resins is first reported. The topological polar surface area of SO_3^{2-} is 82.4 \AA^2 , having the same order of magnitude as PFOA (37.3 \AA^2) (PubChem, 2021). The sizes are sufficiently smaller than the distance (0.5-20 nm) between neighboring hydrocarbon chains in gel-based resins (Zagorodni, 2006). Because of diffusion driven by its concentration gradient between pore water and bulk solution, SO_3^{2-} could transport into pore water within the resin framework with little influence of size exclusion or hindered diffusion (Cui & Deng, 2022). Moreover, hydrophilicity of the polyacrylic matrix facilitated more water migration into the resin matrix (Cui & Deng, 2022). Once part of UV light could transmit into the resins, SO_3^{2-} in pore water could be activated to generate e_{aq}^- for degradation of adjacent PFOA, which are in pore water and/or on the resins (Cui & Deng, 2022).

UV transmission through the resins is plausible at the studied conditions (e.g., strong UV irradiation strength, a short light path length due to the small resin sizes, and a highly mixed state

of the resins in the ARP system), though UV photons can be increasingly adsorbed as the UV light travels from the resin surface to its center. The hypothesis can be supported in two aspects (Cui & Deng, 2022). First, though the gel resin has a poorly porous structure, its long cross-linking bridge ascertains a flexible polymer matrix, in which the space facilitates the water penetration and the exchange of large organic molecules (Zagorodni, 2006). Similarly, the void spaces in the polymer matrix can permit the transmission of UV light. Second, the UV transmittance through the IRA67 material was estimated in this study. Because the UV absorbance of the IRA67 resins is unavailable in the literature or from the manufacture documents, it was scanned in a 1-cm quartz cell over 200-400 nm, as shown in **Figure 4-11**. The maximum and minimum absorbance of the UV light was 3.711 and 2.785 AU·cm⁻¹ at 367 and 400 nm, respectively. Because the IRA67 resin beads (500 – 750 μm) has an average radius of 313 μm, the UV absorbance between the surface and center of a resin bead ranged within 0.0009 – 0.0011 AU when a linear relationship exists between the UV absorbance and the length of light path. Even though the low UV absorbance might have been underestimated if the absorbance was not linearly increased with the path length, the resin material is UV-transparent, to some extent (Cui & Deng, 2022). Moreover, the UV irradiation of polymer and resin materials has been widely applied in many other fields, such as analysis of dental resin composites having the path length ranges similar to the sizes of IRA67 beads in this study (Dos Santos et al., 2008; Masotti et al., 2007). In a growing UV curing technology for coating on different substrates (e.g., wood, paper, metal, and glass), UV light can also transmit into photo-curable resin materials to rapidly generate highly cross-linked polymer networks (Endruweit et al., 2006; Sangermano et al., 2014; Shukla et al., 2004). Furthermore, the UV transmission can occur to the adsorbents rather than IX resins (Cui & Deng, 2022). In a study to regenerate NOM-exhausted GAC with

UV/persulfate, radicals were generated to chemically oxidize sorbed NOM, including these NOM molecules within the pores, for recovering the adsorption capacity, suggesting the occurrence of UV transmission through GAC (An et al., 2015).

Another interesting question is whether the PFOA degradation products in the bulk solution, particularly as they accumulated in the solution, might have enhanced the PFOA desorption from the resins through ion exchange or other mechanisms. As shown in **Figure 4-7**, after the PFOA and NOM-preloaded resins were added to the solution containing complex PFOA degradation products, the PFOA sorbed on the WBA exchange resins remained nearly constant. This finding suggests that the PFOA degradation intermediates could not noticeably influence the desorption of PFOA on the resins over the UV/SO₃²⁻ treatment.

In the UV/SO₃²⁻-resin system, higher SO₃²⁻ doses enhanced the overall PFOA degradation (**Figure 4-5**) due to generation of more e_{aq}⁻. Noticeably, e_{aq}⁻ preferentially decomposes PFOA in solution rather than on the resins (**Figure 4-5**). The finding can be explained from three aspects. First, the e_{aq}⁻ yield is expected to decline from the resin surface to its center because of the strengthened UV shielding as the UV path length increases within the resin mass. Second, different from homogenous reactions between e_{aq}⁻ and PFOA in water, e_{aq}⁻ degradation of sorbed PFOA requires the transport of short-lived e_{aq}⁻ from water to the vicinity of resin surface before reactions with sorbed PFOA. Decay of e_{aq}⁻ (e.g., self-decay at $2k = 1.1 \times 10^{10} \text{ M}^{-1} \cdot \text{s}^{-1}$) during the travel reduces the concentration of e_{aq}⁻ to access to sorbed PFOA. Third, NOM co-sorbed on the resins may have more significant competition for e_{aq}⁻ with the sorbed PFOA. As shown in **Figure 4-3a**, the mass ratio of DOC:PFOA on the resin (2.62 mg/g: 6.49 μg/g) was more than twice that in water (1.24 mg/L: 6.76 μg/L), implying that NOM on the resins or in pore water might be much more than in the bulk solution. Moreover, SUVA of the desorbed NOM in

solution had a low value of 0.08 L/mg·m, suggesting that the released NOM possessed a high fraction of non-humic and HPI NOM molecule, while more HPO NOM was still associated with the resins (Edzwald & Association, 2011). Our recent study reveals that e_{aq}^- favorably reacts with HPO organics (Albalgane et al., 2022). Thus, the more plentiful HPO NOM on the resins could more significantly scavenge e_{aq}^- and thus suppress the degradation of co-sorbed PFOA.

Cyclic tests provide complex information. The recovered PFOA adsorption capability of the UV/SO₃²⁻-treated resins gradually declined with the increasing cycle number. The primary reason is the buildup of NOM on the resins for inhibiting the PFOA adsorption. Although the UV irradiation alone or e_{aq}^- can degrade certain NOM moieties, particularly EWGs (e.g., carboxyl groups), it cannot effectively cleave C-C bonds to mineralize NOM, as evidenced by **Figures 4-8** and **4-9**. The resulting NOM accumulation on the resins increased the number of occupied active sites, thus inhibiting the adsorption at the following cycles.

Of interest, the UV/SO₃²⁻-treated WBA exchange resins at 5.0 and 25.0 mM SO₃²⁻ both performed better than their non-regenerated counterparts in terms of PFOA removal ($p < 0.05$). This phenomenon might be due to the partial desorption of NOM in the alkaline solution (pH = 10.0), thus freeing up the occupied active sites for subsequent adsorption of NOM and PFOA. Meanwhile, the UV/SO₃²⁻-treated resins at 25.0 and 5.0 mM SO₃²⁻ could degrade 87% and 84% of overall PFOA sorbed over the six cycles, respectively. The excellent performance is related to the selectivity of e_{aq}^- . As the reactive functional groups on NOM were consumed via different pathways, such as UV absorption and reactions with different reactive species (e.g., e_{aq}^-), over the UV/SO₃²⁻ treatment, the scavenging effect of residual NOM for e_{aq}^- gradually became insignificant. Consequently, the overall PFOA was effectively degraded, regardless of the presence of substantial NOM. Based on the aforementioned findings, though UV/SO₃²⁻ cannot

function as a standalone resin regeneration option, it may be a promising on-site regeneration process for PFAS destruction if combined with proper strategies for effective mitigation of NOM in natural water and/or on the resins (Cui & Deng, 2022).

Degradation of PFOA sorbed on the WBA exchange resins with e_{aq}^- demonstrates a potential approach to on-site destruction of PFAS on spent IX resins produced from practical water treatment. Although SBA and WBA exchange resins are both known for effective PFOA adsorption (Boyer et al., 2021; Dixit, Dutta, et al., 2021), we argue that WBA exchange resins perform better than SBA exchange ones for the proposed regeneration scheme. Because UV/SO₃²⁻ requires a basic pH for minimal H⁺ scavenging of e_{aq}^- and SBA exchange resins have a broad service pH range (0-14), SO₃²⁻ and its oxidation products (i.e., SO₄²⁻) can largely adsorb to SBA exchange resins during regeneration in an alkaline environment. Consequently, the UV/SO₃²⁻-regenerated SBA exchange resins, when reused for PFOA adsorption, are expected to poorly capture aqueous PFOA because SO₃²⁻ and SO₄²⁻ have masked substantial functional sites. Nevertheless, the adsorption of SO₃²⁻ to WBA exchange resins at such a pH is limited over the UV/SO₃²⁻ treatment. Moreover, WBA exchange resins have a lower affinity with NOM than SBA exchange resins (Croué et al., 1999). Given that NOM, rather than PFAS, governs the resin saturation, NOM has less negative impacts on the WBA exchange resins for the PFOA removal and resin saturation (Cui & Deng, 2022).

4.5 Conclusions

Based on the knowledge summarized from the previous study, the potential on-site IX resin regeneration process integrated with ARPs can take the complementary advantages of IX and ARPs while overcoming their restrictions. Specifically, IX resins can concentrate trace amounts of PFAS from substantial water onto a small volume of resins to generate PFAS-free

water in an adsorption phase. In the subsequent regeneration phase, the IX resins are irradiated by UV in a small volume of SO_3^{2-} solution. Thus, the technical issues (i.e., increased TDS in effluent, pH adjustment, and creation of an anoxic environment) can be addressed in water treatment plants. Moreover, conventional PFAS-spent resin regeneration is typically achieved with high concentrations of salts and/or organic solvents, producing PFAS-containing toxic regeneration waste. Instead, a relatively small volume of regenerant waste primarily containing inert SO_4^{2-} is generated in the proposed method, which can be easily disposed of. More importantly, it is well known that e_{aq}^- -induced reductive degradation of PFOA occurs through H/F exchange and/or carbon chain shortening (Bentel et al., 2019; Cui et al., 2020). Because either of the reaction can also lead to the degradation of PFASs or other PFCAs, the UV/ SO_3^{2-} ARP treatment is highly likely to degrade other PFAS sorbed on resins rather than the simple phase transferring from water to solid (i.e., IX resin adsorption) (Cui & Deng, 2022). Thus, the proposed method deserves further investigation for its engineering applications, especially the evaluation of the role of NOM in the IX adsorption and ARP regeneration phase.

Significant findings in this chapter further advance the current knowledge on the novel ARP-based IX resin regeneration approach tailed for PFAS removal in drinking water treatment. The major contributions from this work are summarized as follows.

- 1) In the regenerated scheme, PFOA can be effectively degraded through e_{aq}^- degradation of PFOA sorbed on the IRA67 or desorbed in the solution.
- 2) e_{aq}^- generated from the UV/ SO_3^{2-} ARPs preferentially attacks PFOA in the solution rather than that on the resins.
- 3) The saturation of IRA67 in the removal of PFOA in water treatment is primarily ascribed to the adsorption of NOM (more abundant in the water).

4) UV/SO₃²⁻ ARPs, though effectively degrading sorbed PFAS, cannot well decompose co-sorbed NOM effectively to recover the resin adsorption.

5) Although UV irradiation alone or e_{aq}^- can degrade specific NOM moieties, particularly EWGs (e.g., carboxyl groups), it cannot effectively cleave C-C bonds to mineralize NOM.

6) The buildup of NOM on the resins finally leads to the loss of the resin capacity for removing PFOA in water with increasing cycle number of adsorption-regeneration, even if PFOA sorbed can be effectively degraded.

The aforementioned information shows new opportunities for decomposing aqueous PFOA sorbed on IX resins in water, but reveals new challenges resulting from NOM being ubiquitous in drinking water sources. In other words, ARPs alone is not technically feasible for the effective regeneration of PFAS/NOM-laden IX resins because ARPs barely decompose co-sorbed NOM to recover the resin adsorption capacity. Therefore, this study suggests that the combination of ARPs with other strategies targeting the mitigation of co-sorbed NOM needs to be considered to realize the promising ARP-based resin regeneration approach to aqueous PFAS pollution. Here, two possible pathways deserve forthcoming investigation for alleviation of co-sorbed NOM on IRA67 to achieve ARP-based IX resin regeneration for PFOA removal in water: 1) pre-removal of NOM (e.g., coagulation and AOPs) in water prior to IX for mitigating the NOM loading in the subsequent resins adsorption phase; and 2) proper chemical processes (e.g., pH adjustment) for alleviation of co-sorbed NOM on the resins. These two routes will be examined in the next chapter.

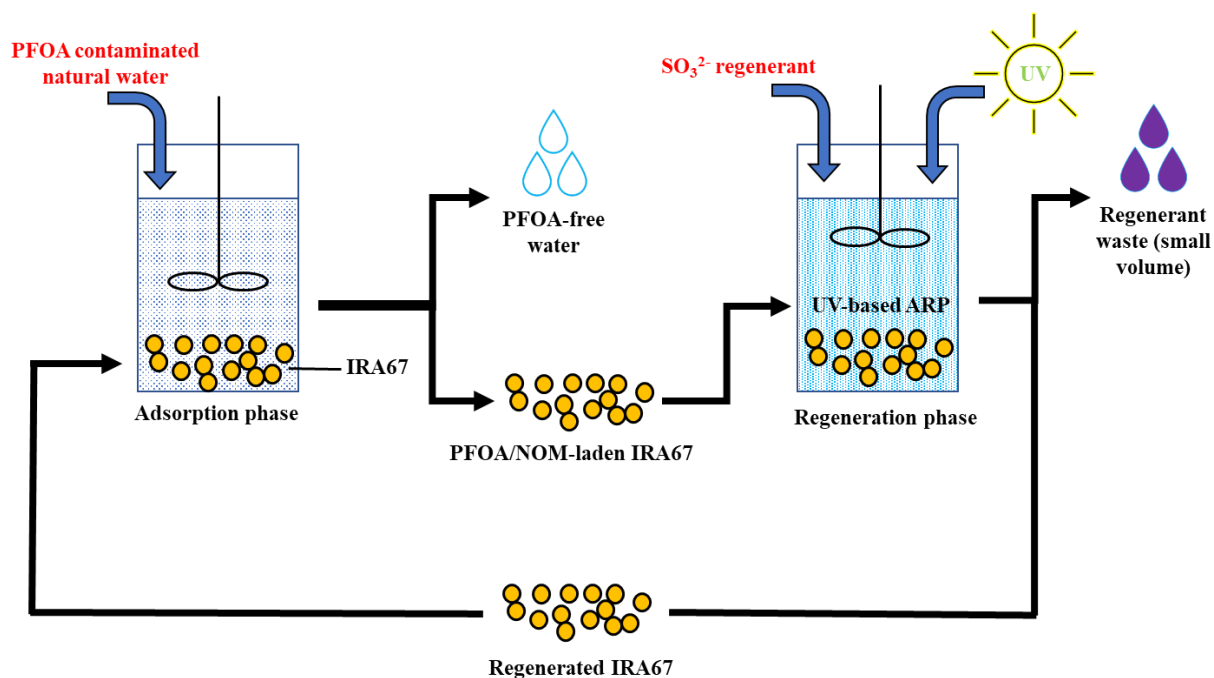


Figure 4-1 Schematic overview of the cyclic adsorption-regeneration test using UV/ SO_3^{2-} as an on-site PFOA/NOM-laden IRA67 regeneration method

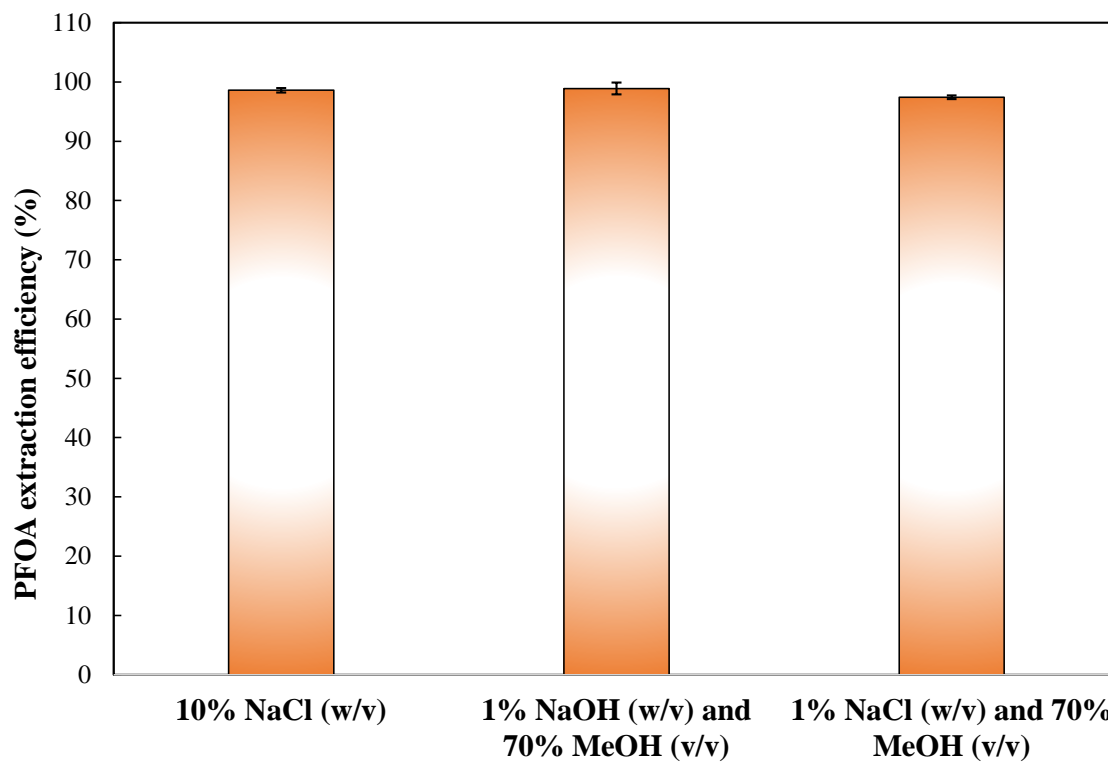


Figure 4-2 Efficiencies of PFOA extracted from PFOA-preloaded resins in different extraction solutions (Experimental condition: PFOA preloaded resins = 13.25 $\mu\text{g/g}$, 1 g/L resins, pH 10.0, 1 L solution, and 24 hours)

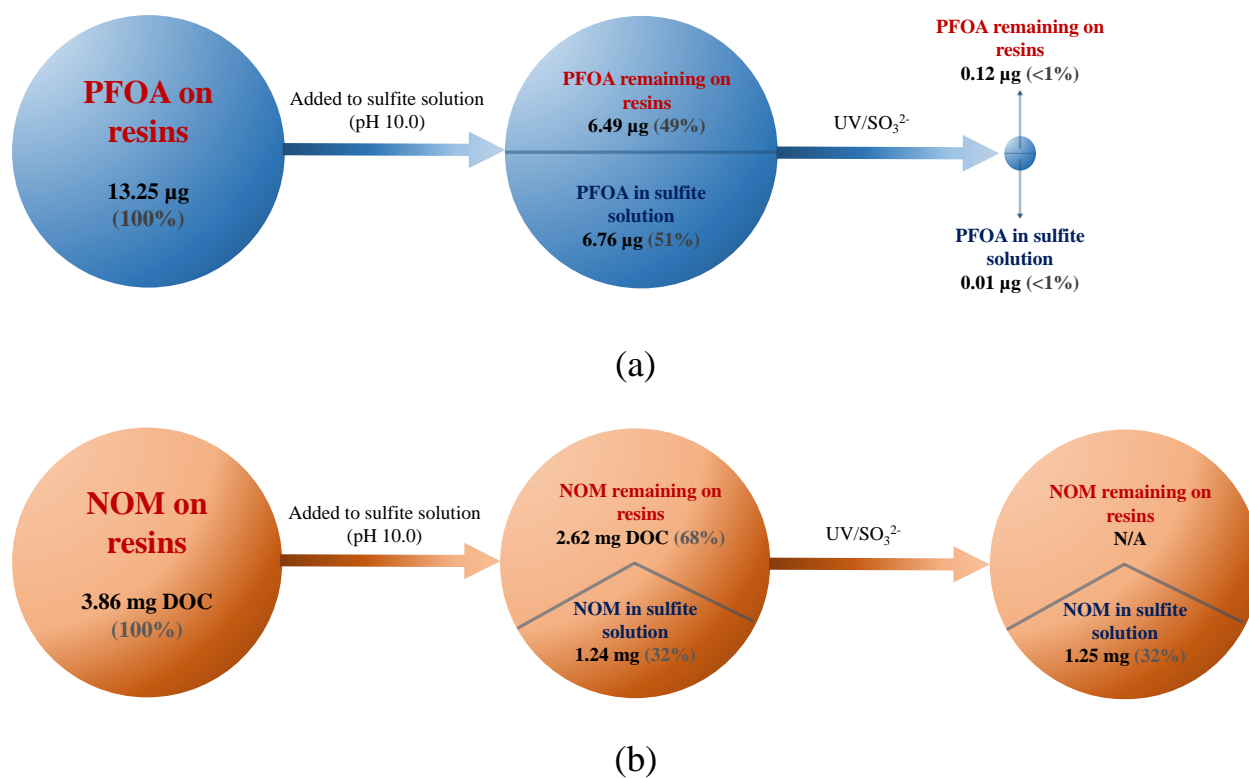


Figure 4-3 Fate of PFOA and NOM in different phases over the UV/SO₃²⁻ ARP treatment of PFOA and NOM-preloaded IRA67 (Experimental condition: 1.0 L solution at pH 10.0, 1.0 g/L resins, and 5.0 mM SO₃²⁻)

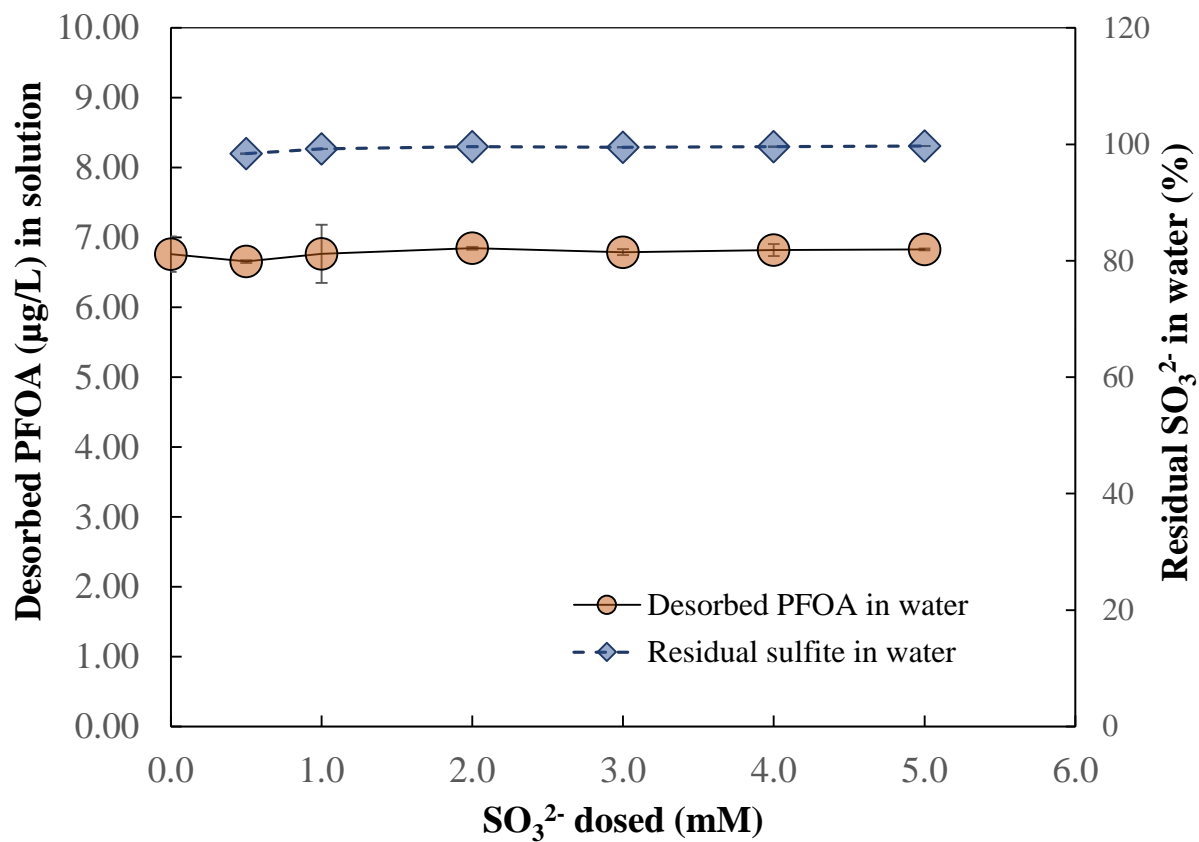


Figure 4-4 Desorbed PFOA in the sulfite solution in the presence of SO_3^{2-} (Experimental condition: pH 10.0, 1 L SO_3^{2-} solution, resin dose = 1.0 g/L, and 13.25 $\mu\text{g/g}$ PFOA on the resin before dosed to the solution)

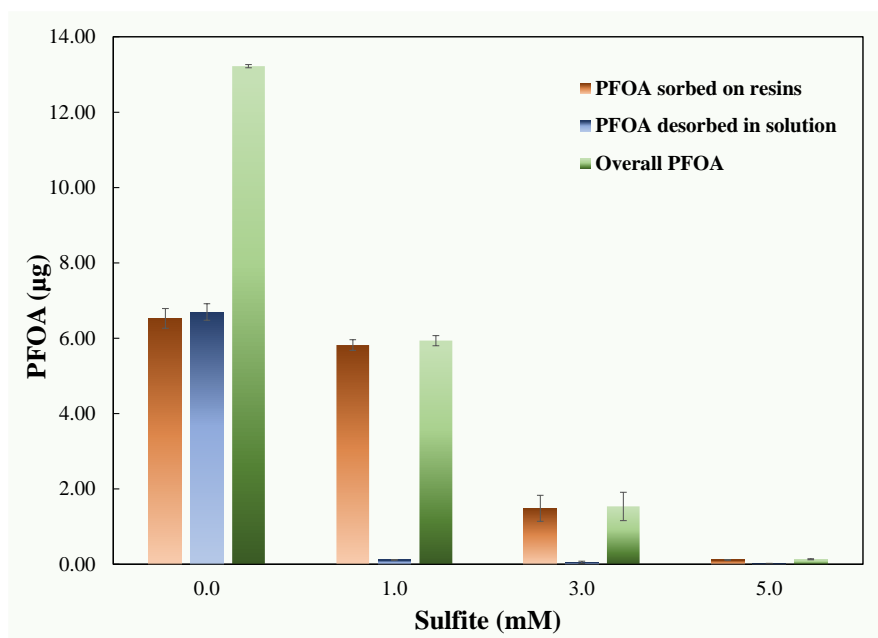
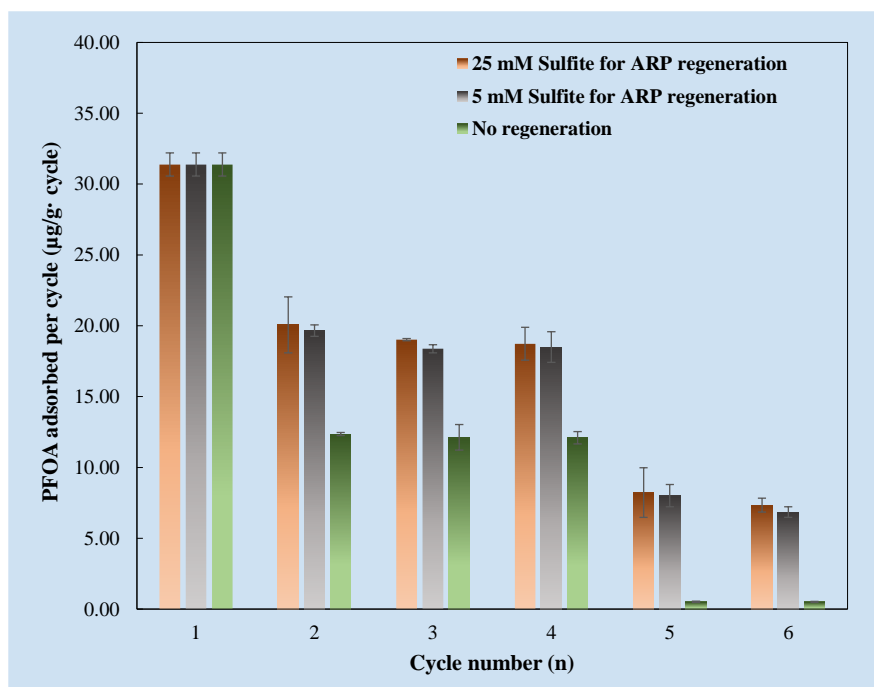
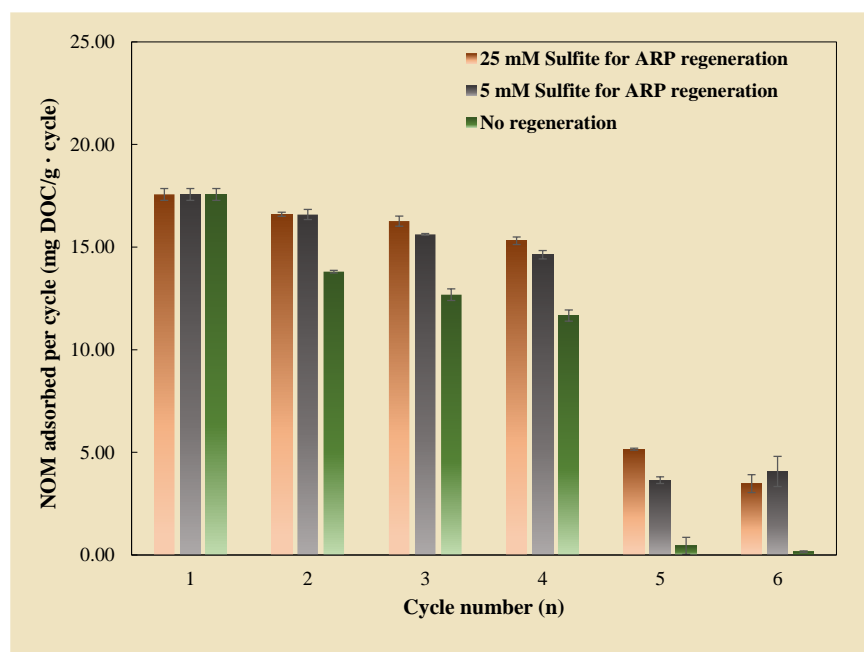


Figure 4-5 PFOA degradation in different phases over the UV/SO₃²⁻ treatment of PFOA and NOM-preloaded IRA67 (Experimental condition: 1.0 L solution at pH 10.0, 1.0 g/L resins, and 0.0-5.0 mM SO₃²⁻)



(a)



(b)

Figure 4-6 PFOA and NOM adsorbed on IRA67 after each adsorption phase during six cyclic adsorption – regeneration tests: (a) PFOA adsorbed; and (b) NOM adsorbed (Experimental condition: no regeneration: no UV/SO₃²⁻ regeneration phase in each cycle; ARP treatment: UV/SO₃²⁻ used in the regeneration phase in each cycle, [SO₃²⁻] = 5.0 or 25.0 mM)

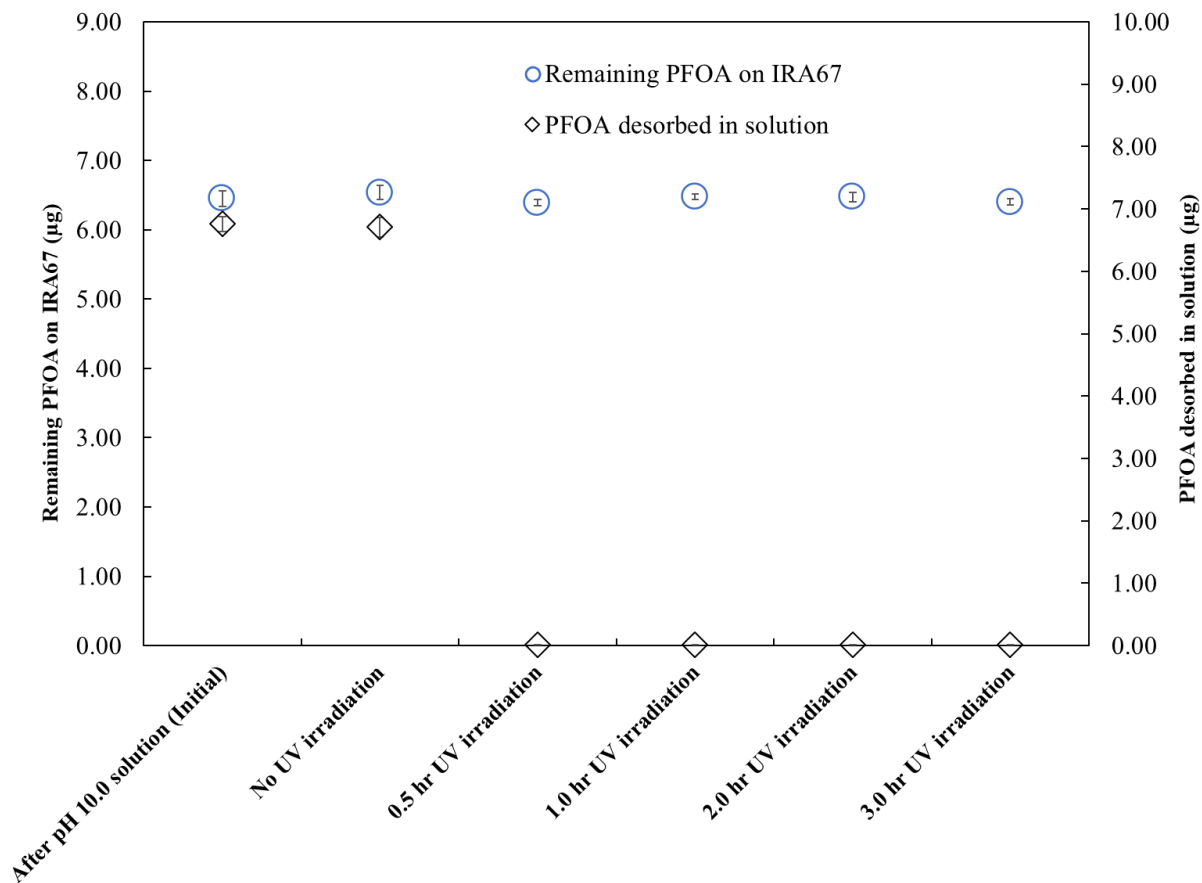


Figure 4-7 Residual PFOA on WBA exchange resins and PFOA desorbed in solution under different experimental conditions (Experimental conditions: after addition of PFOA and NOM preloaded resins in pH 10.0 solution, the solutions were collected and then treated again by UV/SO₃²⁻ at 0.0-3.0 hrs. Then the collected resins were added to the UV/SO₃²⁻ treated solutions for the PFOA desorption tests. Reaction volume = 1.0 L; resin dose = 1.0 g/L; no oxygen during the UV/SO₃²⁻ treatment or desorption tests)

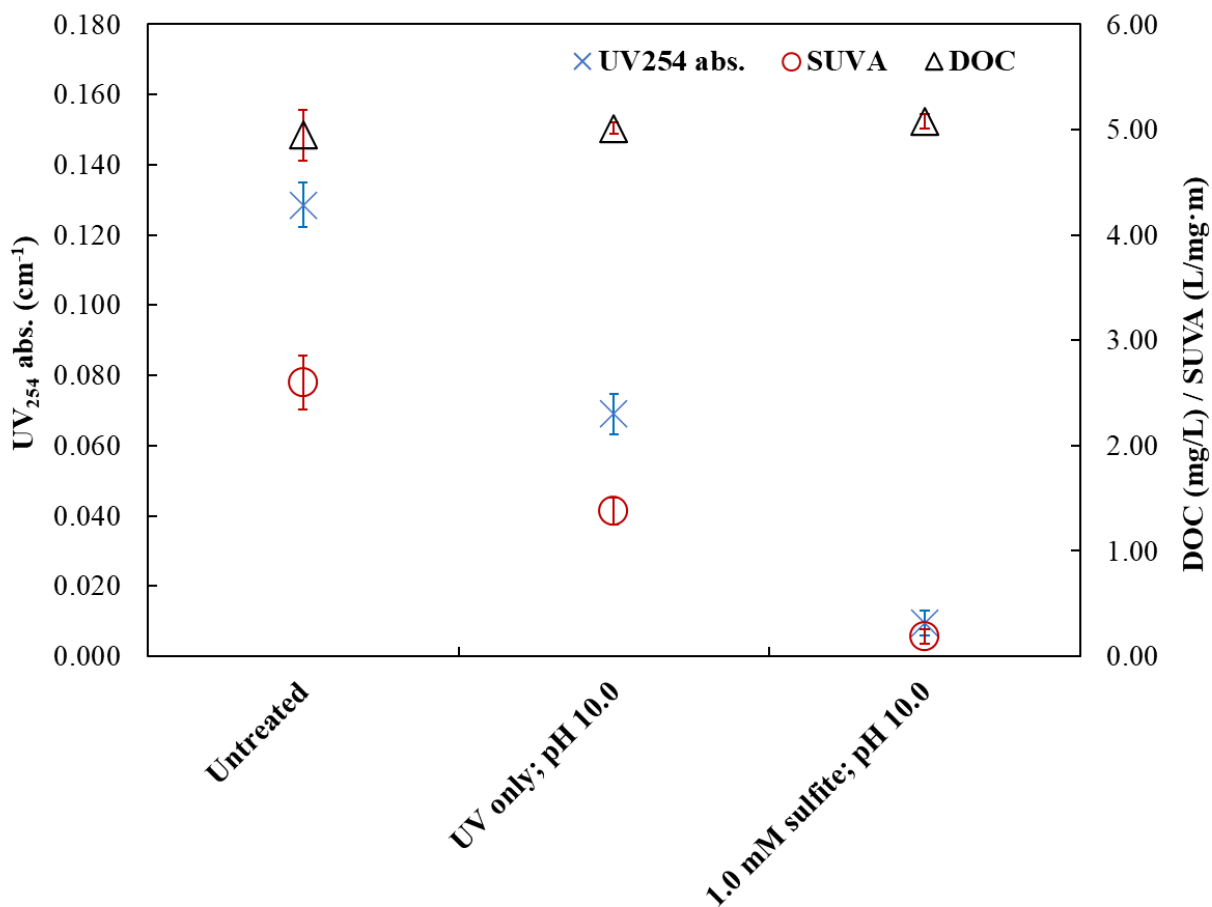


Figure 4-8 Residual UV₂₅₄ absorbance, SUVA, and DOC in the NOM-simulated natural water at different experimental conditions (Experimental condition: Untreated: NOM-simulated natural water; UV only; pH 10.0: the control for ARP; pH 10.0; 1.0 mM sulfite; pH 10.0; UV irradiation time = 40 mins)

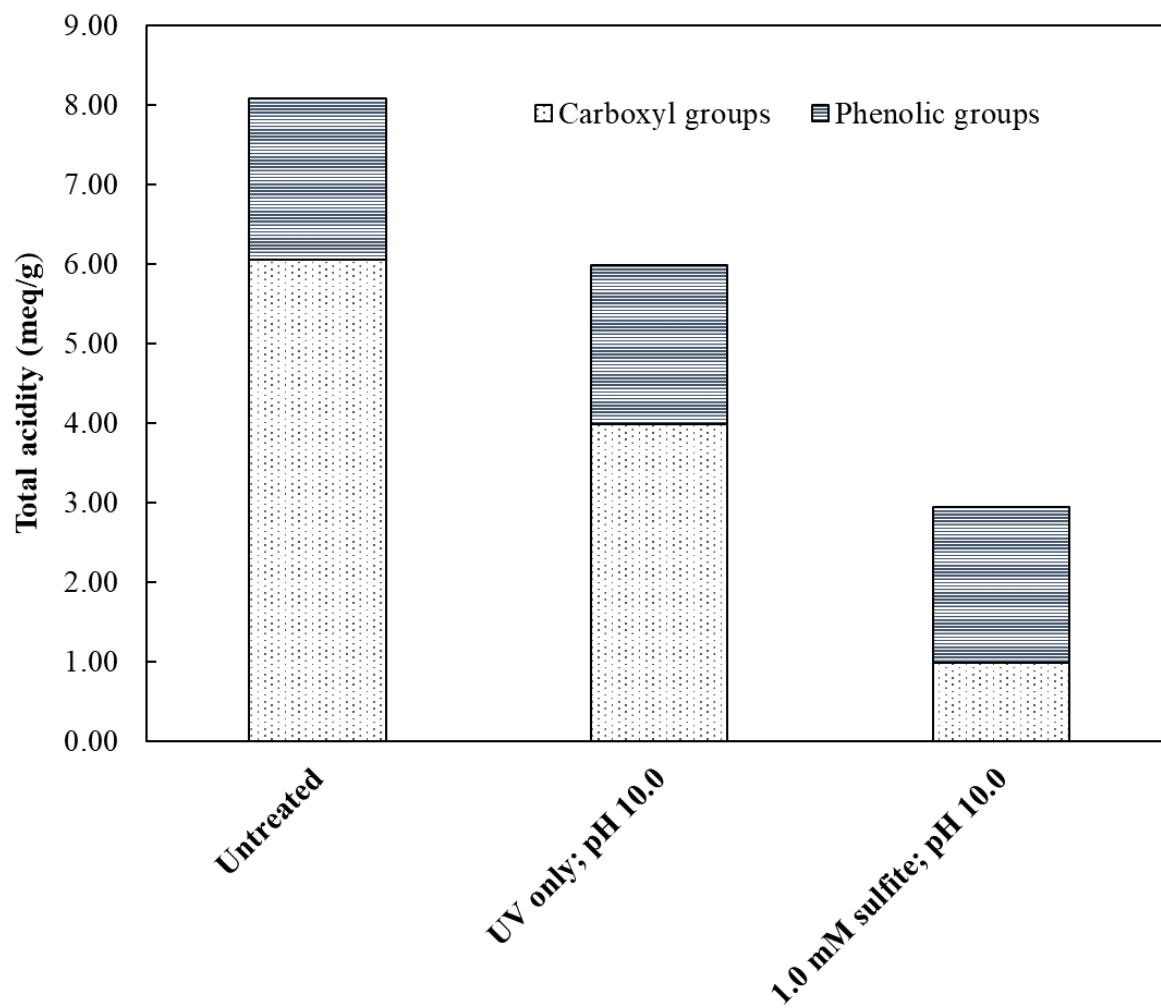
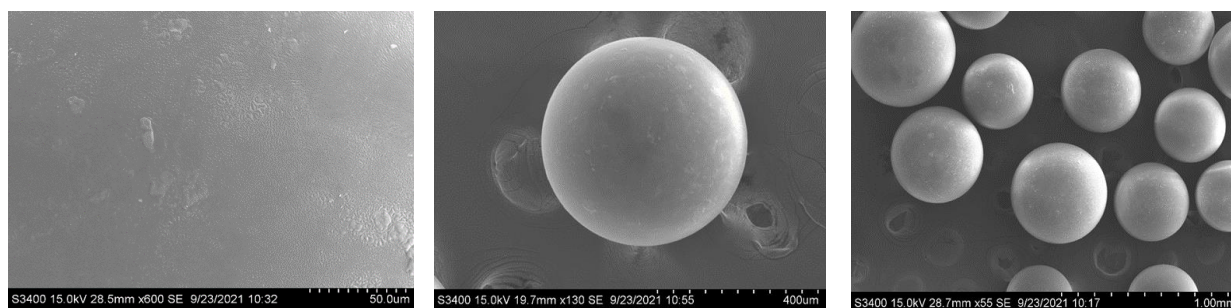


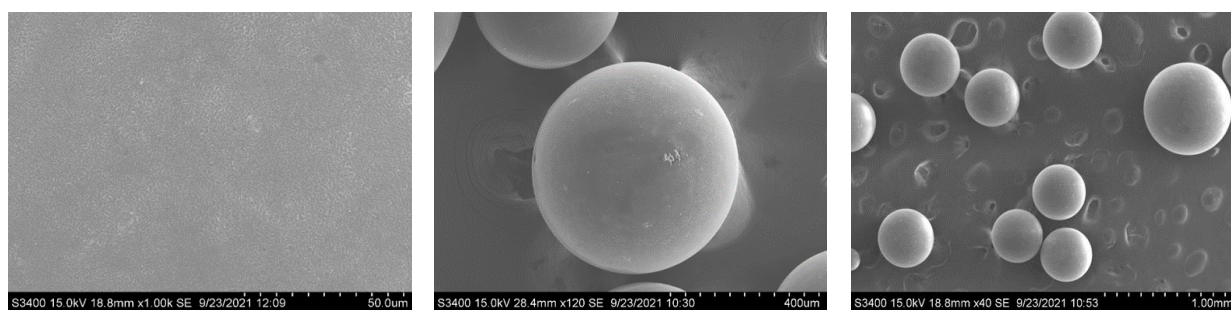
Figure 4-9 The contents of carboxyl and phenolic functional groups in the NOM-simulated natural water at different experimental conditions (Experimental condition: Untreated: NOM-simulated natural water; UV only; pH 10.0: the control for ARP; 1.0 mM sulfite; pH 10.0, and UV irradiation duration = 40 mins)



(a-1)

(a-2)

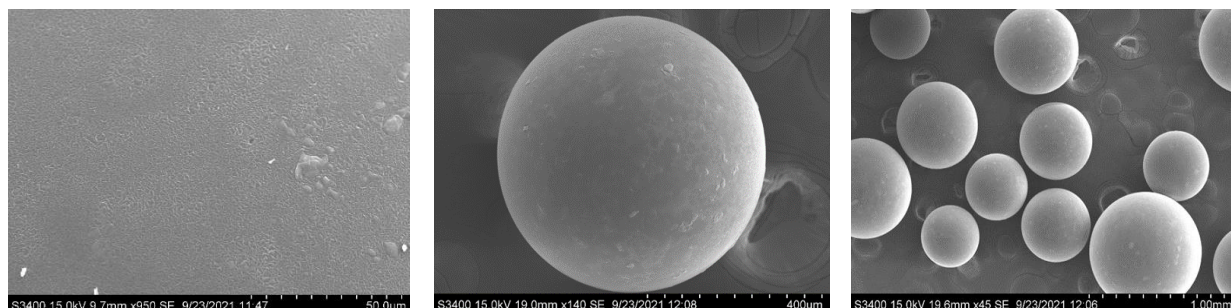
(a-3)



(b-1)

(b-2)

(b-3)



(c-1)

(c-2)

(c-3)

Figure 4-10 Comparison of SEM images of resins at three different conditions: a) fresh IRA67, b) IRA67 with UV irradiation only, and c) IRA67 with ARP treatment using 5 mM sulfite (Experimental condition: reaction volume = 1.0 L; solution pH = 10.0; UV irradiation time = 3.0 hours)

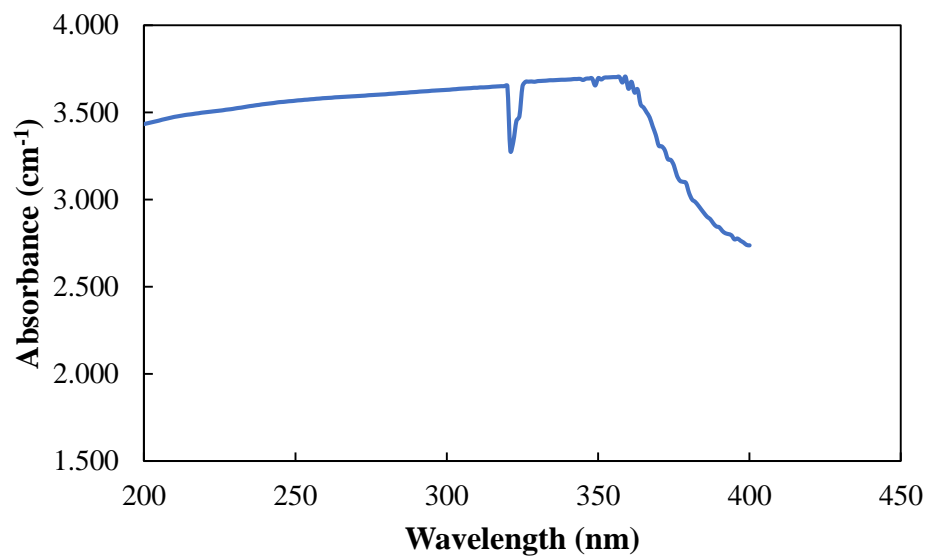


Figure 4-11 UV absorbance scan of IRA67 resins in water in a 1-cm quartz cell (wavelength = 200 – 400 nm)

References

- Albargane, A., Cui, J., Song, W., & Deng, Y. (2022). Advanced Reduction Processes for Degradation of Refractory Organics in Landfill Leachate. *Journal of Environmental Engineering*, 148(9), 04022046.
- An, D., Westerhoff, P., Zheng, M., Wu, M., Yang, Y., & Chiu, C.-A. (2015). UV-activated persulfate oxidation and regeneration of NOM-Saturated granular activated carbon. *Water research*, 73, 304-310.
- Ben-Amotz, D., & Mendes de Oliveira, D. (2021). Surfactant aggregate size distributions above and below the critical micelle concentration. *The Journal of chemical physics*, 155(22), 224902.
- Benjamin, M. M. (2014). *Water chemistry*. Waveland Press.
- Bolto, B., Dixon, D., & Eldridge, R. (2004). Ion exchange for the removal of natural organic matter. *Reactive and Functional Polymers*, 60, 171-182.
- Bolto, B., Dixon, D., Eldridge, R., King, S., & Linge, K. (2002). Removal of natural organic matter by ion exchange. *Water research*, 36(20), 5057-5065.
- Boyer, T. H., Fang, Y., Ellis, A., Dietz, R., Choi, Y. J., Schaefer, C. E., Higgins, C. P., & Strathmann, T. J. (2021). Anion exchange resin removal of per- and polyfluoroalkyl substances (PFAS) from impacted water: A critical review. *Water research*, 117244.
- Burns, D. C., Ellis, D. A., Li, H., McMurdo, C. J., & Webster, E. (2008). Experimental p K_a determination for perfluorooctanoic acid (PFOA) and the potential impact of p K_a concentration dependence on laboratory-measured partitioning phenomena and environmental modeling. *Environmental science & technology*, 42(24), 9283-9288.
- Canonica, S., Hellrung, B., Müller, P., & Wirz, J. (2006). Aqueous oxidation of phenylurea herbicides by triplet aromatic ketones. *Environmental Science & Technology*, 40(21), 6636-6641.
- Chellam, S., & Sari, M. A. (2016). Aluminum electrocoagulation as pretreatment during microfiltration of surface water containing NOM: A review of fouling, NOM, DBP, and virus control. *Journal of hazardous materials*, 304, 490-501.
- Croué, J.-P., Violleau, D., Bodaire, C., & Legube, B. (1999). Removal of hydrophobic and hydrophilic constituents by anion exchange resin. *Water Science and Technology*, 40(9), 207-214.
- Cui, J., & Deng, Y. (2022). Hydrated Electron Degradation of PFOA Laden on Ion-Exchange Resins in the Presence of Natural Organic Matter. *ACS ES&T Engineering*.

- Cui, J., Gao, P., & Deng, Y. (2020). Destruction of per- and polyfluoroalkyl substances (PFAS) with advanced reduction processes (ARPs): A critical review. *Environmental Science & Technology*, 54(7), 3752-3766.
- Dixit, F., Barbeau, B., Mostafavi, S. G., & Mohseni, M. (2020). Removal of legacy PFAS and other fluorotelomers: optimized regeneration strategies in DOM-rich waters. *Water research*, 183, 116098.
- Dixit, F., Barbeau, B., Mostafavi, S. G., & Mohseni, M. (2021). PFAS and DOM removal using an organic scavenger and PFAS-specific resin: Trade-off between regeneration and faster kinetics. *Science of The Total Environment*, 754, 142107.
- Dixit, F., Dutta, R., Barbeau, B., Berube, P., & Mohseni, M. (2021). PFAS removal by ion exchange resins: A review. *Chemosphere*, 129777.
- Dos Santos, G., Alto, R. M., Sampaio Filho, H., Da Silva, E., & Fellows, C. (2008). Light transmission on dental resin composites. *Dental materials*, 24(5), 571-576.
- Du, Z., Deng, S., Chen, Y., Wang, B., Huang, J., Wang, Y., & Yu, G. (2015). Removal of perfluorinated carboxylates from washing wastewater of perfluorooctanesulfonyl fluoride using activated carbons and resins. *Journal of hazardous materials*, 286, 136-143.
- Edzwald, J., & Association, A. W. W. (2011). *Water quality & treatment: a handbook on drinking water*. McGraw-Hill Education.
- Endruweit, A., Johnson, M., & Long, A. (2006). Curing of composite components by ultraviolet radiation: A review. *Polymer composites*, 27(2), 119-128.
- Exner, M., & Färber, H. (2006). Perfluorinated surfactants in surface and drinking waters (9 pp). *Environmental Science and Pollution Research*, 13(5), 299-307.
- Gao, P., Cui, J., & Deng, Y. (2021). Direct regeneration of ion exchange resins with sulfate radical-based advanced oxidation for enabling a cyclic adsorption-regeneration treatment approach to aqueous perfluorooctanoic acid (PFOA). *Chemical Engineering Journal*, 405, 126698.
- Kissa, E. (2001). *Fluorinated surfactants and repellents* (Vol. 97). CRC Press.
- LeBard, D. N., Levine, B. G., DeVane, R., Shinoda, W., & Klein, M. L. (2012). Premicelles and monomer exchange in aqueous surfactant solutions above and below the critical micelle concentration. *Chemical physics letters*, 522, 38-42.
- Ma, H., Allen, H. E., & Yin, Y. (2001). Characterization of isolated fractions of dissolved organic matter from natural waters and a wastewater effluent. *Water research*, 35(4), 985-996.

- Masotti, A. S., Onófrío, Á. B., Conceição, E. N., & Spohr, A. M. (2007). UV–vis spectrophotometric direct transmittance analysis of composite resins. *Dental materials*, 23(6), 724-730.
- Matilainen, A., Vepsäläinen, M., & Sillanpää, M. (2010). Natural organic matter removal by coagulation during drinking water treatment: A review. *Advances in colloid and interface science*, 159(2), 189-197.
- Miyazaki, Y., & Nakai, M. (2011). Protonation and ion exchange equilibria of weak base anion-exchange resins. *Talanta*, 85(4), 1798-1804.
- Park, M., Daniels, K. D., Wu, S., Ziska, A. D., & Snyder, S. A. (2020). Magnetic ion-exchange (MIEX) resin for perfluorinated alkylsubstance (PFAS) removal in groundwater: Roles of atomic charges for adsorption. *Water research*, 181, 115897.
- PubChem. (2021). Sulfite (URL: <https://pubchem.ncbi.nlm.nih.gov/compound/1099>) (Access Date: August 16, 2021).
- Rahmani, S., & Mohseni, M. (2017). The role of hydrophobic properties in ion exchange removal of organic compounds from water. *The Canadian Journal of Chemical Engineering*, 95(8), 1449-1455.
- Ritchie, J. D., & Perdue, E. M. (2003). Proton-binding study of standard and reference fulvic acids, humic acids, and natural organic matter. *Geochimica et Cosmochimica Acta*, 67(1), 85-96.
- Sangermano, M., Razza, N., & Crivello, J. V. (2014). Cationic UV-curing: Technology and applications. *Macromolecular Materials and Engineering*, 299(7), 775-793.
- Shukla, V., Bajpai, M., Singh, D., Singh, M., & Shukla, R. (2004). Review of basic chemistry of UV-curing technology. *Pigment & Resin Technology*.
- Siddiqi, M., Krissmann, J., Peters-Gerth, P., Luckas, M., & Lucas, K. (1996). Spectrophotometric measurement of the vapour-liquid equilibria of (sulphur dioxide+ water). *The Journal of Chemical Thermodynamics*, 28(7), 685-700.
- Traina, S. J., Novak, J., & Smeck, N. E. (1990). An ultraviolet absorbance method of estimating the percent aromatic carbon content of humic acids. *Journal of environmental quality*, 19(1), 151-153.
- Weishaar, J. L., Aiken, G. R., Bergamaschi, B. A., Fram, M. S., Fujii, R., & Mopper, K. (2003). Evaluation of specific ultraviolet absorbance as an indicator of the chemical composition and reactivity of dissolved organic carbon. *Environmental Science & Technology*, 37(20), 4702-4708.

- Xu, B., Liu, S., Zhou, J. L., Zheng, C., Weifeng, J., Chen, B., Zhang, T., & Qiu, W. (2021). PFAS and their substitutes in groundwater: Occurrence, transformation and remediation. *Journal of hazardous materials*, 412, 125159.
- Zagorodni, A. A. (2006). *Ion exchange materials: properties and applications*. Elsevier.
- Zareitalabad, P., Siemens, J., Hamer, M., & Amelung, W. (2013). Perfluorooctanoic acid (PFOA) and perfluorooctanesulfonic acid (PFOS) in surface waters, sediments, soils and wastewater—A review on concentrations and distribution coefficients. *Chemosphere*, 91(6), 725-732.
- Zhang, D., Yan, S., & Song, W. (2014). Photochemically induced formation of reactive oxygen species (ROS) from effluent organic matter. *Environmental Science & Technology*, 48(21), 12645-12653.
- Zhang, Y., Del Vecchio, R., & Blough, N. V. (2012). Investigating the mechanism of hydrogen peroxide photoproduction by humic substances. *Environmental Science & Technology*, 46(21), 11836-11843.

Chapter 5 Mitigation of Co-sorbed NOM on PFOA/NOM-laden Ion

Exchange Resins for Enhanced Hydrated Electron-induced Regeneration of Resins

5.1 Introduction and Objectives

Studies in **Chapter 4** demonstrate the potential of on-site generated e_{aq}^- for degradation of sorbed PFOA on IX resins (IRA67) in the presence of NOM. When UV/SO₃²⁻ ARP is applied to the treatment of PFOA/NOM sorbed IX resins in water, PFOA, regardless of an aqueous or sorbed state, can be effectively degraded. Meanwhile, this study highlights that the saturation of IRA67 in the removal of PFOA in the presence of NOM is primarily ascribed to the adsorption of NOM, which is much more abundant than PFOA in water.

The encouraging findings build a basis for development of a promising cyclic IX adsorption – ARP regeneration approach to the PFAS pollution in drinking water treatment. The new PFAS treatment route takes complementary advantages of IX and ARPs, while overcoming their respective restrictions (i.e., high costs and production of toxic PFAS-containing regenerant for IX resins; TDS increase, pH adjustment, and DO elimination for ARPs). This study represents the first scientific and engineering attempt to probe the interactions between e_{aq}^- and PFOA/NOM-laden IX resins. ARP, though effectively decomposing sorbed PFOA, cannot significantly degrade co-sorbed NOM to fully or largely recover the adsorption capacity of the resins. The accumulation of NOM on IRA67 may increasingly reduce the recovered capability for the PFOA adsorption with an increasing cycle number. Consequently, the proposed adsorption – on-site ARP regeneration approach cannot be truly applied.

To overcome the issue, an applicable approach is to mitigate the impact of co-sorbed NOM during the ARP regeneration of PFOA/NOM co-sorbed IX resins. Thus, further investigations are needed to combine the UV/SO₃²⁻ ARP with NOM mitigation strategies for

enhancing the regeneration of IX resins and permitting the capture of more PFOA in the following adsorption cycles.

In this chapter, two pathways for alleviation of co-sorbed NOM on IRA67 are proposed, including 1) pretreatment of PFOA-polluted water prior to IRA67 addition for mitigating NOM loading on IRA67, and 2) pH adjustment for desorption of NOM co-sorbed on IRA67 during the ARP regeneration.

The objectives of the research described in this chapter include 1) to evaluate two pretreatment strategies (i.e., coagulation and UV/H₂O₂-based AOP) for alleviating NOM loading on IRA67 in the adsorption phase; 2) to assess the effect of regenerant pH on the extents of co-sorbed NOM desorption during the IRA67 regeneration process; 3) to optimize the resin regeneration for effective degradation of sorbed PFOA on PFOA/NOM-laden IRA67; and 4) to evaluate whether the optimized cyclic adsorption-regeneration processes using appropriate co-sorbed NOM mitigation strategies can effectively and repeatedly remove PFOA in water. The study described in **Chapter 5** targets the NOM in raw water for maximizing the PFOA treatment efficiency in the IX adsorption – ARP regeneration approach.

5.2 Materials and Methods

5.2.1 Chemical and Reagents

All the reagents used were at least analytical grade, except as noted. WBA exchange resin (Amberlite™ IRA67) and CH₃CO₂NH₄ (> 97%) were obtained from Sigma-Aldrich. PFOA (96%, ACROS Organics™), hydrogen peroxide (H₂O₂; 30% w/w), potassium chromate (K₂CrO₄; 5% w/v indicator solution), NaCl (>99%), NaHCO₃ (>99%), HCl (37% solution in water), sulfuric acid (H₂SO₄; 0.5 M standard solution), and NaOH (> 97%) were purchased from Fisher Scientific. Aluminum sulfate hydrate (Alum; Al₂(SO₄)₃•(14-18)H₂O; >97%) and

silver nitrate (AgNO_3 ; 0.1N standardized solution) were purchased from Alfa Aesar. PFOA analytical standard solution (100 $\mu\text{g}/\text{mL}$ in methanol), non-ionic resin (Supelite™ DAX-8), Na_2SO_3 (> 98%), and methanol (LC-MS grade) were purchased from Millipore Sigma (Burlington, MA, USA.). SRNOM was purchased from the International Humic Substance Society (IHSS, St. Paul, MN, USA). All the solutions were prepared using ultrapure water (> 18.2 $\text{M}\Omega\cdot\text{cm}$) generated from a Milli-Q® water purification system (Milli-Q Direct 8). SRNOM stock solution (DOC = 100.0 mg/L) was prepared by adding an appropriate weight of SRNOM in the DI water and subsequently filtered with 0.45 μm microfiltration membrane to remove suspended matter. PFOA stock solution (PFOA = 100.0 mg/L) was prepared by adding an appropriate weight of PFOA in the DI water and subsequently filtered with 0.45 μm microfiltration membrane.

5.2.2 Experiments

5.2.2.1 Pretreatment of Simulated Natural Water by Alum Coagulation. To synthesize the simulated natural water (DOC = 5.0 mg/L), DI water was spiked with an appropriate aliquot of the SRNOM stock solution. Prior to alum coagulation, the fresh alum stock solution (10.0 g/L) was prepared. The NOM treatment efficiency of alum coagulation was maximized by optimizing pH and alum dose. To determine the optimal coagulation pH, different pH levels (i.e., 4.0, 5.0, 6.0, 7.0, 8.0, and 9.0) were tested at a fixed alum dose of 40.0 mg/L . Once the most favorable pH was found, different alum dosages (i.e., 0.0, 20.0, 40.0, 60.0, 80.0, 100.0, and 120.0 mg/L) were tested at the optimal pH.

All the alum coagulation tests were performed in 600 mL beakers with 500 mL simulated natural water on a four-paddle programmable jar tester (Phipps & Bird - 7790-950). The initial solution pH was adjusted to the required value with 0.1 mM NaOH or HCl solution. The alum

coagulation process was initiated once an aliquot volume of alum stock solution was introduced to each solution. Within two minutes, a rapid mixing (150 rpm) was applied to disperse the added alum stock solution rapidly and completely. In the following 40 mins, a slow mixing (30 rpm) was used to ascertain a complete mixing state. The solution pH was monitored with a pH meter and adjusted with 0.1 mM NaOH or HCl solution during the alum coagulation process. After the mixing was stopped, sedimentation proceeded for one hour to permit the settling of the formed flocs. The supernatant was collected and filtered with 0.45 μm nylon membrane (Corning™ nylon syringe filters). The filtrate was sampled for further analysis. The visualization of the alum coagulation process for simulated natural water is shown in **Figure 5-1**.

5.2.2.2 UV/H₂O₂-based AOP Treatment of Pre-coagulated Water. The UV/H₂O₂-based AOP treatment of pre-coagulated water was performed in a 1 L closed thermostatic cylindrical quartz photo-reactor (model 7840-185, ACE Glass Inc.) (**Figure 3-1**). Two hundred milliliters of pre-coagulated water after alum coagulation processes (alum 60.0 mg/L; pH 6.0) were loaded into the reactor. The cylinder-shaped reactor had a height of 440 mm and a diameter of 85.5 mm. The inner and outer diameters of a 450-mm high quartz immersion well in the cylinder center were 31 and 48 mm, respectively. A 450 W medium-pressure (200 to 400 nm) mercury lamp with a UV intensity of 187 $\mu\text{W}/\text{cm}^2$ was placed in the quartz immersion well. Of total energy radiated, approximately 40% to 48% is in the ultraviolet portion of the spectrum. Before UV/H₂O₂-based AOP treatment, an aliquot volume of H₂O₂ (30% w/w) was introduced into the reactor to achieve an initial H₂O₂ concentration at 15.0 mg/L. The selected initial H₂O₂ concentration falls within the typical H₂O₂ range reported in the commercial UV/H₂O₂-based process (H₂O₂; <15.0 mg/L) for drinking water treatment (Sarathy et al., 2011; Sillanpää et al., 2018). The initial pH was adjusted to 7.5 with 0.1 mM NaOH or HCl solution. The AOP

treatment was launched once the UV lamp was turned on. During the UV irradiation, pH was not controlled or buffered. Cooling water was continuously circulated to control the solution temperature at 25 ± 1 °C. A magnetic stirrer was used to ensure a thoroughly mixed state. All the UV irradiation tests were conducted in a photochemical safety cabinet. The UV/H₂O₂ treatment proceeded for one hour, within which all the added H₂O₂ was depleted. After AOP treatment, the solution in the UV reactor was filtered with 0.45 µm nylon membrane and collected for further analysis.

5.2.2.3 IRA67 Adsorption of NOM in Simulated Natural Water and Pre-coagulated Water. IRA67 adsorption behaviors of NOM were compared in diluted simulated natural water and pre-coagulated water. IRA67 resins were first rinsed to remove impurities on the surface, as described in **Chapter 3**. One liter of pre-coagulated water treated at the optimal conditions (i.e., alum 60.0 mg/L; pH 6.0) was prepared. One liter of diluted simulated natural water was prepared by diluting initial simulated natural water with DI water to achieve the same DOC as the pre-coagulated water.

The NOM adsorption tests were performed in 1 L beakers with 1.0 L diluted simulated natural water or pre-coagulated water on a four-paddle programmable jar tester. The rinsed fresh resins (5.0 g/L) were introduced to either solution. The initial pH was adjusted to 7.5 with 0.1 mM NaOH or HCl solution. The adsorption proceeded for 24 hours with a 120 rpm stirring at 25 °C before the solution was filtered with a 0.45 µm nylon membrane. The filtrate was collected for further analysis.

5.2.2.4 NOM Characterization after Different Treatment Processes. MW fractionation tests were carried out to determine the MW distribution of NOM in simulated natural water, pre-coagulated water, and pre-coagulated water after resin (5.0 g/L) adsorption.

Three hundred milliliter of simulated natural water, pre-coagulated water, or pre-coagulated water after resin (5.0 g/L) adsorption was sequentially filtered by different ultrafiltration (UF) membranes on a stirred cell (Amicon 8200, Millipore, Billerica, USA) driven by pressured N₂ gas. Two MW cut-off UF membranes (i.e., 100 and 10 kDa) (EMD Millipore, regenerated cellulose) were used. Before the MW fractionation, each UF membrane was used to filter 2.0 L DI water. All the filtrates were collected for further analysis. The visualization of the MW fractionation process with a UF stirred cell is shown in **Figure 5-2(a)**.

Furthermore, a solid phase extraction (SPE) technique was used to extract fulvic acid (FA), humic acid (HA), and HPI fractions from dissolved NOM. The method was used as described in detail elsewhere (Christensen et al., 1998). Briefly, each NOM solution was initially filtered with a 0.45 μm nylon membrane. Thereafter, the filtrate was acidified to pH 2.0 with 10 mM HCl, and before acidified solution stood on a bench overnight at room temperature (25 ± 1 °C). All the precipitates were HA that could be separated from the solution with 30-min centrifugation at 4,500 rpm. The HA precipitates were then collected, redissolved in 0.05 M NaOH, and purified using dialysis against 0.1 mM HCl and ultrapure water. The solution, after removing the HA fraction, was pumped through the clean DAX-8 resins (20-60 mesh). The portion retained on the resin was the FA fraction, while the portion passed through the resin column was HPI isolates (Thurman & Malcolm, 1981). The visualization of the SPE process for the separation of FA and HPI isolates is shown in **Figure 5-2(b)**.

5.2.2.5 Adsorption Isotherms of IRA67 for PFOA in Different PFOA-containing Waters. Adsorption isotherm experiments using IRA67 were carried out in different PFOA-containing water systems. Prior to adsorption tests, an appropriate aliquot of the PFOA stock solution was first spiked into simulated natural water, pre-coagulated water (alum 60.0 mg/L; pH

6.0), and pre-coagulated water after UV/H₂O₂-based AOP, separately, to achieve the initial PFOA concentration at 20.0 µg/L. The initial pH was adjusted to 7.5 with 0.1 mM NaOH or HCl solution. A typical batch adsorption run was performed in a 200 mL flask with 100 mL of PFOA-containing solution on a shaker (Thermo Scientific MaxQ™ 2508). Resins were dosed from 0.1 to 2.0 g/L (i.e., 10 to 200 mg) in each flask. The flasks were shaken on the shaker at 150 rpm for 24 hours at 25 °C. After 24 hours, the solution was filtered with a 0.45 µm nylon membrane. The filtrate was stored to measure residual PFOA for quantifying the PFOA sorbed on IRA67, while IRA67 was collected for further analysis.

5.2.2.6 NOM and PFOA Desorption from PFOA/NOM Preloaded IRA67. PFOA and/or NOM preloading tests were first performed. Fresh IRA67 resins (0.1g) were introduced to 0.1 L of four different PFOA and/or NOM containing solutions, separately. The solution included 1) PFOA-containing (20.0 µg/L) water; 2) PFOA-containing (100.0 µg/L) water; 3) PFOA/NOM containing water (20.0 µg/L PFOA and 5.0 mg/L DOC); and 4) PFOA/NOM containing water (100.0 µg/L PFOA and 25.0 mg/L DOC). The initial pH of each solution was adjusted to 7.5 with 0.1 mM NaOH or HCl solution. Each solution was loaded in a 200 mL flask on the shaker. The flasks were shaken on the shaker at 150 rpm for 24 hours at 25 °C before the solution was filtered with a 0.45 µm nylon membrane. All the preloaded resin beads were collected for subsequent PFOA and/or NOM desorption tests. The extent of PFOA and/or NOM adsorption on each preloaded IRA67 was 1) 20.0 µg PFOA/g IRA67; 2) 100.0 µg PFOA/g IRA67; 3) 13.25 µg PFOA and 3.86 µg DOC/g IRA67; 4) 21.12 µg PFOA and 11.55 mg DOC/g IRA67.

Each PFOA and/or NOM preloaded IRA67 was then loaded into 0.1 L DI water with different pH levels (9.0 to 12.0) in a 200 mL flask. The flasks were shaken on the shaker at 150

rpm for 24 hours at 25 °C before filtration with 0.45 µm nylon membrane. The filtrates at different pH levels were collected for further analysis.

5.2.2.7 NOM and PFOA Multiple Loading Tests on IRA67 in Pre-coagulated Water.

NOM and PFOA multiple loading tests on IRA67 were performed over ten cycles to synthesize the PFOA/NOM-laden IRA67. The PFOA-containing pre-coagulated water (20.0 µg/L PFOA) was first prepared by spiking with an appropriate aliquot of the PFOA stock solution into pre-coagulated water after alum coagulation processes (alum 60.0 mg/L; pH 6.0). The initial pH of each solution was adjusted to 7.5 with 0.1 mM NaOH or HCl solution. Thereafter, 0.1g fresh IRA67 was introduced to 200.0 mL PFOA-containing pre-coagulated water in a 600 mL beaker on a four-paddle programmable jar tester. The adsorption proceeded for 30 mins with a 150 rpm stirring at 25 °C before the solution was filtered with a 0.45 µm nylon membrane. The IRA67 from the previous adsorption process was subsequently collected and transferred to the following adsorption process using a new 200.0 mL PFOA-containing pre-coagulated water. The filtrates from each adsorption solution were collected to measure PFOA and DOC concentration. The visualization of NOM and PFOA loading processes on IRA67 in PFOA-containing pre-coagulated water using a jar tester is shown in **Figure 5-3(a)**.

5.2.2.8 Desorption of NOM and PFOA on IRA67 from Multiple Loading Tests.

Experiments concerning the desorption of NOM and PFOA on IRA67 from multiple loading tests were conducted at different pH levels. Prior to desorption tests, IRA67 (4.23 mg DOC/g and 106.4 µg PFOA/g IRA67) was initially prepared using multiple loading tests. 0.1 g PFOA and NOM preloaded IRA67 was introduced in a 200 mL flask with 100 mL DI water on the shaker. The initial pH of DI water in the flask ranged from 9.0 to 14.0, which was adjusted with 1 M NaOH or HCl solution. The flasks were shaken on the shaker at 150 rpm for 24 hours at 25 °C.

After 24 hours, the solution was filtered with a 0.45 μm nylon membrane. The filtrate at each pH level was stored to measure the desorbed PFOA and NOM from IRA67. The visualization of the desorption of NOM and PFOA on IRA67 from multiple loading tests at different pH solutions using a shaker is shown in **Figure 5-3(b)**.

5.2.2.9 UV/SO₃²⁻ Treatment for PFOA Degradation on IRA67 from Multiple Loading Tests. Prior to UV/SO₃²⁻ treatment, IRA67 (4.23 mg DOC/g and 106.4 μg PFOA/g IRA67) was initially prepared using multiple loading tests. A 100 mL solution containing 0.1 g PFOA and NOM preloaded IRA67 was loaded in a 1 L closed thermostatic cylindrical quartz photo-reactor for the UV/SO₃²⁻ treatment. In this study, different sulfite dosages (0.0, 5.0, 10.0, 20.0, and 40.0 mM) were introduced in the reactor, respectively, with the addition of appropriate amounts of Na₂SO₃. A 450 W medium-pressure mercury lamp (200-400 nm) placed in a quartz tube was inserted in the center of the reactor. Before reactions, the solution was purged with N₂ for 40 min to eliminate DO. The initial pH was adjusted to 10.0 with 1.0 mM NaOH solution. During the UV irradiation, pH was not controlled or buffered. Cooling water was continuously circulated to control the solution temperature at 25 ± 1 °C. A magnetic stirrer was used to ensure a completely mixed state. The UV/SO₃²⁻ ARP treatment was launched once the UV lamp was turned on. All the UV irradiation tests were conducted in a photochemical safety cabinet. The UV/SO₃²⁻ treatment proceeded for three hours. Control tests were carried out at identical conditions in the absence of UV irradiation and Na₂SO₃. After ARP treatment, the solution was filtered with a 0.1 μm nylon membrane. The filtrate at each treatment was stored to measure the residual PFOA. The IRA67 after each treatment was collected to quantify the sorbed PFOA on IRA67.

5.2.2.10 PFOA and Sulfite Decay during UV/SO₃²⁻ ARP Treatment. PFOA and sulfite decay experiments were carried out during UV/SO₃²⁻ ARP treatment of PFOA/NOM-laden IRA67. Prior to UV/SO₃²⁻ ARP treatment, IRA67 (4.23 mg DOC/g and 106.4 µg PFOA/g IRA67) was initially prepared using multiple loading tests. A 100 mL solution containing 0.1 g PFOA and NOM preloaded IRA67 was loaded in a 1 L closed thermostatic cylindrical quartz photo-reactor for the UV/SO₃²⁻ treatment. A 450 W medium-pressure mercury lamp (200-400 nm) placed in a quartz tube was inserted in the center of the reactor. Before reactions, the solution was purged with N₂ for 40 min to eliminate DO. Initial pH was adjusted to 10.0 with 1.0 mM NaOH solution. During the UV irradiation, pH was not controlled or buffered. Cooling water was continuously circulated to control the solution temperature at 25 ± 1 °C. A magnetic stirrer was used to ensure a completely mixed state. To initiate the e_{aq}⁻ generation, appropriate amounts of Na₂SO₃ were dosed to the solution to make the initial sulfite concentration at 20 mM before the UV lamp was turned on. All the UV irradiation tests were conducted in a photochemical safety cabinet. In this study, the UV/SO₃²⁻ treatment time for IRA67 ranged from 0 to 3 hours (i.e., 0, 5, 10, 20, 30, 45, 60, 90, 120, and 180 min). After each selected ARP treatment time, the UV lamp was switched off. After that, the solution was filtered with a 0.1 µm nylon membrane. The filtrate was immediately collected to measure the residual PFOA and sulfite concentration. The IRA67 after each treatment was collected to quantify the sorbed PFOA on IRA67.

5.2.2.11 Cyclic Adsorption-regeneration Tests. Cyclic adsorption-regeneration tests were carried out over six cycles. Each cycle was composed of a NOM/PFOA multiple loading phase and a UV/SO₃²⁻ treatment. The NOM/PFOA multiple loading tests were identical to the NOM/PFOA multiple loading tests, as described in **Section 5.2.2.7**. The following UV/SO₃²⁻

treatment experiments were performed at conditions similar to the UV/SO₃²⁻ treatment tests as described in **Section 5.2.2.9.**, except that the initial sulfite dose was fixed at 20.0 mM. Control experiments were conducted without the UV/SO₃²⁻ treatment phase in each cycle. The visualization of fresh IRA67, IRA67 with no regeneration after six cyclic adsorption-regeneration tests, and ARP regenerated IRA67 after six cyclic adsorption-regeneration tests is shown in **Figure 5-4.**

5.2.2.12 IRA67 Ion-exchange Capacity Measurement Tests. The experiments concerning the measurement of IRA67 ion-exchange capacity (IEC) were conducted. Fresh resin and the resins from the cyclic adsorption-regeneration test as well as the control experiment in **Section 5.2.2.11** were selected in this study. The measurement of IRA67 IEC was composed of three parts. The first part was to convert the free base (OH⁻) form of IRA67 into its chloride (Cl⁻) form, as described in detail elsewhere (Deng et al., 2010; Moldes et al., 2003). Briefly, IRA67 in Cl⁻ form was obtained by washing 0.1 g IRA67 sequentially with 1 M HCl solution, DI water, 1 M NaOH solution, DI water, 1 M HCl solution, and DI water (until pH =7.0). Thereafter, IRA67 was collected and air-dried until free flowing. The second part was to extract the Cl⁻ sorbed on IRA67 to the solution. Specifically, 0.1 g IRA67 was introduced in a 200 mL flask with 100 mL of 1 M NaOH solution on the shaker. The flasks were shaken on the orbital shaker at 150 rpm for 24 hours at 25 °C. After 24 hours, the solution was filtered with a 0.45 μm nylon membrane and collected for the following experiment. The third part was to determine chloride ion concentration by titration using Mohr's method (Korkmaz, 2001). Briefly, 50.0 mL of solution from the second part was transferred into a 100 mL volumetric flask. Thereafter, the solution was diluted to 100.0 mL by adding DI water. The solution pH was adjusted to 8.3 with 0.1 mM NaOH or H₂SO₄ solution. After that, 1.0 mL of K₂CrO₄ indicator solution was introduced to the

solution. Then, the mixed solution was titrated with 0.1 M AgNO_3 standard solution. The endpoint of the titration was identified as the first appearance of a red-brown color of silver chromate. The total volume of used 0.1 M AgNO_3 standard solution was measured to calculate the chloride ion concentration in the solution.

5.2.3 Sample Analyses

Solution pH was measured with a Thermo Scientific Orion 5-Star Plus pH meter. DOC was analyzed by measuring TOC in the water filtered by a 0.45 μm nylon membrane with a TOC analyzer (TOC-LCPH, Shimadzu Corp., Kyoto, Japan). UV_{254} absorbance was analyzed using a UV/Vis spectrophotometer (HACH, DR5000). SO_3^{2-} concentration in water was quantified using sulfite test kits (Model SU-5, HACH). PFOA in water was analyzed with a HPLC-MS/MS (Agilent 6460C). To quantify PFOA sorbed on the resins, the sorbed PFOA was extracted from the resins to water before analysis of aqueous PFOA. PFOA measurement and extraction are described in detail in **Chapter 4**. After the cyclic adsorption-regeneration tests, PFOA remaining on the resins was extracted to aqueous phase before analyses of aqueous PFOA, which represented overall residual PFOA on the resins. After the $\text{UV}/\text{SO}_3^{2-}$ treatment of the resin beads, the amount of degraded PFOA was the difference between PFOA sorbed on resins before the treatment and aqueous PFOA after treatment and extraction. Morphology and elemental analysis of the resins were determined using SEM (Hitachi S-3400N) with EDS. Two adsorption isotherm models were used to fit the experimental data at chemical equilibrium, including the Langmuir and Freundlich models, as shown in Eq. (3-1) and (3-2), respectively (Rahimi et al., 2014). The non-linear least-square optimization technique was used to evaluate the fit of the aforementioned adsorption isotherm models as well as pseudo-first order reaction models in PFOA decomposition using the Solver Add-In in Microsoft Excel (Version 2020). Chi-square tests were

used as a statistical “goodness-of-fit” criterion. The chi-square goodness-of-fit test is based on Eq. (3-3) and (3-4). The equilibrium sorption amount of PFOA on IRA67 in different PFOA-containing water systems were compared with the Students’ t-tests (95% confidence limits) using the Solver Add-In of Microsoft Excel. All analytical results reported represent the mean of three replicate samples, with error bars corresponding to one standard deviation.

5.3 Results

After the pretreatment of simulated natural water (DOC = 5.00 mg/L; UV₂₅₄ absorbance = 0.130 cm⁻¹) with alum coagulation, the residual DOC and UV₂₅₄ absorbance are shown in **Figure 5-5**. As seen in **Figure 5-5(a)**, the residual DOC gradually declined from 4.84 to 1.47 mg/L as the pH increased from 4.0 to 6.0, at a fixed alum dose of 40.0 mg/L. However, when the pH level increased from 6.0 to 9.0, the residual DOC steadily went back to 4.95 mg/L, indicating that the optimal coagulation pH was 6.0 during alum coagulation. Similar patterns of residual UV₂₅₄ absorbance were observed (**Figure 5-1(b)**). With the pH increase from 4.0 to 5.0, the UV₂₅₄ absorbance dramatically decreased from 0.100 to 0.000 cm⁻¹. No UV₂₅₄ absorbance was observed at pH 5.0 - 7.0. As the pH level further increased from 7.0 to 9.0, the UV₂₅₄ absorbance significantly increased to 0.130 cm⁻¹. In contrast, the residual DOC and UV₂₅₄ absorbance at pH 6.0 with different alum dosages are displayed in **Figures 5-5(c)** and **(d)**, respectively. As shown in **Figure 5-5(c)**, the residual DOC gradually decreased from 1.92 to 1.24 mg/L with the increasing alum dose from 20.0 to 60.0 mg/L. As the alum dose further increased from 60.0 to 120.0 mg/L, the residual DOC remained constant. Meanwhile, no UV₂₅₄ absorbance was observed when the applied alum dose was between 40.0 and 120.0 mg/L. Thus, when the 60.0 mg/L alum was applied at pH 6.0, the maximum DOC and UV₂₅₄ absorbance removals were achieved in the simulated natural water.

DOC in UV/H₂O₂-based AOP treatment of pre-coagulated water is shown in **Figure 5-6**. Residual DOC in the control solution (i.e., pre-coagulated water after optimized alum coagulation (alum 60.0 mg/L; pH 6.0)) was 1.32 mg/L. As shown in **Figure 5-6**, the DOC (i.e., 1.31 mg/L) was not further reduced after one-hour UV irradiation in the absence of H₂O₂. The finding indicates that UV/H₂O₂-based AOP cannot effectively mineralize remaining NOM in simulated natural water after alum coagulation.

The DOC levels in diluted simulated natural water and pre-coagulated water before and after fresh IRA67 (5.0 g/L) adsorption are presented in **Figure 5-7**. The initial DOC values in diluted simulated natural water and pre-coagulated water were approximately 1.30 and 1.30 mg/L, respectively. After IRA67 adsorption, the DOC in diluted simulated natural water was significantly decreased to 0.31 mg/L. In contrast, the residual DOC slightly declined to 1.12 mg/L in pre-coagulated water after IRA67 adsorption, indicating that a majority of NOM in pre-coagulated water cannot be removed by IRA67.

DOC and UV₂₅₄ absorbance in different MW fractions (i.e., >100 kDa, 10-100 kDa, and <10 kDa) of the simulated natural water, pre-coagulated water, and pre-coagulated water after resin (5.0 g/L) adsorption are shown in **Figures 5-8(a)** and **(b)**, respectively. As shown in **Figure 5-8(a)**, the DOC levels in the simulated natural water of >100 kDa, 10-100 kDa, and <10 kDa were 0.15, 3.28, and 1.56 mg/L, respectively. As shown in **Figure 5-8(b)**, UV₂₅₄ absorbance in simulated natural water of >100 kDa, 10-100 kDa, and <10 kDa was 0.007, 0.122, and 0.001 cm⁻¹, respectively. The medium MW group possessed the major portions of the overall NOM in terms of DOC and UV₂₅₄ absorbance. Of note, the DOC in pre-coagulated water of >100 kDa, 10-100 kDa, and <10 kDa was 0.02, 0.26, and 1.43 mg/L, respectively. This result showed that high and medium MW groups were preferentially removed during alum coagulation, while only

a slight reduction in the low MW group could be achieved in terms of DOC. Moreover, the DOC in pre-coagulated water after resin (5.0 g/L) adsorption of >100 kDa, 10-100 kDa, and <10 kDa was 0.01, 0.05, and 1.46 mg/L, respectively, indicating that only medium MW fraction was further removed during resin adsorption in pre-coagulated water in terms of DOC. As shown in **Figure 5-8(b)**, the UV₂₅₄ absorbance of >100 kDa, 10-100 kDa, and <10 kDa in pre-coagulated water as well as pre-coagulated water after resin (5.0 g/L) adsorption was not detected.

The DOC and UV₂₅₄ absorbance in the HPO and HPI fractions of NOM (i.e., HA, FA, and HPI) in the simulated natural water, pre-coagulated water, and pre-coagulated water after resin (5.0 g/L) adsorption are presented in **Figures 5-8(c)** and **(d)**, respectively. As shown in **Figure 5-8(c)**, DOC in the simulated natural water of HA, FA, and HPI was 0.15, 3.37, and 1.50 mg/L, respectively. As shown in **Figure 5-8(d)**, UV₂₅₄ absorbance of HA, FA, and HPI in the simulated water was 0.007, 0.122, and 0.001 cm⁻¹, respectively. The FA fraction played a critical role in contributing to the overall DOC and UV₂₅₄ absorbance. Of interest, the DOC in pre-coagulated water of HA, FA, and HPI declined to 0.01, 0.27, and 1.48 mg/L, respectively. This result showed that the primary reduction of NOM during alum coagulation was attributed to the removal of the HPO fractions, particularly FA.

Moreover, DOC in the pre-coagulated water after resin (5.0 g/L) adsorption of HA, FA, and HPI further declined to 0.01, 0.05, and 1.48 mg/L, respectively, suggesting that only the FA fraction was effectively removed during the resin adsorption from the pre-coagulated water in terms of DOC. As shown in **Figure 5-8(d)**, the UV₂₅₄ absorbance of HA, FA, and HPI in the pre-coagulated water as well as pre-coagulated water after resin (5.0 g/L) adsorption was not obtained.

Adsorption isotherms of PFOA on the fresh IRA67 in PFOA-containing simulated natural water, pre-coagulated water, and AOP-treated pre-coagulated water are shown in **Figure 5-9**. Two different adsorption isotherm models were attempted to fit experimental data at chemical equilibrium for six IRA67 dosages (i.e., 0.2, 0.3, 0.4, 0.5, 1.0, and 2.0 g/L). At a 95% confidence level, the Langmuir and Freundlich model passed the goodness-of-fit tests in all the studied experimental conditions. Results showed that the adsorption isotherm of PFOA on IRA67 in pre-coagulated PFOA-containing water was significantly different ($p < 0.05$) from the adsorption isotherm without coagulation pre-treatment, indicating that more PFOA was adsorbed on IRA67 after the optimized alum coagulation of simulated natural water. In contrast, the adsorption isotherm of PFOA on IRA67 in AOP-treated pre-coagulated PFOA-containing water was not significantly different ($p > 0.05$) from that with pre-coagulated treatment in the studied experimental conditions, highlighting that no additional PFOA was further adsorbed on IRA67 after the UV/H₂O₂-based AOP treatment of pre-coagulated water.

Desorption of PFOA from 20.0 µg PFOA/g IRA67 and 100.0 µg PFOA/g IRA67 in DI water at different pH levels is shown in **Figures 5-10(a)** and **(b)**, respectively. Results showed that PFOA initially sorbed on IRA67 was gradually desorbed as the solution pH increased from 9.0 to 12.0, suggesting that the solution pH contributes to the desorption of sorbed PFOA on PFOA-laden IRA67. At pH 11.0 or greater, most PFOA sorbed on IRA67 (>97%) were desorbed in solution regardless of the mass of PFOA sorbed on the resins in the studied experimental conditions. Furthermore, the fate of PFOA and NOM on 13.25 µg PFOA and 3.86 mg DOC/g IRA67 as well as 21.12 µg PFOA and 11.55 mg DOC/g IRA67 in DI water at different pH levels is shown in **Figures 5-10(c)**, **(d)**, **(e)**, **(f)**, **(g)**, and **(h)**, respectively. As shown in **Figures 5-10(c)** and **(d)**, PFOA initially sorbed on IRA67 was also gradually desorbed in solution as the pH

increased from 9.0 to 12.0, highlighting that solution pH played a critical role in the desorption of sorbed PFOA on PFOA/NOM-laden IRA67. At pH 11.0 or greater, most PFOA sorbed on IRA67 (>97%) were desorbed in solution in the presence of co-sorbed NOM on IRA67 in the studied experimental conditions. Of interest, the portion of desorbed PFOA from IRA67 in the presence of co-sorbed NOM at each pH level in **Figures 5-10(c)** and **(d)** was similar to that of desorbed PFOA on IRA67 in the absence of sorbed NOM in **Figures 5-10(a)** and **(b)**, spotlighting that the mass of co-sorbed NOM on IRA67 little affects the extent of PFOA desorption from IRA67. Furthermore, as shown in **Figures 5-10(e)** and **(f)**, NOM initially sorbed on IRA67 was gradually desorbed in solution as solution pH increased from 9.0 to 12.0, implying that solution pH significantly influences the desorption of sorbed NOM on IRA67. However, different from the complete PFOA desorption at pH 12.0, approximately 25% of NOM remained on IRA67, as shown in **Figures 5-10(e)** and **(f)**. Meanwhile, the mass of co-sorbed NOM on resins had little effect on the portion of sorbed NOM on IRA67 desorbed to the solution in the studied experimental conditions. Additionally, UV₂₅₄ absorbance in solution increased as solution pH increased from 9.0 to 12.0, as shown in **Figures 5-10(g)** and **(h)**. Of note, the UV₂₅₄ absorbance in solution had a relatively low value at each pH as compared to the UV₂₅₄ absorbance of corresponding DOC in solution, suggesting that the released NOM possessed a high fraction of non-humic and HPI NOM molecule, while more HPO NOM molecules were still associated with the IRA67.

The residual DOC and accumulative NOM adsorbed on IRA67 in PFOA-containing pre-coagulated water after each NOM/PFOA loading cycle are shown in **Figure 5-11(a)**. As shown in **Figure 5-11(a)**, the residual DOC in solution decreased from an initial 1.19 to 0.98 mg/L after the first loading cycle. As the cycle number increased, the residual DOC in each solution almost

remained constant. After the 10th loading cycle, the residual DOC in solution was approximately 1.01 mg/L, indicating that the adsorption capability of IRA67 on NOM was not significantly changed in PFOA-containing pre-coagulated water. Meanwhile, after ten loading cycles, 4.23 mg DOC/g was cumulatively adsorbed on IRA67. Moreover, the residual PFOA and accumulative PFOA adsorbed on IRA67 in PFOA-containing pre-coagulated water after each loading cycle are shown in **Figure 5-11(b)**. Specifically, the PFOA in the solution was reduced from the initial 20.0 to 13.4 $\mu\text{g/L}$ after the first loading cycle. As the loading cycle increases from one to ten, the residual PFOA gradually increased from 13.4 to 16.2 $\mu\text{g/L}$, suggesting that the adsorption capability of IRA67 on PFOA was significantly decreased in PFOA-containing pre-coagulated water. Eventually, 106.4 $\mu\text{g PFOA/g}$ was cumulatively adsorbed on IRA67 after ten loading cycles.

The fate of NOM and PFOA on 106.4 $\mu\text{g PFOA}$ and 4.23 mg DOC/g IRA67 in DI water at different pH levels (9.0-14.0) is shown in **Figures 5-12(a)** and **(b)**, respectively. As shown in **Figure 5-12(a)**, NOM initially sorbed on IRA67 was gradually desorbed in solution as solution pH increased from 9.0 to 14.0. Specifically, only half of the NOM sorbed on IRA67 was desorbed in solution at pH 9.0. At pH 10.0, the majority of sorbed NOM (i.e., 92.8%) was desorbed in solution, which was significantly different from the results shown in **Figures 5-10(e)** and **(f)**, indicating that the sorbed NOM from pre-coagulated water was readily desorbed in solution as compared to the sorbed NOM from simulated natural water. At pH 11.0 or greater, most NOMs sorbed on IRA67 (>97%) were desorbed in solution in the studied experimental conditions. As shown in **Figure 5-12(b)**, PFOA initially sorbed on IRA67 was also gradually desorbed in solution as solution pH increased from 9.0 to 14.0. Different from the complete

NOM desorption at pH 10.0, only half of the PFOA sorbed on IRA67 was desorbed in solution at pH 10.0.

Residual PFOA in solution and sorbed on the resin after the UV/SO₃²⁻ treatment of IRA67 (106.4 µg PFOA and 4.23 mg DOC/g) from ten cyclic NOM and PFOA loading tests at different sulfite dosages is shown in **Figure 5-13**. Specifically, PFOA desorbed in solution and sorbed on resins after each treatment process was demonstrated. In the control test and 0 mM sulfite test, approximately half of PFOA remained on IRA67, while the other half desorbed to the solution. At 5 mM sulfite, PFOA in the solution was completely degraded. Nevertheless, only half of the PFOA sorbed on resins was degraded. As the sulfite concentration increased, PFOA sorbed on resins were increasingly decomposed. When the sulfite dose reached 20 mM, PFOA, both desorbed in solution and sorbed on resins, was completely degraded within three hours.

Kinetic results of PFOA and sulfite decomposition during the UV/SO₃²⁻ ARP treatment of IRA67 from the NOM and PFOA cyclic loading tests (106.4 µg PFOA and 4.23 mg DOC/g) are shown in **Figures 5-14(a)** and **(b)**, respectively. As shown in **Figure 5-14(a)**, PFOA desorbed in solution was completely degraded in the UV/SO₃²⁻ ARP treatment process within 90 mins, while PFOA sorbed on resins was fully decomposed within 180 mins in the studied experimental conditions. Thus, 180 mins were needed to fully degrade the overall PFOA in this study. As shown in **Figure 5-15**, the decomposition of PFOA desorbed in the solution, PFOA sorbed on IRA67, and overall PFOA all followed pseudo-first order reaction patterns ($R^2=0.99$), with their corresponding rate constants of 0.061, 0.021, and 0.028 min⁻¹. Meanwhile, as shown in **Figure 5-14(b)**, less than half of the sulfite in the solution decayed in the UV/SO₃²⁻ ARP treatment process within 180 mins, indicating that more than half of the sulfite remained in the solution after the ARP treatment.

The residual DOC and accumulative NOM adsorbed on IRA67 after each loading test during six cyclic adsorption-regeneration tests are shown in **Figures 5-16(a)** and **(b)**, respectively. As shown in **Figure 5-16(a)**, the initial DOC in pre-coagulated water was 1.19 mg/L. Of interest, the residual DOC in the control test after each loading test dramatically increased from 0.96 mg/L to 1.09 mg/L during six cyclic adsorption-regeneration tests. In contrast, a slight increase of residual DOC from 0.96 to 0.99 mg/L was observed in the ARP-treated test after each loading test during six cyclic adsorption-regeneration tests. As shown in **Figure 5-16(b)**, cumulative NOM adsorbed on IRA67 in the control test increased to 18.60 mg DOC/g after six cyclic adsorption-regeneration tests, while cumulative NOM adsorbed on IRA67 in the ARP-treated test increased to 24.98 mg DOC/g, showing that more NOM was adsorbed on the IRA67 after ARP regeneration processes.

Moreover, the residual PFOA and accumulative PFOA adsorbed on IRA67 after each loading test during six cyclic adsorption-regeneration tests are shown in **Figures 5-16(c)** and **(d)**, respectively. As shown in **Figure 5-16(c)**, the initial PFOA in pre-coagulated water was 20.0 $\mu\text{g/L}$. Of interest, the residual PFOA in the control test after each loading test dramatically increased from 13.4 to 19.4 $\mu\text{g/L}$ during six cyclic adsorption-regeneration tests. However, the relatively less enhancement of residual PFOA from 13.4 $\mu\text{g/L}$ to 16.9 $\mu\text{g/L}$ was obtained in the ARP-treated test as compared to the results in the control test. As shown in **Figure 5-16(d)**, cumulative PFOA adsorbed on IRA67 increased to 290.7 and 566.4 $\mu\text{g PFOA/g}$ in the control and the ARP-treated test, respectively, after six cyclic adsorption-regeneration tests, suggesting that the optimized cyclic adsorption-regeneration processes using appropriate co-sorbed NOM mitigation strategies can constantly remove PFOA in PFOA contaminated water. Meanwhile, the overall PFOA degradation was 97.7% during six cyclic adsorption-regeneration tests,

highlighting that effective PFOA degradation occurred through optimized ARP regeneration. Furthermore, DOC in solution before and after ARP regeneration is shown in **Figure 5-16(e)**. The results showed that the DOC in the regenerant before ARP regeneration was not significantly different from the DOC in the regenerant after ARP regeneration, indicating that UV/SO₃²⁻ ARP cannot effectively mineralize NOM in solution.

5.4 Discussion

As discussed in **Chapter 4**, the saturation of IRA67 in the treatment of PFOA-contaminated simulated natural water is governed by the NOM adsorption. Thus, alum coagulation was applied to the pretreatment of simulated natural water prior to IRA67 for alleviating the NOM loading on IRA67. Solution pH and coagulant dose are two key operating factors affecting the coagulation behaviors. Therefore, the alum coagulation pre-treatment should be optimized to maximize the NOM removal. As shown in **Figures 5-1(a)** and **(b)**, the lowest residual DOC and UV₂₅₄ absorbance were obtained at pH 6.0 in this study. Generally, the NOM removal with alum coagulation can be realized by different mechanisms, including charge neutralization, entrapment, adsorption and complexation (Matilainen et al., 2010). As coagulant hydrolyzates derived from alum are positively charged at pH 6.0 (e.g., Al(OH)²⁺, Al(OH)₂⁺, Al₂(OH)₂⁴⁺, and Al₃(OH)₄⁵⁺), they preferentially interact with negatively charged functional groups on NOM molecules. Therefore, when pH is optimized (pH 6.0 in this study), charge neutralization has been proven to be the primary mechanism for NOM removal in simulated natural water (Bond et al., 2010; Zhao et al., 2008). However, NOM was not effectively removed in terms of DOC and UV₂₅₄ absorbance at a too low (e.g., pH = 4.0) or a too high pH level (e.g., pH = 9.0) during alum coagulation. This finding is because aluminum exists predominantly as Al(H₂O)₆³⁺ at a too low pH (pH < 5.0), which may prevent, at least partially, the occurrence of

alum coagulation (Krupińska, 2020). Moreover, the positive charge on aluminum coagulants is dramatically decreased at a too high pH, which can cause a coagulated particle to redisperse (Krupińska, 2020). Meanwhile, as the solution pH increases, NOM becomes more ionized because the carboxyl groups lose protons (Crittenden et al., 2012). Thus, an optimal pH exists for the alum coagulation of NOM. In this study, the most favorable pH was 6.0.

Furthermore, as shown in **Figure 5-1(c)**, DOC was gradually reduced as the alum dose increased from 20.0 to 60.0 mg/L at pH 6.0 because more alum coagulants are available to provide more positive charges on the aluminum hydroxide floc surface to remove negatively charged functional groups on NOM via a charge neutralization mechanism (Bose & Reckhow, 2007). However, no further DOC reduction was observed once the applied alum dose was greater than 60.0 mg/L at pH 6.0, suggesting that the residual NOM molecules are recalcitrant to alum coagulation even at a high alum dose.

The extent of overall NOM removal during the alum coagulation process is highly dependent on the nature of NOM. As shown in **Figure 5-8**, the HPO fraction (i.e., HA and FA) and high MW group (i.e., >10 kDa) of NOM were more readily removed during alum coagulation as compared to HPI fraction and low MW group, which is in agreement with the findings reported in other studies (Bond et al., 2010; Crittenden et al., 2012; Matilainen et al., 2010). Because of the abundance of aromatic carbon, phenolic structure, and conjugated double bonds, the HPO fraction of NOM possesses more electrochemically negative charges (Świetlik et al., 2004). Thus, this portion can be more efficiently removed via charge neutralization during alum coagulation. Similarly, the observation of a better removal of the high MW NOM groups was because they contain greater portions of aromatic compounds, which are classified as HPO in nature (Świetlik et al., 2004). Different from the DOC removal pattern, more UV_{254}

absorbance was reduced during alum coagulation in **Figures 5-5(d)** and **5-8**, indicating that aromatic materials are removed more effectively than other NOM fractions (Uyak et al., 2007; Uyguner et al., 2007). In contrast, the HPI fraction and low MW group of NOM mainly encompass organic compounds (e.g., aliphatic carbon and nitrogenous compounds) with low charge density (Matilainen et al., 2010). Therefore, their removal is challenging even with a high alum dose (Chong Soh et al., 2008; Chow et al., 2008). Consequently, the optimal alum dose was 60.0 mg/L for the following alum coagulation of simulated natural water, because the application of a higher alum dose can produce more aluminum sludge that requires prohibitive disposal. Meanwhile, a too high alum dose may lead to a high concentration of Al in finished water, which has potential health hazards or results in other issues in the distribution system (e.g., spontaneous flocculation) (Matilainen et al., 2010).

To further mitigate the NOM loading on IRA67, the pretreatment using UV/H₂O₂-based AOP was applied for the removal of NOM in pre-coagulated water. Although the UV/H₂O₂-based AOP was a well-established process commonly reported in other studies to significantly alleviate the NOM from natural water (Sillanpää et al., 2018; Wang et al., 2000), the DOC remained constant in the applied condition (i.e., UV irradiation time = 60 mins; H₂O₂ = 15.0 mg/L), as shown in **Figure 5-6**. These results were in agreement with those reported in other studies (Philippe, 2010; Sarathy & Mohseni, 2007; Sarathy et al., 2011; Sillanpää et al., 2018). There are two possible reasons for this phenomenon. First, the yield of generated •OH using the commonly applied H₂O₂ concentrations for the treatment of drinking water supplies in this study may not be sufficient to mineralize NOM. Better NOM removal was reported at high H₂O₂ concentrations and UV fluences (Kleiser & Frimmel, 2000; Sindelar et al., 2014; Toor & Mohseni, 2007). Second, the advanced oxidation can alter the structural properties of NOM after

the advanced oxidation treatment, such as decreasing MW, the enhanced hydrophilicity, and the less aromaticity, when economically acceptable UV fluences and H₂O₂ concentrations were applied to treat NOM (Sillanpää et al., 2018). This suggests that the advanced oxidation preferentially removes high MW, more hydrophobic, and aromatic NOM fractions, which overlap with the NOM portion removed by coagulation. Therefore, it might be challenging to further mineralize NOM in pre-coagulated NOM water in this study.

The DOC in diluted simulated natural water and pre-coagulated water before and after the addition of IRA67 (5.0 g/L) was compared to determine the fractions of NOM loaded on IRA67 in pre-coagulated water. As shown in **Figure 5-7**, a small portion of NOM was removed in pre-coagulated water after the introduction of IRA67 in terms of DOC. Based on **Figure 5-8**, the adsorbed NOM fraction on IRA67 in pre-coagulated water was mainly from the medium MW group (10-100 kDa) and FA fraction of NOM. In contrast, a significant reduction of DOC was observed in diluted simulated natural water after the introduction of IRA67. Interestingly, NOM was not completely removed in diluted simulated natural water or pre-coagulated water even though a high IRA67 dose was applied. The mechanisms governing IX resin removal of NOM are complex due to the involvement of multiple interacting phenomena (Rahmani & Mohseni, 2017), relying heavily on the properties of both resins and NOM (Bolto et al., 2004; Bolto et al., 2002). For WBA exchange resin removal of NOM in water, one of the plausible mechanisms is the electrostatic interaction of the positively charged tertiary amine functional groups on IRA67 with negatively charged functional groups on NOM molecules (Bolto et al., 2004; Bolto et al., 2002). Other mechanisms may also be involved in removing NOM in water. For instance, a non-electrostatic mechanism involving H bonding of undissociated acidic species (e.g., carboxylic acid and phenol) in NOM molecules with amino groups on the resins was

proposed (Bolto et al., 2002). The NOM in diluted simulated natural water has more negatively charged functional groups than that in pre-coagulated water, resulting in the better NOM removal after IRA67 addition. The incomplete removal of NOM with a high IRA67 dose is ascribed to the presence of the low MW group (i.e., <10 kDa) and HPI fraction of NOM in the diluted simulated natural water or pre-coagulated water, as evidenced by the results from **Figure 5-8**. As discussed above, the HPI fraction and low MW group of NOM are mainly composed of aliphatic carbon and nitrogenous compounds (e.g., carboxylic acids, carbohydrates, and protein) with low charge density, which significantly restrict the electrostatic interactions between IRA67 and NOM.

Furthermore, the adsorption capacity of PFOA on fresh IRA67 in PFOA-containing simulated natural water, pre-coagulated water, and AOP-treated pre-coagulated water were compared to evaluate whether pretreatment of simulated natural water prior to the IRA67 addition can improve the PFOA adsorption by IRA67. As shown in **Figure 5-9**, the PFOA adsorption on IRA67 in PFOA-containing pre-coagulated water was significantly enhanced compared to in PFOA-containing simulated natural water. As discussed in **Chapter 4**, the primary mechanism for PFOA removal by IRA67 is attributed to the electrostatic interaction of charged tertiary amine functional groups on IRA67 with deprotonated PFOA, indicating that the competition between NOM and PFOA in solution for interacting with charged tertiary amine functional groups on IRA67 exists. Because the high MW HPO fraction of NOM, which is preferentially adsorbed by IRA67, is largely removed during alum coagulation, less NOM strongly competes with PFOA for the limited occupied sites on IRA67. Therefore, more PFOA in the solution can be adsorbed by IRA67 via electrostatic interactions. Nevertheless, further PFOA adsorption by IRA67 in AOP-treated pre-coagulated water was observed in **Figure 5-9**

because AOP cannot mineralize remaining NOM in the studied experimental conditions. Thus, UV/H₂O₂-based AOP is not a feasible pretreatment option for alleviating NOM loading on the PFOA/NOM-laden IRA67.

The desorption of NOM and PFOA sorbed on IRA67 in DI water at different pH solutions was evaluated. As solution pH increased from 9.0 to 12.0, more NOM and PFOA were desorbed in the solution. This finding is because the tertiary amine moieties on the IRA67 ($pK_a = 9.3$ (Miyazaki & Nakai, 2011)) were gradually deprotonated as the solution pH increased. Therefore, the PFOA or NOM adsorbed on IRA67 via electrostatic interactions is released. Based on **Figure 5-10**, the portion of desorbed PFOA from IRA67 at each pH level is not affected by the masses of PFOA and co-sorbed NOM in the studied experimental conditions, suggesting that the interaction of PFOA and NOM (i.e., PFOA adsorption by NOM) is limited. A small portion of PFOA remained on the IRA67 at a high pH (e.g., pH >11.0), validating the involvement of PFOA adsorption mechanisms other than electrostatic interactions. Meanwhile, the fraction of desorbed NOM from IRA67 at each pH is barely influenced by the mass of NOM or co-sorbed PFOA in the studied experimental conditions. Additionally, non-humic and HPI NOM molecules are readily desorbed in solution compared to more HPO fraction of NOM, as evidenced by the low value of UV₂₅₄ absorbance in solution at each pH solution compared to the corresponding DOC value in **Figure 5-10**. This is because the HPO fraction or aromatic carbon content of the NOM has a relatively higher charge density, which can form a higher magnitude of the electrostatic force of attraction with the positively charged tertiary amine functional groups on IRA67. Thus, as tertiary amine moieties are gradually deprotonated with the increase of solution pH, the desorption of non-humic and HPI NOM molecules with lower charge density was first obtained.

The residual DOC and accumulative NOM adsorbed on IRA67 in PFOA-containing pre-coagulated water after each NOM/PFOA loading cycle are shown in **Figure 5-11(a)**. As discussed above, the majority of adsorbed NOM on IRA67 after each NOM/PFOA loading cycle in pre-coagulated water was proven to be FA and medium MW fraction of NOM. Meanwhile, the adsorption capability of IRA67 on NOM remained constant in the studied experiment, as evidenced by the linear enhancement of cumulative NOM adsorbed on resins after each loading cycle, suggesting that the IRA67 was still far from saturation after ten loading cycles. However, the adsorption capability of IRA67 on PFOA steadily decreased as the number of loading cycles increased in PFOA-containing pre-coagulated water, as shown in **Figure 5-11(b)**. This phenomenon can be ascribed to the competition of co-existing NOM with PFOA in pre-coagulated water. Although a significant reduction of overall NOM was observed after alum coagulation, the concentration of remaining DOC (~1.2 mg/L) was still two orders of magnitudes greater than PFOA (20.0 $\mu\text{g/L}$). Thus, the accumulation of NOM on IRA67 can increasingly inhibit the PFOA adsorption with the increasing cycle number of NOM/PFOA loading.

Furthermore, the effect of pH (9.0-14.0) on the fate of sorbed NOM and PFOA on IRA67 after ten loading cycles was evaluated. As shown in **Figure 5-12**, as solution pH increased from 9.0 to 14.0, more NOM and PFOA were desorbed in the solution, which is in agreement with the previous results shown in **Figure 5-10**. The release of NOM and PFOA to the solution is primarily due to the deprotonation of tertiary amine moieties. Of interest, a higher portion of sorbed NOM from pre-coagulated water was desorbed at each pH level compared to the sorbed NOM from simulated natural water. For instance, 92.8% of NOM from pre-coagulated water was desorbed at pH 10.0, whereas nearly 30.0% of NOM from simulated natural water was released. This finding is because the composition of the sorbed NOM from pre-coagulated water was

dramatically different from that of the simulated natural water. Specifically, sorbed NOM on IRA67 from pre-coagulated water possesses a relatively higher fraction of HPI and lower MW group than the sorbed NOM on IRA67 from simulated natural water. Meanwhile, no UV-absorbing aromatic compounds were adsorbed on IRA67 from pre-coagulated water. Thus, the sorbed NOM from pre-coagulated water was readily desorbed at each pH level because of its relatively lower charge density. In this study, pH 10.0 was chosen as the optimized pH in the following ARP regeneration process for three reasons. First, the majority of sorbed NOM on IRA67 from ten loading cycles can be desorbed at pH 10.0, implying that this pH level sufficiently releases most NOM-occupied tertiary amine functional groups for capturing more PFOA in the adsorption phase. Second, half of the PFOA was still adsorbed on IRA67 at pH 10.0, which facilitates the ensuing UV/SO₃²⁻ ARP treatment of sorbed PFOA on IRA67. If the solution pH was greater than 10.0, most PFOA were desorbed in solution, as evidenced by the results in **Figure 5-12**, indicating that UV/SO₃²⁻ ARP treatment method may no longer be feasible for degradation of sorbed PFOA on IRA67. Third, a higher pH (i.e., ≥ 11.0) solution can potentially increase the difficulties in the post-treatment of ARP regenerant owing to its corrosive properties.

The degradation of sorbed PFOA on IRA67 (106.4 μg PFOA and 4.23 mg DOC/g) from the ten cyclic loading tests at different sulfite dosages during the UV/SO₃²⁻ treatment was investigated. As discussed above, the partial desorption of sorbed PFOA is attributed to the deprotonation of tertiary amine moieties on the resins. PFOA sorbed on the resins or in the solution could not be degraded by the direct UV irradiation, as evidenced by **Figure 5-13**. As sulfite was dosed during the UV/SO₃²⁻ treatment, the degradation of PFOA was observed, highlighting the principal role of e_{aq}^- in the PFOA degradation. Similar to the results from

Chapter 4, though PFOA in the two phases was both degraded, e_{aq}^- generated preferentially attacked PFOA in the solution rather than PFOA on the resins. The detailed mechanisms behind the PFOA degradation in the solution and on the IRA67 during the UV/SO₃²⁻ treatment were explained in **Chapter 4**. Based on **Figure 5-13**, 20 mM was chosen as the optimal sulfite concentration for the following ARP regeneration process because both PFOA desorbed in solution and sorbed on resins were entirely degraded within three hours. As shown in **Figure 5-14(a)**, PFOA desorbed in solution was completely degraded in the UV/SO₃²⁻ ARP treatment process within 90 mins, while PFOA sorbed on resins was fully decomposed within 180 mins in the studied experimental conditions, indirectly suggesting the preferences of e_{aq}^- on degradation of PFOA in the solution.

Information from the results of six cyclic adsorption-regeneration tests provide is mixed. The cumulative PFOA sorption to UV/SO₃²⁻ ARP-treated resins was linearly increased with the cycle number ($R^2 \geq 0.99$). At any specific cycle excluding the first one, the ARP-treated resin consistently exhibited a greater cumulative PFOA removal than the control one. This observation is because most sorbed NOM on IRA67 was desorbed in the solution during the ARP regeneration (**Figure 5-16**) via the deprotonation of tertiary amine moieties on resins. Thus, more functional groups on IRA67 are available for capturing PFOA through electrostatic interactions in the subsequent adsorption phase. In contrast, because e_{aq}^- cannot effectively degrade co-sorbed NOM due to its selective reactivity, the accumulation of NOM on resins leads to the continuous decline of the PFOA adsorption capability in the control tests. More importantly, the ARP-treated resins at 20 mM sulfite could degrade most PFOA sorbed over the six cycles. The excellent performance is also ascribed to the selectivity of e_{aq}^- , which can considerably degrade PFOA even though substantial NOM co-exists. Based on the

aforementioned findings, the combination of alum coagulation with UV/SO₃²⁻ can function as a promising resin regeneration option to realize both ARP-based resin regeneration and effective PFOA degradation.

The physical and chemical properties of IRA67 after six cyclic adsorption-regeneration tests were evaluated. The SEM method was applied to visualize the morphologic evolution of the resins. The SEM images were compared before and after six cyclic adsorption-regeneration tests. As shown in **Figure 5-17**, all resin beads still possessed intact, smooth, and spherical structures. No cracks were observed on the resins, indicating that UV/SO₃²⁻ ARP treatment does not damage the matrix of IRA67 in this study. Moreover, to gain insights into the change of elemental compositions on the resins at different phases, EDS (**Figure 5-18**) analysis was made. The results showed no significant changes in elemental compositions of IRA67 before and after six cyclic adsorption-regeneration tests. This finding indirectly implies that SO₃²⁻ or SO₄²⁻ was not adsorbed on IRA67 during the ARP treatment process. Furthermore, to better understand if the functional groups (i.e., tertiary amine moieties) on IRA67 are affected by UV/SO₃²⁻ ARP treatment, the IEC of resins at different phases were compared in **Figure 5-19**. The results showed that the IEC of fresh resin was not significantly different from the resins after six cyclic adsorption-regeneration tests ($p > 0.05$), highlighting that UV/SO₃²⁻ ARP treatment little destructs the functional groups on IRA67. This is because e_{aq}⁻ selectively reacts with electron-withdrawing groups instead of electron-donating groups (e.g., tertiary amines). Thus, the property of IRA67 is less impacted by UV/SO₃²⁻ ARP treatment.

5.5 Conclusions

Based on the knowledge summarized from the previous study, ARPs alone is not technically feasible for the effective regeneration of PFOA/NOM-laden IX resins to repeatedly

remove PFOA in water. Specifically, PFOA can be effectively degraded through e_{aq}^- degradation of PFOA sorbed on PFOA/NOM laden IRA67 or desorbed in the solution because of the selectivity of e_{aq}^- . However, UV/SO₃²⁻ ARPs cannot well decompose co-sorbed NOM because UV irradiation alone or e_{aq}^- cannot effectively cleave C-C bonds to mineralize NOM. Of note, the saturation of IRA67 in the removal of PFOA in water treatment is primarily ascribed to the adsorption of NOM (more abundant in the water). Namely, the buildup of NOM on the resins finally leads to the loss of the resin capacity for removing PFOA in water with the increasing cycle number, even if PFOA sorbed can be effectively degraded. Thus, further investigation is needed for the mitigation of co-sorbed NOM to accomplish the ARP-based IX resin regeneration method for PFOA removal in real water treatment.

In **Chapter 5**, the combination of the UV/SO₃²⁻ treatment process with appropriate NOM treatment strategies was investigated. Specifically, two water pretreatment options (i.e., coagulation and UV/H₂O₂-based AOP) were evaluated to alleviate NOM loading on PFOA/NOM-laden IRA67. Adsorption of NOM in pre-coagulated water and diluted simulated natural water by IRA67 was compared. The fate of NOM and PFOA in PFOA-containing pre-coagulated water after each loading cycle during a set of ten-cycle loading tests was evaluated. The effect of pH on the fate of sorbed NOM and PFOA on IRA67 was also assessed. Furthermore, the resin regeneration operation was optimized (e.g., sulfite dose, solution pH, and UV irradiation time) for effective degradation of sorbed PFOA on PFOA/NOM-laden IRA67. Meanwhile, the optimized cyclic adsorption-regeneration processes for the on-site PFOA/NOM-laden IRA67 ARP regeneration were evaluated. Finally, IRA67, after six cyclic adsorption-regeneration tests, was characterized.

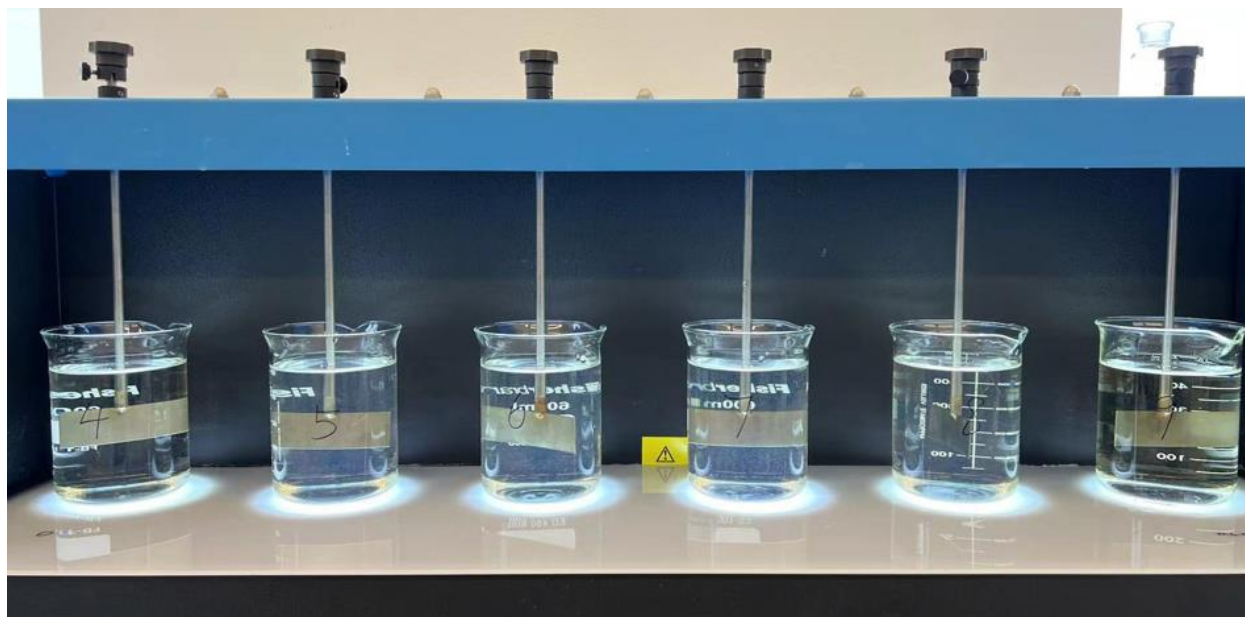
Significant findings in this chapter further advance the current knowledge on the novel ARP-based IX resin regeneration approach tailed for PFAS removal in drinking water treatment. The major contributions from this work are summarized as follows.

- 1) Pretreatment with alum coagulation at the optimized operational conditions (i.e., alum 60.0 mg/L; pH 6.0) significantly alleviates NOM loading on IRA67. The coagulation preferentially removes the HPO fraction and high MW group.
- 2) UV/H₂O₂ treatment of pre-coagulated water (H₂O₂ =15 mg/L; UV irradiation time = 60 mins) poorly mitigates NOM loading in this study. Therefore, the AOP is less effective for the abatement of NOM than alum coagulation.
- 3) IRA67 cannot effectively adsorb the HPI fraction and low MW group of NOM in simulated natural water.
- 4) PFOA adsorption on IRA67 in PFOA-containing pre-coagulated water is significantly enhanced compared to that in PFOA-containing simulated natural water. However, PFOA adsorbed on IRA67 in AOP treated pre-coagulated water is not significantly different from in PFOA-containing pre-coagulated water.
- 5) NOM from the PFOA-containing pre-coagulated water governs the saturation of IRA67, which can decrease the co-sorption of PFOA on IRA67 as the loading cycle increases.
- 6) The solution pH plays a critical role in desorbing sorbed NOM and PFOA on IRA67. Most sorbed NOM from pre-coagulated water is desorbed at pH 10.0, whereas half of PFOA is sorbed on IRA67.

- 7) The optimized ARP regeneration conditions for effective degradation of sorbed PFOA on PFOA/NOM-laden IRA67 are three-hour ARP treatment at 20 mM sulfite at pH 10.0.
- 8) The decomposition of PFOA desorbed in the solution, PFOA sorbed on IRA67, and overall PFOA removal follows pseudo-first order reaction patterns during the UV/SO₃²⁻ ARP regeneration process. PFOA desorbed in the solution can be completely degraded in the UV/SO₃²⁻ ARP treatment process within 90 mins, while PFOA sorbed on resins was fully decomposed within 180 mins in the studied experimental conditions.
- 9) The continuous adsorption of PFOA by IRA67 in the cyclic IX adsorption-regeneration process is ascribed to NOM desorption at pH 10.0 during the UV/SO₃²⁻ ARP regeneration process to release more occupied sites on IRA67. The PFOA sorbed on IRA67 during the cyclic IX adsorption-regeneration process can be completely degraded via UV/SO₃²⁻ ARP treatment.
- 10) The physical and chemical properties of IRA67 are little affected by UV/SO₃²⁻ ARP treatment during six cyclic adsorption-regeneration tests.
- 11) The UV/SO₃²⁻ process, if jointly used with an optimized alum coagulation pretreatment for alleviating NOM loading on IRA67, can enable a promising on-site PFOA/NOM-laden IRA67 ARP regeneration process for PFOA elimination in drinking water.

The aforementioned information further demonstrates that a pre-treatment can enable the innovative, on-site ARP-based IX regeneration approach for the cyclic use of regenerated IRA67 resins to control the PFAS pollution in drinking water treatment. In addition to the technical facets of the proposed ARP-based resin regeneration methods, it is also critical to

comprehensively assess the profound implications of the proposed method in terms of economic, environmental, and social aspects, which will be discussed in the next chapter. Meanwhile, the major conclusions from this dissertation will be summarized. And, future research directions will be identified in the following chapter.



(a)



(b)

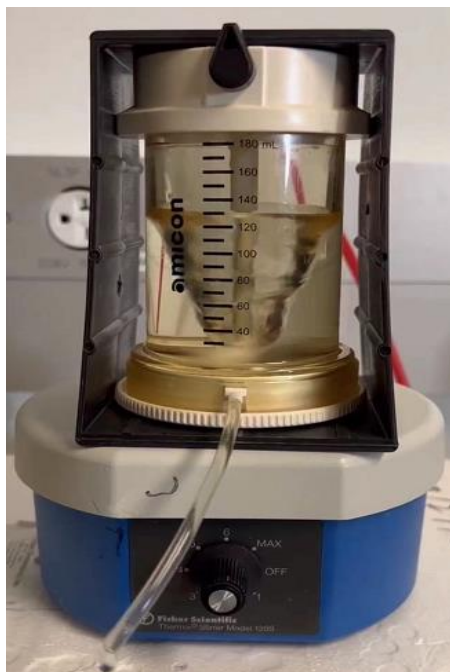


(c)



(d)

Figure 5-1 Visualization of alum coagulation process for simulated natural water: (a) mixing during coagulation; (b) collection of the supernatant; (c) membrane filtration; (d) simulated natural water before (left) and after (right) alum coagulation (alum 60.0 mg/L; pH 6.0)



(a)



(b)

Figure 5-2 Visualization of (a) MW fractionation with a UF stirred cell; (b) SPE for the separation of FA and HPI isolates



(a)



(b)

Figure 5-3 Visualization of (a) NOM and PFOA loading tests on IRA67 in PFOA-containing pre-coagulated water using a jar tester; and (b) desorption of NOM and PFOA on IRA67 from multiple loading tests at different pH solutions using a shaker



Figure 5-4 Visualization of fresh IRA67 (left), IRA67 with no regeneration after six cyclic adsorption-regeneration tests (middle), and ARP regenerated IRA67 after six cyclic adsorption-regeneration tests (right)

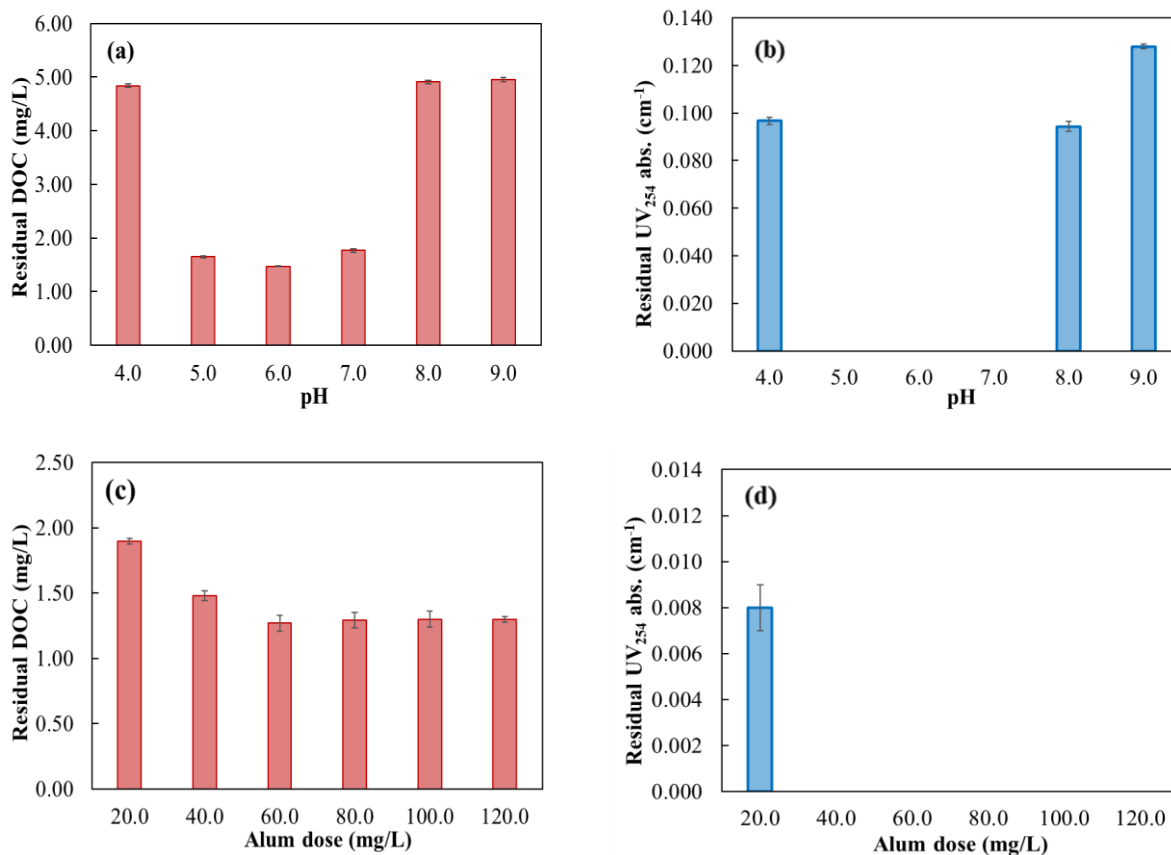


Figure 5-5 Effect of coagulation pH and chemical dose: effect of pH (4.0 to 9.0) on (a) residual DOC and (b) residual UV₂₅₄ absorbance of simulated natural water during alum coagulation (Experimental condition: alum dose = 40.0 mg/L; 500 mL); and effect of alum dose (20.0 to 120.0 mg/L) on (c) residual DOC and (d) residual UV₂₅₄ absorbance in simulated natural water during alum coagulation (Experimental condition: pH = 6.0; 500 mL)

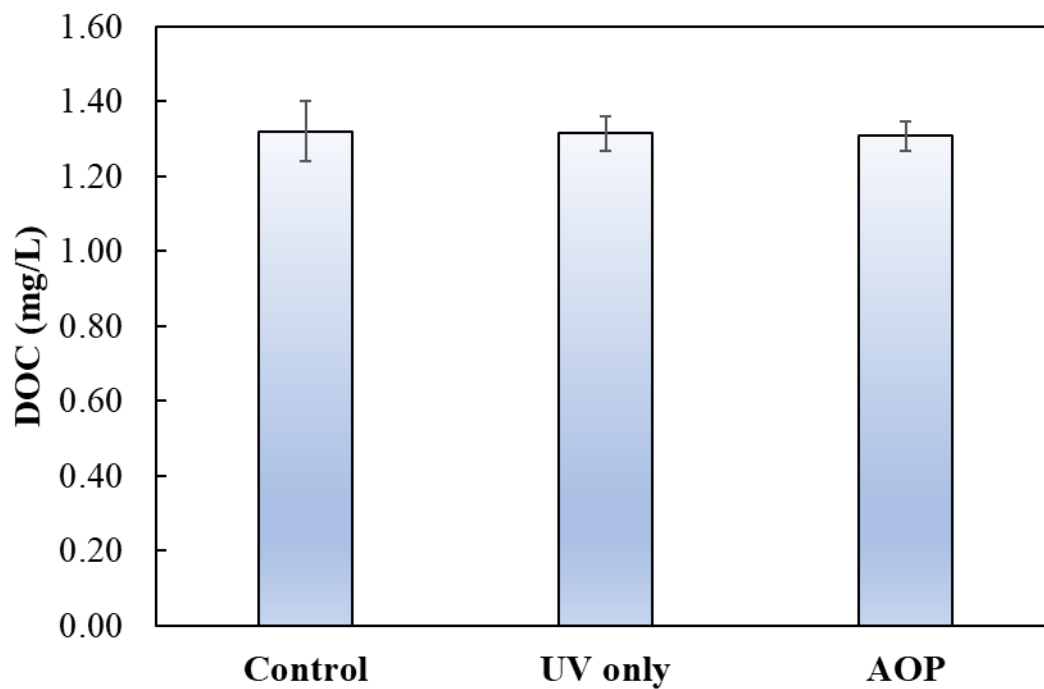


Figure 5-6 Residual DOC after the UV/H₂O₂-based AOP treatment of pre-coagulated water (Experimental condition: H₂O₂ = 15.0 mg/L; initial pH = 7.5; UV irradiation time = 1 hour; reaction volume = 200 mL)

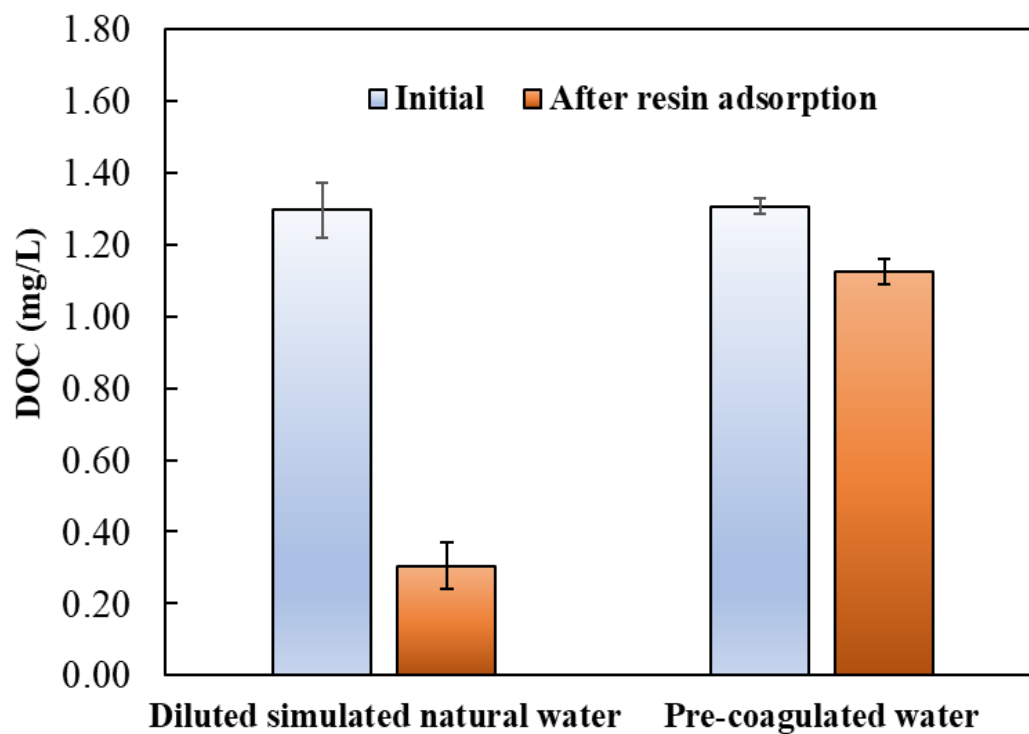


Figure 5-7 Residual DOC in diluted simulated natural water and pre-coagulated water before and after IRA67 adsorption (Experimental condition: IRA67 dosage = 5.0 g/L; initial pH = 7.5; adsorption time = 24 hours; volume = 1.0 L)

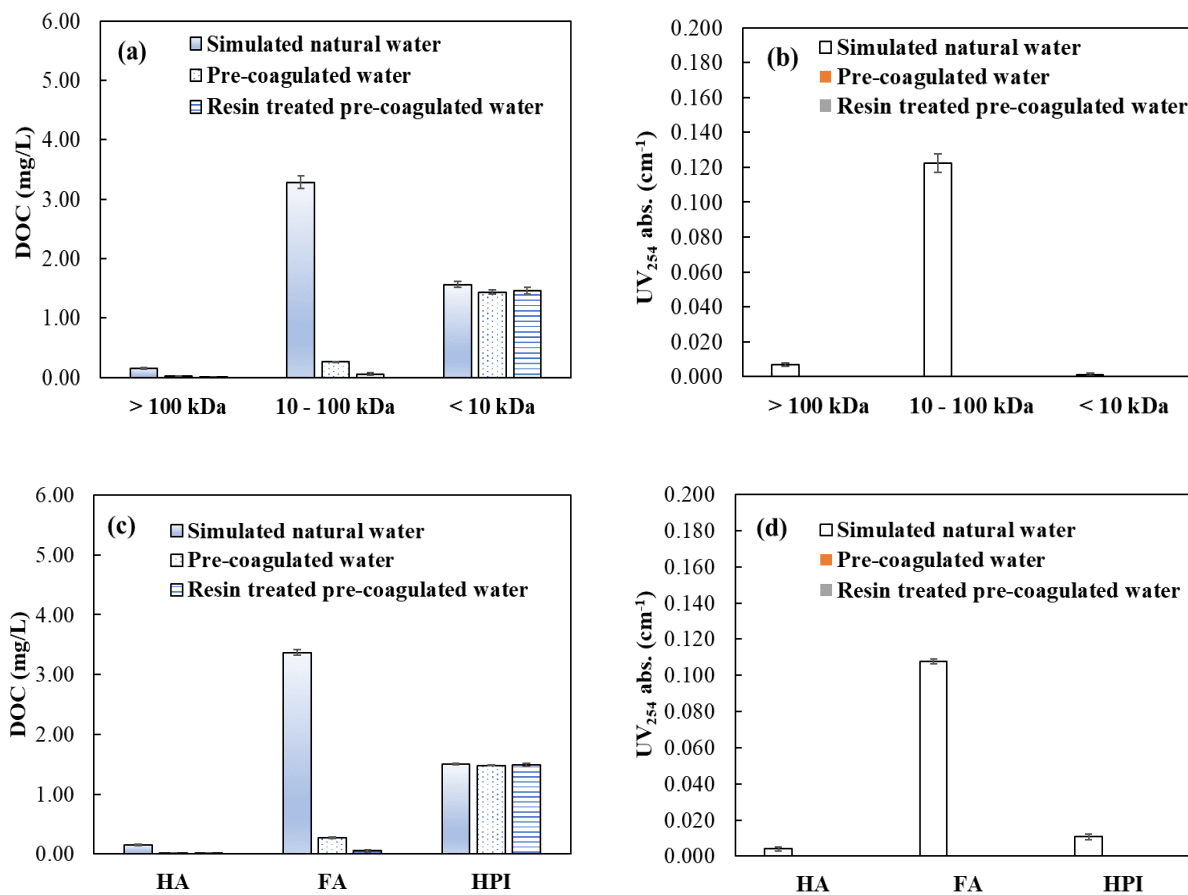


Figure 5-8 Molecular size distribution of (a) residual DOC and (b) residual UV₂₅₄ absorbance as well as hydrophobic/hydrophilic fraction of (c) residual DOC and (d) residual UV₂₅₄ absorbance in simulated natural water, pre-coagulated water, and pre-coagulated water after resin (5.0 g/L) adsorption

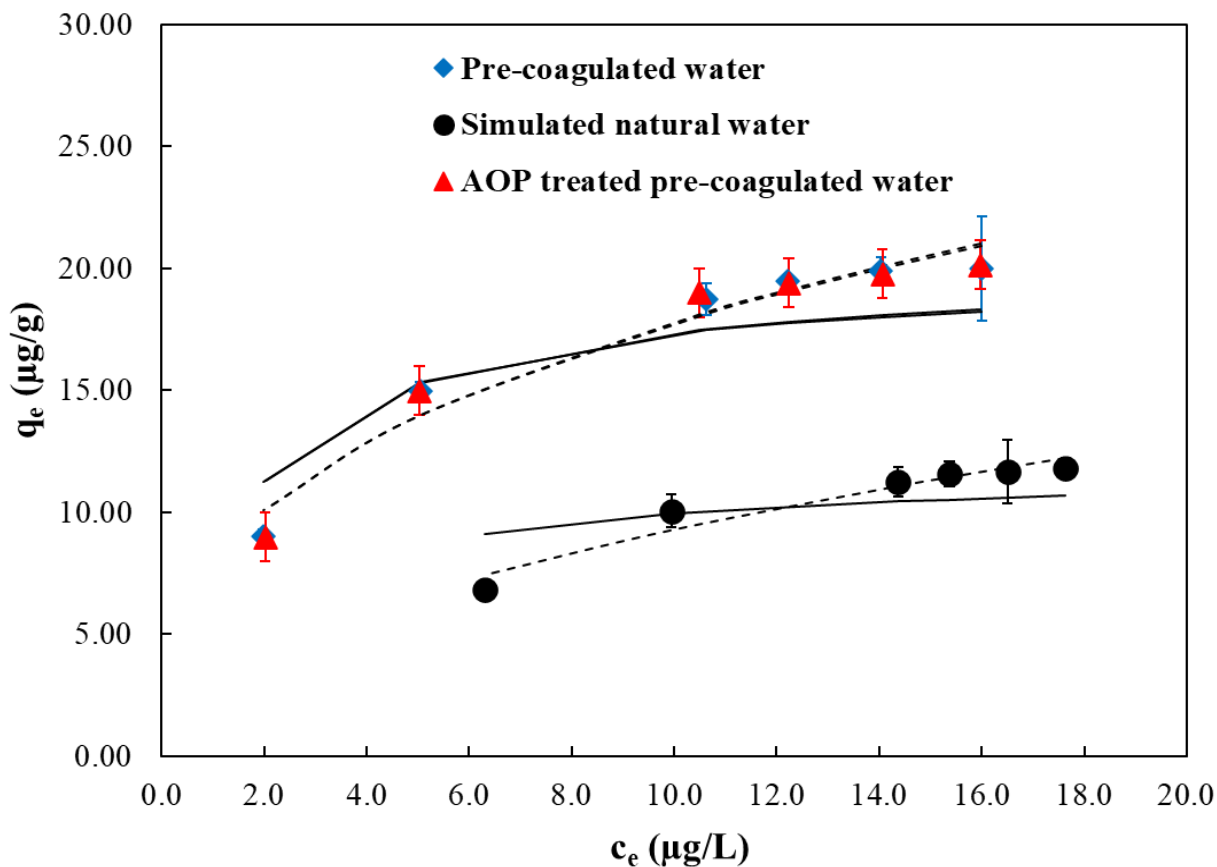
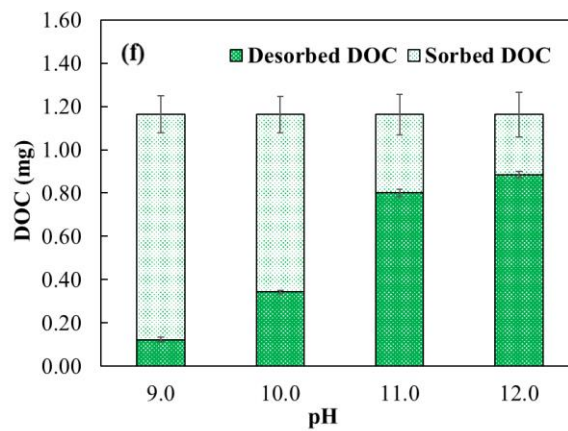
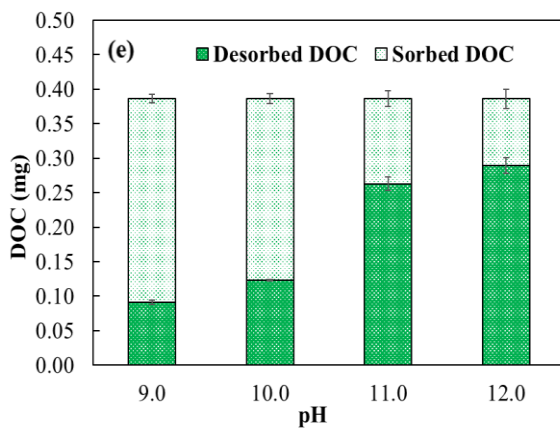
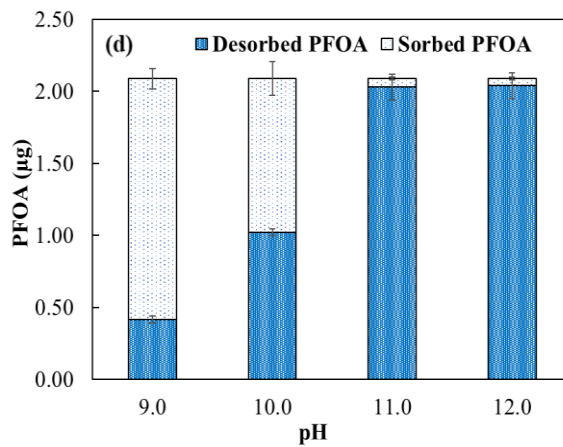
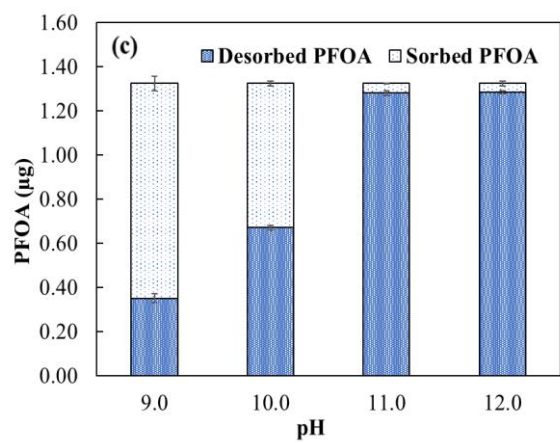
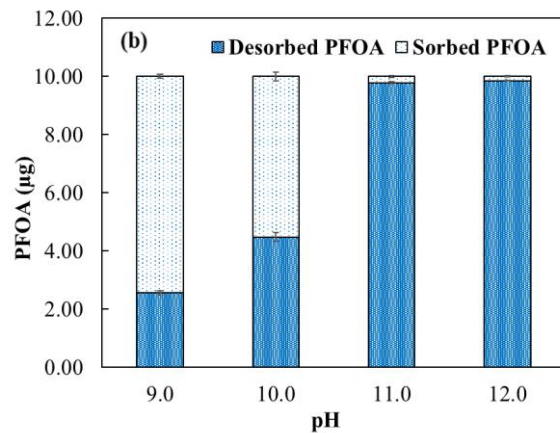
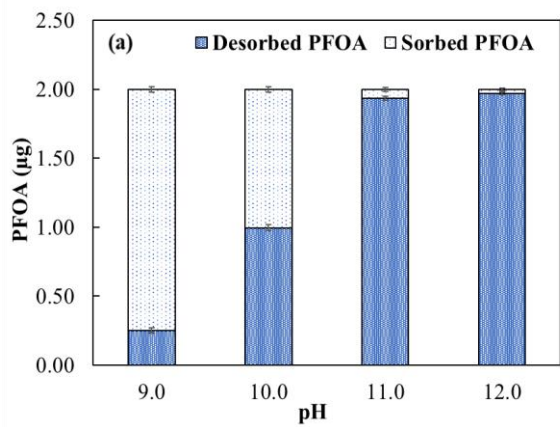


Figure 5-9 Measured and modeled adsorption isotherms of PFOA in different PFOA-containing water systems (Experimental condition: initial pH = 7.5; reaction volume = 0.1 L; IRA67 dosage = 0.1 to 2.0 g/L; adsorption time = 24 hours; scattered symbols, scattered lines, and solid lines represent measured, Freundlich modeled, and Langmuir modeled data, respectively)



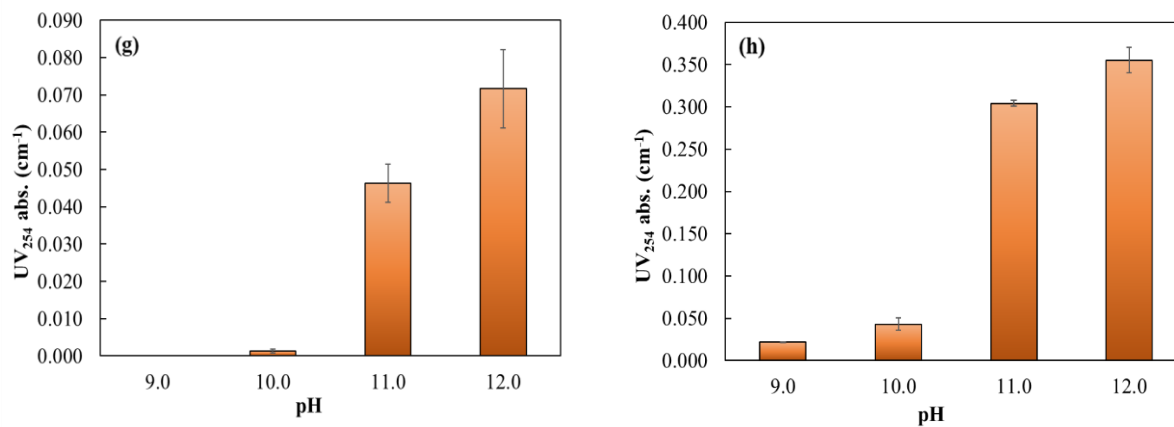


Figure 5-10 Effect of pH on the residual NOM and PFOA after the desorption from IRA67 (Experimental condition: (a) 20.0 μg PFOA/g IRA67; (b) 100.0 μg PFOA/g IRA67; (c, e, and g) 13.25 μg PFOA and 3.86 mg DOC/g IRA67; (d, f, and h) 21.12 μg PFOA and 11.55 mg DOC/g IRA67; volume = 0.1 L; IRA67 dosage = 1.0 g/L; desorption hour = 24 hours)

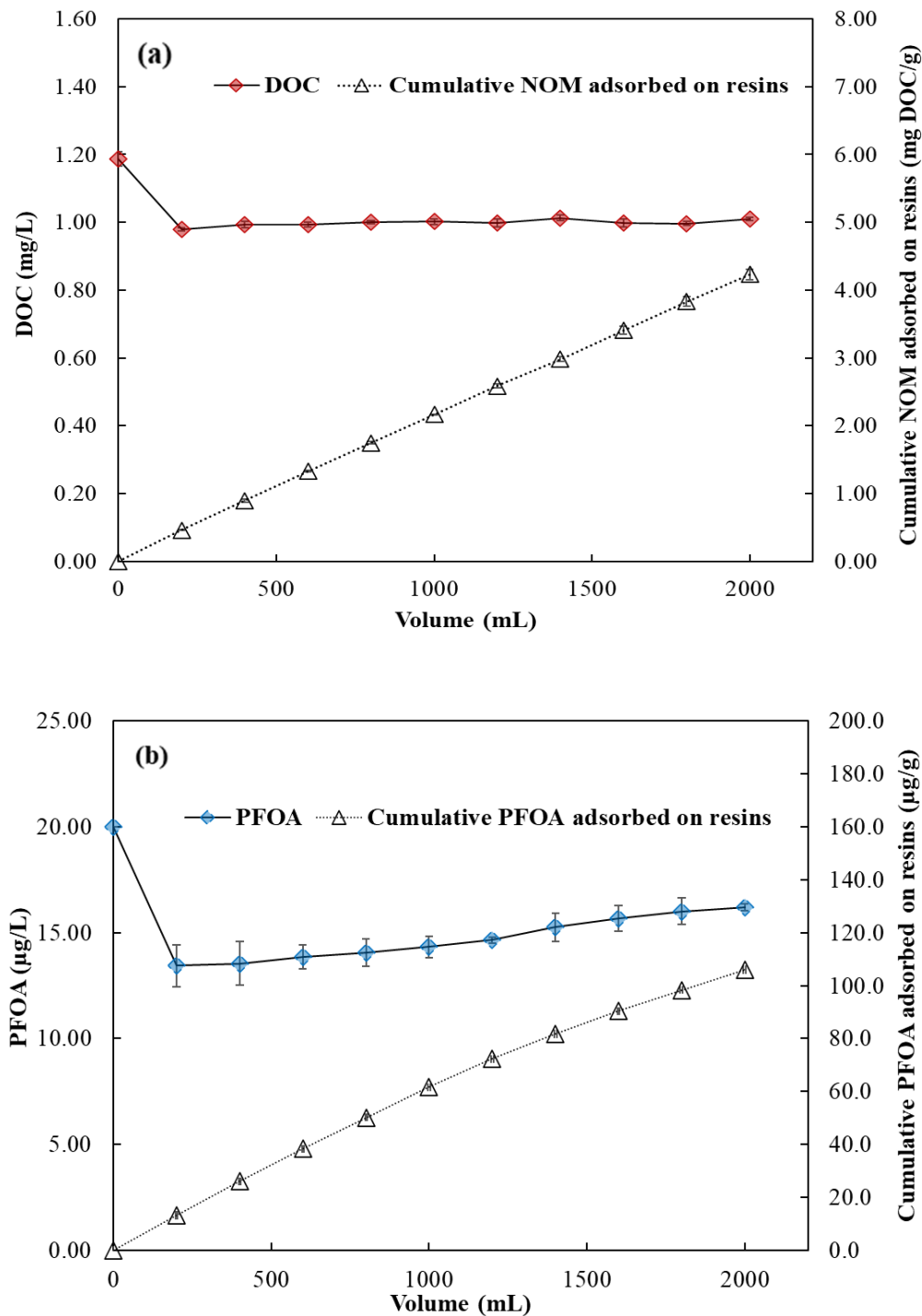


Figure 5-11 Fate of NOM and PFOA in PFOA-containing pre-coagulated water after each loading cycle during ten cyclic NOM and PFOA loading tests: (a) residual DOC in solution after each loading test and accumulative NOM adsorbed; and (b) residual PFOA in solution after each loading test and accumulative PFOA adsorbed (Experimental condition: pH = 7.5; volume = 0.2 L; IRA67 dosage = 0.5 g/L; reaction hour = 30 mins)

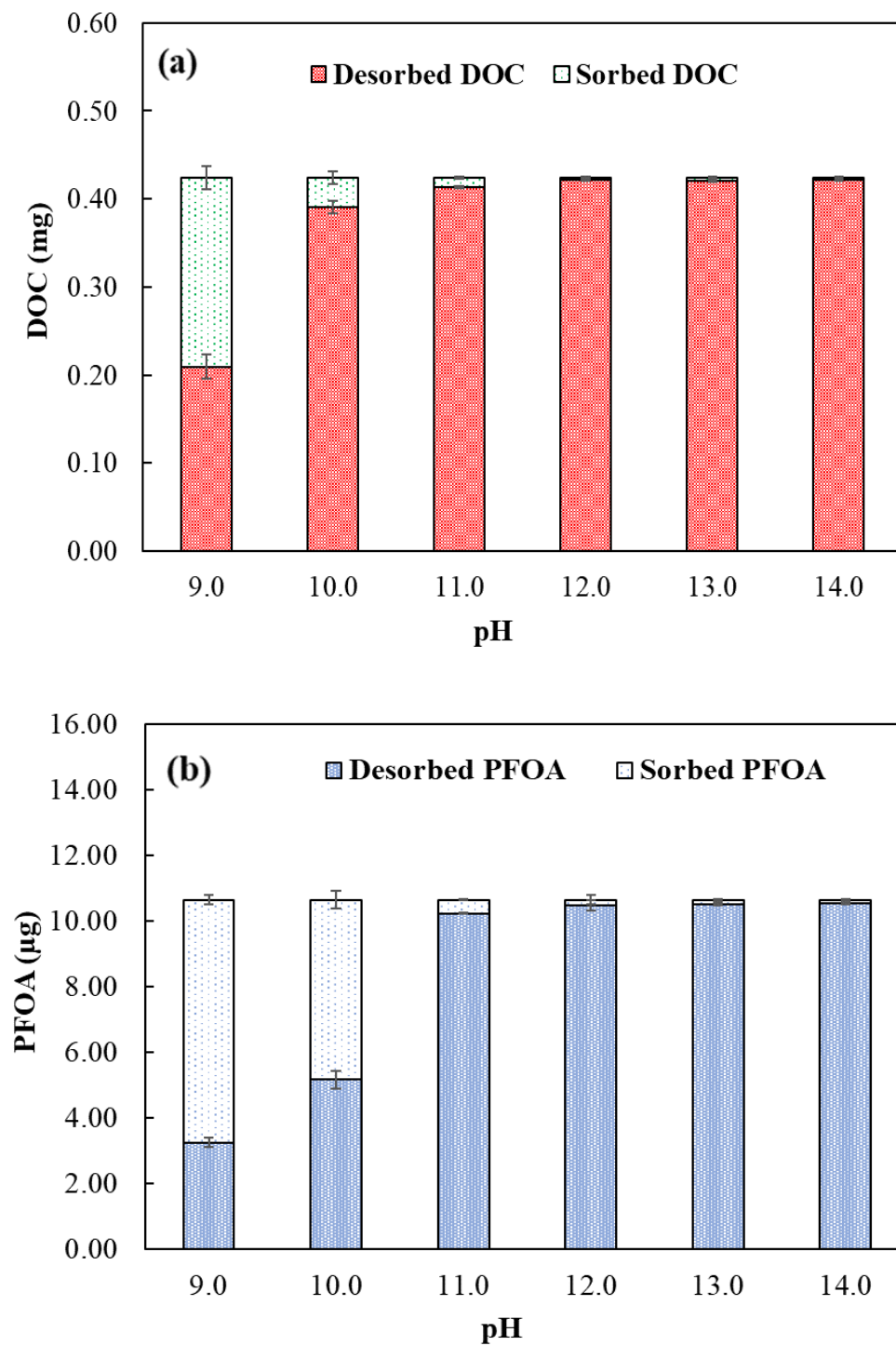


Figure 5-12 Effect of pH on the fate of sorbed NOM and PFOA on IRA67 after ten cyclic loading tests: (a) NOM in solution (b) PFOA in solution (Experimental condition: volume = 0.1 L; IRA67 dosage = 1.0 g/L; desorption hour = 24 hours)

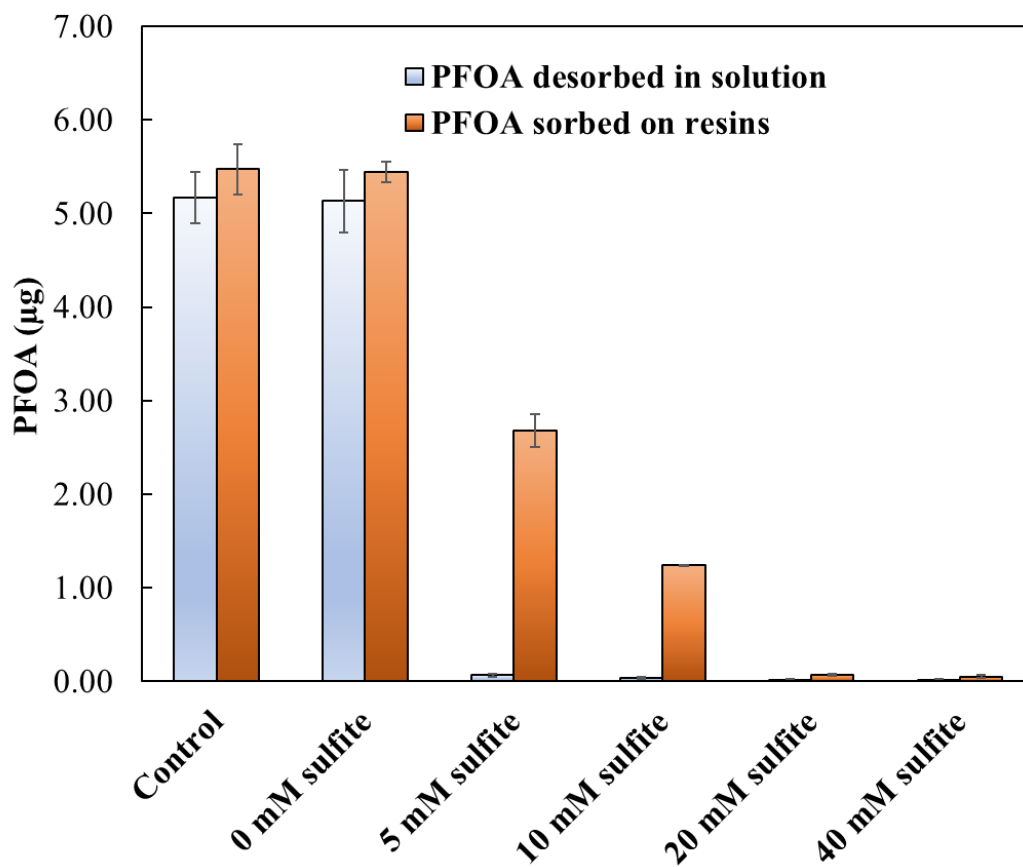


Figure 5-13 PFOA degradation at different sulfite dosages during the UV/SO₃²⁻ treatment of IRA67 from ten cyclic NOM and PFOA loading tests (Experimental condition: pH = 10.0; volume = 0.1 L; IRA67 dosage = 1.0 g/L; reaction hour = 3 hours)

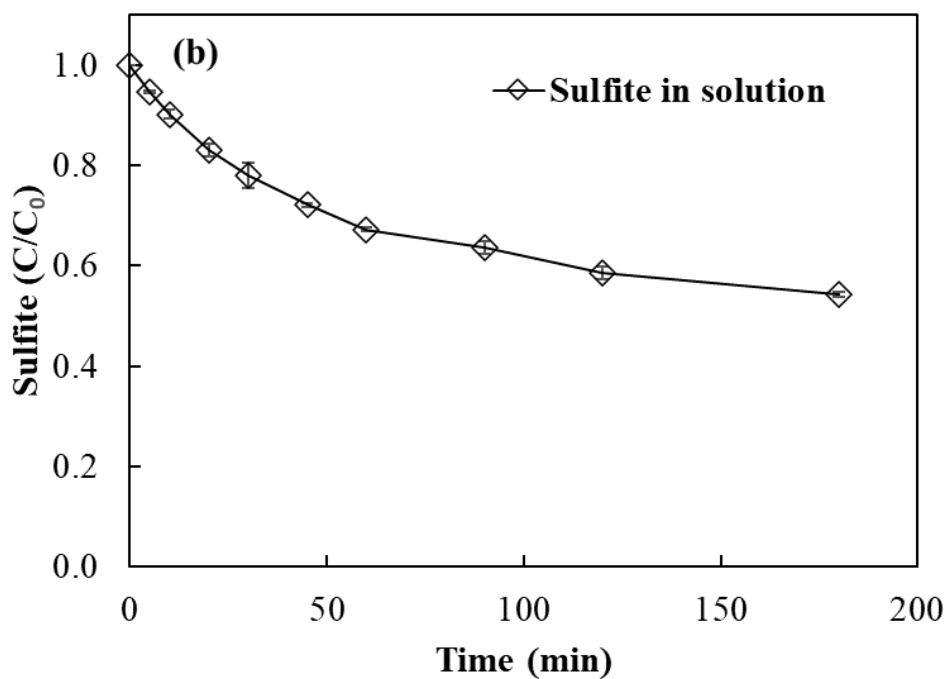
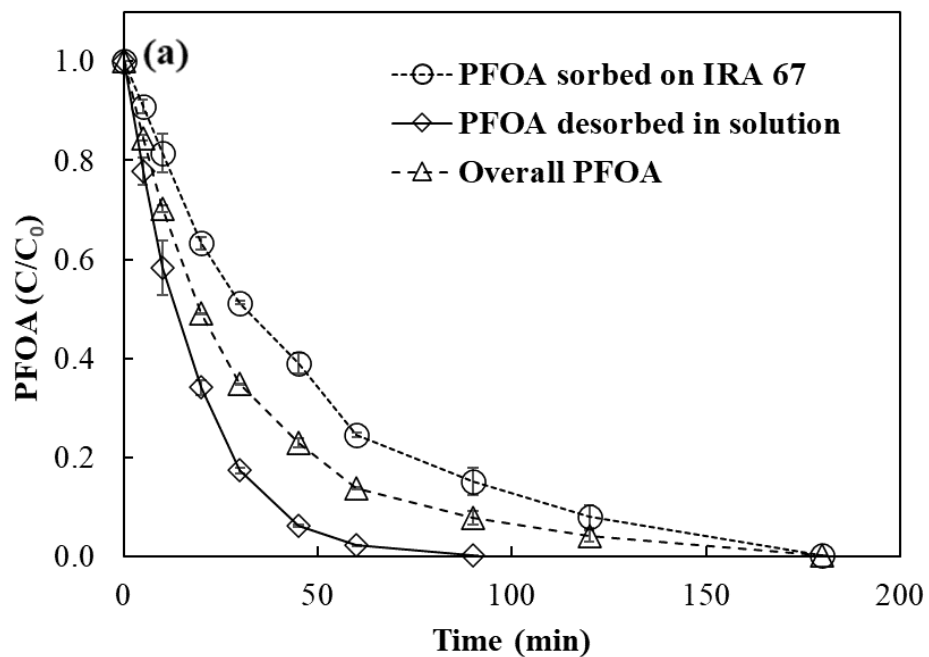


Figure 5-14 Kinetic tests of the UV/SO₃²⁻ ARP treatment of IRA67 from ten cyclic NOM and PFOA loading tests: (a) PFOA decomposition and (b) sulfite decay (Experimental condition: pH = 10.0; volume = 0.1 L; IRA67 dosage = 1.0 g/L; reaction hour = 0 to 3 hours; sulfite dosage = 20.0 mM); symbols and lines represent measured data and the fit of the hypothetical reaction model, respectively

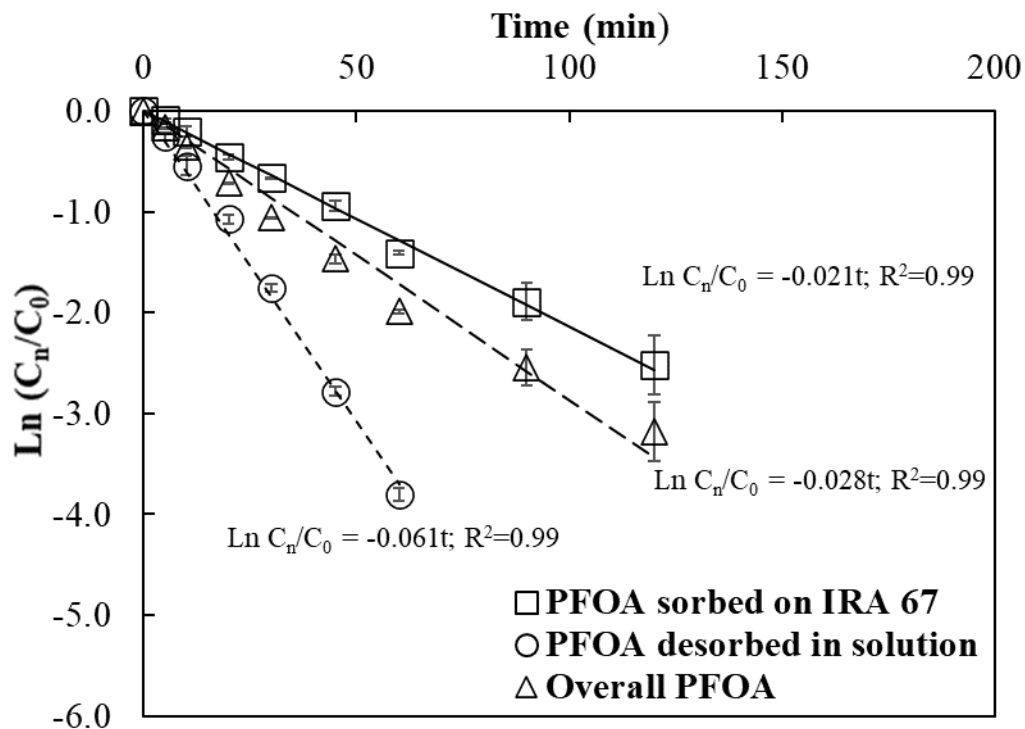
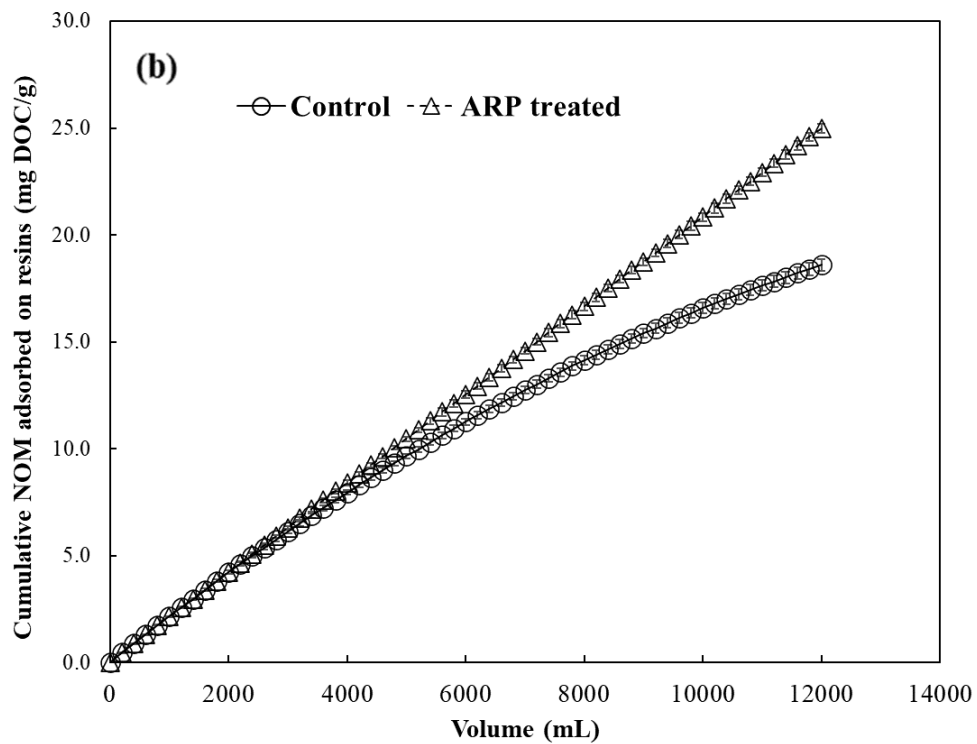
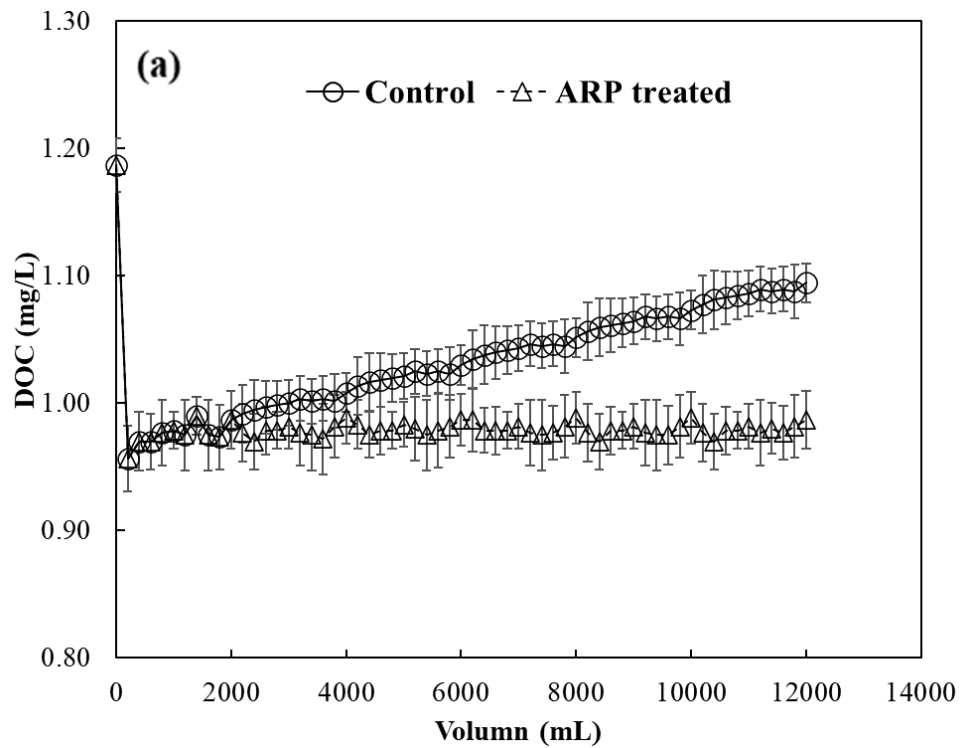
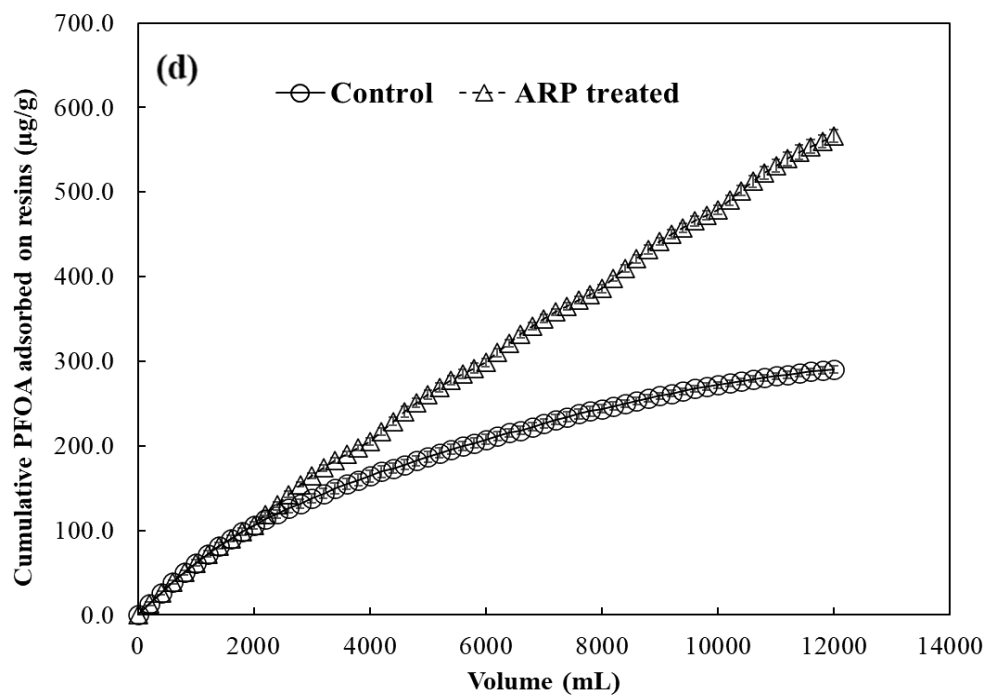
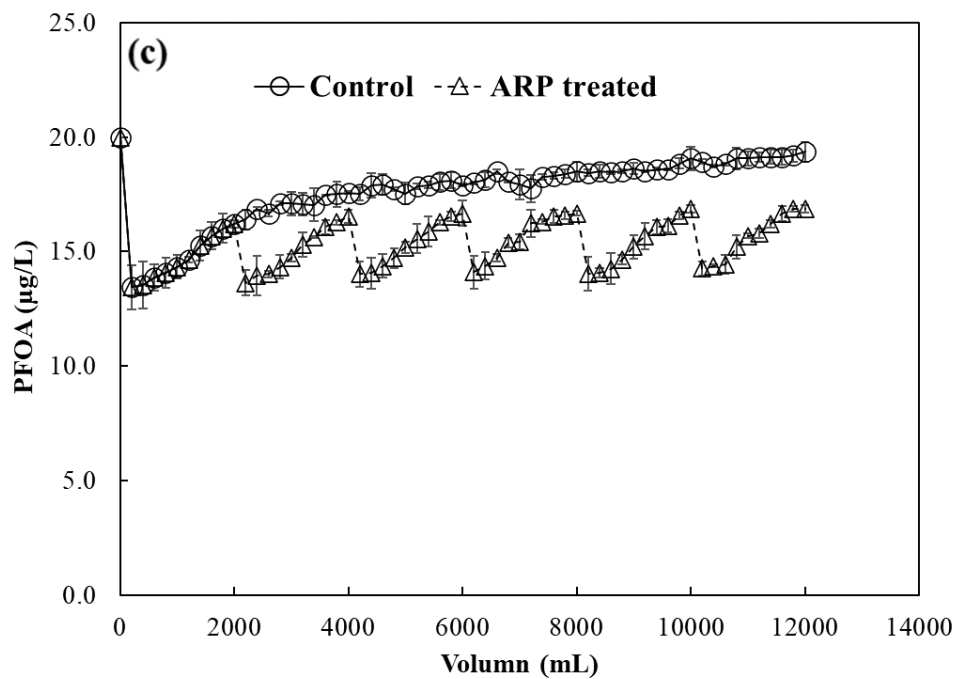


Figure 5-15 Ln C_n/C₀ vs. t for PFOA decomposition during the UV/SO₃²⁻ ARP treatment of IRA67 from ten cyclic NOM and PFOA loading tests (Experimental condition: pH = 10.0; volume = 0.1 L; IRA67 dosage = 1.0 g/L; reaction hour = 0 to 3 hours; sulfite dosage = 20.0 mM); symbols and lines represent measured data and non-linear regression modeled data, respectively)





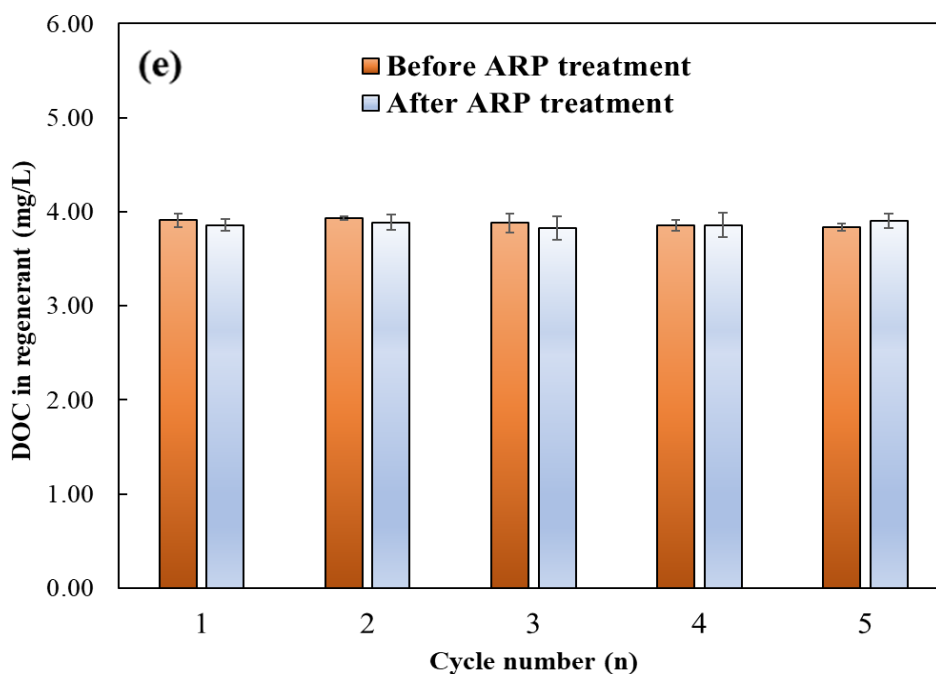


Figure 5-16 NOM and PFOA during six cyclic adsorption-regeneration tests: (a) residual NOM in solution after each loading test; (b) accumulative NOM adsorbed; (c) residual PFOA in solution after each loading test; (d) accumulative NOM adsorbed; (e) DOC in solution before and after ARP regeneration (Experimental condition: adsorption phase: pH = 7.5; volume = 0.2 L; IRA67 dosage = 0.5 g/L; reaction hour = 30 mins; Control: no UV/SO₃²⁻ regeneration in each cycle; ARP treatment: pH = 10.0; volume = 0.1 L; IRA67 dosage = 1.0 g/L; reaction hour = 3 hours; sulfite dosage = 20.0 mM)

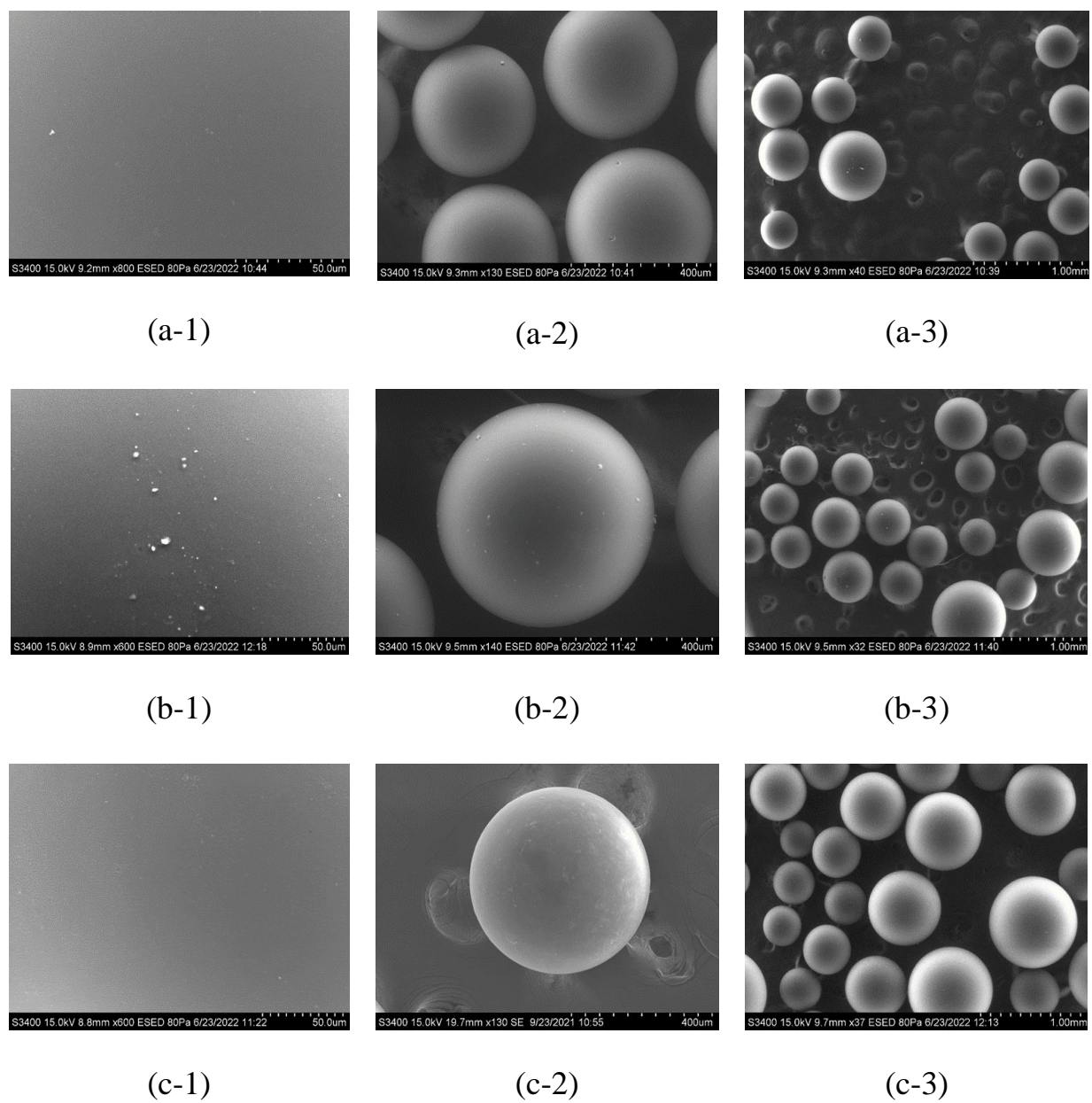
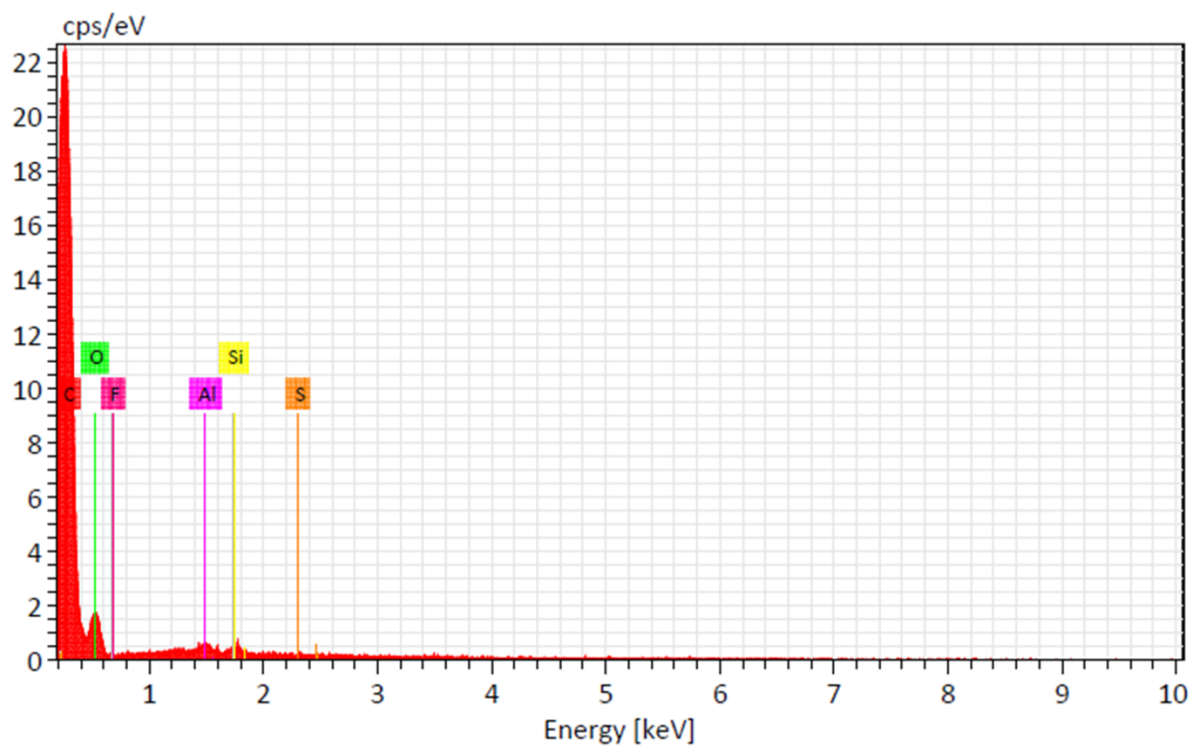
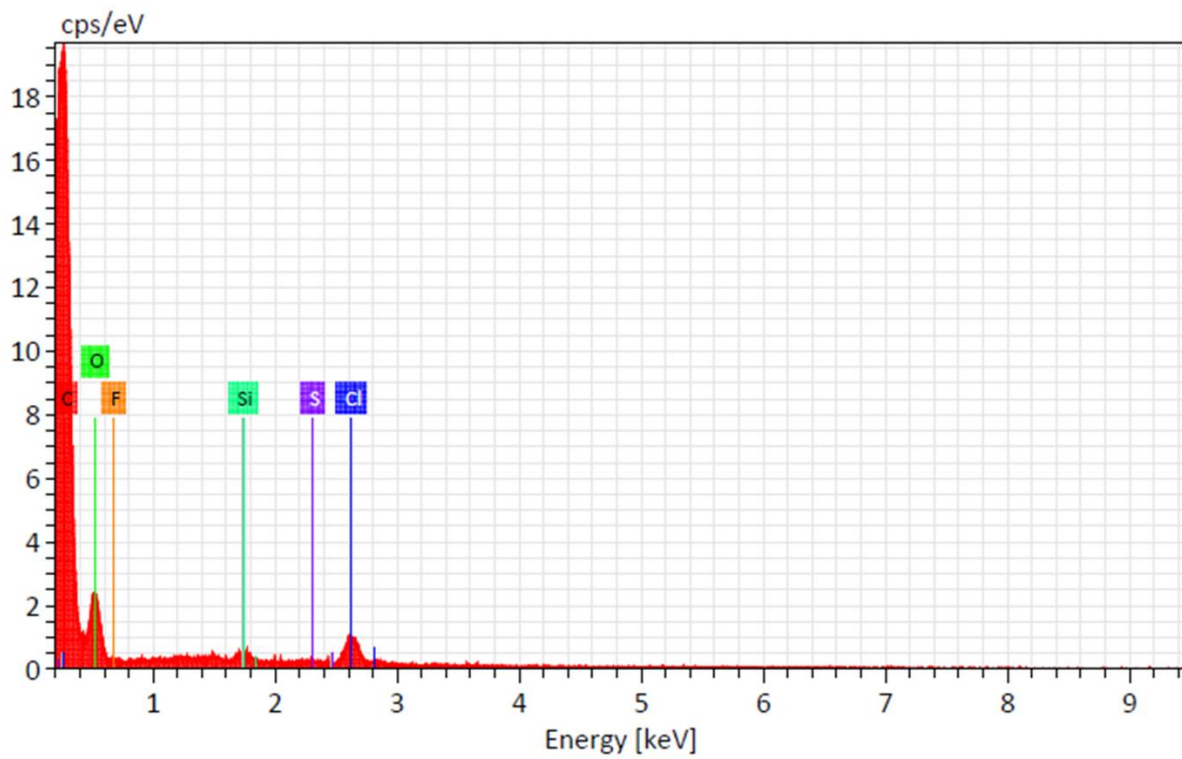


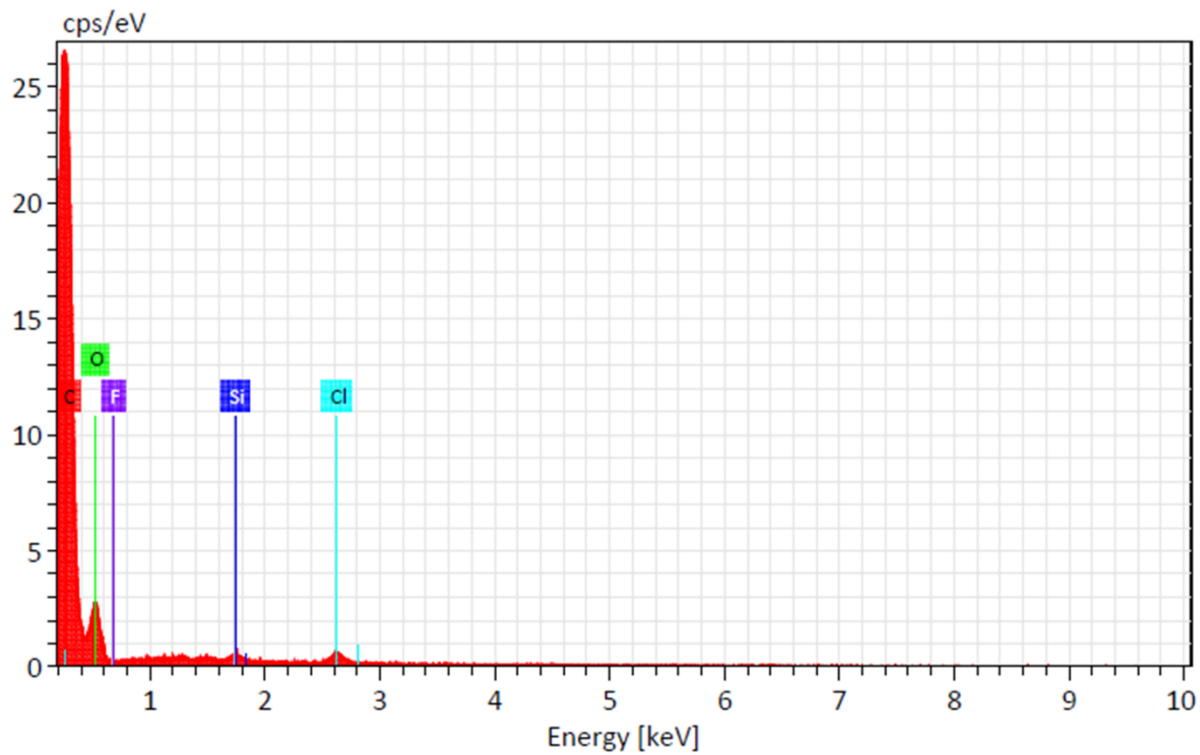
Figure 5-17 Comparison of SEM images of three resins: a) fresh IRA67, b) IRA67 with no ARP regeneration after six cyclic adsorption-regeneration tests and c) ARP regenerated IRA67 after six cyclic adsorption-regeneration tests



(a)



(b)



(c)

Figure 5-18 Comparison of EDS spectra of three resins: a) fresh IRA67, b) IRA67 with no ARP regeneration after six cyclic adsorption-regeneration tests and c) ARP regenerated IRA67 after six cyclic adsorption-regeneration tests

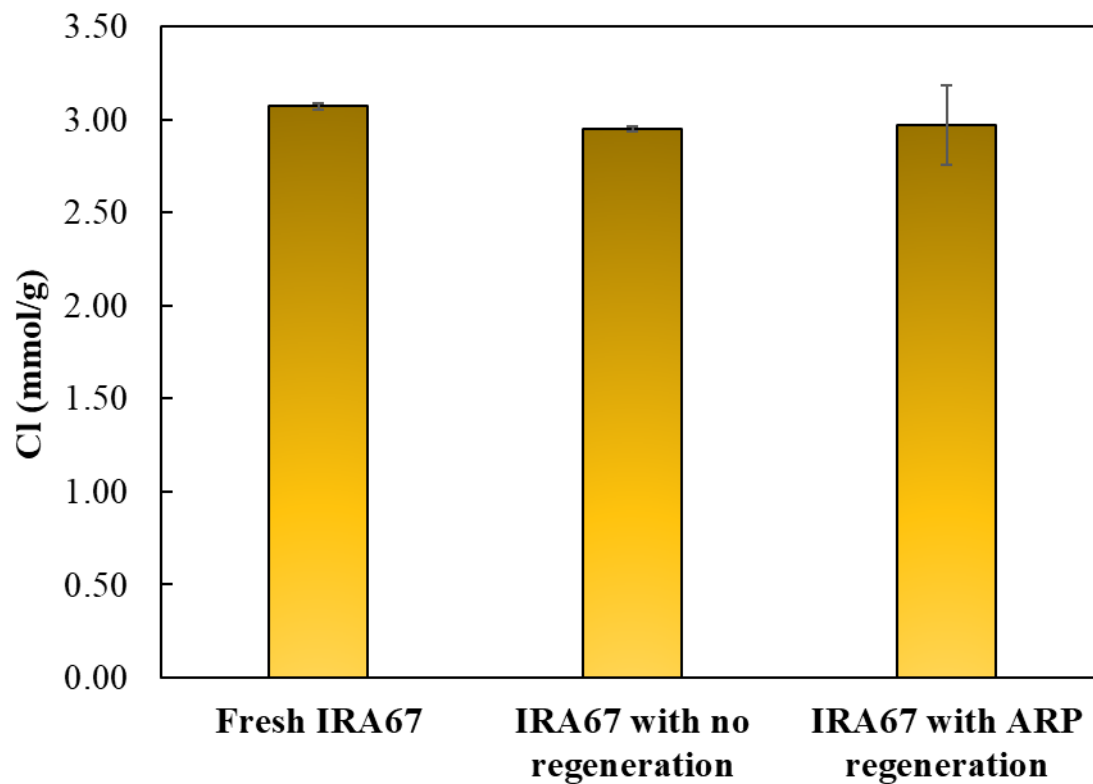


Figure 5-19 Comparison of IEC of fresh IRA67, IRA67 with no regeneration after six cyclic adsorption-regeneration tests, and ARP regenerated IRA67 after six cyclic adsorption-regeneration tests

References

- Bolto, B., Dixon, D., & Eldridge, R. (2004). Ion exchange for the removal of natural organic matter. *Reactive and Functional Polymers*, 60, 171-182.
- Bolto, B., Dixon, D., Eldridge, R., King, S., & Linge, K. (2002). Removal of natural organic matter by ion exchange. *Water research*, 36(20), 5057-5065.
- Bond, T., Goslan, E., Parsons, S., & Jefferson, B. (2010). Disinfection by-product formation of natural organic matter surrogates and treatment by coagulation, MIEX® and nanofiltration. *Water research*, 44(5), 1645-1653.
- Bose, P., & Reckhow, D. A. (2007). The effect of ozonation on natural organic matter removal by alum coagulation. *Water research*, 41(7), 1516-1524.
- Chong Soh, Y., Roddick, F., & Van Leeuwen, J. (2008). The impact of alum coagulation on the character, biodegradability and disinfection by-product formation potential of reservoir natural organic matter (NOM) fractions. *Water Science and Technology*, 58(6), 1173-1179.
- Chow, C. W., Fabris, R., Leeuwen, J. v., Wang, D., & Drikas, M. (2008). Assessing natural organic matter treatability using high performance size exclusion chromatography. *Environmental Science & Technology*, 42(17), 6683-6689.
- Christensen, J. B., Jensen, D. L., Grøn, C., Filip, Z., & Christensen, T. H. (1998). Characterization of the dissolved organic carbon in landfill leachate-polluted groundwater. *Water research*, 32(1), 125-135.
- Crittenden, J. C., Trussell, R. R., Hand, D. W., Howe, K. J., & Tchobanoglous, G. (2012). *MWH's water treatment: principles and design*. John Wiley & Sons.
- Deng, S., Yu, Q., Huang, J., & Yu, G. (2010). Removal of perfluorooctane sulfonate from wastewater by anion exchange resins: Effects of resin properties and solution chemistry. *Water research*, 44(18), 5188-5195.
- Kleiser, G., & Frimmel, F. (2000). Removal of precursors for disinfection by-products (DBPs)—differences between ozone-and OH-radical-induced oxidation. *Science of the Total Environment*, 256(1), 1-9.
- Korkmaz, D. (2001). Precipitation titration:“determination of chloride by the Mohr method”. *Methods*, 2(4), 1-6.
- Krupińska, I. (2020). Aluminium drinking water treatment residuals and their toxic impact on human health. *Molecules*, 25(3), 641.

- Matilainen, A., Vepsäläinen, M., & Sillanpää, M. (2010). Natural organic matter removal by coagulation during drinking water treatment: A review. *Advances in colloid and interface science*, 159(2), 189-197.
- Miyazaki, Y., & Nakai, M. (2011). Protonation and ion exchange equilibria of weak base anion-exchange resins. *Talanta*, 85(4), 1798-1804.
- Moldes, A., Alonso, J., & Parajo, J. (2003). Recovery of lactic acid from simultaneous saccharification and fermentation media using anion exchange resins. *Bioprocess and biosystems engineering*, 25(6), 357-363.
- Philippe, K. K. (2010). The role of advanced oxidation processes in drinking water treatment.
- Rahimi, M., Wadi, D., & Vadi, M. (2014). Langmuir, freundlich and temkin adsorption isotherm of captopril an ace inhibitor (or angiotensin-converting-enzyme inhibitor) is a pharmaceutical drug used for the treatment of hypertension by multi-wall carbon nanotube. *Ind. J. Fund. Appl. Life Sci*, 4, 933-937.
- Rahmani, S., & Mohseni, M. (2017). The role of hydrophobic properties in ion exchange removal of organic compounds from water. *The Canadian Journal of Chemical Engineering*, 95(8), 1449-1455.
- Sarathy, S. R., & Mohseni, M. (2007). The impact of UV/H₂O₂ advanced oxidation on molecular size distribution of chromophoric natural organic matter. *Environmental Science & Technology*, 41(24), 8315-8320.
- Sarathy, S. R., Stefan, M. I., Royce, A., & Mohseni, M. (2011). Pilot-scale UV/H₂O₂ advanced oxidation process for surface water treatment and downstream biological treatment: effects on natural organic matter characteristics and DBP formation potential. *Environmental technology*, 32(15), 1709-1718.
- Sillanpää, M., Ncibi, M. C., & Matilainen, A. (2018). Advanced oxidation processes for the removal of natural organic matter from drinking water sources: A comprehensive review. *Journal of Environmental Management*, 208, 56-76.
- Sindelar, H. R., Brown, M. T., & Boyer, T. H. (2014). Evaluating UV/H₂O₂, UV/percarbonate, and UV/perborate for natural organic matter reduction from alternative water sources. *Chemosphere*, 105, 112-118.
- Świetlik, J., Dąbrowska, A., Raczyk-Stanisławiak, U., & Nawrocki, J. (2004). Reactivity of natural organic matter fractions with chlorine dioxide and ozone. *Water research*, 38(3), 547-558.
- Thurman, E. M., & Malcolm, R. L. (1981). Preparative isolation of aquatic humic substances. *Environmental Science & Technology*, 15(4), 463-466.

- Toor, R., & Mohseni, M. (2007). UV-H₂O₂ based AOP and its integration with biological activated carbon treatment for DBP reduction in drinking water. *Chemosphere*, 66(11), 2087-2095.
- Uyak, V., Yavuz, S., Toroz, I., Ozaydin, S., & Genceli, E. A. (2007). Disinfection by-products precursors removal by enhanced coagulation and PAC adsorption. *Desalination*, 216(1-3), 334-344.
- Uyguner, C., Bekbolet, M., & Selcuk, H. (2007). A comparative approach to the application of a physico-chemical and advanced oxidation combined system to natural water samples. *Separation Science and Technology*, 42(7), 1405-1419.
- Wang, G.-S., Hsieh, S.-T., & Hong, C.-S. (2000). Destruction of humic acid in water by UV light—catalyzed oxidation with hydrogen peroxide. *Water research*, 34(15), 3882-3887.
- Zhao, H., Hu, C., Liu, H., Zhao, X., & Qu, J. (2008). Role of aluminum speciation in the removal of disinfection byproduct precursors by a coagulation process. *Environmental Science & Technology*, 42(15), 5752-5758.

Chapter 6 Conclusions

6.1 Economic Analysis

Cost is one of the most critical factors for market adoption and technology commercialization. The expenses can be typically divided into capital and operational and maintenance (O&M) costs. In the proposed technology, the capital costs have been associated with the buildup of an ARP reactor, pumps, pipes, valves, measuring meters, and contractor overhead and profit (O&P). Of note, the capital cost is amortized over a span of years at a given amortization rate. The O&M costs may be used for part replacement and repair (e.g., UV lamps), labor, chemical transport and storage, waste transport and disposal, and sample analysis.

However, it is not suitable to conduct cost analyses and compare the new IX-regeneration method with established PFAS treatment technologies due to two reasons. First, the data acquired from this dissertation study is preliminary. Second, technical data without technology optimization cannot be input into economic assessments because this may lead to a cost.

However, the potential economic advantages of the proposed ARP-driven on-site IX resin regeneration process are briefly discussed as follows. First, the conventional IX resin regeneration is commonly off-site implemented. Thus, compared to the conventional resin regeneration methods, the proposed on-site ARP-based IX resin regeneration can decrease costs related to transportation between the treatment and regeneration facilities. Second, different from the toxic regenerant wastes containing aqueous PFAS, brine solution, and organic solvent generated from conventional resin regeneration processes, a relatively small volume of non-toxic PFAS-free regenerant (pH =10.0) is expected to be produced from the proposed method. The regenerant pH can be readily neutralized acid before discharge (Bengtsson et al., 2008; Patterson, 1985). Third, as discussed in **Chapter 1**, the successful implementation of the proposed method

can repeatedly utilize IX resins to maximize their commercial values to significantly decrease the resin consumption.

6.2 Implications in Environmental Management

Water treatment plays a critical role in water resource management to ensure water security and improve water quality for meeting different intended uses. This dissertation research represents the first scientific and engineering attempt to apply ARP-driven on-site IX resin regeneration for concurrently restoring the resin capacity for PFAS adsorption and degrading sorbed PFAS. This effort is made to explore a new ultimate solution to the PFAS pollution in drinking water. The encouraging findings from the bench-scale studies in this dissertation indicate that the novel ARP-driven on-site IX resin regeneration approach has the potential to revolutionize the way PFAS-contaminated water is treated due to the benefits unmatched by existing treatments. Their profound impacts on environmental management are delineated in the following three aspects: water treatment industry, environmental benefits, and social benefits.

6.2.1 Implication to the Water Treatment Industry

Safe and sufficient water is essential in society. Water treatment plants utilize technological barriers to the mitigation of various pollutants in a bulk volume of the raw water to meet federal, state, and local water standards. However, PFAS, a family of emerging persistent organic pollutants, seriously challenge traditional water treatment processes (Gao et al., 2021; Rahman et al., 2014; Ratola et al., 2012). Although IX, as an established PFAS treatment technology, has been extensively applied to drinking water treatment practices due to its adsorption capability and technology maturity, IX is challenged by prohibitive off-site regeneration and the production of toxic PFAS-containing regenerant waste, which requires proper disposal. Therefore, the development of novel IX regeneration methods is urgently

needed. Interestingly, e_{aq}^- has been appreciated over the past decade because of its effective degradation of PFAS in water (Bentel et al., 2019; Tenorio et al., 2020). However, e_{aq}^- -driven ARPs for PFAS treatment is restricted in drinking water treatment due to increased TDS in the effluent, pH adjustment, and practical difficulty in eliminating DO from substantial water (Cui et al., 2020). Thus, new strategies need to be explored to apply e_{aq}^- in a drinking water treatment scenario. Of note, the new approach proposed in this dissertation research takes complementary advantage of IX and ARPs, while overcoming their respective restrictions, enabling the true ARP application to the water treatment industry. The key findings can bring an immediate and profound impact on the water treatment industry, considering that PFAS are one of the highest priority pollutants, IX is widely applied for PFAS removal, and the fundamental knowledge on e_{aq}^- -based ARP is increasingly advanced (Cui et al., 2020).

Meanwhile, the proposed ARP-based IX resin regeneration approach can be readily accepted and adopted by the industrial community due to 1) commercially available UV equipment for water treatment; 2) a relatively small volume of easily managed regenerant waste; 3) extensive experience in UV system design, installation, operation, and maintenance; and 4) on-site regeneration.

It should be noted that this dissertation research has two significant implications for the industrial sector. First, an innovative approach (i.e., ARP-driven on-site IX resin regeneration) is proposed in this dissertation to tackle the PFAS issues in drinking water. Although this dissertation targets IX resins, the ARP regeneration approach can be similarly applied to other commercialized and emerging adsorbents (e.g., AC, zeolite, and biochar) (Cantoni et al., 2021; Gagliano et al., 2020; Qian et al., 2022). Second, although this dissertation mainly focuses on

removing one of the representative PFAS, the proposed approach can be readily transferred to the abatement of other trace and persistent contaminants in drinking water.

For example, it is well known that e_{aq}^- -induced reductive degradation of PFOA occurs through H/F exchange and/or carbon chain shortening (Cui et al., 2020). Because either of the reaction routes can also lead to degradation of PFASs or other PFCAs, the UV/SO₃²⁻ ARP treatment is highly likely to degrade other PFAS sorbed on resins. This pioneering research is the first step toward the technology innovation and eventually finds a sustainable pathway to the PFAS issues confronted by the water treatment industry.

6.2.2 Environmental Benefits

The innovative ARP-based IX resin regeneration schemes for water treatment can benefit the environment, at least in the following two aspects, including 1) the improvement of environmental quality and 2) the environmental friendliness of the technology.

Improving environmental quality. As discussed in **Chapter 1**, PFAS exhibit a high mobility in the aquatic environment (e.g., groundwater and surface water) (Hatton et al., 2018), strong partitioning behavior (e.g., liquid/solid and gas/liquid interface) (Munoz et al., 2019), and high resistance to biotic and abiotic transformation of perfluorinated moieties (i.e., the carbon center possessing only C-C or C-F bonds) in the environment (Bentel, 2020). Thus, various PFAS have been ubiquitously identified in most environmental media, including contaminated soil, air, drinking water, and groundwater, with high concentrations detected in fire-fighting facilities near military bases (Evich et al., 2022).

Of note, mitigating these emerging anthropogenic chemicals in the environment can dramatically decrease the potential risks to environmental health. Application of the innovative ARP-based IX resin regeneration can minimize the occurrence of PFAS in drinking water,

thereby safeguarding environmental quality. As illustrated in this dissertation research, the PFOA can be predominantly adsorbed on IRA67 and subsequently degraded after the UV/SO₃²⁻-ARP-based IX resin regeneration. Unlike the conventional IX regeneration practices that require cautions for PFAS-containing regenerant, the novel IX regeneration method can effectively degrade a vast majority of PFAS with the production of a small volume of easily managed regenerant waste.

Additionally, the new ARP-based IX resin regeneration method has proven effective for NOM adsorption in drinking water. NOM is defined as a complex matrix of organic material, which is ubiquitously present in natural waters (Matilainen et al., 2010). Mitigating the NOM in the water system can promote water quality due to the following two reasons. First, NOM might be the precursors of harmful identified and unidentified disinfection byproducts (DBPs) (Song et al., 2016). Second, NOM can play a vital role in enhancing the solubility of toxic heavy metals (e.g., cadmium and lead) in water via complexation, which can challenge the removal of toxic metals in the subsequent water treatment processes (Matilainen et al., 2010).

Environmentally friendly technology. The novel ARP-based IX resin regeneration approach in this dissertation study is relatively environmentally friendly compared to the conventional PFAS-laden IX resin regeneration and disposal.

The conventional method to desorb PFAS from IX resin for regeneration is to apply salts (e.g., NaCl), alkaline (e.g., NaOH), and/or organic solvents (e.g., methanol, ethanol, and propanol) at high concentrations (Boyer et al., 2021; Dixit et al., 2021; Du et al., 2014). These unwanted chemicals will largely remain in the regenerant for the following disposal. In contrast, the ARP regeneration is expected to produce a waste solution containing sulfate at a relatively low level. Moreover, traditional IX resin regeneration methods are mostly off-site implemented,

requiring the storage and management of PFAS-containing IX resins and toxic organic solvents. The transport and storage may cause a secondary pollution. Furthermore, because the common IX resin regeneration method only transfers PFAS from IX resins to another phase (i.e., regenerant) without PFAS degradation, the PFAS toxicity for environmental health remains. Meanwhile, the incineration (i.e., thermally destruction of resin) approach is commonly used for disposal of non-regenerable IX resins once IX resins reach service lifetime (Taylor et al., 2014; Zaggia et al., 2016). After the incineration of PFAS-spent IX resins, PFAS (e.g., PFOA and PFOS) sorbed on IX resins can be chemically broken down to prevent their re-introduction into the environment (Khan et al., 2020; Krusic et al., 2005). Then, the treatment residuals and incineration wastes (e.g., ash) are landfilled in most scenarios. Nevertheless, the treatment method will lead to the emission of gaseous perfluorocarbon (Boyer et al., 2021).

In contrast, the proposed IX resin regeneration approach can overcome the aforementioned shortcomings in four aspects. First, rather than the PFAS-containing bulk solution, a relatively small volume of residual is generated after the ARP regeneration for proper disposal. Second, the major final product in the regenerant may be non-toxic (e.g., Na_2SO_4) rather than PFAS-containing toxic organic solvents. Third, because this method is an on-site IX resin regeneration, which can largely avoid the unwanted pollution to the environment during off-site IX resin regeneration, such as resin handling, storage, and transportation. Fourth, the PFAS-spent IX resins can be repeatedly applied for abatement of PFAS in drinking water without considering the disposal of single-use PFAS-spent IX resin (e.g., incineration and landfilling) for potential environmental pollution.

6.2.3 Social Benefits

The novel, effective, and resilient PFAS treatment technology can also engender multiple social benefits in our community. At a minimum, five social benefits are expected from this dissertation study.

- 1) *Life quality and public health.* Human exposure to PFAS is potentially associated with cancer, obesity, fertility reduction, enhanced cholesterol, liver diseases, immune suppression, and hormone interference. Consumption of PFAS-polluted drinking water represents a major route of human exposure to PFAS. Approximately 200 million U.S. residents, i.e., nearly two-thirds of the U.S. population, consume water from municipal water supply systems that are contaminated by PFAS (Andrews & Naidenko, 2020; Cordner et al., 2021). Thus, the alleviation of PFAS pollution in drinking water with the innovative UV/SO₃²⁻ ARP-based IX resin regeneration approach will significantly improve human health, thereby promoting the life quality of residents in the community.
- 2) *Local economic development.* Safe and sufficient water can significantly enhance a community's economic growth. Specifically, the community residents and local businesses utilize clean water to boost the local economy through farming, recreation, energy production, tourism, manufacturing, and other economic sectors. The clean water-induced economic growth can appreciably attract more people to the local companies, thereby concurrently creating more job opportunities for the community.
- 3) *Clean water supply reliability.* The wide-ranging application of PFAS in different industrial and consumer goods results in the release of these emerging anthropogenic chemicals into the water system. Widespread PFAS contamination in surface water

(e.g., rivers, lakes, and reservoirs) is now a severe issue in the U.S. and globally.

Despite the lack of enforceable federal MCLs for any PFAS chemicals in U.S. drinking water, the USEPA has tightened its lifetime health advisory (LHD) levels for certain PFAS. Furthermore, many U.S. states (e.g., New Jersey) have established statewide mandatory drinking water standards for different PFAS compounds. It is challenging to meet the federal or state standard levels to supply PFAS-safe water to the community. To maintain a clean water supply for the residents, municipalities may purchase less PFAS-contaminated water from other distributors. However, this option can burden public utilities heavily due to the increased capital costs for new infrastructure and ongoing maintenance costs. In contrast, as a technically viable and low-cost water treatment option, the innovative UV/SO₃²⁻ ARP-based IX resin regeneration method can lower the levels of PFAS in the locally produced drinking water to meet different required or recommended levels and enhance clean water supply, thereby lessening the dependence upon water conveyance from other distributors in remote areas.

- 4) *Enhancing the awareness of sustainability.* Resin regeneration represents a sustainable method to reactivate spent resin for continuous water purification. In this dissertation study, the ability of multiple regeneration of PFAS-laden IX resin using the UV/SO₃²⁻ ARPs will increase the environmental and economic sustainability (a lower resin demand and less production of resin wastes) of water treatment processes. The successful implementation of the on-site ARP-based IX resin regeneration scheme for drinking water treatment will increasingly promote public awareness and understanding of sustainability in their daily life. Strengthening public awareness of sustainability can enhance the quality of our lives, protect our ecosystem, and preserve

natural resources for future generations. Meanwhile, the knowledge obtained from the emerging IX resin regeneration technology can also be integrated into sustainability education, thereby encouraging students, schools, and communities to act for sustainability.

- 5) *Aesthetics*. As discussed in this dissertation, the IX resins can concurrently adsorb PFAS and NOM in the surface water. Meanwhile, the resin saturation during IX application to drinking water treatment is principally governed by the sorption of substantial NOM instead of trace PFAS. Although the PFAS are colorless in water, the co-existing NOM can impact the color of water, which causes aesthetic effects. The proposed UV/SO₃²⁻ ARP-based IX resin regeneration method removes the PFAS in water and reduces the NOM-induced color. Therefore, the aesthetic values of water will be improved, which is important to drinking water and vital to certain recreational purposes (e.g., swimming) in local communities.

6.3 Overall Conclusions

This dissertation aimed to assess the technical aspect of the novel UV/SO₃²⁻ ARP-based IX resin regeneration approach to effective mitigation of PFOA in drinking water and elucidate the underlying mechanisms. The proposed on-site resin regeneration scheme builds on complementary advantages of IX and ARPs, while overcoming their respective restrictions, thus enabling the application of ARPs to water treatment. Bench-scale studies were conducted to validate that the ARP treatment can reductively degrade PFOA sorbed on exhausted WBA exchange resins, while having limited destruction on physical and chemical properties of the resin materials. Initial screening tests indicate that IRA67 is the optimal resin for the proposed approach because of its excellent adsorption capacities for PFOA, regeneration capabilities

during the ARP treatment, and durable physical/chemical properties under the exposure to the UV irradiation and e_{aq}^- -driven reduction.

This study demonstrates that e_{aq}^- -driven ARP treatment is effective for the degradation of PFOA sorbed on PFOA/NOM-laden IRA67 and desorbed in the solution in the presence of NOM. Specifically, e_{aq}^- generated preferentially attacks PFOA in the solution rather than PFOA on the resins. In the meantime, the saturation of IRA67 in the removal of PFOA in water treatment is ascribed to the adsorption of NOM (more abundantly present in the water). Unfortunately, the UV/SO₃²⁻ ARP treatment cannot effectively decompose and mineralize co-sorbed NOM to effectively recover the resin adsorption, though UV irradiation alone or e_{aq}^- can degrade certain NOM moieties, particularly EWGs (e.g., carboxyl groups). Therefore, strategies for mitigating co-sorbed NOM need to be jointly applied with ARPs to alleviate the NOM impacts.

Pretreatment of simulated natural water with alum coagulation prior to the IX was demonstrated to significantly alleviate the NOM loading on IRA67 and increase PFOA adsorption on IRA67. Coagulation performance relies heavily on two operating factors, i.e., alum dose and solution pH. Nevertheless, the UV/H₂O₂-based AOP for treatment of pre-coagulated water does not further remove NOM loading on IRA67 because the AOP cannot sufficiently mineralize the remaining NOM after alum coagulation. Although PFOA adsorption on IRA67 in pre-coagulated PFOA-containing water is significantly enhanced compared to the sorption to IRA67 in simulated natural water, the remaining NOM from the pre-coagulated PFOA-containing water remains the dominant contribution to the saturation of IRA67. Consequently, the co-sorbed PFOA on IRA67 declines as the loading cycle increases. However, the coagulation pretreatment alleviates the impact of NOM on the PFOA adsorption. Of note, results show that

co-sorbed NOM on IRA67 is largely desorbed in the optimal alkaline solution to release the occupying sites on IRA67 because of the deprotonation of tertiary amine at a higher pH solution.

The dissertation builds a basis for an innovative ARP-enabled on-site IX regeneration approach to the PFAS pollution in drinking water treatment. It targets two purposes, that is, cost-efficient removal of PFOA and regeneration of saturated IX resin. The approach can be significantly favored when coagulation pretreatment is applied to abate NOM in raw water prior to IX adsorption. Meanwhile, a small volume of easily managed regenerant waste is produced. The regenerated IRA67 can be repeatedly used to alleviate PFOA in water to significantly reduce the overall PFOA treatment cost. In addition to PFAS, the proposed regeneration approach is expected to mitigate other persistent micropollutants in drinking water. Although the ARP is still at an early stage, it has the potential to be widely accepted by the water industry. Thus, the innovative ARP-based IX resin regeneration method can profoundly impact our society in the technical, environmental, economic, and social aspects.

6.4 Current Limitations of the Proposed IX Resin Regeneration Method

Although this study demonstrates the potential of the ARP-driven on-site IX resin regeneration approach advantageous over conventional PFAS treatment technologies, there is still an uphill struggle in its application. Three potential barriers to the application are discussed below. First, a relatively high pH condition (i.e., pH 10.0) was selected for the IX resin regeneration process in this dissertation, which prevents e_{aq}^- from scavenging by H^+ in the solution. Although the pH of the regenerant can be neutralized before water discharge, an alkaline pH solution might cause corrosion on the equipment during the ARP regeneration to reduce its lifetime. Second, over 4,700 PFAS were identified on the global market in 2018 (OECD, 2018). However, only certain PFAS (e.g., PFOA and PFOS) and their replacements

(e.g., GenX) have been extensively studied in the laboratory- and pilot-scale studies using the ARP treatment. There is still the limited information on whether the emerging ARP technology can effectively or even completely destruct other PFAS (e.g., short-chain PFAS) and their degradation intermediates (e.g., sulfur-containing byproducts) to truly generate a non-toxic or PFAS-free regenerant. Third, the PFOA-contaminated water samples used in this study are prepared using DI or simulated natural water, which are not real water samples from natural water sources. Namely, besides NOM, the roles of other common water matrix constituents (e.g., nitrate and chloride) and other PFAS (e.g., PFASs) in real water samples during the PFOA adsorption and ARP-based resin regeneration phases were not studied in this dissertation. However, these water matrix constituents or other PFAS may positively or adversely influence the PFOA adsorption capacity and degradation efficiencies in the proposed method.

6.5 Future Research

This dissertation research represents the first step towards an innovative on-site ARP-based IX resin regeneration approach capable of repeatedly using regenerated IX resin for removal and degradation of PFAS in drinking water. Although the current study demonstrates encouraging results in the regeneration of PFOA/NOM-laden IRA67, further investigations are needed to advance the application of this novel on-site ARP-based IX resin regeneration process for PFAS elimination in drinking water. The future research directions, which deserve in-depth investigations, are discussed below.

- 1) *Other PFAS*. Although PFOA was chosen as a model PFAS species in this dissertation owing to its prevalence in the aquatic environment, other commonly identified PFAS (e.g., PFOS and GenX) in drinking water were not investigated in this study. It is inappropriate to directly translate the knowledge acquired from this dissertation to treat

other PFAS in drinking water, because of their different structures (e.g., chain length and functional group). When various PFAS are present in drinking water, the information regarding how these PFAS chemicals may compete for the limited active sites on IX resins remains limited. Whether e_{aq}^- -driven ARP can effectively degrade short-chain PFAS sorbed on IX resins is also unknown. Although the proposed treatment method is a promising solution to other PFAS in drinking water, the assumption needs to be validated through systematic laboratory experiments.

- 2) *Effect of other common water matrix constituents.* The effect of NOM on the IX adsorption and the UV/SO₃²⁻ ARP degradation has been investigated in this dissertation. However, very few efforts were made to examine the effect of other common water matrix constituents (e.g., chloride, nitrate, phosphate, and sulfate) on the proposed regeneration route. Of note, the concentrations of many common water matrix constituents in surface water are several magnitudes greater than those of PFAS. Although WBA exchange resins do not effectively adsorb anions (e.g., chloride and nitrate) around a neutral condition as compared to the SBA exchange resins, the potentially sorbed anions may not only compete with PFAS for active functional sites during the adsorption phase but also scavenge e_{aq}^- to adversely affect PFAS degradation during the ARP treatment. Therefore, a future study is needed to identify the role of other common water matrix constituents in the proposed resin regeneration scheme.
- 3) *Identification and quantification of fluorinated intermediates.* Species and toxicity of PFAS transformation products over the ARP treatment should be elucidated in the future study. The formation of undesirable degradation byproducts is a concern.

Various fluoride-containing degradation products may be produced, of which some remain toxic or are greenhouse gases. Moreover, the effects of solution chemistry parameters and operating conditions on the formation of these unwanted byproducts deserve in-depth evaluation. Special attention should be paid to the production of transformation products derived from the reactions of e_{aq}^- with both PFAS and water matrix constituents (e.g., NOM) and to the formation of the byproducts due to the incorporation of dosed solutes (e.g., sulfite). If the regenerant after ARP treatment still contains considerable amounts of toxic fluorinated intermediates, it needs to be properly disposed of. Thus, future studies should focus on identifying and quantifying the fluorinated intermediates (i.e., daughter products from their parent PFAS) after UV/SO₃²⁻ ARP treatment to truly generate the PFAS-free non-toxic regenerant.

- 4) *Durability of IX resin.* The durability and resistance of the IX resin materials exposed to the UV or UV/SO₃²⁻ treatment needs to be examined. In this dissertation, the SEM image and IEC of the resins were compared before and after cyclic adsorption-regeneration tests. Results showed that the resin beads remained intact, smooth, and spherical structure, indicating that UV irradiation or UV/SO₃²⁻ treatment cannot noticeably alter the resin morphology. At the same time, the functional groups of resins were barely destructed during the UV irradiation or UV/SO₃²⁻ treatment. Further studies are needed to assess the impacts of the UV/SO₃²⁻ ARP process on other material properties.
- 5) *Lifecycle assessment of on-site ARP-based IX resin regeneration.* Developing cost and energy-saving on-site ARP-based IX resin regeneration technologies using less energy-demanding activation methods (e.g., visible light) with minimal environmental impacts

is essential to address PFAS pollution in the future. There is a need for system-level analysis of the entire life cycle costs and environmental impacts of on-site ARP-based IX resin regeneration. It is critical to compare the information with established or other emerging technologies, such as off-site IX resin regeneration by a high concentration of salt or other regenerant chemicals (e.g., organic solvent) and subsequent management operations (e.g., energy for distillation processes to recover solvent). The optimal treatment solutions can be identified only through such analyses that consider the integrated treatment systems. Life cycle cost assessment will play a critical role in evaluating the trade-offs in operating and capital costs over the lifetime of the cyclic regeneration-adsorption system. Meanwhile, life cycle assessment frameworks need to be developed to compare the comprehensive environmental impacts of other existing resin regeneration technologies for PFAS mitigation. However, it is inappropriate now to carry out the TEA and LCA for on-site ARP-based IX resin regeneration technologies and compare the technologies with existing treatment options, considering that the emerging treatment process is still at the early stage. With the advances in ARP chemistry and technology, the TEA and LCA will be needed in a future and more-developed phase. Furthermore, residual disposal and management will also need to be considered during these assessments.

References

- Andrews, D. Q., & Naidenko, O. V. (2020). Population-wide exposure to per-and polyfluoroalkyl substances from drinking water in the United States. *Environmental science & technology letters*, 7(12), 931-936.
- Bengtsson, S., Hallquist, J., Werker, A., & Welander, T. (2008). Acidogenic fermentation of industrial wastewaters: Effects of chemostat retention time and pH on volatile fatty acids production. *Biochemical Engineering Journal*, 40(3), 492-499.
- Bentel, M. J. (2020). *Understanding Structure–Reactivity Relationships for Aqueous Per-and Polyfluoroalkyl Substances (PFAS) Within the UV/Sulfite System UC Riverside*].
- Bentel, M. J., Yu, Y., Xu, L., Li, Z., Wong, B. M., Men, Y., & Liu, J. (2019). Defluorination of Per-and Polyfluoroalkyl Substances (PFASs) with Hydrated Electrons: Structural Dependence and Implications to PFAS Remediation and Management. *Environmental science & technology*.
- Boyer, T. H., Fang, Y., Ellis, A., Dietz, R., Choi, Y. J., Schaefer, C. E., Higgins, C. P., & Strathmann, T. J. (2021). Anion exchange resin removal of per-and polyfluoroalkyl substances (PFAS) from impacted water: A critical review. *Water research*, 200, 117244.
- Cantoni, B., Turolla, A., Wellmütz, J., Ruhl, A. S., & Antonelli, M. (2021). Perfluoroalkyl substances (PFAS) adsorption in drinking water by granular activated carbon: Influence of activated carbon and PFAS characteristics. *Science of the Total Environment*, 795, 148821.
- Cordner, A., Goldenman, G., Birnbaum, L. S., Brown, P., Miller, M. F., Mueller, R., Patton, S., Salvatore, D. H., & Trasande, L. (2021). The true cost of PFAS and the benefits of acting now. *Environmental Science & Technology*, 55(14), 9630-9633.
- Cui, J., Gao, P., & Deng, Y. (2020). Destruction of per-and polyfluoroalkyl substances (PFAS) with advanced reduction processes (ARPs): A critical review. *Environmental Science & Technology*, 54(7), 3752-3766.
- Dixit, F., Dutta, R., Barbeau, B., Berube, P., & Mohseni, M. (2021). PFAS removal by ion exchange resins: A review. *Chemosphere*, 272, 129777.
- Du, Z., Deng, S., Bei, Y., Huang, Q., Wang, B., Huang, J., & Yu, G. (2014). Adsorption behavior and mechanism of perfluorinated compounds on various adsorbents—A review. *Journal of hazardous materials*, 274, 443-454.
- Evich, M. G., Davis, M. J., McCord, J. P., Acrey, B., Awkerman, J. A., Knappe, D. R., Lindstrom, A. B., Speth, T. F., Tebes-Stevens, C., & Strynar, M. J. (2022). Per-and polyfluoroalkyl substances in the environment. *Science*, 375(6580), eabg9065.

- Gagliano, E., SgROI, M., Falciglia, P. P., Vagliasindi, F. G., & Roccaro, P. (2020). Removal of poly-and perfluoroalkyl substances (PFAS) from water by adsorption: Role of PFAS chain length, effect of organic matter and challenges in adsorbent regeneration. *Water research*, 171, 115381.
- Gao, P., Cui, J., & Deng, Y. (2021). Direct regeneration of ion exchange resins with sulfate radical-based advanced oxidation for enabling a cyclic adsorption–regeneration treatment approach to aqueous perfluorooctanoic acid (PFOA). *Chemical Engineering Journal*, 405, 126698.
- Hatton, J., Holton, C., & DiGuseppi, B. (2018). Occurrence and behavior of per-and polyfluoroalkyl substances from aqueous film-forming foam in groundwater systems. *Remediation Journal*, 28(2), 89-99.
- Khan, M. Y., So, S., & da Silva, G. (2020). Decomposition kinetics of perfluorinated sulfonic acids. *Chemosphere*, 238, 124615.
- Krusic, P. J., Marchione, A. A., & Roe, D. C. (2005). Gas-phase NMR studies of the thermolysis of perfluorooctanoic acid. *Journal of fluorine chemistry*, 126(11-12), 1510-1516.
- Matilainen, A., Vepsäläinen, M., & Sillanpää, M. (2010). Natural organic matter removal by coagulation during drinking water treatment: A review. *Advances in colloid and interface science*, 159(2), 189-197.
- Munoz, G., Budzinski, H., Babut, M., Lobry, J., Selleslagh, J., Tapie, N., & Labadie, P. (2019). Temporal variations of perfluoroalkyl substances partitioning between surface water, suspended sediment, and biota in a macrotidal estuary. *Chemosphere*, 233, 319-326.
- OECD. (2018). *Toward a new comprehensive global database of perand polyfluoroalkyl substances (PFASs)*.
- Patterson, J. W. (1985). Industrial wastewater treatment technology.
- Qian, L., Kopinke, F.-D., Scherzer, T., Griebel, J., & Georgi, A. (2022). Enhanced degradation of perfluorooctanoic acid by heat-activated persulfate in the presence of zeolites. *Chemical Engineering Journal*, 429, 132500.
- Rahman, M. F., Peldszus, S., & Anderson, W. B. (2014). Behaviour and fate of perfluoroalkyl and polyfluoroalkyl substances (PFASs) in drinking water treatment: a review. *Water research*, 50, 318-340.
- Ratola, N., Cincinelli, A., Alves, A., & Katsoyiannis, A. (2012). Occurrence of organic microcontaminants in the wastewater treatment process. A mini review. *Journal of hazardous materials*, 239, 1-18.

- Song, Y., Deng, Y., & Jung, C. (2016). Mitigation and degradation of natural organic matters (NOMs) during ferrate (VI) application for drinking water treatment. *Chemosphere*, *146*, 145-153.
- Taylor, P., Yamada, T., Striebich, R., Graham, J., & Giraud, R. (2014). Investigation of waste incineration of fluorotelomer-based polymers as a potential source of PFOA in the environment. *Chemosphere*, *110*, 17-22.
- Tenorio, R., Liu, J., Xiao, X., Maizel, A., Higgins, C. P., Schaefer, C. E., & Strathmann, T. J. (2020). Destruction of per-and polyfluoroalkyl substances (PFASs) in aqueous film-forming foam (AFFF) with UV-sulfite photoreductive treatment. *Environmental Science & Technology*, *54*(11), 6957-6967.
- Zaggia, A., Conte, L., Falletti, L., Fant, M., & Chiorboli, A. (2016). Use of strong anion exchange resins for the removal of perfluoroalkylated substances from contaminated drinking water in batch and continuous pilot plants. *Water research*, *91*, 137-146.